LASER INDUCED DAMAGE IN THIN FILMS AND THEIR SUBSTRATES

by

DAVID MICHAEL ROWLEY

Thesis presented for the
Degree of Doctor of Philosophy
in the University of London

October 1971

Department of Physics,
Royal Holloway College

A B S T R A C T

The design parameters and the construction of a pulsed solid state laser are described.

Q - switching techniques are reviewed and a novel form of the exploding film Q - switch is decribed. This Q - switch was capable of generating high power giant pulses which were comparable with those obtained using conventional dye - stuff switches.

Techniques for generating ultra - short optical pulses are reviewed and in particular the author's procedures for generating mode locked pulses in ruby are described. The successful use of a random stack mirror circumvented the damage problem which besets thin film dielectric mirrors in the presence of mode locked pulses. The construction and use of random stack mirrors with lasers operating in various modes were also investigated.

Spatially modulated structures defined to 0.2 μ were thermally etched on thin metallic films and such structures were found to be duplicated on the substrate. Assessments of such structures for applications to the manufacture of optical diffraction gratings and grid polarizers have also been made.

The hologram of the laser cavity, recorded in gold film, was found to be capable of instant 'read out'.

Spatially modulated thin films have been deposited on

glass substrates by a process in which the condensation of the film material was inhibited by the intense electromagnetic fields within the cavity of a giant pulse ruby laser. Such an inhibitive process constitutes a new phenomenon, discovered by the author and reported very recently in Nature.

"...or if they list to try
Conjecture, he his Fabric of the Heav'ns
Hath left to thir disputes, perhaps to move
His laughter at thir quaint Opinions wide
Hereafter, when they come to model Heav'n
And calculate the Starrs, how they will weild
The mightie frame, how build, unbuild, contrive
To save appeerances, how gird the Sphear
With Centric and Eccentric scribl'd ore,
Cycle and Epicycle, Orb in Orb:"

Milton, "Paradise Lost", VIII, 75 - 84.

C O N T E N T S

C O N T E N T S (continued) Page

C H A P T E R 4

MODE LOCKED RUBY LASER

C H A P T E R 5

RANDOM STACK MIRRORS

C H A P T E R 6

LASER INDUCED THERMAL ETCHING IN THIN FILMS

CHAPTER 1

SURVEY OF RELEVANT AREAS IN PHYSICS

1.1 THE GIANT PULSE LASER

The irregular pulsations of a free running laser[1,2] are unsuitable for most applications where timing and control of the pulse are important. Even by pumping in excess of threshold for oscillation the enhancement of peak power is negligible. The reason is that the peak power of the output $P \alpha \phi \Delta N$ where ϕ is the flux density and ΔN the inversion defined as $\Delta N = N_2 - N_1$. In a given system the quality factor or Q is a measure of the strength and lifetime of ϕ and the value of ΔN for the onset of oscillations. Thus for a fixed Q, large ϕ and large ΔN, necessary for peak power, are not simultaneously attainable.

The threshold for oscillation is reached when the gain for each double transit exactly compensates for the losses i.e.

$$\exp 2(AL - \gamma) = 1 \qquad 1.$$

where A is the absorption coefficient, L the length of the active medium and γ the total loss of the system. At threshold therefore

$$AL = \gamma \qquad 2.$$

Now the absorption coefficient A for an excited material is given by

$$A = Z\kappa(N_2 - N_1)$$

and for an unexcited material the relevant coefficient is

$$\alpha = Z\kappa N_o$$

where Z is a factor dependent on the line shape and κ is the

integrated absorption. N_1 and N_2 are the population densities of the upper and lower levels respectively and N_o the total number of active ions per unit volume.

Using equation 2 the threshold inversion is given by

$$N_1 - N_2 = \frac{\gamma N_o}{aL} = \frac{\gamma}{L\sigma_o} \qquad 3.$$

where $\sigma = \frac{a}{N_o}$ is the absorption cross section per atom.

Equation 1 may be written as

$$\exp 2(N_2 - N_1)ZKL = \frac{1}{\exp -2\gamma}$$

and if γ is small

$$\exp(N_2 - N_1)2\sigma_o L = \frac{1}{(1-\gamma)^2}$$

also defines the threshold.

In 1961 Hellworth[3,4] proposed a technique for enhancement of peak power by modulation of the feedback by means of shuttering or rotating an external reflector. Because of the losses introduced with the shutter closed the Q is reduced such that the threshold condition

$$\exp(2\Delta N \sigma_o L) \geqslant \frac{1}{(1-\gamma)^2} \qquad 4.$$

is not satisfied. During this time ΔN rises to a high value and when the loss is removed, and the Q restored, the radiation builds up rapidly as the inequality (equation 4) is more than satisfied. The excess excitation is discharged in a single high power pulse called a 'giant pulse'. If the shutter is left open after the first giant pulse, threshold may be reached again and ordinary relaxation pulses ensue.[5]

For mathematical formulation[6] and generation of the shortest pulses with the highest powers the speed of switching or shuttering the cavity is an important parameter. If the switch is so slow that a significant change in population inversion occurs the number of quanta within the cavity increases more slowly, the output pulse becomes broader and is no longer characterized by exponential slopes. Multiple pulses may also be generated.

Q - Switching Techniques.

The techniques available for Q - switching may conveniently be divided into fast and slow speed devices. The distinction between fast and slow switches is not sharp, but when the switching time reaches the order of magnitude of the total pulse length multiple pulses develop.

Slow Switches.

Rotating Mirrors.[7] The triggering of the flash tube is synchronized with the position of the mirror so that at the peak of the inversion the mirror is parallel to the second reflector. Slowness, vibration and noise are undesirable features of such opto - mechanical switches.

Rotating Slits.[8] This simple, but very slow switch consists of a rotating slit inside a statically aligned laser cavity. The synchronization problems and inherent instability of mechanical systems are reasons for the adoption of other devices.

Suppressed Total Internal Reflection[9] T.I.R. Using a 90° prism as a reflector, a dielectric is moved to within a fraction of a wavelength of the face and T.I.R. suppressed by

the tunnel effect. The dielectric is then moved away by a piezoelectric drive and T.I.R. restored.

Ultrasonic Switch Cell.[10] The transient diffraction of light in passing through a liquid in which a stationary ultrasonic wave is excited, allows one cavity mirror to be set at an angle to the direction of zero diffracted order. By shock exciting the ultrasonic cell the optical path can be gated open for a short period.

Faraday Rotator.[11] The plan of polarization is rotated by 90° for a double pass in a P bO Faraday rotator. In the case of a ruby laser with its polarization dependent gain (ch. 2.3) the Q at this time is low. The resonator is then gated open by switching off the field current to the coils. The slowness of this device, caused by inductive reactance, makes it of little use in practice.

Intensity Dependent Reflectivity.[12] By using a polished semi conductor material (In Sb) as a cavity reflector, increasing laser emission increases the carrier density in the semi conductor. This can produce a change in reflectivity typically from 40% to 90% with a corresponding variation in cavity Q. Apart from its slowness the reflecting surface is often damaged by the laser radiation.

Exploding Films.[13, 14] A thin absorbing layer is placed inside the laser cavity. Increasing laser emission vaporises the material reducing the losses within the cavity and increasing the Q factor. Being a slow, single shot, device broad multiple pulses are formed. However, chapter 3.3 of this thesis shows that by analysing the losses available from a thin film it is possible to generate short single pulses from a ruby laser Q - switched by this technique.

Fast Switches.

Kerr and Pockels Cell.[15, 16] By rotating the plane of polarization using electro - optic devices, very fast (order of ns) switching can be obtained, in contrast to the equivalent Faraday rotator. This method remains the most popular when it is essential that the timing of the output pulse be synchronized with some external event, as in plasma diagnostics. If nitrobenzene is used stimulated Raman scattering[17] occurs and the parasitic lines can be annoying in liquid Kerr cells. Electro-optic crystals, for example KDP and ADP (potassium and ammonium dihydrogenphosphate) have the advantage of requiring control voltages in the region of 5KV depending on electrode arrangement and material, compared with the 20KV for a Kerr cell. However, the crystals are often damaged by the laser radiation.

Saturable Absorbers.[18, 19] Many of the phthalocyanines and cyanine dyes are highly absorbent but become transparent with strong illumination. Such an intensity dependent loss within the cavity forms the simplest and most economical high speed Q - switch. The only disadvantage, apart from reports of mode selection,[20] is that such devices are passive and the giant pulse produced cannot easily be synchronized with external events. Dye stuff switches are, however, completely self synchronizing in that the bleaching occurs close to the time for maximum gain in the crystal. Furthermore, the power handling capability is unrestricted.

The bleaching is caused by saturation of the dye due to the optical pumping of its absorption transition near oscillation threshold. If the energy levels of the absorber are denoted E_1 and E_2 then

$$E_2 - E_1 = h\nu$$

ν_L being the laser frequency.

The initial (low level) transmission is given by

$$T_o = \exp(-\sigma_s N_o L) \qquad 5.$$

where N_o is the ground state population density and σ_s the absorption cross section.

When the absorber is partially excited the transmission becomes

$$T = \exp(N_2 - N_1)\sigma_s L$$

and when $N_2 = N_1 \cong \frac{N_o}{2}$ $\quad T \to 1$

The pump power P to maintain saturation is

$$P = \frac{N_o}{2} \frac{h\nu_L}{\tau} \qquad 6.$$

where τ is the relaxation time of the absorber. From equations 5 and 6

$$P = \text{Log}_e \frac{T_o h\nu_L}{2\sigma_s L \tau}$$

Typical values for dye stuffs are $\tau \sim 10^{-12}$ sec. and $\sigma_s = 10^{-16} \text{cm}^2$. For the ruby laser line the power required for saturation is in the region of 15 KW/cm^2.

The saturation power increases if the laser frequency is not at the peak of the absorption line of the dye and conversly should decrease if the laser line width is less than the absorption line width. In the latter case the laser radiation selectively saturates the absorption line as is the case with the dye cryptocyanine.

To generate a giant pulse the absorber need not be highly saturated. A very small non linearity leads to the generation

of shortened pulses.[21] Chapter 3.3 explores this fact and experimental results are presented showing the generation of single giant pulses by pumping a small absorption edge found in Kodak Neutral Density Filters.

By use of these 'conventional' Q - switching techniques giant pulse ruby lasers are capable of peak powers in the region of 100MW with pulse widths from 10 to 50 ns.

1.2 SUBNANOSECOND LASER PULSES

There has been considerable interest in generating shorter optical pulses with peak powers in excess of those obtainable by conventional Q - switching methods. Such pulses have applications in non linear experiments where the efficiency of the process is proportional to the square of the light intensity, transient response of atomic systems, information processing and optically generated plasmas. Whilst such applications have a need for extremely high powers 10^9 - 10^{12} W the result is generally the catastrophic damage to the laser medium. Increasing the peak power of a laser by generating the same energy in a shorter pulse appears to circumvent this limitation. The damage appears to have an energy threshold rather than a peak power threshold. Bliss[22] examined a number of damage mechanisms in transparent dielectrics both theoretically and experimentally, looking for a pulse duration dependence. Although such relationships are not understood the observation of this dependence formed the motivation for developing shorter optical pulses.

Time Variable Reflectivity or Cavity Dumping.

This method of peak power enhancement was suggested and

analysed theoretically by Vuylsteke[23,24] and several variations of technique are possible. The first method, called 'First Pulse Reflection Mode' consists of a laser resonator closed by a 100% mirror and an 'effective' zero reflectivity mirror during the pump cycle. At the maximum of inversion the output mirror is switched to 99% reflectivity, the inversion is rapidly dumped within the cavity and 1% is coupled out. Such a system is characterized by minimum output coupling of the photon flux and maximum coupling between stored energy and photon density inside the cavity. Vuylsteke calculated that a $1cm^3$ ruby should yield a 17 MW pulse with a width of 10^{-8} sec. when operated in this mode.

The 'Second Pulse Reflection Mode' is similar to the above, but the output reflectivity is switched to some critical value between zero and 100%, which optimizes the output with respect to the necessary regeneration. Vuylsteke showed that the optimum reflectivity is such that the total cavity loss rate due to absorption, scattering etc., is equal to the loss rate due to output coupling. Calculations predict 170 MW peak power with 8 ns half width for a $1cm^3$ ruby.

'Pulse Transmission Mode' combines the best of First and Second P.R.M. After pumping to a high inversion with a low Q cavity the Q is suddenly increased by switching the output mirror to 100%. A rapid conversion of the stored energy to photon flux results. At the peak of the photon flux the output mirror is switched back to zero reflectivity and the stored photon energy within the cavity is effectively dumped in the cavity transit time ($\sim$ 1 ns). Peak power in this case is 920 MW for a $1cm^3$ ruby.

The main difficulty with T.V.R. and P.T.M. in particular is that the timing and speed of the switching operations are at the limit of the 'state of the art' in optical control. The methods used[25,26,27] utilize Glan Thomson polarizers and polarization switches driven by an optically triggered Marx - Bank pulser. The P.T.M. technique, when used with a 4 x 3/8 inch ruby, produces a triangular pulse with a rise time of 3.0 ns and a pulse width of 5.3 ns. Peak powers are in the region of 1.5×10^8 watts.[27] Even with these shortened pulses the calcite surfaces of the 'switch gear' are often damaged in pure P.T.M. operation and such components are expensive to replace.

Mode Locking

An alternative approach to shorter pulses is available by the technique of mode locking. A mode locked crystal laser can produce pulses as short as 10^{-12} seconds; the properties of such short pulses are of inherent interest besides the gigawatt power levels involved.[28, 29] A mode locked laser may be compared with the microwave regenerative pulse oscillator developed by Cutler.[30] Such an oscillator comprises a filter, amplifier, delay line and an 'expandor'. The purpose of the latter is to emphasize the peak region of a recirculating pulse, whilst reducing lower amplitude regions, thereby shortening the pulse until the pulse width is limited by the frequency response of the circuit. Cutler was able to generate microwave pulses having a carrier frequency of 4 GHz and pulse widths of 2 ns. A laser possesses all the basic elements for an optical regenerative pulse oscillator. The laser medium acts as combined filter and amplifier and the time taken by the light to bounce between mirrors(2 L/C) is the corollary of the delay line.

The action of the expandor is translated from the time domain to the frequency domain and pulse shortening achieved by amplitude modulation and side band generation.

Early attempts to operate the laser as a pulse regenerative oscillator involved modulating the cavity by means of electro-optic devices. Hargrave et al[31] used a c.w. He Ne gas laser and an acoustic diffraction modulator. The R.F. frequency was 56 MHz and 2.5 ns pulses were obtained. The R.F. signal had to be synchronized exactly with the axial mode difference frequency (see chapter 4). A similar device was used to mode lock an argon ion laser.[32]

The oscillating bandwidth of solid state lasers is greater by an order of magnitude and shorter pulses are expected from ruby lasers. Deutsch[33] used a K.D.P. polarization modulator working at 50 MHz and a pulsed ruby laser. Though not realized at the time, the change in optical path, caused by thermal transients, made complete locking unlikely. Neodymium - glass lasers were investigated for locking effects by Michon[34] using a K.D.P. phase modulator. A c.w. solid state Y.Al.G.: Nd laser was mode locked by the use of a diffraction modulator[35] and pulse widths < 0.15 ns estimated by comparing the relative intensities of second harmonic radiation[36] produced in locked and unlocked cases.

Self (automatic) mode locking with use of saturable absorber Q - switches was reported for ruby using crypto-cyanine in methanol (low power absorption $\alpha = 0.24$).[37] Automatic mode locking, now as then, is a volatile commodity

particular to a given laser rod, laboratory and operator. In chapter 4 procedures are outlined that were adopted to obtain a reproducible self mode locked output from a ruby laser. In particular the damage problem associated with the output mirror[38] was alleviated by the use of a random stack mirror.[39] The theory, fabrication and use of such mirrors with a free running and a conventionally Q - switched ruby laser is the subject of chapter 5.

By 1966 Nd^{3+}:glass lasers had become acceptable and the advantages of a wide ($\sim$ 100Å) bandwidth realized. Eastman 9740 Q - switch solution was found capable of simultaneously Q - switching and mode locking the laser[40] giving pulses with a theoretical width of 3.7×10^{-13} seconds.

Since the pulse widths had reached the limit of the opto - electronic detection systems and were having to be derived from the inverse bandwidth relation

$$\Delta\tau = \frac{1}{\Delta f} \qquad 7.$$

which assumes simultaneous excitation over the whole oscillating bandwidth, the spectra of mode locked pulses were examined. Stetser et al.[41] took random sections of the 180Å spectrum of the output from a mode locked Nd^{3+}:glass laser. Even over a region defined by 0.5Å the pulse widths were detection limited and they concluded that mode coupling was complete over the 180Å bandwidth, inferring a lower limit of 2×10^{-12} seconds and peak powers of 10^{10} W. Time resolved spectroscopic data, to check simultaneous excitation over the entire bandwidth was sketchy.

Several papers[42,38] discussed the influence of mode discrimination by various resonator elements on the spectral

composition of the radiation. When pulsed solid state lasers were used the problem of output mirror damage and the possibility of frequency 'chirp' were discussed.[43,38]

The first attempt at direct measurement of pulse widths was by Weber.[44] Although the experiment had an intrinsic resolution of 10^{-12} seconds it assumed that the pulse sequences were reproducible. It was realized by Weber that the phase matching condition[45,36] can be attained for more than one direction in a non linear crystal. The second solution requires a beam split into 'o' and 'e' parts and second harmonic is generated by the interaction i.e. in the overlap time. The incident beam was split and orthogonal polarizations obtained for two optically delayed pulses in a Michelson type arrangement. By adjusting the relative delay the harmonic content produced in a 1 mm thick K.D.D. crystal was measured as a function of path difference and the pulse width deduced.

Direct measurement without resorting to multiple shots was achieved by the standing wave excitation of two photon fluorescence in solutions of organic molecules.[46,47] This technique is discussed further in chapter 4.

Single Pulses.

A mode locked laser generates a train of high power picosecond pulses. This is disturbing for many scattering experiments and for these it becomes necessary to select a single pulse. This can be achieved in two ways. Firstly, selection can be made external to the oscillator[48] with a high speed optical gate. Alternatively, the recirculating ultra short pulse can be switched out of the cavity.[49,50,51] This amounts to a

combination of P.T.M. and mode locking. However, the introduction of so many surfaces within the laser cavity tends to disrupt the delicate locking conditions. This is particularly important with ruby lasers where the conditions for mode locking are hypercritical.

By amplifying a single picosecond light pulse with five cascaded amplifiers Basov[52] obtained a 30 Joule pulse believed to be 10^{-11} seconds long. Focused on a lithium deuteride target the 3 terrawatt pulse resulted in four coincident neutrons.

1.3 HOLOGRAPHY

From the diffraction theory of image formation[53] it is known that the process of diffraction can be regarded as a Fourier analysis. For a periodic function such as a diffraction grating a series of orders of diffraction correspond to the Fourier coefficients and for a non periodic object the general pattern of diffraction is the Fourier transform. A diffraction pattern is seen as the square of the Fourier transform and from such a pattern the relative amplitudes of the light diffracted into various directions can be obtained. The relative phases are unknown. Since all the information concerning the image of an object is contained in the diffraction pattern such information should be 'storable' on a photographic plate. The main difficulty is the recording of the relative phases of the different parts of the optical transform. Photographic films only record intensities, the information contained in the phase portion is lost.

The problem of image formation by an electron microscope

led Gabor[54] to demonstrate the reconstruction of images from optical diffraction patterns. The phase problem was solved by using an object consisting of a small amount of black detail on a large transparent background (on line system); the background produced a uniform phase and the variation in phase of the diffraction pattern was recorded as a difference in intensity. Gabor called the photographic record a hologram from the Greek 'holos' or whole, indicating that the entire wave pattern consisting of amplitude and phase was recorded. The method did not work very well even for optical patterns and was never applied to the problem of increasing the resolution of electron microscopes. The application of the laser, with its intense beam of spatially coherent light, allowed the hologram approach of image formation to be used successfully. The laser enabled the reference (uniform phase) beam to be split off at an angle from the beam impinging on the object, thereby removing the necessity for a large transparent background (skew hologram).[55,56]

The extension of holography to colour and the applications to image storage and retrieval have been reviewed by Stroke.[57]

Holographic Materials

Other storage media besides photographic plates are capable of recording holographic information. There are two basic requirements: firstly, the medium must be able to resolve fringes of a few wavelengths separation; secondly, it must be able to retain the information recorded whilst interrogation takes place. Ideally, additional requirements are:

a) Infinite resolution for high density information storage without noise

b) Dimensional stability for faithful reproduction of the original wave-front

c) Real time recording without processing, which can be erased for further use

d) Freedom from loss for high efficiency reconstruction

e) No thickness limitation so that storage capacity can be increased.

The most widely used recording media are summarized in the following paragraphs.

Photographic emulsions[58] Agfa 10E 70 and Kodak 649F plates. The resolution claimed for these plates under exacting conditions is 3,000 line pairs per mm. The hologram needs processing, is not re-usable, lacks dimensional stability, possesses grain noise and the thickness must be less than 50 μm for uniform processing.

Photochromic materials. Photochromism is the property of some compounds to show reversible colour and optical density changes under the influence of light. Photochromic glass[59] consists of borosilicate glass with silver halide crystals and is similar to photographic emulsions but the host (glass) is non permeable and the halide atoms are available for recombination when the exposing field is removed. This is called thermal fading and can take between minutes and weeks depending on temperature. The 'speed' of the system is four orders of magnitude slower than 649F photographic plates. Photochromic glass is suitable for real time systems and possesses a resolution of 2,000 line pairs per mm.

Alkali Halide Crystals.[60] Potassium bromide (KBr) is incorporated into potassium hydride (KH) during the formation

of the crystal. The crystal is first exposed to ultra violet radiation and the spatially modulated laser field bleaches the affected areas. The bleaching process is temperature dependent and hot air turbulence causes an unstable interference pattern, requiring the whole system to be placed in a vacuum chamber. The resolution depends on crystal quality but is in the region of 1,500 line pairs per mm.

Photoresist[61] is a formulation of resins sensitive to the ultraviolet. The resist polymerizes when exposed and may be dissolved selectively by a 'developer' e.g. trichloroethylene.

Thermoplastics[62]. This is basically a Xerograph technique. The plastic is coated on a photoconducting substrate and in full darkness equal and opposite charges are placed on the film and its substrate. When exposed to the spatially periodic light field the charges move towards each other at the exposed parts, resulting in a higher static potential. If the plate is heated the differing static potentials allow differing amounts of deformation.

Photosensitive Plastics[63] consist of a plastic resin coating containing light sensitive diazonium salts (Kalvar process). The salt releases nitrogen on exposure to ultra violet radiation and by heating the air bubbles expand, forming microscopic vesicules. After cooling the image is permanent as long as the remaining diazonium salt is allowed to decompose. The process has a resolution of 500 line pairs per mm.

Ferroelectric Crystals[64] e.g. lithium niobate. When a single crystal of $LiNbO_3$ is exposed to light of short wavelengths photoexcitation frees trapped charges which drift a short distance before becoming retrapped. The field created by the space charges causes a change in refractive index due to electro-

optical effects. The image can be erased by heating and the resolution is 1,600 line pairs per mm.

Dichromated Gelatin[65] consists of gelatin treated with water soluble dichromates and chromates. The gelatin becomes hardened and less soluble when exposedto light. Development is by agitating in water for 30 seconds and dipping in isopropanol for rapid drying. The structure of the developed grains is unknown. Dichromates are as fast as 649F photographic plates in the blue region of the spectrum and the resolution can be as high as 4,000 line pairs per mm.

Photopolymer[66] consists of a monomer, catalyst, photo-oxident and fixer. The photo-oxident is activated by photons with resultant oxidation of the catalyst causing free radical polymerization. Fixing is by heating or ultra violet light which de-activates the oxident. A resolution of 1,000 line pairs per mm is claimed, but scattering by long polymer chains causes noise.

Holographic Diffraction Gratings

The simplest form of hologram is that recorded without an object. Classically this is simply the interference pattern produced between two beams of light. For two beams making angles θ_1 and θ_2 to the surface normal, the distance between adjacent fringes in the plane of a photographic emulsion surface is given by

$$d = \frac{\lambda}{2\cos\frac{\theta_2-\theta_1}{2}\sin\frac{\theta_2+\theta_1}{2}} \qquad 8.$$

where λ is the wavelength of the source.

The idea of photographically produced diffraction gratings is certainly not new. Early work on interferometric methods for the photographic production of gratings was reported by Burch.[67] The intense, spatially coherent light of the laser permitted gratings to be recorded over larger areas. The shorter exposures requires also enabled less stringent control over mechanical and thermal stability.[68,69,70,71] Holographically produced diffraction gratings are now available commercially[72,73] and their performance extends the generally accepted limits of machine ruled gratings.[74,75] The light sources used to produce the gratings are the prominent gas laser lines (6328A He Ne and 4880A argon ion) and the beam is separated by a Kösters prism arrangement. Two plane mirrors then bring about interference fringes on the film plate.

More recently the high powers developed by pulsed solid state lasers have enabled metallic surfaces to be used as recording media. The intensity distribution is recorded by the evaporation of metal in the interference antinodes produced by the superposition of two laser beams.[76,77,78] A hologram of a resolution test pattern has also been achieved in a 75A thick bismuth film.[79]

In the work described in chapter 6, instead of splitting the beam into two parts, the corollary of the Gabor 'on line' hologram was used. This allowed the metallic film to fulfil a dual role as combined recording medium and Q - switch film. A large number of metallic films were investigated and their diffraction properties and resolution are reported.

Holographic recording on metallic surfaces has the following advantages: an increased resolving power; no processing; exposure in full light and truly panchromatic range. Furthermore, because of the short 'exposure' time the metallic film is more tolerant of vibration and the resulting hologram is permanent.

In chapter 6 the instant read out capability of the thin film hologram is demonstrated, as is an extension of the technique, using gold vapour as the recording medium.[80] It is also shown that it is possible to record a two beam interference pattern on a surface which is normally non-absorbing, such as glass.

1.4 LASER INDUCED DAMAGE

The technique for recording holograms on metals, described above, relies on sufficient energy being absorbed to raise the temperature of the surface layer to its boiling point. The energy must be absorbed in a time that is short compared with the time it takes the thermal energy to diffuse. The recording process is then the result of localised high power laser damage and from a study of such recordings more information can be obtained about the damage processes themselves.

Damage due to the absorption of laser radiation resulted in early workers with lasers measuring the output energy in 'Gillette power', this being the number of razor blades the focused radiation could penetrate. Subsequently research has been supported by 'the military', whose 'top brass' still think the laser is the nonpareil of weapons, blasting enemy missiles

from the skies. Real lasers are confined to welding, cutting and boring operations at the focus of a lens. Low power, high energy pulses cause surface melting and are used for welding. High power, low energy systems cause vaporization of small quantities of material and are used in resistor trimming type applications. This is not to mention the K watt powers from c.w. CO_2 lasers, used for material processing in bulk.[81]

Ready[82] was the first to show that an ordinary thermodynamic approach could be used for calculating the effects produced by laser beams absorbed at opaque surfaces when the surface either vaporized or was simply heated. When high power Q - switched lasers were used experimental evidence was not in accord with such a treatment. Calculations by Ready[83] indicated that a 10^9 W/cm^2 laser pulse, 30 ns long, would bring the surface layer of any metal to boiling point in less than 1 ns. Vaporization then appeared to proceed slowly, tending to maximum emission from the vapour plume (carbon in air) 120 ns after the giant pulse had reached its peak. Ready interpreted this delay in terms of a super heated liquid state close to the surface. Material below the surface reached its vaporization temperature before the surface layer had absorbed its latent heat. This led to a high pressure pulse and subsequent superheating of the underlying material until the temperature rose above the critical point. At this point there was no distinction between the superheated solid and the highly condensed gas. The emission of vaporized material then proceeded like a thermal explosion.

This phenomenological model was further supported by microscopic examination of the surface damage caused by the irradiation of 2 mm thick metal targets.[84] The radiation damage area showed a concentric zone structure. The central zone was characterized by melting and re-solidification. The concentric crater zone was dominated by two types of crater formations with diameters in the region of 10 microns. The so-called ejection crater possessed a central peak, usually a drop like formation, and in later stages the crater was surrounded by a ring. The other craters were similar to impact craters and lacked the central peak. In general the size and number of the craters decreased with increasing distance from the irradiation centre. With increased power densities the microstructure was not significantly influenced, the main feature being an increase in ejection and evaporation from the melting zone. At the highest power densities radially directed grooves usually terminated in a drop like formation. The formation of the craters was related to defects on the surface as they appeared closely packed along surface scratches. Crystal structure was not considered important. Microcraters were also observed in shielded sections of the target area, thus excluding their interpretation as an effect of a high intensity micromode. An assessment of the crater depth was made by lowering a tapered tungsten stylus into the crater.[85] Depths were typically 16 microns. Experiments conducted in vacuum showed no change in surface microstructure. Shielding part of the target resulted in a sharp boundary between the crater region and undisturbed metal, contrary to previous work.[84] Assuming the metal was ejected from the craters in the form of a vapour jet the energy required would be in the region of 10^{-4}

Joules and it has been suggested that the spatial distribution of picosecond components in the laser pulse could be responsible for blasting the craters.[86] Alternatively the filamentary structure due to self trapping[82] in the ruby rod could have concentrated the energy from the laser to form intense localized hot spots of the order of a micron in size. The similar nature of a spark eroded crater presents another possibility regarding the laser produced craters. The formation of a hot, dense ionized plasma near the irradiated metal surface has been observed by Ehler.[87] A localized microdischarge would be consistent with the formation of craters at surface irregularities. The observation of ordered microcraters[88] on pure polished specimens favoured the crater formation by unipolar arcs at points of high potential resulting from a wavelike instability within the plasma.

Giant pulse laser damage has also been investigated from the properties of the evaporated material. Weichel[89] used a streak camera to measure the velocity of the vapour leaving the target and, whilst the initial velocity agreed with the sublimation temperature (of graphite), subsequent vapour absorption of the laser radiation accelerated the plume front from 5×10^5 cm/sec to 7×10^6 cm/sec in a distance of 0.3 cm. Other techniques include time of flight measurements,[90] high speed photography[83] and time resolved temperature measurement of laser heated surfaces.[91]

The discussion so far has concerned material in bulk. When thin metal films are considered the rate of heating and evaporation depends on the ratio of the bulk specific heats of the layer and the heated region of the substrate.[92] A metal layer

is termed thin when the thermal skin depth $d = (a\tau)^{1/2}$ is greater than the film thickness. Where τ is the pulse length and a the diffusivity defined as $a = \frac{K}{\rho c}$, . K thermal

conductivity, ρ density, c specific heat. If the film thickness is less than $(a\tau)^{1/2}$ and the incident pulse energy is sufficient to vaporize the film, the boiling point can be taken as the threshold for the total destruction of the film.[93]

In chapter 6 the microtopography of the laser evaporated films and their substrates is examined and several surface features elucidated.

* * *

CHAPTER 2

EQUIPMENT USED IN THE EXPERIMENTS

2.1 LASER DRIVE UNIT AND FLASH TUBES

The method of creating a population inversion in the majority of solid state lasers is by strong pulsed illumination. This pump light must have an emission spectrum that covers the absorption band of the laser material.

In ruby there are two absorption bands, at 5500 ∓ 500Å and 4100 ∓ 500Å. The emission spectrum of xenon has peaks at 4500Å, 4624Å and 4671Å and matches the lower absorption wavelength of ruby. By using a suitable mixture of xenon and other gases, a flash tube can be made to emit in the 5500Å region and provide a better match to ruby than a pure xenon filling. These tubes are commercially available in standard sizes or can be made to specification. The specification for the tube used was as follows:

Arc length 6"	Maximum voltage 2.5 KV
Quartz tube 3/8" diameter	Minimum trigger 10 KV
	Maximum input 5000 J in 2 ms

The filling pressure was in the region of 100 mm of Hg.

The tube is connected across a capacitor bank charged to a voltage that, by itself, would not cause breakdown of the gas. The tube is then pre-ionized by a large, low capacity, over voltage applied by a trigger wire wound around the tube. This acts as ignition and the plasma grows rapidly in luminosity.

A SPECTRAL OUTPUT OF FLASHTUBES AND ABSORPTION SPECTRUM OF RUBY

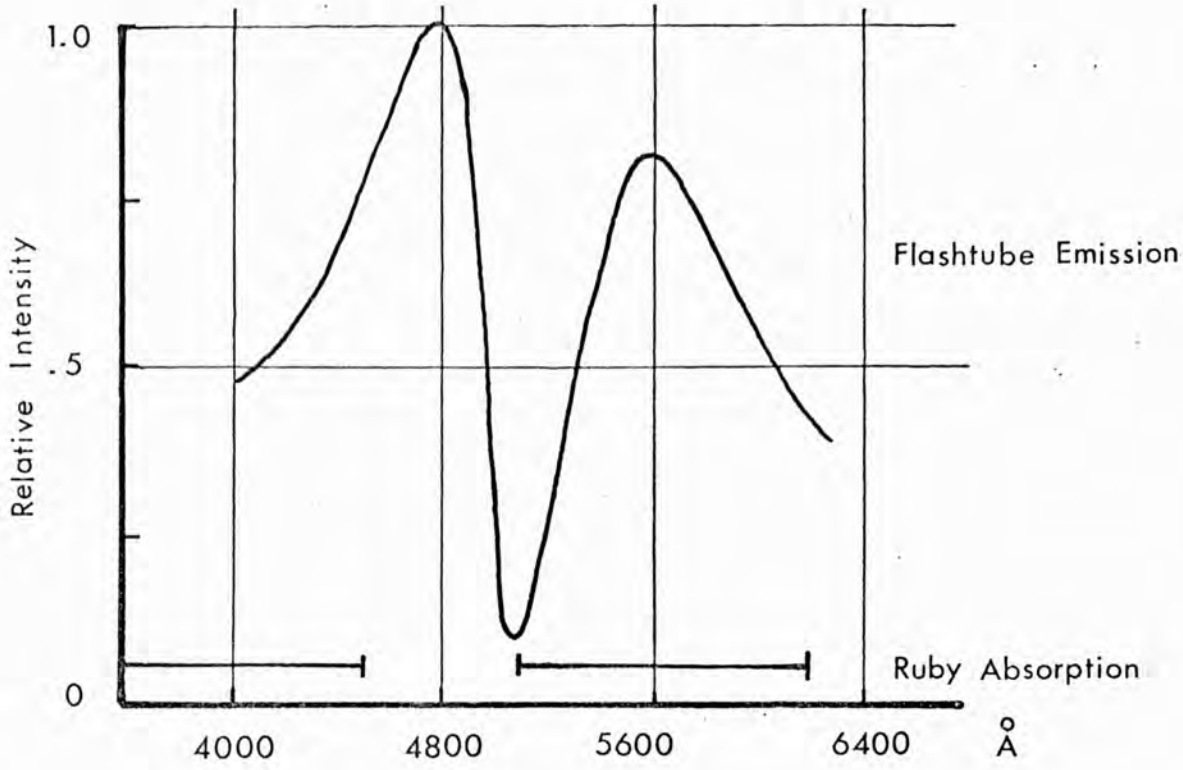

B CALIBRATION CURVES FOR C_B

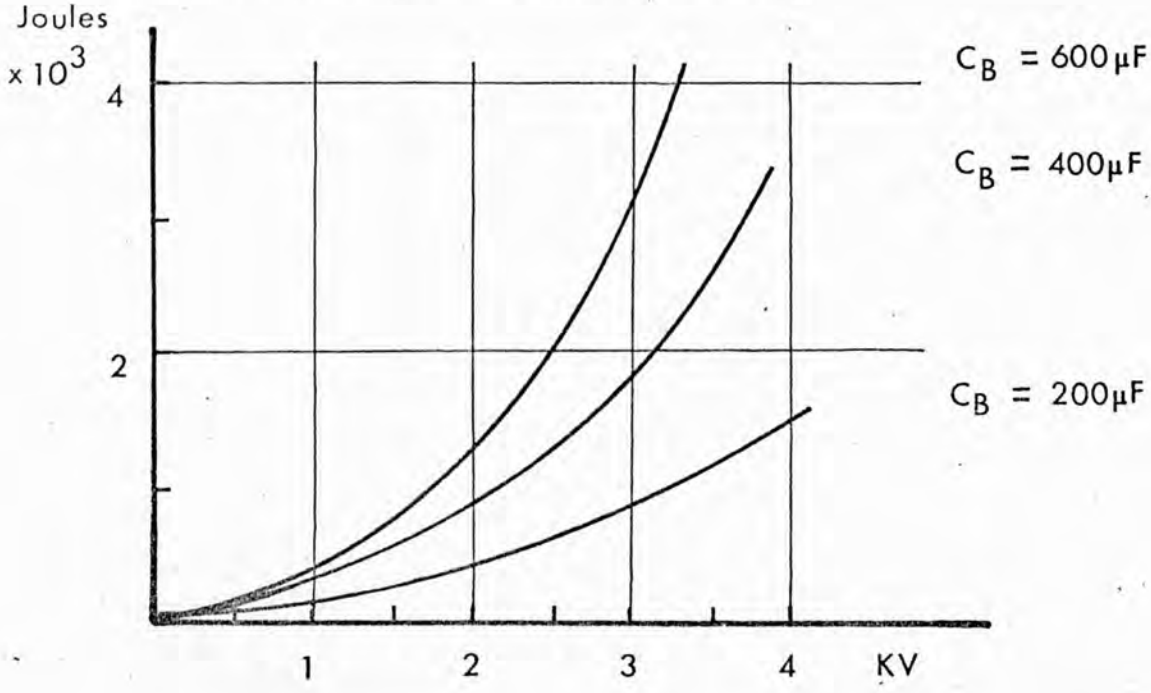

Fig 2·1

A PRE-IONIZATION PULSE
MONITORED AT SKT.1

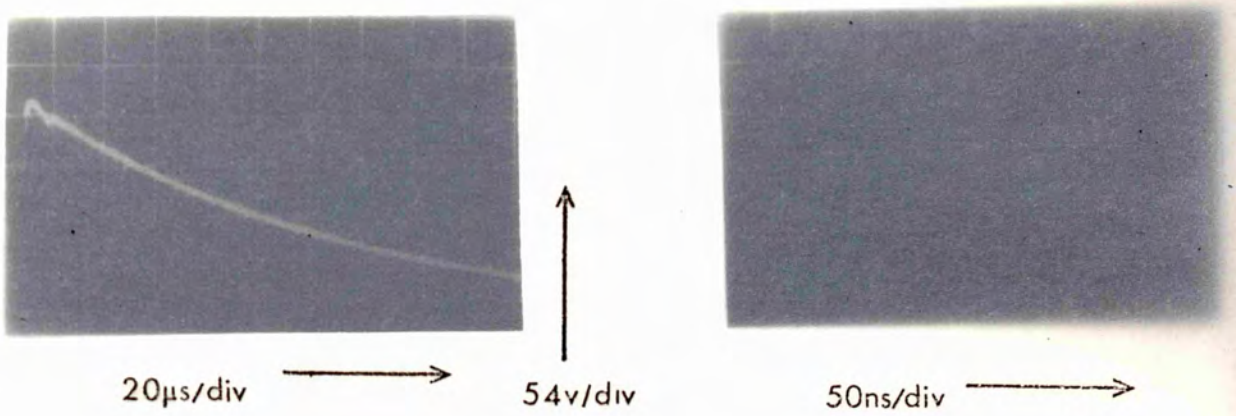

B FLASHTUBE OUTPUT
FOR VARIOUS SERIES INDUCTANCES

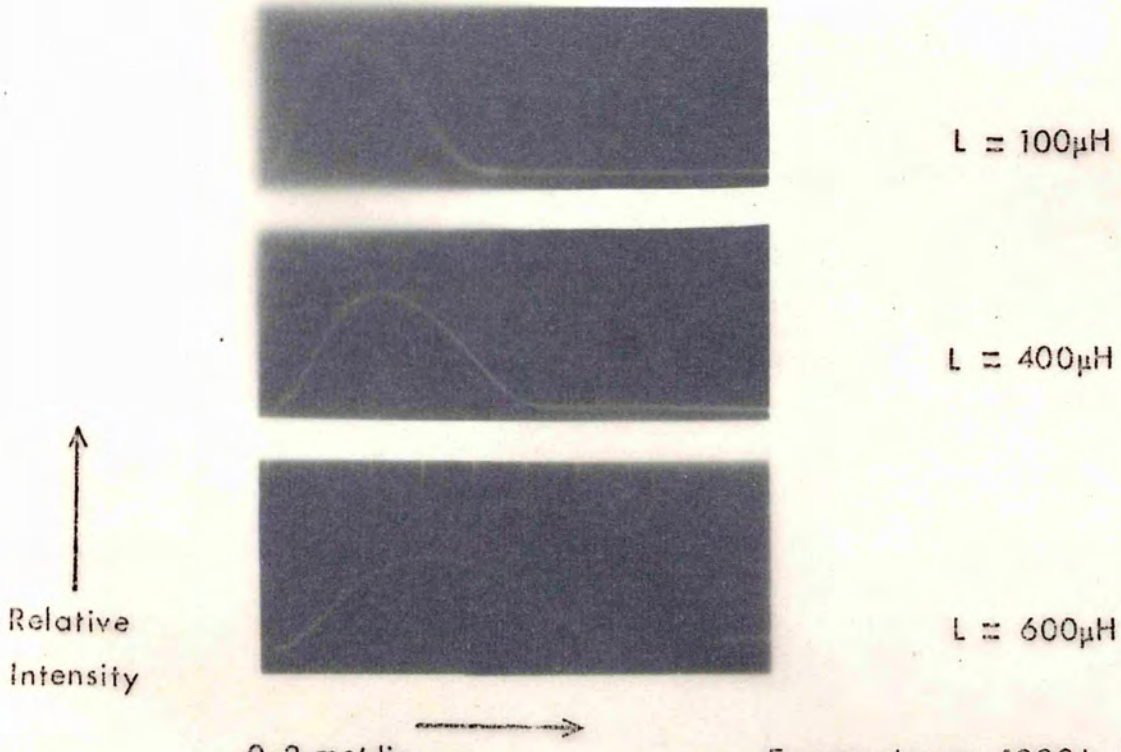

Fig 2·2

The pump light must cause inversion in a time comparable with the metastable lifetime of the lasing level involved. For ruby this amounts to 2.9 ms. The plasma lifetime, and therefore pump lifetime, depends on the resistance, capacitance and inductance in the circuit. The resistance of the plasma was typically $\frac{1}{2}$ ohm and the storage capacity 400 μF. Fig. 2.2B shows the effect of varying the series inductance. With an inductance of 100 μH the luminous flash lasted 0.8 ms. At the input energy of 10^3 Joules the power level was approaching the advised 2 MW maximum for the tube. At 600 μH the output was a non-monatonic function unsuitable for laser excitation. With the inductance at 400 μH the output was critically damped and the power within the advised limit.

Laser Power Supply.

The circuit for the drive unit constructed is shown in fig. 2.3. The output from T_2 is rectified by bridge D_1 and charges the capacitor bank C_B through the limiting resistance R_2. The dump system R_4 - R_{EL} allows C_B to be discharged quickly if necessary. Closing S_5 shorts C_5 to ground and the resulting -90 V pulse is inverted by T_4 before being applied to the -14 V biassed grid of V_1 causing it to conduct for a short period equal to $5R_7C_5$ = 25 μs. The resulting 200V pulse is transformed by T_5 to the 20 KV required for pre-ionization. The pulse at the monitor SKT_1 is shown in fig. 2.2A. The thyratron V_1 switches 150 V in 50 ns into the pulse transformer. In the experiments the signal at SKT_1 was used as a high impedance trigger for the laser light detecting systems. The energy stored in the capacitor bank was $\frac{1}{2}C_BV^2$ and fig. 2.1B shows a series of calibration curves calculated for various values of C_B and V.

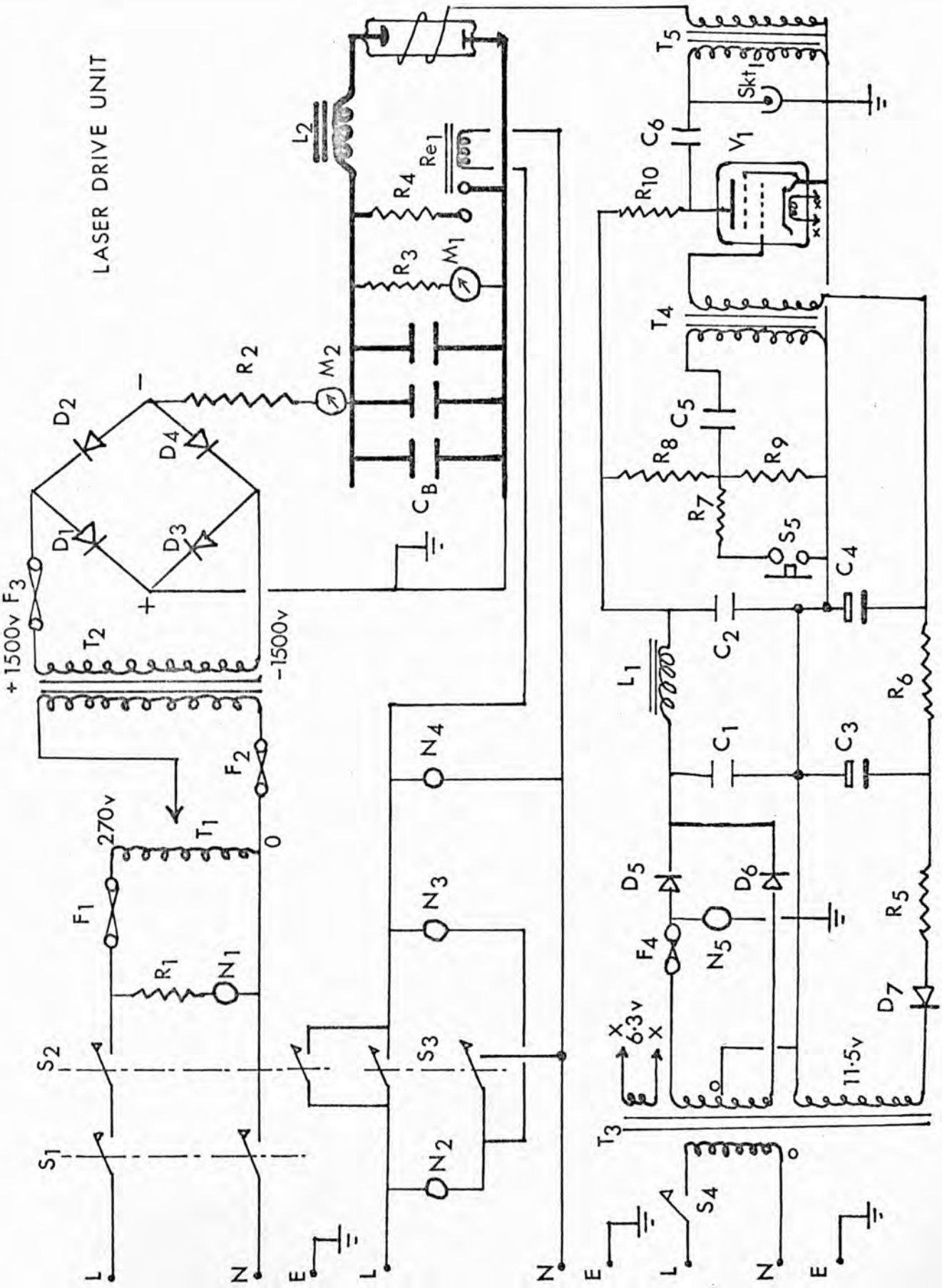
LASER DRIVE UNIT
L2
Re1
R4
R3
M1
M2
R2
CB
D2
D4
D1
D3
+ 1500v F3
T2
-1500v
F2
270v
T1
0
F1
R1
N1
S2
S1
L
N
E
N4
N3
N2
S3
T5
Skt1
C6
V1
R10
T4
C5
R8
R9
R7
S5
C4
C2
L1
C1
C3
R6
D5
D6
F4
N5
R5
D7
X
6·3v
X
11·5v
T3
S4
L
N
E

Fig 2·3

Most of the components used were standard and are listed below:

R_1	270	D_{1-4}	IN 2378	M_1	100 µA f.s.d.
R_2	34 K	$D_{5,6}$	BYX 22/400	M_2	50 µA f.s.d.
R_3	30 M	$C_{1,2}$	16µ		
R_4	2 K	C_3	4 µ		
R_5	22	C_4	1 µ		
$R_{6,7}$	100	C_5	0.05µ		
R_8	100 K	C_6	0.5 µ		
R_9	47 K	L_1	20 H 60 mA		
R_{10}	220 K	V_1	2D21 (CV 4018)		
T_1	3 Amp Variac				
T_2	R.C.A. plate transformer 1.75 KVA				
T_3	radio transformer				
T_5	Ferranti PT60 100:1 pulse transformer				
R_{EL}	Philtrol mains solenoid relay				

The inductor unit L_2 and the inverting transformer T_4 were not commercially available and their construction is outlined in the following paragraphs.

L_2 was made from 18 gauge copper strip one inch wide. The winding was in pancake form to minimise insulation problems. Insulation was provided by a paper layer between the windings. Forty feet of copper were used, increasing from two inches to nine inches in diameter. The inductance, as measured on a Marconi Universal Bridge, was 405 µH.

The inverting transformer T_4 consisted of a primary of 100 turns and a secondary of 115 turns of 26 swg on a ferrite core 1 cm in diameter and 4 cm long. The ratio was checked using a wide band oscillator.

2.2 LASER HEAD DESIGN

The main design feature of the laser head was the efficiency with which it coupled the exciting radiation into the active medium. The design used was that of an exfocal elliptical cylinder of the type used for Raman spectroscopy. Such illumination projection geometries provide a factor of ten reduction in lasing threshold compared with close coupled helical flash tubes.[94,95] By placing the rod and flash tube symmetrically about the focii, fig. 2.4A, the rod was in a uniform field of illumination. Centring the rod and flashtube at the focii (focal ellipse geometry) would have caused strong focusing of the pump light of the rod centre and a corresponding variation of inversion.

The elliptical cylinder was machined from solid aluminium in two halves. These were fitted together accurately by metal dowels and Alan screws. The ends of the cylinder were closed by flat aluminium plates suitably machined to hold the ruby rod and flash tube in their exfocal positions.

The reflectivity of the inner elliptical surface was of crucial importance if full advantage was to be taken of this kind of pump geometry. Ideally the surface should have a reflectivity of unity. Direct polishing of the aluminium surface did not give the desired effect because of impurities in the aluminium. The method used was therefore that of high reflectivity shim liners. These shims were made of springy, 0.05 mm thick steel and were accurately cut to length so that, with their ends abutted, they contoured the inner surface of the cylinder exactly. The shims were electropolished in a saturated solution of chromium trioxide in orthophosphoric acid at 120 C. A current of 10 Amps

A COMPARISON OF FOCAL AND NON-FOCAL ELLIPTICAL CYLINDERS

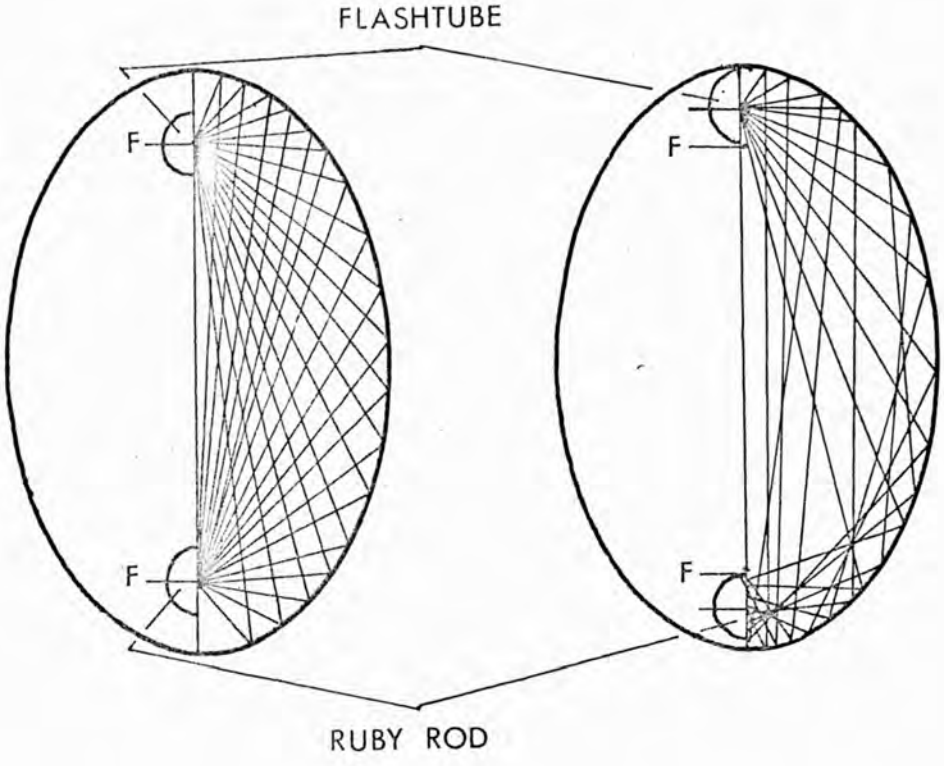

B SPRING MOUNTED MIRROR SUSPENSION

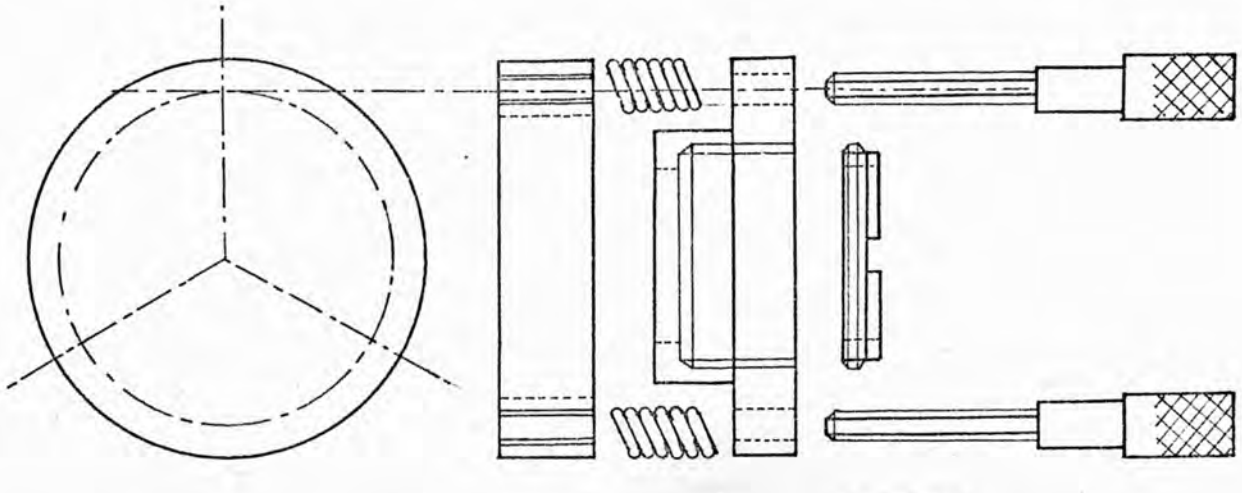

Full Size

Fig 2·4

for 5 minutes was sufficient to remove all processing marks and give the surface a high polish. After thorough rinsing in distilled water a slight bloom appeared which was removed with 0.05 μm polishing powder dispersed in distilled water. The shims were then coated with a 1.0 μm layer of silver. This care taken with the finishing of the shims was the reason for the low threshold values obtained.

Cooling.

The energy released in relaxation to the metastable state and that caused by absorption, which is not involved in the lasing transition, is a source of heat. This thermal energy would have created non-stable threshold conditions, perturbations in the resonator and undesirable excitation of atoms to other levels. The rated life expectancy of the flash tube was quoted for a free environment. Heating of the flash tube would reduce the reasonable lifetime loading of the tube by 50% in the image forming pump arrangement used. Independent water jackets are often employed for cooling, but here a cooled nitrogen draught was used. This had the advantage of preventing oxidization of the silver coatings on the shim liners. An oxygen free nitrogen cylinder with a control valve passed the gas at 300 cc per minute into a helical heat exchanger immersed in liquid nitrogen. The cooled gas then entered the cavity, its only exit being through the clearance around the ruby rod. This arrangement enabled the laser to be operated every two minutes without any appreciable temperature rise. When deliberate cooling below ambient was required the gas flow was increased. The system was purged with nitrogen when the laser was not being used and the gas entry point sealed off. This procedure lengthened the life of the silver coated shim liners to approximately nine months

compared with three days in a free air environment. After nine months degradation of the liners resulted in a steady increase of 30% in threshold. The liners could be taken from the cavity, cleaned in H_2O_2 and recoated.

2.3 THE OPTICAL CAVITY AND ALIGNMENT

The active medium used in the experiments was a 6" x 3/8" Vernoillii ruby cut at the Brewster angle. The outer cylindrical sidewall of the rod was polished. This had the disadvantage of causing partial focusing within the rod. This effect can be avoided by roughening the surface of the rod. However, an increase in threshold results because of the diffuse reflection at the surface. In the particular pump geometry used roughened rods would have threshold values comparable with those obtained using helical flash tubes. Further more, a rough surface is less stable and in ruby such a surface breaks down gradually under the action of the pump light.

Ruby consists of chromium doped Al_2O_3, the aluminium and oxygen being inert. The most suitable doping rate is 0.035% Cr^{3+} or the equivalent of 0.05% by weight Cr_2O_3. This rate gives the number of active ions per cc $N_o = 1.6 \times 10^{19}$ which is generally called pink ruby. With higher doping unwanted laser action can be observed in satellite lines of coupled chromium atoms.

The ruby laser is an example of a three level laser system and the energy level scheme is shown in fig. 2.5A. At room temperature the ground state and the upper levels are taken as equally degenerate $g_1/g_2 = 1$ and inversion occurs at $N_2 = N_1 = N_o/2$. As can be seen there are two possible transitions to the ground

A ENERGY LEVELS OF CHROMIUM ION IN RUBY

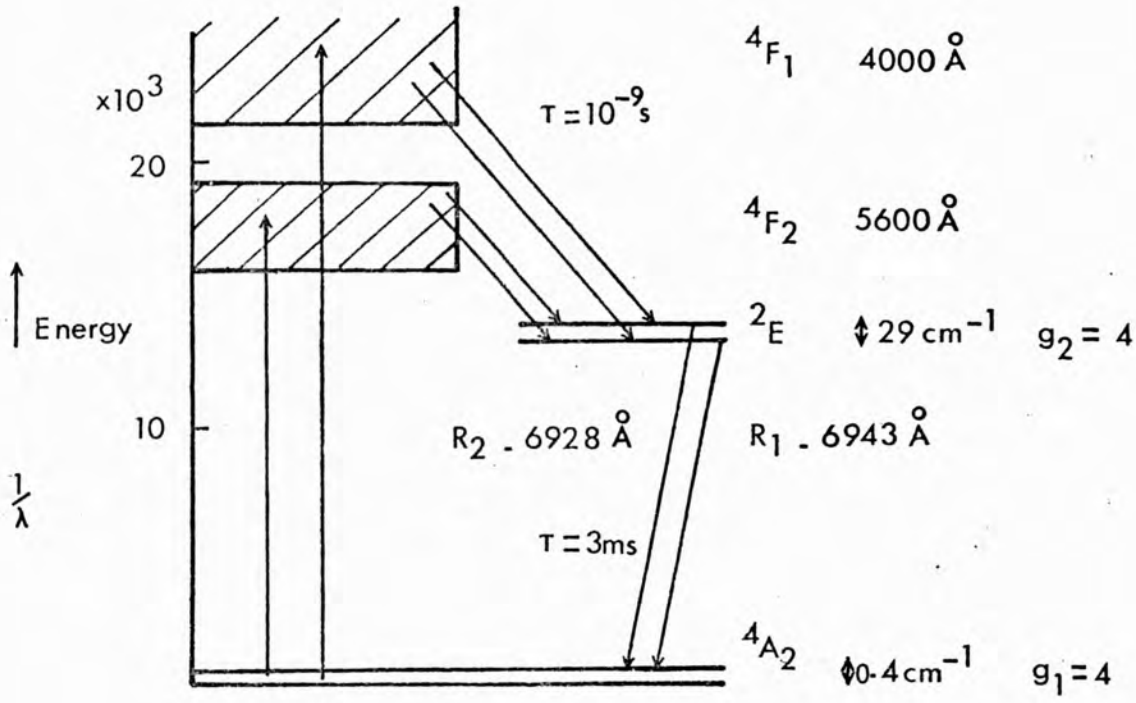

B ORIENTATION OF OSCILLATING E VECTOR, BREWSTER FACES AND CRYSTAL C AXIS

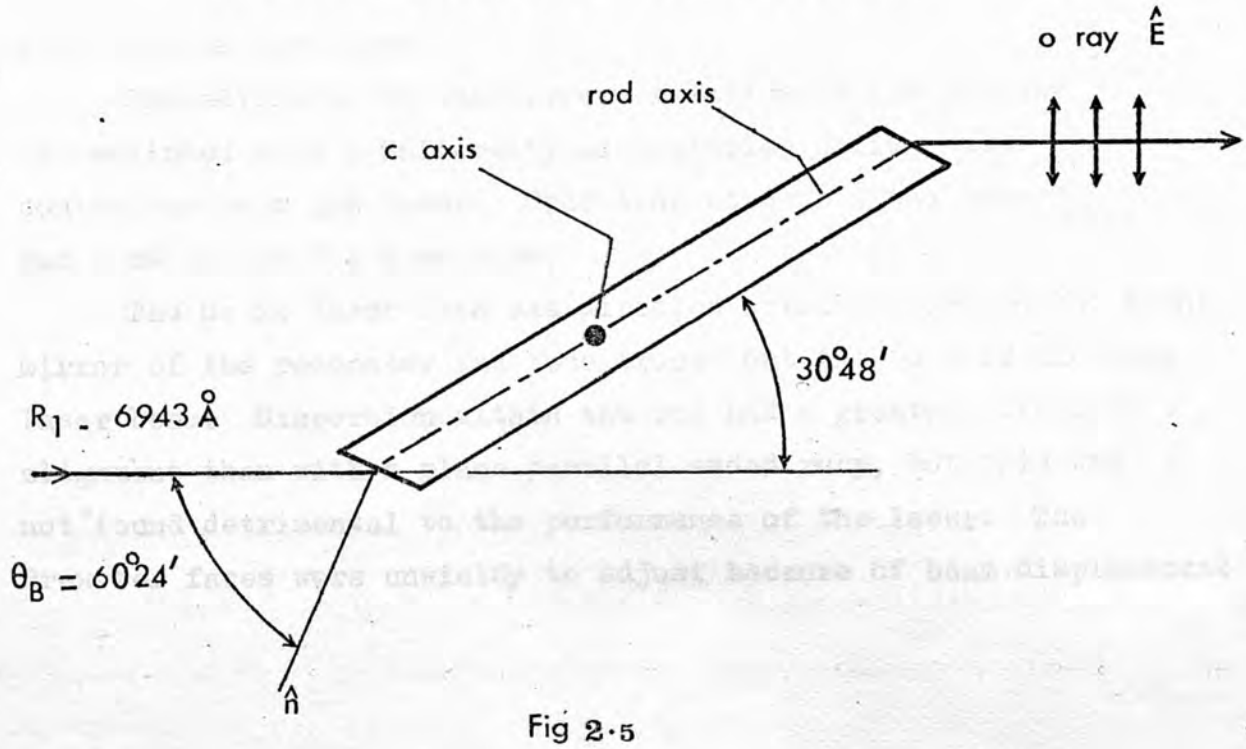

Fig 2·5

state described as the R_2 (6929 Å) and R_1 (6943 Å) lines. The R_1 line is polarized at right angles to the optic axis and travels as the ordinary ray in the birefringent crystal. The R_2 line is polarized along the optic axis in the crystal and travels as the extra-ordinary ray. Only the R_1 line oscillates under normal conditions, since it attains inversion before the R_2 line on account of its higher thermal population.[96] Both transitions are operative in amplifiers but the amplification of the R_1 line is larger because of its larger spontaneous transition probability. Cutting the rod at the Brewster angle for the R_1 line ensured that there were no internal reflections at the rod air interface. The refractive index of ruby at 6943 A is 1.76 and the corresponding Brewster angle ($\tan\theta = \mu$) is 60° 24'.

As will be shown Brewstered surfaces were found to have a strong effect on the mode structure of the laser output. The relative orientations of the rod, Brewster faces and oscillating electric vector are shown in fig. 2.5B.

Alignment of the laser.

The alignment of the mirrors relative to the rod was accomplished with a University Laboratories helium neon continuous wave gas laser. Operating at 6328 Å the power was 1 mW in the T.E.M.oo mode.

The He Ne laser beam was directed normally through the front mirror of the resonator and thus traced out the path of the ruby laser beam. Dispersion within the rod had a greater effect on alignment than with a plane parallel ended ruby, but this was not found detrimental to the performance of the laser. The Brewster faces were unwieldy to adjust because of beam displacement

and the most critical adjustment was the orientation of the Brewster faces relative to the axis of the resonator. This involved two variables; the rotation of the rod about its longitudinal axis and the angle between this axis and the normal reflection from one of its mirrors, fig. 2.5B. To facilitate these adjustments the laser head was held in a mounting which was capable of rotation and trnaslation, thus giving the necessary degree of freedom, fig. 2.6A.

The ruby rod itself was simply held in holes machined in the end plates of the laser head and rotation about the rod axis was effected by pushing the Brewster edge with a cotton bud. Once aligned, this latter adjustment needed no further attention unless the laser head was dismantled for flash tube renewal or recoating of the shim liners.

Mirrors.

In Maiman's original ruby laser the reflectors were formed directly on the end faces of the active material. Arrangements with external mirrors are considerably more flexible and necessary for Q - switched operation.

Quartz glass blanks with a flatness of $\lambda/10$ were used as the supports for the reflective coatings. The blanks were $\frac{1}{2}$" thick, giving extreme mechanical stability. Although metallic coatings of silver, gold and aluminium are suitable for low power operation they are destroyed by pulsed ruby radiation. Dielectric interference coatings are more resilient. Alternate $\lambda/4$ layers of high and low index substances are used for an odd total number of layers. High index materials used are titanium dioxide, cryolite and cerium oxide. Low index materials include magnesium fluoride and silicon dioxide. The coatings used for

A THE LASER HEAD

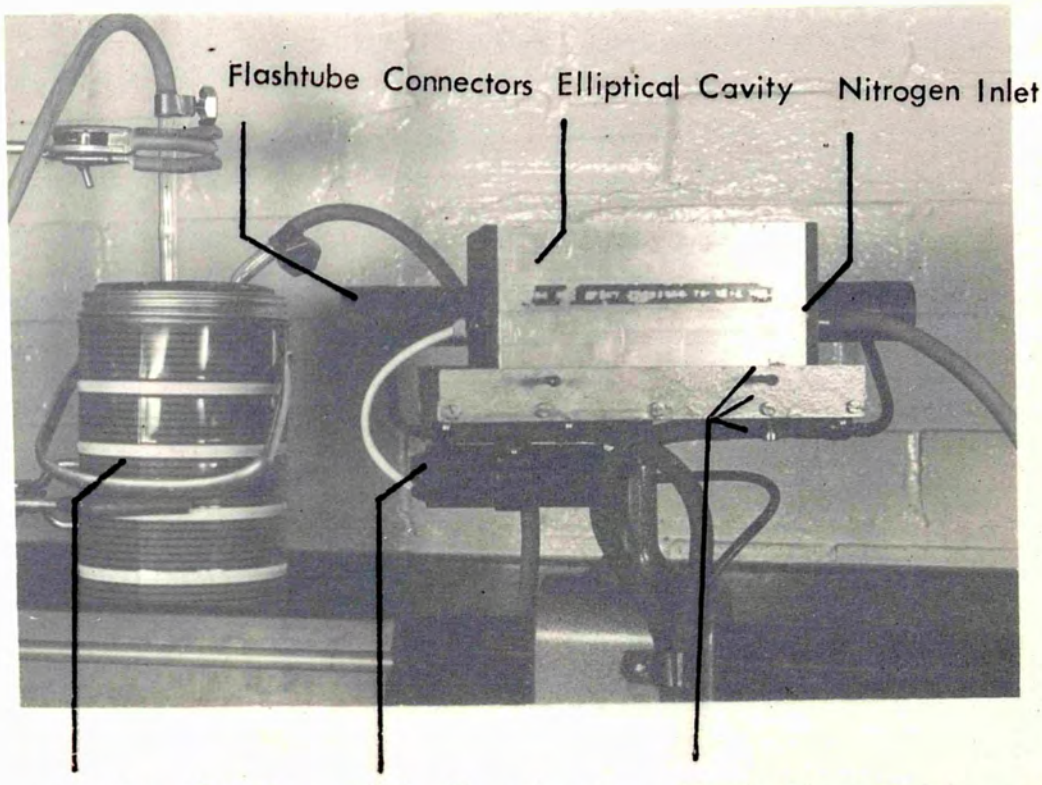

B THE P.I.N. DIODE AND POWER SUPPLY

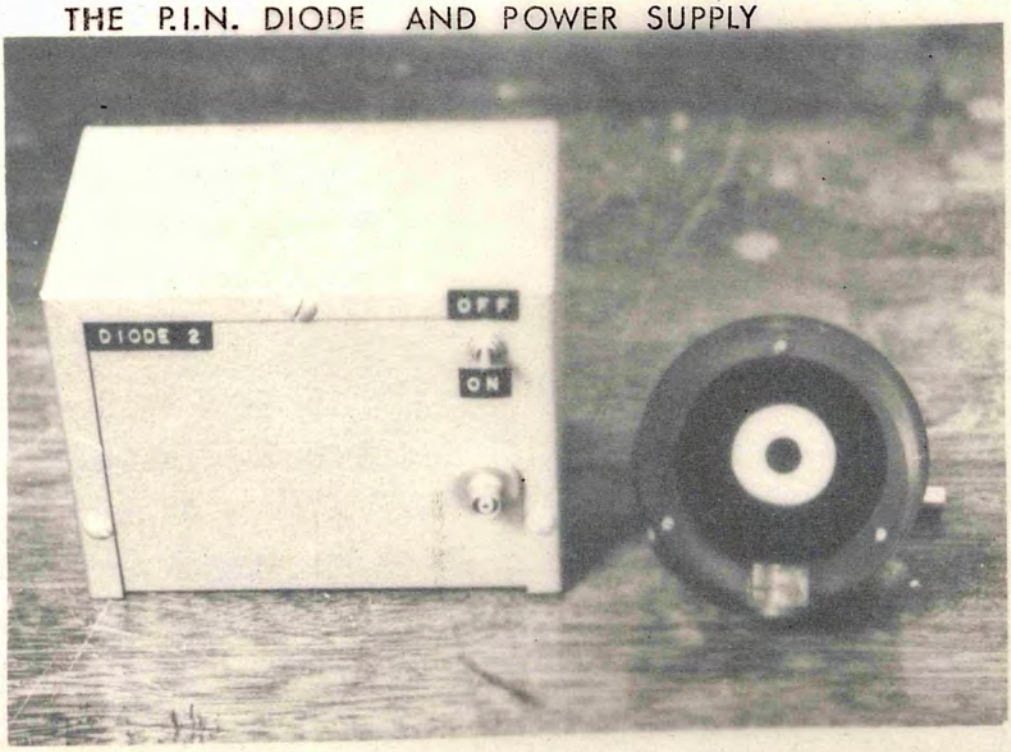

Fig 2·6

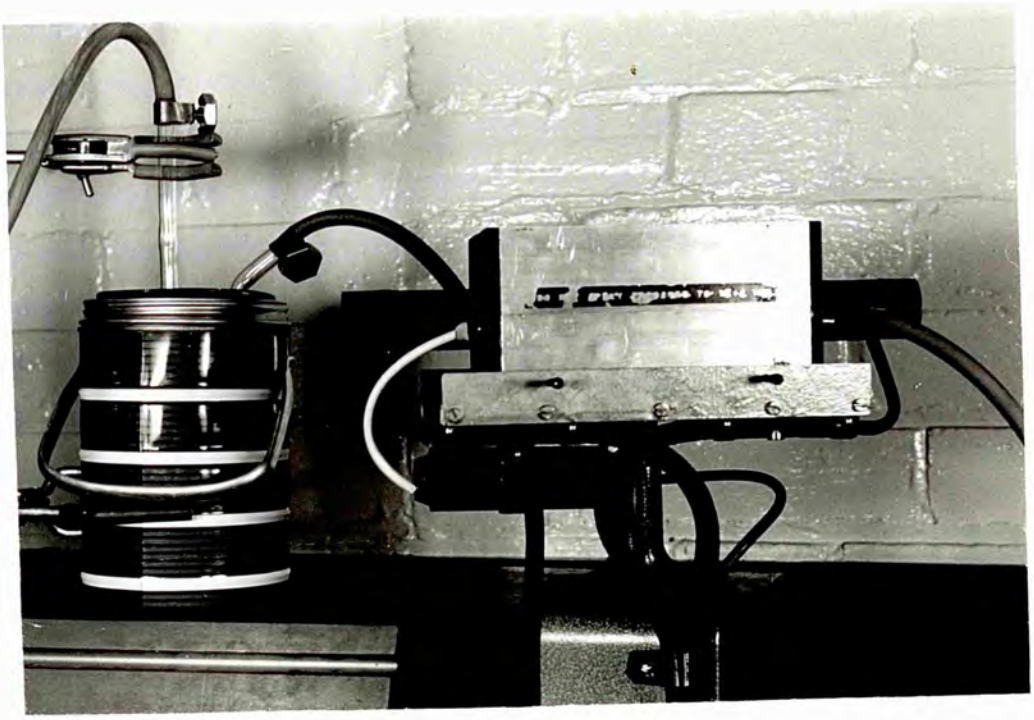


DIODE 2
OFF
ON

the high reflectivity mirrors had the following values, obtained with thirteen layers; R 98.8%, T 0.1%, A 1.1% at 6943 Å.

Mirror adjustment was facilitated by use of a classical three point mounting with spring releases, fig. 2.4B.

An alternative mirror used was a $45^\circ 90^\circ 45^\circ$ roof top prism made from silica glass. The hypotenuse was flat to $\lambda/20$ and the returning ray was parallel to the incident ray to within 1 sec. The alignment of the laser, with this type of reflector, was especially critical in the plane parallel to the roof of the prism.

Output coupling mirrors.

In pulsed lasers optimum decoupling is not the only factor determining mirror transmission. The energy density in the resonator is proportional to $1/(1-R)$ and with R = 95% the energy density is twenty times higher in the cavity than in the emergent beam. It is important to operate with high decoupling so that damage to the laser material and mirrors is reduced. On the other hand, in the special case of mode locked operation, high output coupling is detrimental to the required phase locking conditions and to avoid mirror damage an alternative mirror was developed (chapters 4 and 5).

For normal operation the Fresnel reflection at the ruby air interface can be used to provide feedback. The reflectivity is $\left|\frac{\mu-1}{\mu+1}\right|^2$ which amounts to 8%. This technique, however,

was not available with the Brewster angled rod, but the 4% reflection from an uncoated quartz blank was used. Such a mirror was free from damage at the power levels used. When higher feedback was required dielectric coatings with a reflectivity of 48% and 20% at 6943 Å were used.

2.4 DETECTION OF OUTPUT

Two oscilloscopes and three photodiodes were used to monitor the output of the laser.

Mesh Anode E.M.I. 9648 B. This device required 2 KV potential to give good saturation of high output currents. The S 10 (BiAgOCs) photocathode gave response to 7500 A with an absolute sensitivity of 2 mA/W at 6943 Å. When it was used with a Tektronix T 519 oscilloscope the rise time of the detection system was 3 ns. The rise time of the T 519 alone was 0.3 ns with a vertical sensitivity of 9.3 V/cm.

An I.T.L. high current vacuum diode of the same basic construction was also used. In this case, however, the photocathode was in a carefully matched housing and the output impedance matched directly to the 125 Ohm output impedance of the T 519. This arrangement had an overall rise time of less than one nanosecond.

A series 5082 - 4200 P.I.N. photodiode was also used. This solid state device had an intrinsic rise time of $\sim$ 1 ns when used with a 50 Ohm load. The power requirement was much smaller than that of the other two diodes. A dry cell with a small storage capacitor was used to provide the 18 V negative bias, fig. 2.7B. The output from this diode was not capable of driving the T 519 and a T 454 oscilloscope was used. With a vertical sensitivity of 5 mV/cm the rise time of the detection system was limited by the oscilloscope amplifiers to 2.5 ns. Fig. 2.7A shows the mounting designed to obtain the best possible match between the diode and the 50 Ohm cable.

The light input to all the photodiodes was obtained by reflection from a beam splitter and attenuated by a diffusing screen and neutral density filters. A Kodak no. 70 gelatin

A MATCHED MOUNTING FOR P.I.N. DIODE

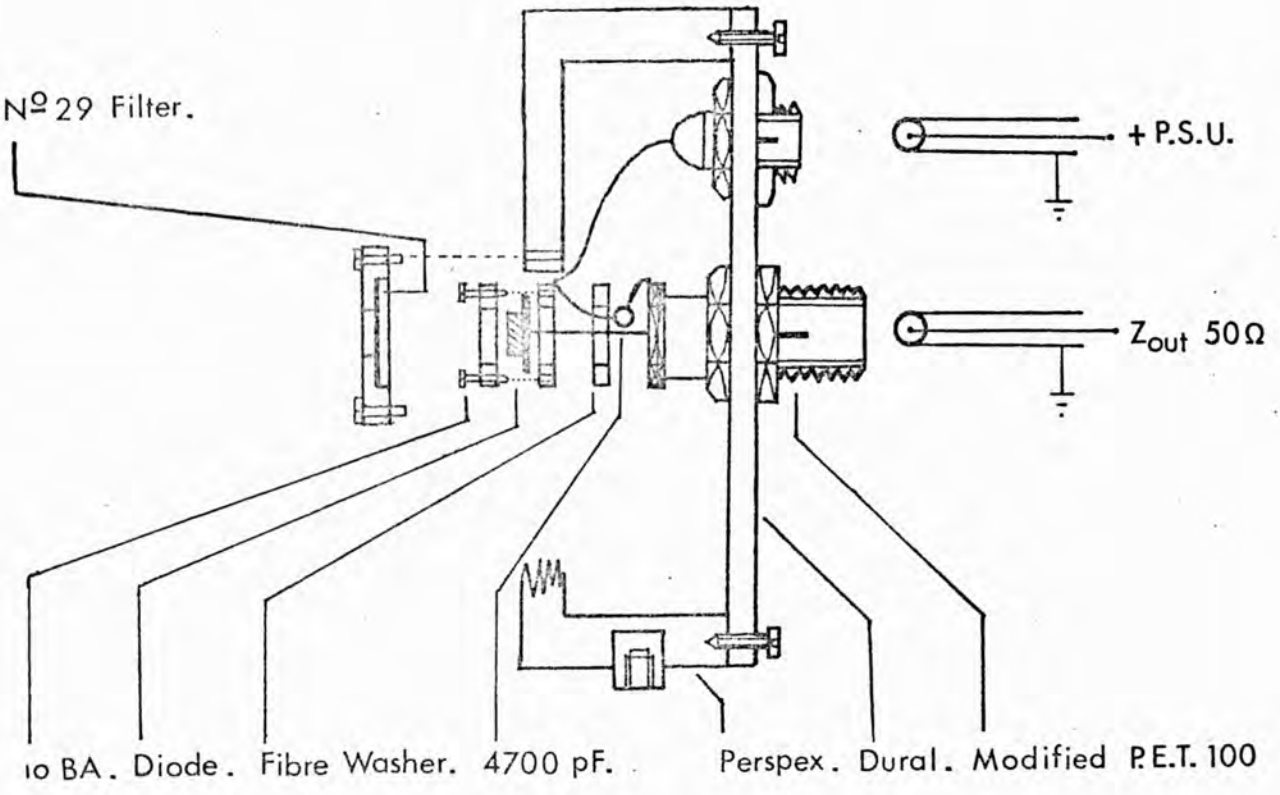

B NEGATIVE BIAS P.S.U.

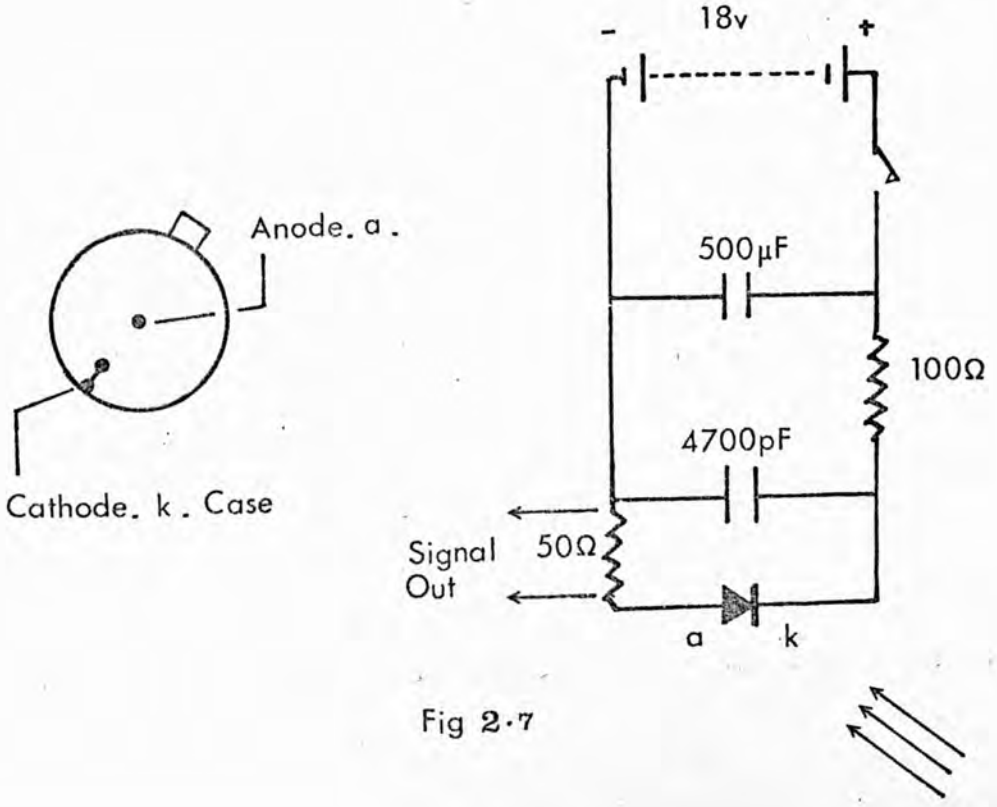

Fig 2·7

filter ensured rejection of any extraneous pump light.

Absolute measurements of the energy of the laser pulse were obtained with a calibrated T.R.G. Type 100 calorimeter. The incident light was directed into a polished, nickel plated, silver cone. After multiple reflections most of the incident radiation was absorbed in the cone. The temperature difference produced in the cone, relative to a reference cone, was detected by ten iron-constantan thermocouples. The e.m.f. produced was measured by a Fluke 845 A high impedance voltmeter. The e.m.f. measured was linearly related to the total input energy by a calibration factor of 199 μV/J. The absolute accuracy of the calorimeter was 5%.

The results of calorimeter measurements of single pulses were used to calibrate the photodiodes (chapter 3).

* * *

CHAPTER 3

STUDY OF PASSIVE Q - SWITCHING MECHANISMS

3.1 LASER OUTPUT - FREE RUNNING

To examine the output of the laser under normal conditions the arrangement shown in fig. 3.1A was used.

The laser cavity, consisting of ruby rod R and two mirrors M_1 and M_2, was aligned using the gas laser F in conjunction with the stop L. A small portion of the output was selected by the glass beam splitter S_1 and in conjunction with the T 454 and P.I.N. diode D_1 recorded the intensity time fluctuations of the output. Triggering of the T 454 was from the monitor SKT_1 on the power supply unit. The sweep of the oscilloscope was delayed by the 'B' triggering facility and adjusted to give a delay of 0.2 ms.

The beam splitter S_2 directed another small proportion of the output to a photographic film P behind the no. 70 filter and several neutral density filters F_2, thereby recording the far field pattern of the radiation.

The main portion of the output then entered the calorimeter C. This optical arrangement prevented the ruby laser radiation impinging on the gas laser mirrors and possibly causing damage.

Variations of the output in space and time.

The photographs, fig. 3.2, show the intensity time traces monitored on the T 454. At threshold (input energy 650 J), 3.2A, oscillations started 830 μs after the beginning of excitation and continued for 200 μs. With the excitation 50% above threshold,

A. MEASUREMENT OF OUTPUT PARAMETERS

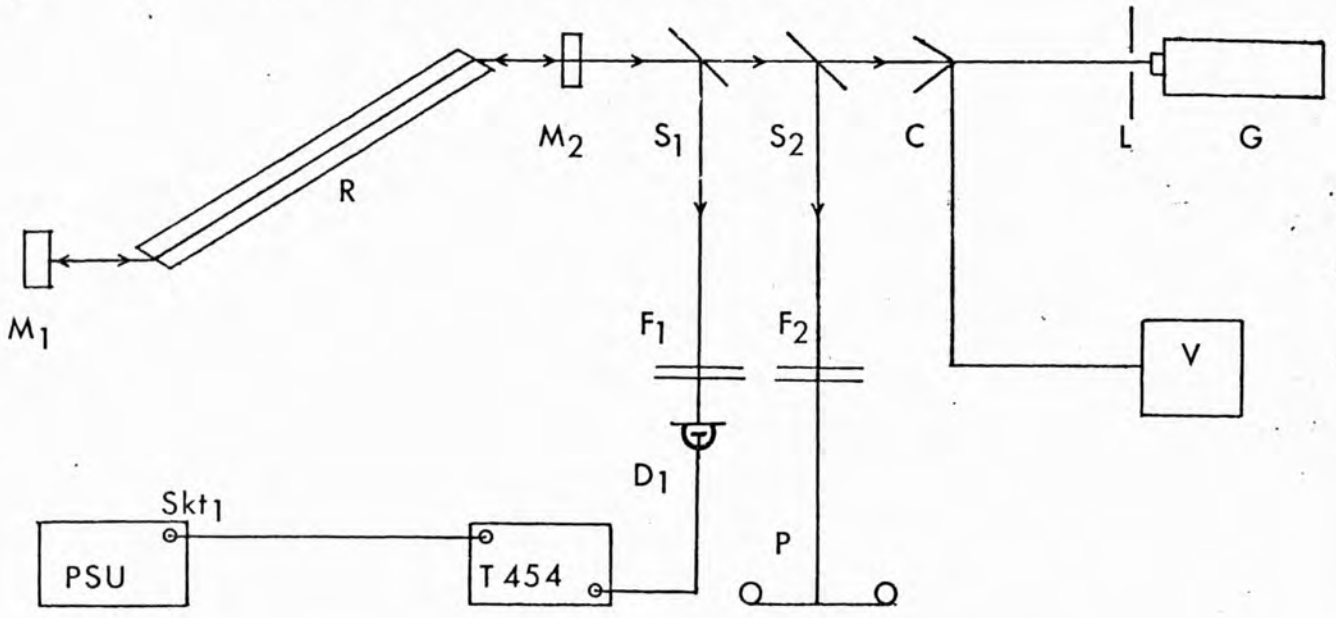

B. LASER OUTPUT AS A FUNCTION OF INPUT ENERGY

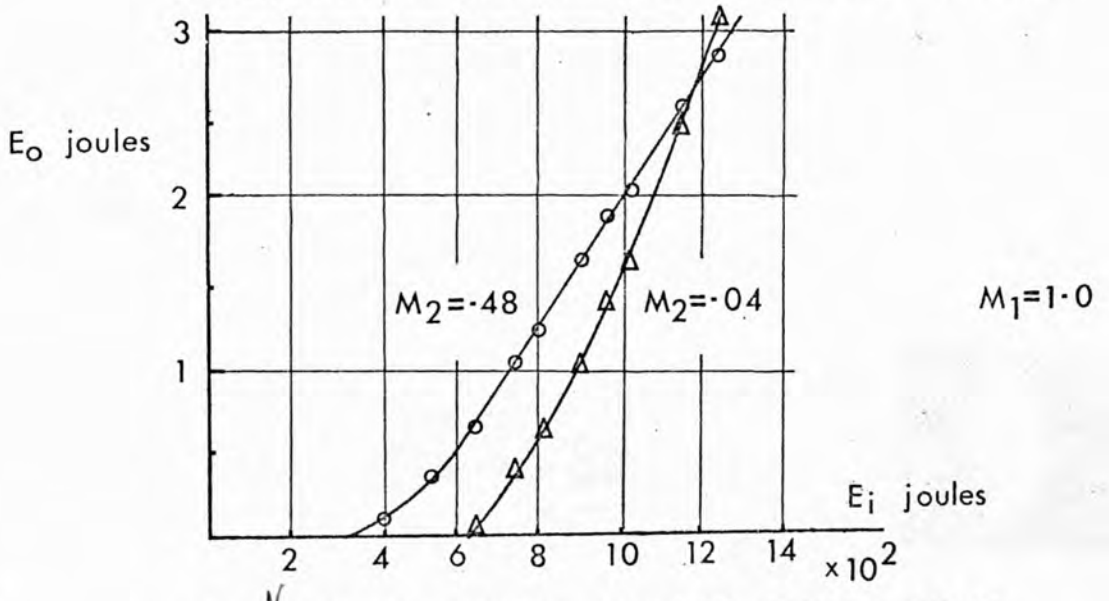

C. INTESITY VARIATION ACROSS OUTPUT BEAM

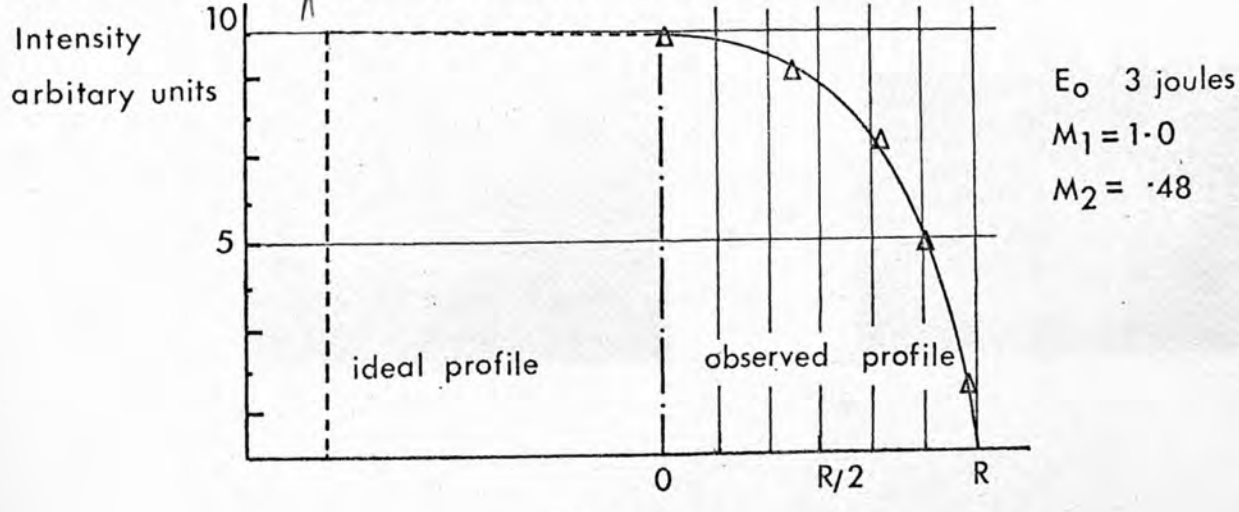

Fig 3·1

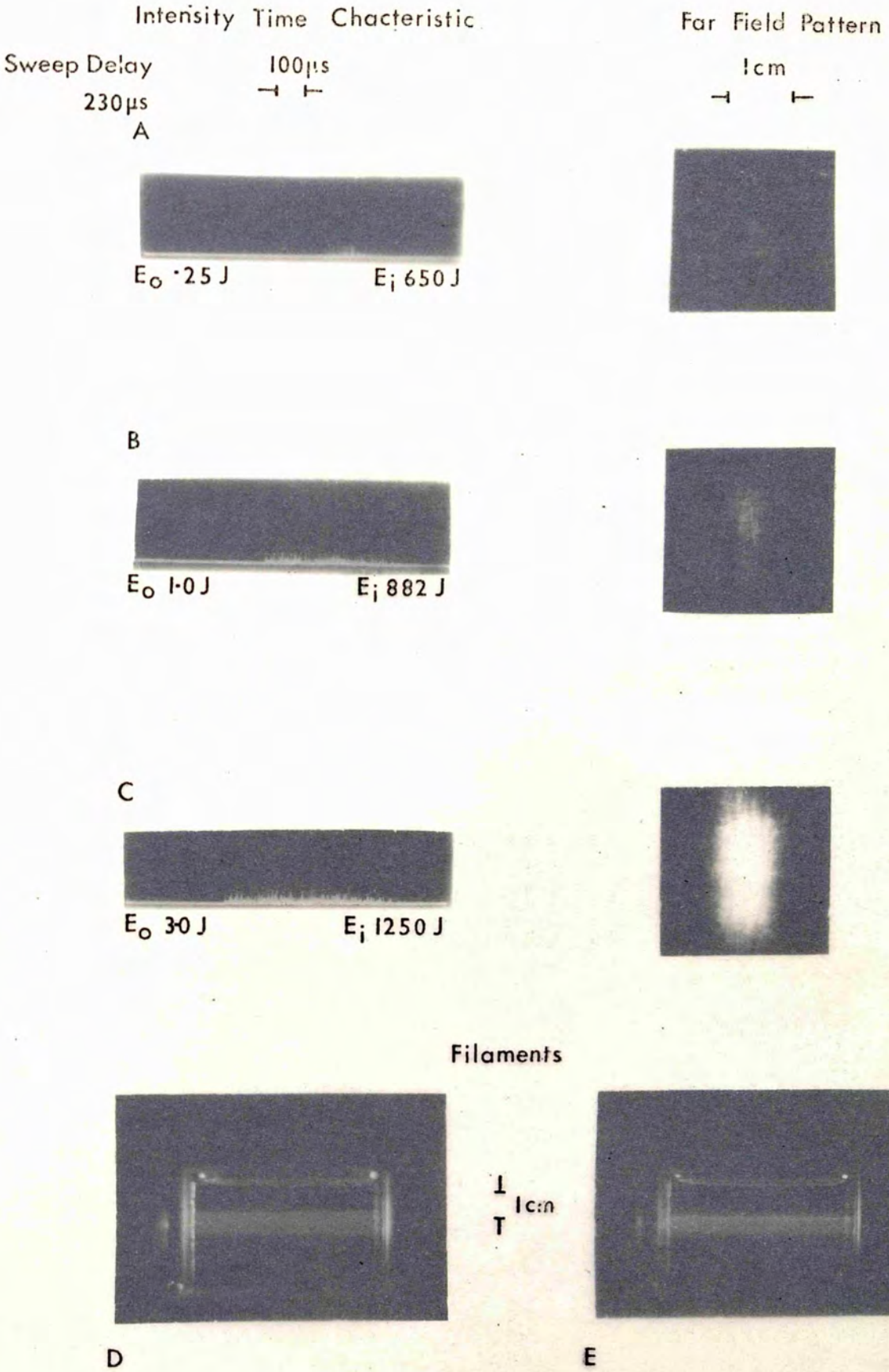
Intensity Time Chacteristic
Far Field Pattern
Sweep Delay
230µs
100µs
1cm
A
E_o ·25 J
E_i 650 J
B
E_o 1·0 J
E_i 882 J
C
E_o 3·0 J
E_i 1250 J
Filaments
1cm
D
E

Fig 3·2

3.2C, oscillations started after 530 μs and continued for a total time of 600 μs.

The far field pattern corresponding to each trace is shown. Near threshold the filamentary structure of the output beam was evident and oscillations were restricted to the central area of the rod. The filaments were approximately 100 μm in diameter and formed clusters which were 800 μm across. Above threshold the oscillations covered the whole area of the rod and the filamentary structure seemed to disappear. Increasing the attenuation by inserting neutral density filters in front of the camera revealed the filaments again. The best method of showing the existence of the filaments, however, was by photographing the scattered light as the laser beam passed through a liquid. A square glass cell was used, containing water with a drop of milk added to scatter the light. The scattered light was recorded on Tri X film in a camera focused on the cell. The photograph, fig. 3.2D,E, shows the clusters of filaments, the formation of which changed with every shot. Sound theoretical reasons for this filamentary action do not exist, but examination of such patterns, with ruby lasers excited barely above threshold, allows tentative identification with possible non-axial modes.[97]

Power and energy output.

The peak power radiated in the non-Q - switched mode is an indefinite quantity since the output consists of a large number of irregular spikes, fig. 3.2. The total energy radiated is a more meaningful quantity in this case. This depends mainly on the degree of excitation and output coupling. Fig. 3.1B shows the total output energy radiated E_o as a function of excitation energy E_i for dielectric mirrors of 4% and 48% reflectivity. The non-linear behaviour close to threshold was

caused by the whole cross section of the rod not being excited. The overall conversion efficiency was in the region of 0.2%.

Beam divergence.

To determine the divergence of the laser beam successive recordings of the far field pattern were taken with the camera P, fig. 3.1A, at different positions. A microdensitometer trace was then made from each negative and the beam width taken as the distance between points where the recorded intensity fell by 1/e of its peak value. The resulting divergence was computed at 1.4×10^{-3} radians. This value was typical for solid state lasers and was larger than would be expected from diffraction theory, assuming the radiation came from an aperture of diameter d radiating in phase with uniform amplitude i.e. $\theta = \frac{1.22\lambda}{d}$

As shown in the previous paragraph, however, the radiation was restricted to filaments and clusters of filaments. It has been shown that when related to these filaments the beam divergence appears to have the correct magnitude. The interpretation of these filaments as associated with non-axial modes is further supported by observations made on lasers with large mirror spacings. Non-axial mode selection in such systems results in smaller beam divergences.

Beam inversion cross section.

As with the filaments discussed previously, which may be attributed to the optical cavity, a further intensity variation across the beam was caused by the pump geometry. This variation was caused by a combination of the self focusing properties of the laser rod and the pump cavity.

Evaluation of the inversion cross section was achieved

using the camera shown in fig. 3.1A, recording the far field pattern for a fixed level above threshold. Fig.3.1C shows the resulting variation of inversion across the rod diameter, derived from microdensitometer traces of the negatives. Though showing a pronounced hump the result compared favourably with other projection pump geometries.[95]

Detail of the spikes..

The detail of the spikes or relaxation oscillations is shown in fig. 3.3A-D. The spacing of the spikes was irregular in the region of 2 μs. Individual pulses had full width at half maximum (F.W.H.M.) in the region of 350 ns. Using the calibrated P.I.N. diode (section 3.2) the largest pulses were found to have peak powers in the region of 600KW whilst the majority were in the region of 400 KW.

This pulsating behaviour has also been observed in c.w. ruby lasers.[98] Qualitatively the pulsations can be explained by the fact that the photon density ϕ builds up rapidly in the laser and, in the presence of a high photon density, stimulated transmissions occur at a much faster rate than excitations are supplied. Consequently the population of the upper level is depleted below the point where oscillations can be sustained.

Statz and De Mars[99] tried to explain the pulsations analytically by deriving a pair of non-linear differential equations, linking the photon density ϕ with the inversion density N.

$$\frac{d\phi}{dt} = BN\phi - C \qquad 9.$$

SPIKE FORMATIONS

A

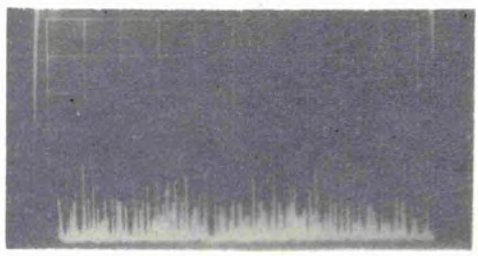

20μs

B

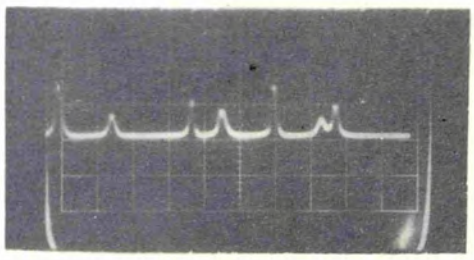

0·2μs

C

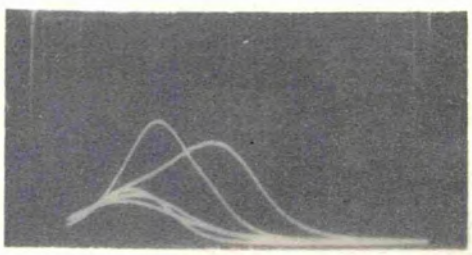

100ns

Threshold E_i 800 J

Peak pulse power 400 KW

D

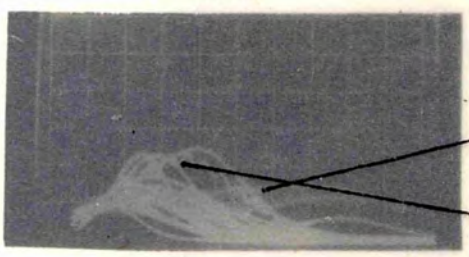

100ns

E_i 900 J

Longitudinal mode beats

$(\Delta f = \frac{c}{2L}) \sim 10^8$ Hz

Transverse mode beats

$(\Delta f = \frac{X_{01}^2 c \lambda}{8\pi^2 r^2}) \sim 10^7$ Hz

E

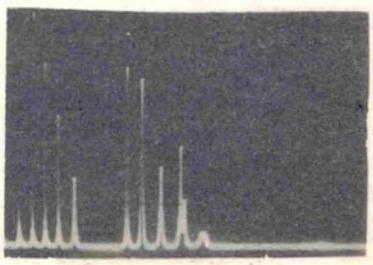

2·0μs

Periodic damped oscillations

Near threshold

Fig 3·3

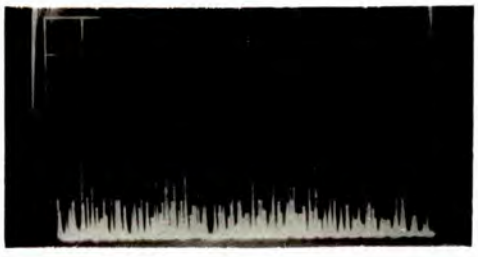

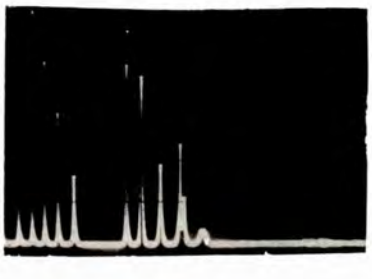

where B is a constant and C the rate at which photons leave the system. The first term on the right of equation 9 is the number of photons created per unit volume by stimulated emission. if the inversion is created at rate A and spontaneously decays at a rate $\frac{1}{\tau}$

$$\frac{dN}{dt} = A - \frac{N}{\tau} - 2BN\phi \qquad 10.$$

The second term on the right is the rate at which the inversion is depleted by the spontaneous process. The third term is the corresponding rate for stimulated transitions.

It is not possible to solve these so-called Statz De Mars equations in a closed form. Small signal solutions for deviations of N from unity (N normalized to unity at threshold) were obtained by Dunsmuir[100] and lead to a rapidly damped oscillation. It must be noted that computer solutions of the equations assume a homogeneous, isotropic medium, uniformly excited and oscillating in a simple mode. As demonstrated, such assumptions are normally invalid. When operated near threshold, however, the latter requirements were partially fulfilled and a sequence of damped oscillations was observed, followed by an undamped, quasi periodic sequence, fig. 3.3E. As the pump level was raised more modes were excited, as evidenced by the beat frequencies observed in fig. 3.3D, the output being the chaotic spike ensemble of fig. 3.3A. The beat frequencies of fig. 3.3D could be related to the axial mode frequency separation for the cavity length concerned.

The reason that the various modes did not radiate independently,

in the damped periodic fashion of fig. 3.3D, was two-fold. In the first place, some sort of mode interaction was inevitable and secondly, spatial modulation of the population inversion caused the output to shift from one mode to another. This phenomenon, called spatial hole burning, is caused by the spatial distribution of population inversion due to one particular mode being more favourable for oscillation in the adjacent mode. This interpretation assumes that the population inversion at any given point was depleted faster than it could be refilled by diffusion from adjacent excited ions. Statz and De Mars[112] showed this to be the case by showing that the spatial cross relaxation time for the Cr^{3+} ion was of the order of 10^{-4} sec whilst from the duration of the individual spikes it was evident that a level was depleted in 10^{-7} sec.

When the effects of spatial hole burning are combined with factors such as inhomogeneities, irregularities in the excitation and temperature variation during excitation it is obvious that the periodic damped output of fig. 3.3D was difficult to achieve and not easily reproducible.

The shifting of the mode pattern results in time coherence not being maintained from one spike to the next. As fig. 3.3C shows, the duration of a single spike was of the order of 300 ns and this may be taken as the phase memory of the laser in this case. Berkley and Wolga[101] found that interference fringes with a ruby laser operated in this regime disappeared with path differences exceeding 3000 cm, corresponding to a time coherence of 100 ns.

3.2 CRYPTOCYANINE Q - SWITCH

To examine the output of the laser when Q - switched by a saturable absorber the arrangement of fig. 3.1A was used. The dye was introduced into the cavity in a quartz glass cell, with a path length of 0.5 cm, positioned near the maximum reflectivity mirror M_1. The cryptocyanine crystals were dissolved in methanol (100 mg per litre) to form a stock solution. The photochemical properties of the dye made it necessary to store the stock solution in a refrigerated dark bottle. The strength of dye required for the generation of a single giant pulse depended on the reflectivity of the cavity mirrors and the pump level. Generally one could just discern a slight blue tinge in the dye. The exact low level transmission T_o of a particular solution was determined using a Perkin Elmer spectrophotometer and the values of T_o quoted refer to 6943 Å. The shift of absorption maxima for cryptocyanine in various solvents (solvatochromy) is discussed in chapter 4. The photograph, fig. 3.4A shows the laser output as monitored on the T 454 using the 'A' triggering facility, i.e. the first signal from the diode triggered the sweep. A reduction in number of pulses was immediately noticed when the cell transmission T_o was 0.8. With initial absorption increasing, the number of pulses was reduced to two for T_o = 0.32 and by slightly reducing the flash tube input energy a single pulse was generated when T_o was 0.25.

The main disadvantage of the dye switch was that, although the process was reversible, degradation of the dye resulted in inconsistencies which had to be compensated for by slight adjustment of dye concentration or flash tube input. Impurities in the dye caused long term degradation and a fresh solution had

CRYPTOCYANINE DYE Q SWITCH

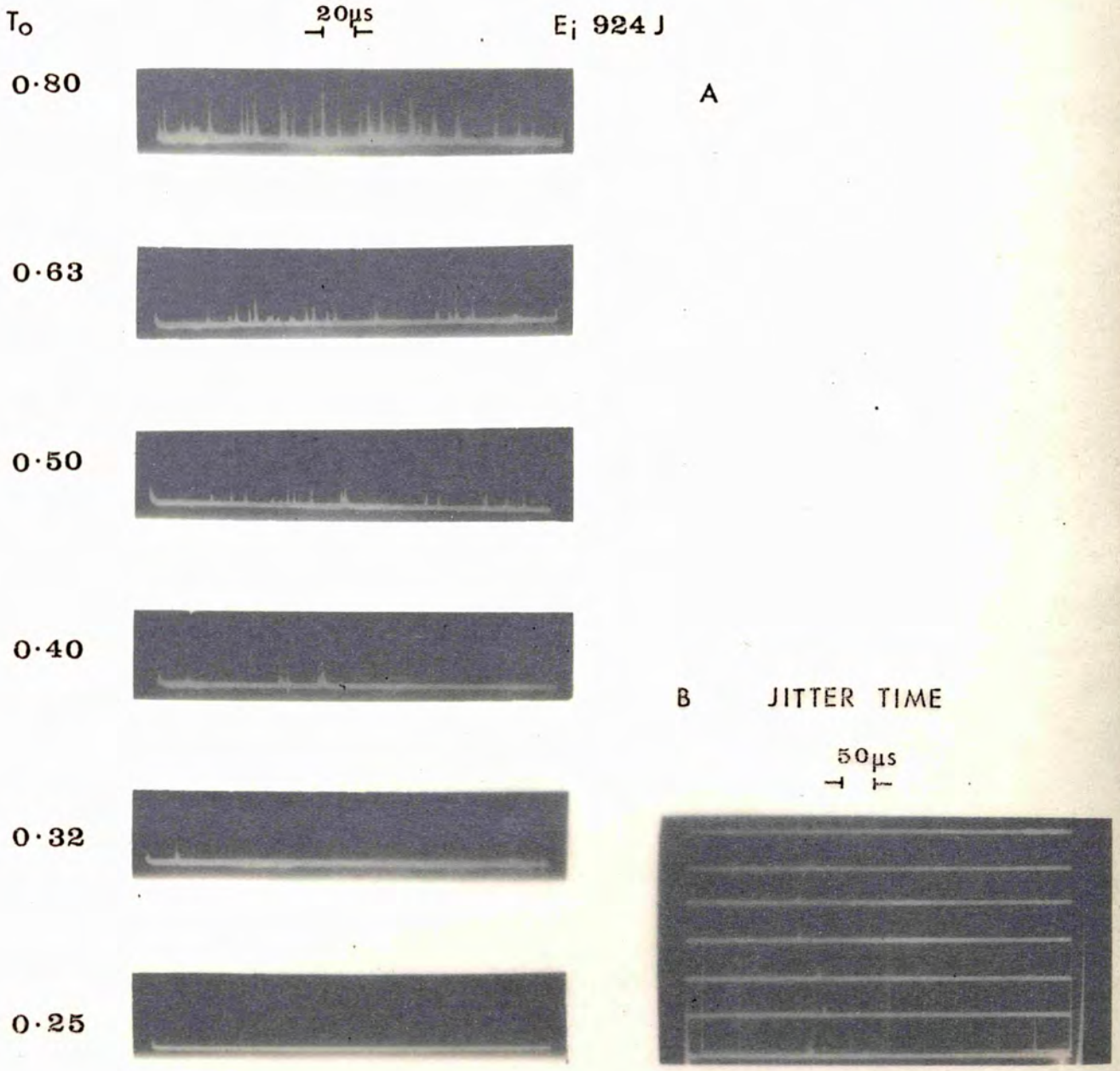

Fig 3.4

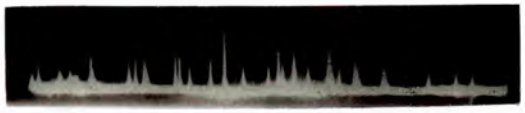

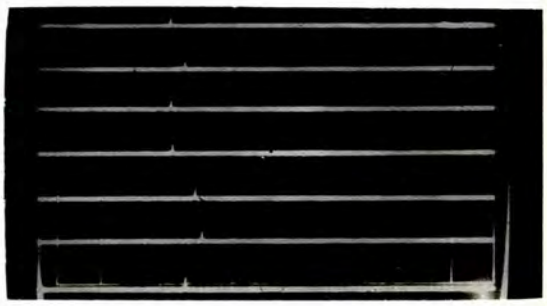

to be made daily from the stock solution.

The jitter time of the giant pulse was investigated using the 'B' triggering facility of the T 454. The sweep of the oscilloscope was delayed by 700 μs relative to the start of the excitation as monitored from SKT_1. As fig. 3.4B shows the giant pulse was radiated after 850 ∓ 25 μs.

Peak power and diode calibration

Photograph fig. 3.4C shows the single giant pulse profile. The F.W.H.M. was 50 ∓ 5 ns and the measured output energy was 8/200 Joule. Assuming a Gaussian profile the area under the curve, fig. 3.4C was F.W.H.M. x peak power = output energy. The value of the attenuation in front of the P.I.N. diode was noted and a power calibration factor S calculated.

$$S = 0{\cdot}1 \times \frac{100}{T} \times 10^6 \quad \text{Watts/Volt}$$

Recalibration of the diode was required if the portion of light selected from the main beam varied.

Increasing the initial absorption of the cell and the excitation level increased the peak pulse power generated. Photograph, fig. 3.4D shows the 10 MW pulse produced with $T_o = 0.1$. The corresponding power density (flux) was 14.5 MW/cm^2 in the output beam. The output mirror in this case was a quartz glass flat so the flux inside the laser cavity was almost the same as in the output beam. Damage thresholds for ruby cited in literature were in the region of 400 MW/cm^2 but operation below 100 MW/cm^2 was recommended for extended ruby life.

3.3I EXPLODING FILM Q - SWITCH

The sudden increase in Q required when the inversion ΔN is high can be achieved using exploding films.[102,103] Such Q - switch films have been classed as slow speed devices because the disappearance of the film cannot be expected instantly due to the film's mass.

A thin film possesses three loss mechanisms; pure reflection, diffraction if the particle size is of the order of a wavelength of light and absorption loss. In the past it has been the rule to rely solely on absorption loss, consequently thick films with a high thermal inertia were used. Such absorption Q - switches generated broad multiple pulses.

The switch time is proportional to $\frac{dQ}{dt} \alpha \frac{d\gamma_s}{dt}$ where γ_s is the total loss consisting of an absorption loss γ_a and a reflection loss γ_r

$$\gamma_s = \gamma_a + \gamma_r$$

assuming there are no diffraction losses. If γ_r is small a thick film is required to obtain sufficient change in Q. If, however, γ_r is high, as in the case of a thin specular metal surface, a large change in Q can be rapidly triggered by the vaporization of the thin film caused by the remnant absorption

Gold films of various thicknesses were vacuum deposited on glass substrates and the films placed in the cavity arrangement shown in fig. 3.1A near the mirror M_1. The total loss γ_s from such a film was variable since the reflection coefficient was a function of angle of incidence θ . The plane of incidence was parallel to the oscillating electric vector and by convention

the reflected beam was denoted R_{pa} in fig. 3.6A. Photograph fig. 3.5 shows the computed reflection coefficients for the gold films.

With 100 Å thick films oscillation proceeded normally with a low Q whilst the 300 Å film prevented lasing completely. When the film thickness was 200 Å a single giant pulse was generated and the peak power could be varied by adjusting θ over a small range. The F.W.H.M. of the giant pulse was 30 ns and no subsequent pulses were observed, implying fast switching of the cavity Q.

The series of photographs fig. 3.5 was taken using different parts of a gold coated 3"x 1" microscope slide at the angle θ indicated. The peak power output for a given varied from one slide to the next, but the expected rise in peak power as θ was varied was consistent for a particular film. The film thicknesses were measured by standard interference techniques.

The interpretation of a low γ_a which triggered a rapid change in γ_r and Q was further substantiated by energy considerations assuming γ_a to be zero (Maxwell's demon vaporizing the film!). The 13 MW pulse radiated when $R_{pa} = 0.5$ had a total energy of 350 mJ. The threshold inversion given by equation 3 is

$$N_1 - N_2 = \frac{\gamma N_o}{a\, l}$$

or $$\exp 2\left(\langle N_1 - N_2 \rangle \sigma_o l - \gamma\right) = 1$$

Assuming the loss coefficient is that due only to leakage loss at the cavity mirrors

$$\exp -2\gamma = r_1 r_2$$

GOLD FILM Q SWITCH

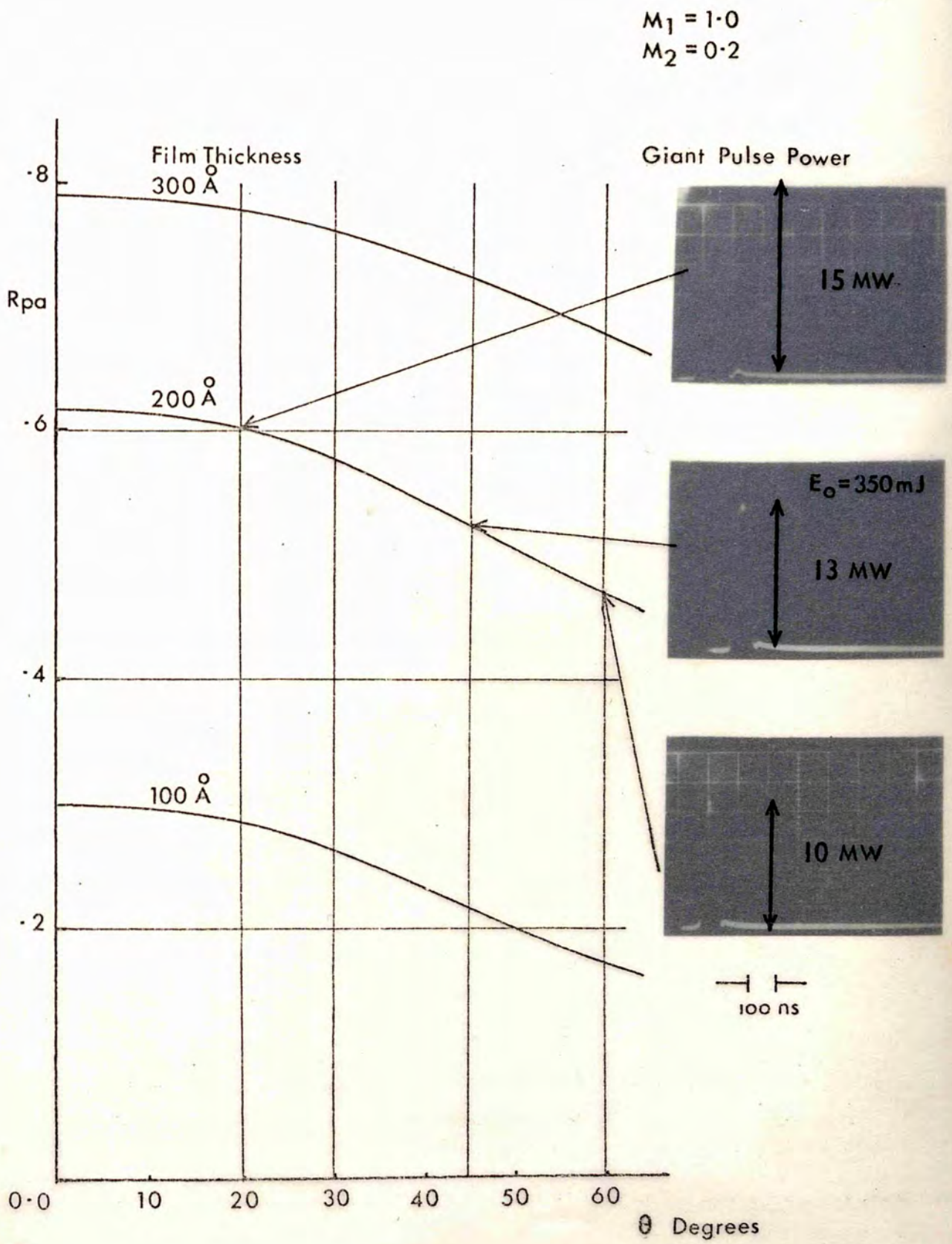

Fig 3·5

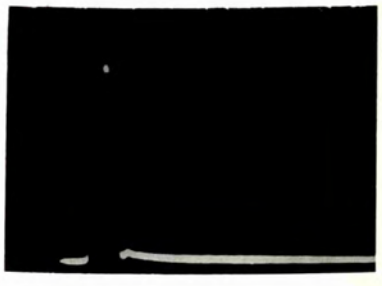

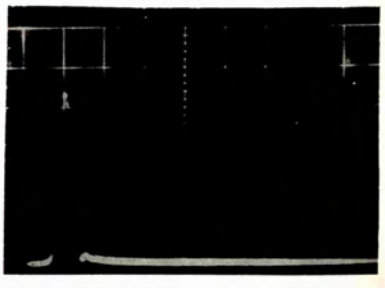

A. ORIENTATION OF $\hat{E}$ VECTOR FOR Au FILM Q SWITCH

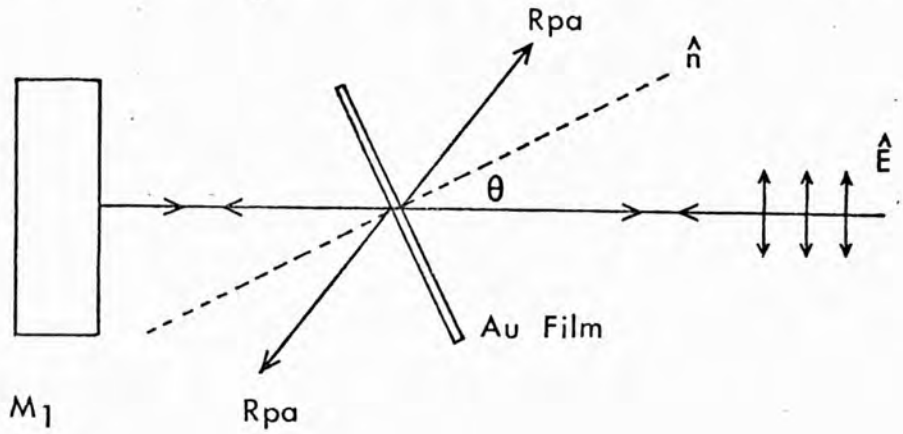

B. ABSORPTION CURVES OF N° 96 DENSITY FILTERS

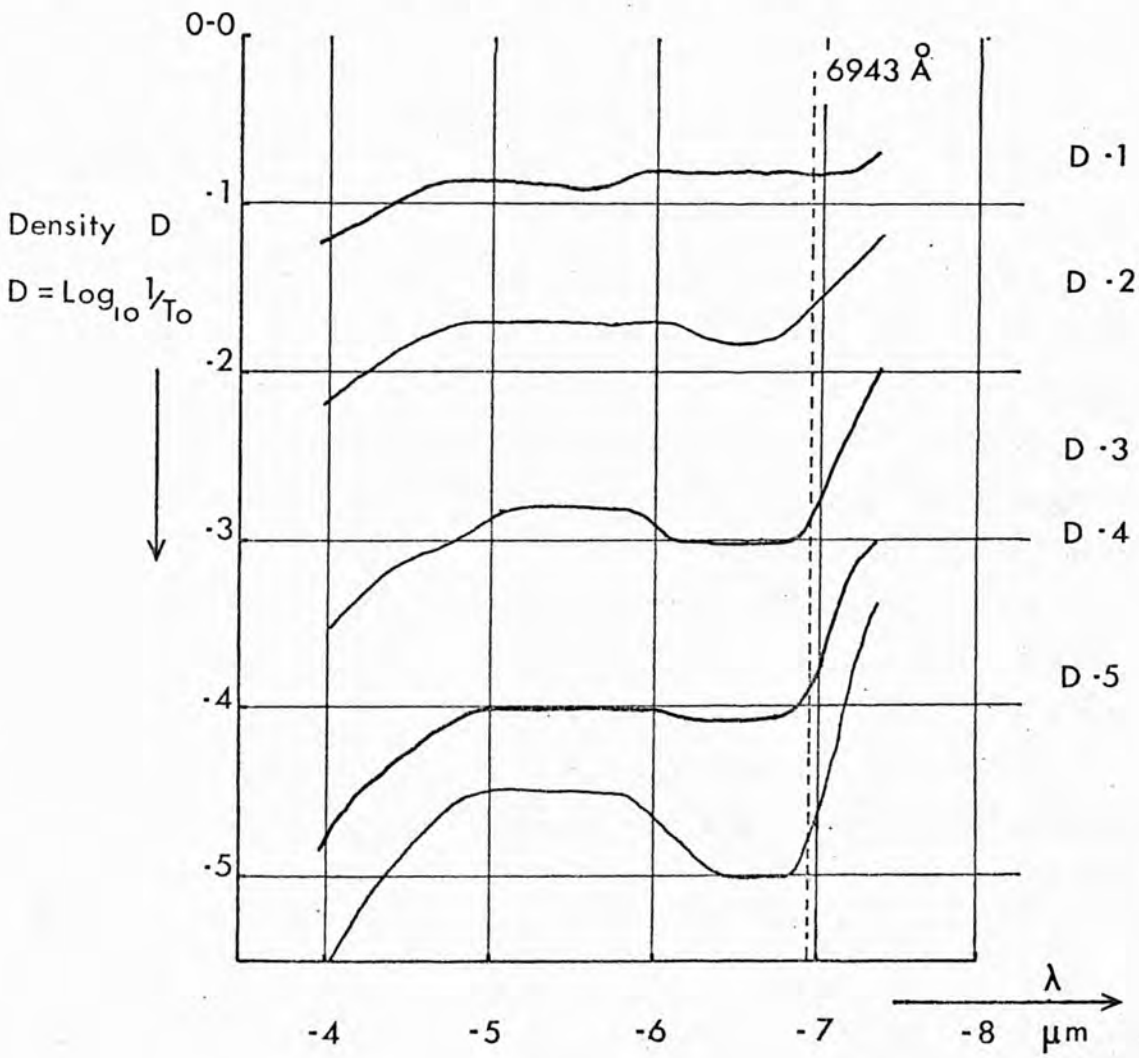

Fig 3·6

$$\gamma = 1 - (r_1 r_2)^{\frac{1}{2}}$$

and 3 may be written

$$N_2 - N_1 = \frac{N_o (1 - (r_1 r_2)^{\frac{1}{2}})}{aL} \qquad 11.$$

The gold film modifies the value of say r_1 to an effective value r_{1g}

$$r_{1g} = r_1(1 - (\gamma_r + \gamma_a))$$

for $\gamma_a \rightarrow 0$

$$r_{1g} = r_1(1 - \gamma_r)$$

After vaporization of the gold film the reflectivity of M_1 returns to its real value of r_1. Using 11 the excess inversion is now

$$\Delta N = \frac{N_o (r_1 r_2)^{\frac{1}{2}}}{aL} - \frac{N_o (r_1 r_2)^{\frac{1}{2}} (1 - \gamma_r)}{aL}$$

$$= \frac{N_o (r_1 r_2)^{\frac{1}{2}} \gamma_r}{aL} \text{ per unit volume}$$

If ν is the frequency associated with the lasing states, the total energy stored is

$$E = N_o h\nu \, aL (r_1 r_2)^{\frac{1}{2}} \gamma_r (aL)^{-1}$$

where a is the ruby cross sectional area. Theoretically one half the stored energy may be radiated in a single pulse and assuming the following values; $a = 0.73$ cm^2, $r_1 = 1.0$, $r_2 = 0.04$, $\gamma_r = 0.5$, $a = 0.4$ cm^{-1}, $N_o h\nu = 4.6$ Joule/cc, the energy radiated is computed at 420 mJ, compared with the 350 mJ actually observed.

Other metallic films were utilized and similar results obtained to those obtained with gold films. The damage caused to the films and their substrates is the subject of chapter 6.

3.3 II NEUTRAL DENSITY FILTERS

To compare the results of the gold reflection switch with a pure absorption switch Kodak Wratten no. 96 density filters were used. Such filters contain carbon particles dispersed in a gelatin base and evaporation of the absorbing loss results in an increased Q. The particle size is such that the Callier factor defined as $\frac{\text{Specular Density}}{\text{Diffuse Density}} = 1.02$ at 6800 Å and therefore no diffraction loss is involved.

The filters were placed in the cavity arrangement shown in fig. 3.1A near the mirror M_1. Photograph fig. 3.7 shows the effect of increasing the density value and correspondingly increasing the change in Q brought about by the destruction of the film. The number of pulses decreased with increasing loss, whilst the peak power increased. The single giant pulse generated with density 0.4 had a F.W.H.M. of 30 ns implying fast switching. However, the set of photographs on the right demonstrates that the switching effect was reversible and a filter continued to Q - switch for at least 10 shots. It was clear that the switching mechanism was not solely the destruction of an absorbing film. The spectral distribution of the filters was examined with a spectrophotometer and the results are reproduced in fig. 3.6B. A true neutral density characteristic would have been a horizontal straight line but as fig. 3.6B shows there was a variation of density value with wavelength. The non-linearity increased with higher density values.

Information supplied by Kodak Ltd. stated that certain dyes were incorporated in the filters. In particular there was an absorption edge in the region of 7000 Å and it was concluded that the optical pumping of this region resulted in partial

NEUTRAL DENSITY FILTER Q SWITCH

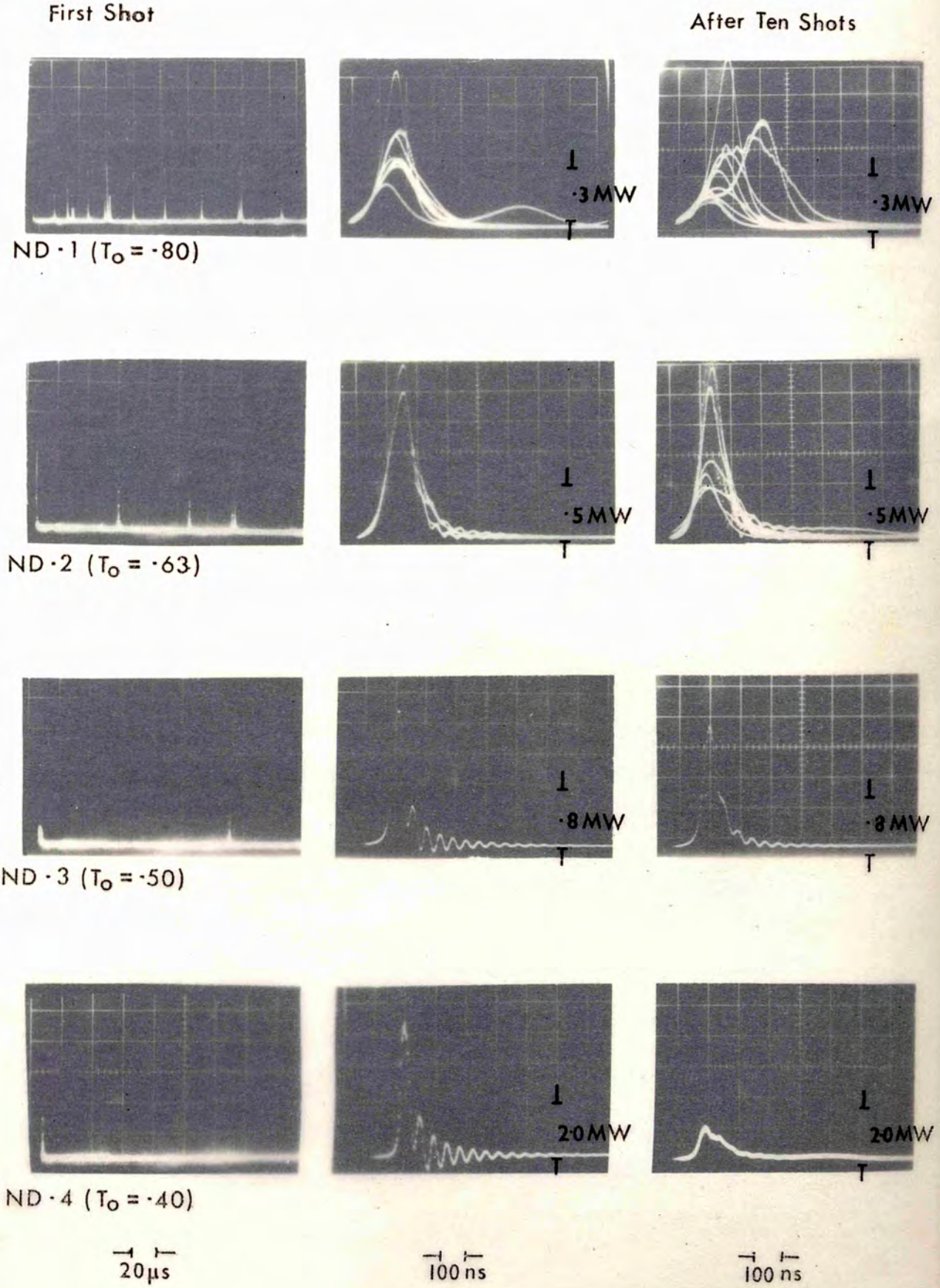

Fig 3·7

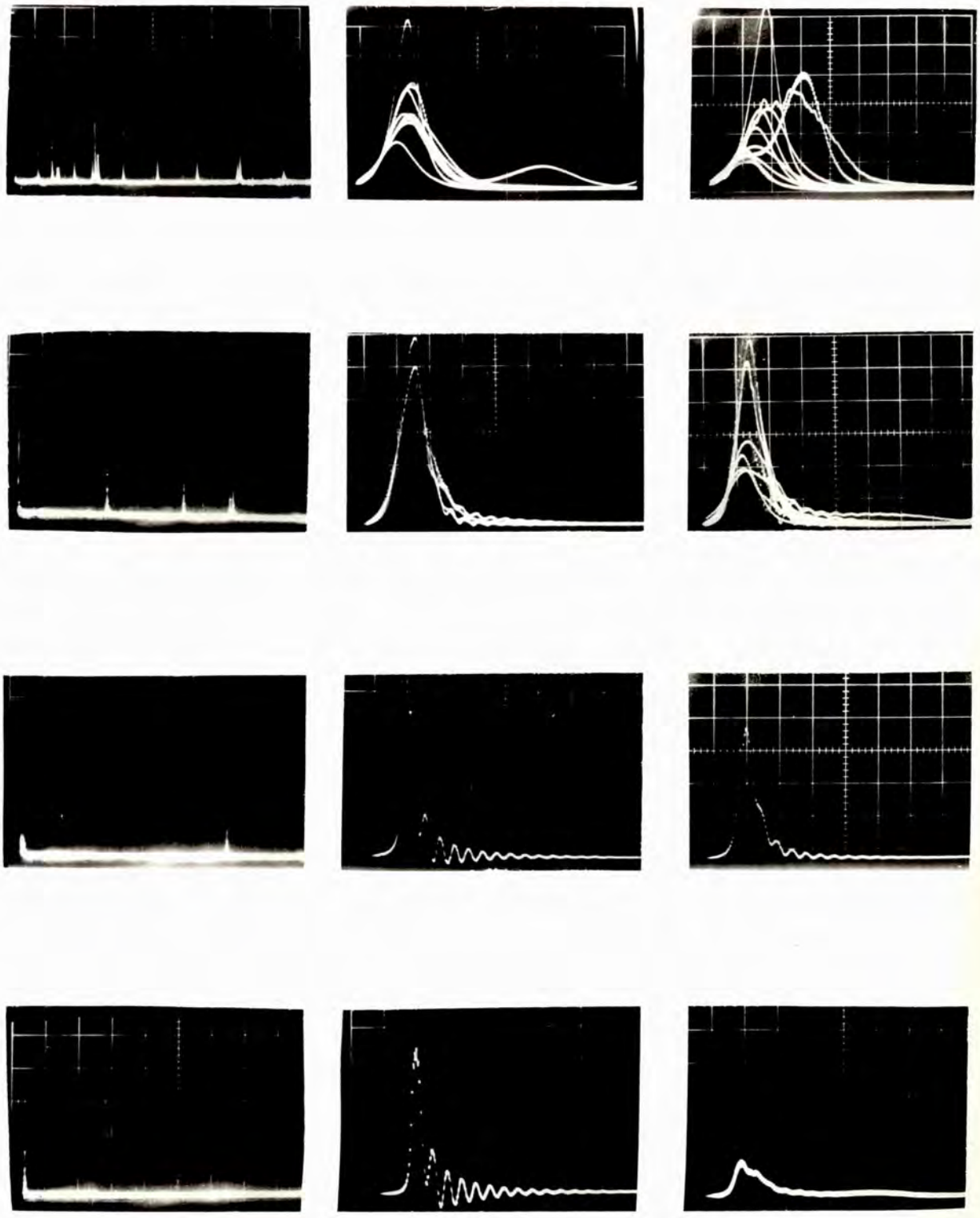

saturation of the contained dye.[21] Such a saturation process would explain the reversible behaviour of this type of Q - switch.

When the pulse power reached 1.5 MW the reversibility was not observed and it was concluded that the structure of the dye had changed due to the high power. This type of behaviour has been observed when the dye triphenylmethane was used as a Q - switch.[103]

3.3 III CARBON LAYERS

To avoid the contaminating effect of dyes in density filters absorbing films were made by depositing carbon films on glass substrates. Acheson Colloids Ltd. dry film lubricant Dag dispersion no. 580 in amyle acetate was used and the glass cover slips dipped into the suspension. Absorption measurements taken when the dispersing agent had dried indicated a diffuse absorption of 0.3.

The films were put in the cavity near the maximum reflectivity mirror, fig. 3.1A, as were previous films. The laser output is shown in photograph fig. 3.8A. At low excitation two giant pulses were generated, followed by low level relaxation oscillations as threshold was reached again. Increasing the excitation increased the number and power of the after pulses. Subsequent operation of the laser revealed normal relaxation oscillations since the vaporization of the carbon caused a step function change in Q.

Coating a cover slip a second time increased the diffuse absorption to 0.6. In this case the first pulse generated had a peak power of 8 MW, fig. 3.8B, but again after pulses

A CARBON LAYER Q SWITCH

Single Layer. Density 0·3 (T_o = 0·5)

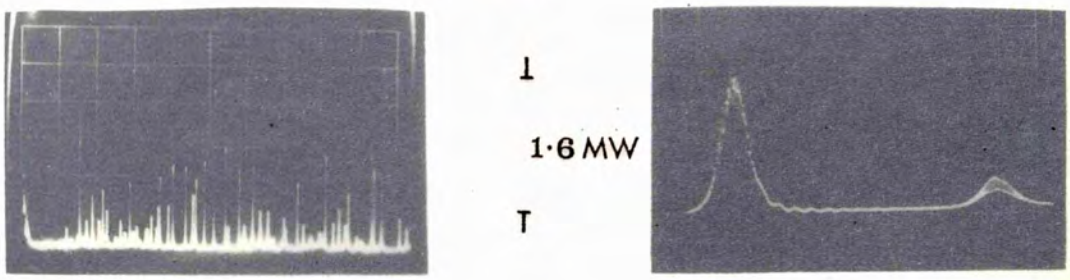

B Double Layer. Density 0·6 (T_o = 0·25)

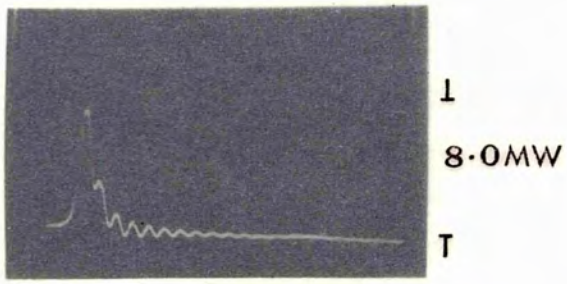

C CARBON DISPERSED IN ETHANOL

Ethanol Alone

Carbon In Ethanol

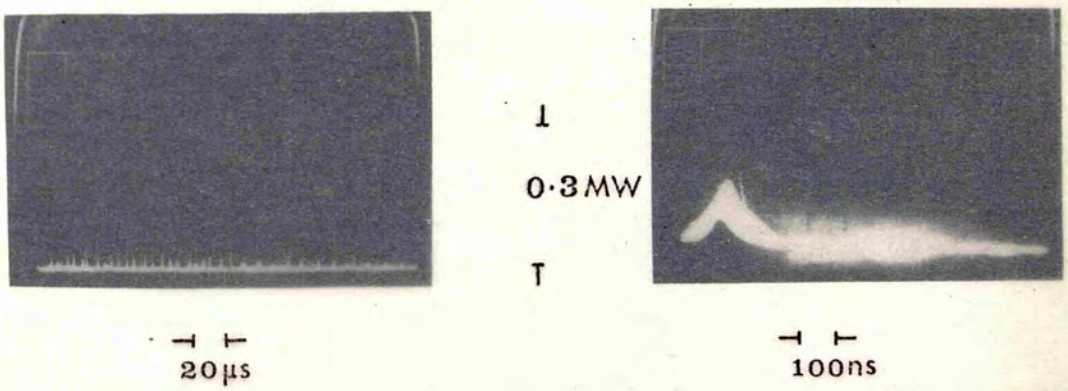

Fig 3·8

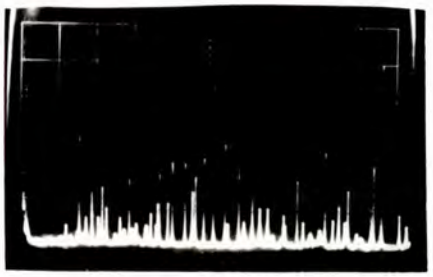

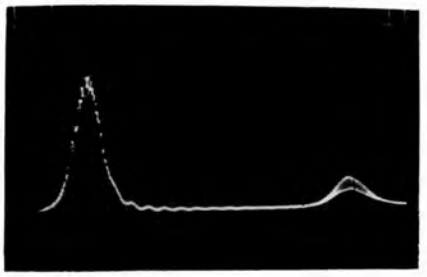

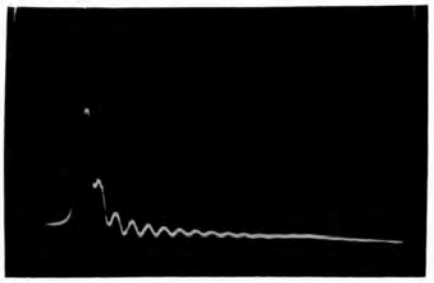

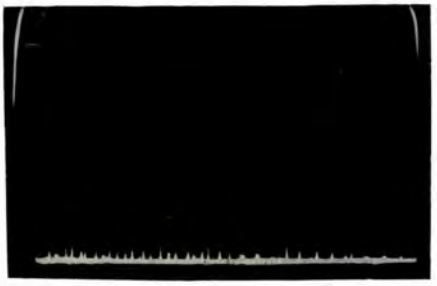

were observed.

Dispersing the carbon particles in ethanol had the advantage of forming a quasi reversible Q - switch, as opposed to the single shot carbon layers. The first giant pulse had a F.W.H.M. of 40 ns and a peak power of 0.3 MW, fig. 3.8C. The reduction in power was due to the absorption in the ethanol, which was also the cause of the partially Q - switched after pulses.

The behaviour of a large number of organic solvents has been investigated by Selden[21,104] who showed that a small absorption edge was sufficient to reduce the number and width of normal relaxation oscillations. The output observed above, with carbon dispersed in ethanol, is seen to be a two stage Q - switch. A single giant pulse, generated by destruction of the absorber, is followed by a series of partially Q - switched pulses, caused by the solvent.

3.3 IV SELF Q - SWITCHING

Szabo and Erickson[105] observed that a ruby laser could be self Q - switched at 77 K if there was a non-uniform photon density in a region of the ruby which was shielded from the pump light. The variation of photon density in their experiments was caused by using a roof top T.I.R. ruby rod and the roof top region was shielded from the pump light.

The pulse shortening mechanism, proposed by Szabo, was that of a saturable absorber effect in the ruby comparable with the Q - switching of CO_2 lasers by CO_2 vapour. The mechanism requires an absorption cross section σ_A of the unpumped atoms to be greater than that of the laser atoms σ_L

for a uniform photon density ϕ . The roof top, however, increased the photon density resulting in a higher effective value for $\sigma_A = M\sigma_L$ where M was a constant depending on the degree of reduction of the beam in the absorber (approximately M = 2 for the roof top). The value of M required for saturation was also a function of temperature. At 100°K, M should be 3, whilst at 77°K a value of 2 was sufficient.

To investigate this process the ruby rod was cooled by increasing the rate of flow of nitrogen to the laser cavity. Photograph, fig. 3.9A shows the free running output of the laser at room temperature. Fig. 3.9B shows the reduction in the number of pulses and peak power enhancement observed when the rod was cooled. The output reverted to normal when the rod warmed to ambient temperature. The slight Q - switching effect observed was attributed to the laser rod supports shielding the chiselled Brewster faces from the pump light. Complete saturation of these sections of the rod was not possible with the degree of cooling used but the pulse shortening and power enhancement was attributed to non-linearities caused by optical pumping of the $^4A_2 \rightarrow E$ transition in ruby.

Self Q - switching of a misaligned ruby laser cavity has been discussed in several papers[106,107,108] and no satisfactory mechanism exists at present. Photograph fig. 3.9C shows the effect produced as a result of misaligning the mirror M_2 of fig. 3.1A by 10^{-3} radians. In common with examples cited in the references an enhancement of peak power and a reduction in pulse width and number was produced. The orientation of the misalignment relative to the oscillating E vector did not alter the observations.

SELF Q SWITCHING

A Normal Output

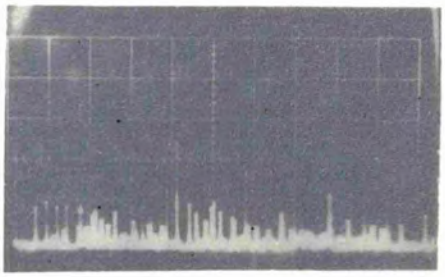

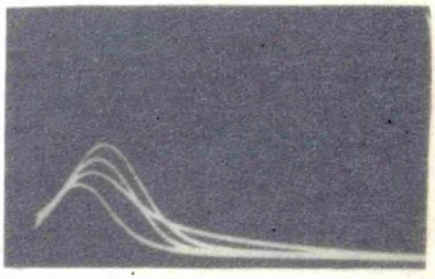

B Cooled Ruby Rod

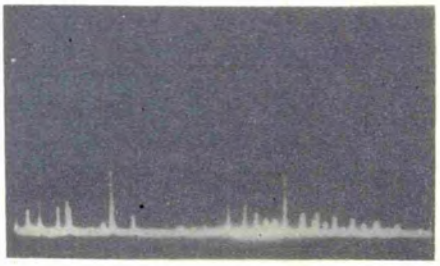

20μs

100ns

C Misaligned Ruby Rod

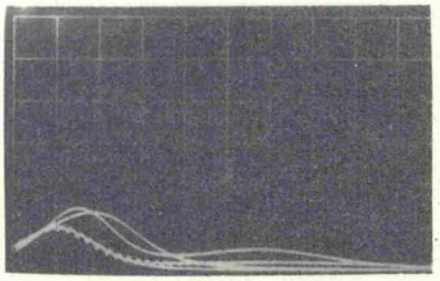

100ns

Aligned

100ns

Misaligned By 10^{-3} Rad

Fig 3·9

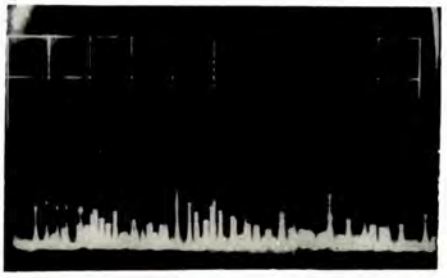

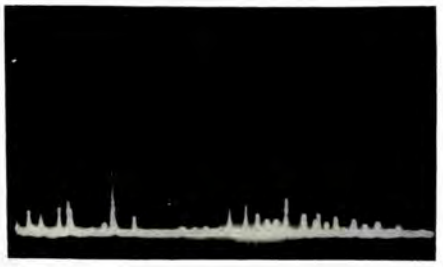

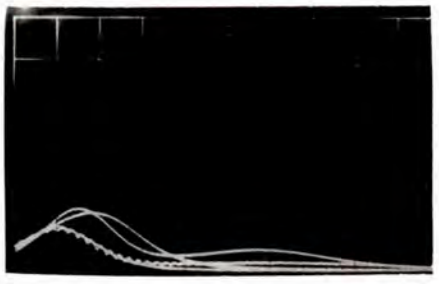

The main experimental results concerning cavity misalignment are as follows.

The effect of misaligning one cavity mirror is known to vary depending on the formation of the ruby rod. For Brewster angled systems and T.I.R. configurations varying degrees of Q - switching have been reported. For plane ended ruby rods a periodic undamped oscillation has been observed.

It is also known that the introduction of a lens into a misaligned plane mirror cavity does not alter threshold if

$$\alpha < D/2f$$

where α is the misalignment angle, D the diameter of the active medium and f the focal length of the lens. It is argued that the lens prevents 'walk off' of a ray which would otherwise occur and causes it instead to oscillate about a mean position.[109]

As shown in chapter 2, the intensity of the pump radiation is concentrated towards the centre of the rod and the resulting thermal differential is known to act as a positive lens.[107]

In such circumstances a ray may oscillate in a misaligned cavity throughout the whole of the active medium and effectively increase the length of the active medium with possible non-axial mode selection as evidenced by the lack of a filamentary structure in the output beam. The latter would satisfy the conditions of the Statz De Mars equations (9,10) and the production of periodic oscillations.

The effective length of the active medium also includes any regions shielded from the pump light. Any non-linearities in the shielded regions, caused by a non-uniform flux density, would be magnified if 'walk off' was prevented. It could be that a saturation process at room temperature is a possible mechanism for the experimental observations with shaped rubies.

* * *

CHAPTER 4

MODE LOCKED RUBY LASER

4.1 MODES IN A LASER RESONATOR

Investigation of the spectral distribution of the light emitted from a solid state laser is usually a great disappointment. Narrowing below a few tenths of a wave number is difficult to achieve. This results in part from a frequency shift during the output caused by changes in length and refractive index and the presence of unresolved modes. Such axial modes can be resolved by a Fabry Perot etalon and the beat frequencies between various modes (chapter 3) confirm these conclusions.

Fig. 4.1A shows the gain profile of ruby and the coverage of the profile is in the form of a fine tooth comb of axial modes separated by $\Delta\nu = c/2L$. These axial modes are the allowed resonances of the Fabry Perot feedback interferometer. The width of the individual modes varies with temperature and resonator geometry between 3 and 20 MHz, Temperature and refractive index changes cause a gradual frequency shift and the variation of mode pattern from one spike to the next means a particular pattern lasts only a short time i.e. independently phased modes.

With the advent of Q - switched lasers mode selecting elements were used to obtain lasers with high spectral brightness[110] by confining the radiation to a single axial mode. Transverse modes could be eliminated by a combination of increasing the resonator length and using stops. Axial mode selection was conveniently achieved by resonant reflectors[111]

A RUBY LASER LINE PROFILE

Δf. 9×10^{10} Hz

($\Delta \bar{\nu}$. $3 cm^{-1}$)

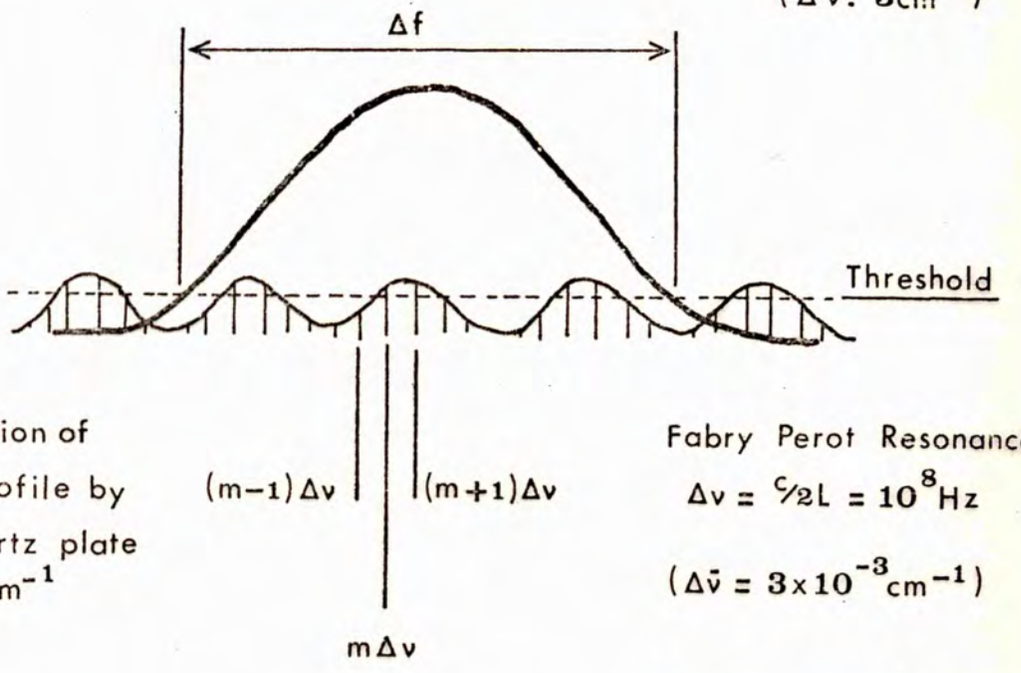

Modulation of mode profile by 1cm quartz plate $\Delta \bar{\nu} = 0.3 cm^{-1}$

Fabry Perot Resonances

$\Delta \nu = c/2L = 10^8$ Hz

($\Delta \bar{\nu} = 3 \times 10^{-3} cm^{-1}$)

Number of modes n

$n = \Delta f / \Delta \nu = 9 \times 10^2$

AXIAL MODE BEAT FREQUENCIES (CHANNELLED SPECTRUM)

B C

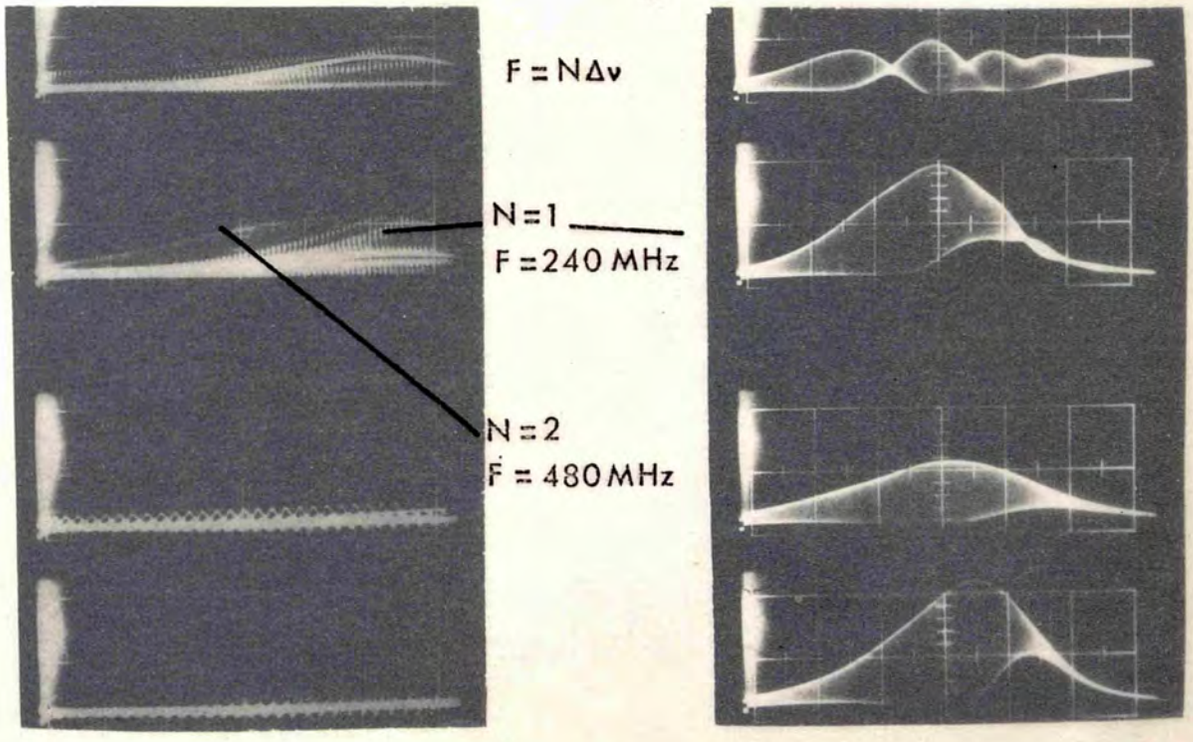

Upper 50 ns

Lower 20 ns

200 ns

Fig 4.1

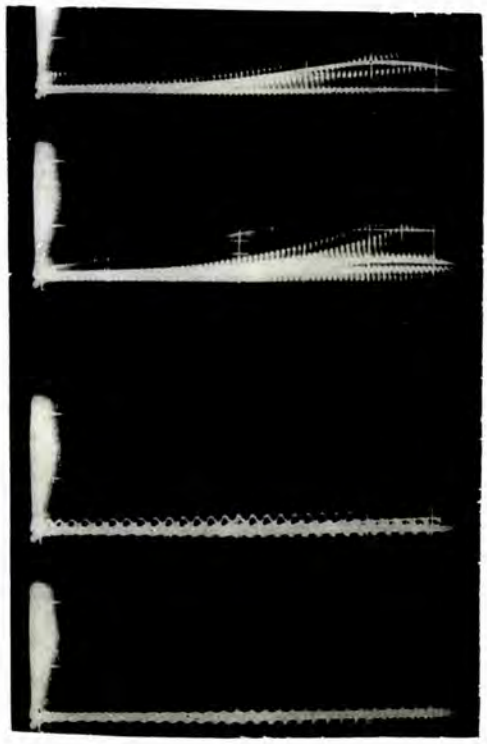

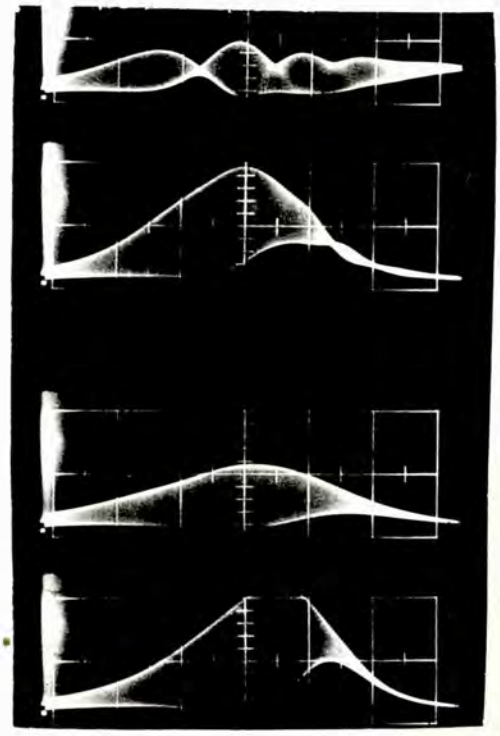

which provided feedback for a very narrow frequency range and, in fact, were able to select a single mode. A laser resonator with a resonant reflector acts as a coupled cavity, the shorter cavity (resonant mirror) determining the principal resonances of which only one lies within the gain profile.

4.2 MODE SELECTION AND BEATS

Without such mode selection the result of a large number (m) of random phased modes and their superposition is an output intensity equal to m times the number of modes. This may be compared with 100 violins, all playing approximately the same note, when no beat frequencies are observed.

The beats previously observed within the spikes (chapter 3) were due to amplitude fluctuations of individual modes caused by the intensity dependent transmission of the ruby.[112] Clearly, if two modes have an amplitude greater than the rest, beats will be observable at the difference frequency and the beat signal will continue until one of the modes undergoes a change in amplitude or phase.

A similar result was consistently obtained by purposely suppressing some of the available modes. Fig. 4.1A shows the result of placing a mode selecting element within the cavity. The mode profile was modulated with a spectral period $\Delta\bar{\nu} = 1/2l\mu$ where l was the length of the element and μ its index. For a quartz plate 1 cm thick $\Delta\bar{\nu} = 0.3\ cm^{-1}$ and the spectral channelling modulated the mode profile so that threshold was reached for groups of 2 or 3 modes. The almost 100% beat modulation observed was at the fundamental beat frequency $\Delta\nu = nc/2L$ $(n = 1)$ which was 240 MHz in this case. With a

faster time base and repetitive triggering the beat frequency between alternate (n = 2) axial modes was observed.

The low finesse coefficient of the quartz plate imposed a very slight modulation on the mode profile and each resonance may have covered several axial modes. If the finesse coefficient had been increased by coating the quartz with a reflecting layer the modulation may have been sufficiently sharp to encompass only a single axial mode. Furthermore, if the spectral period of the element $\Delta\bar{\nu}$ had been greater than the laser line profile only a single axial mode would have oscillated, the beat pattern would have diminished and the plate would have acted as a true mode selector.

When quartz plates 1 mm thick were placed in the cavity (spectral period 3.3 cm^{-1}) the spectral period was at least as broad as the linewidth of the ruby. The imposed modulation encompassed all the available modes and a beat signal was only observed occasionally when the ruby was pumped in excess of threshold. The 100% modulation observed with the thicker plates was never observed with the 1 mm plates.

To ensure that the beat signal observed was not caused by electronic ringing in the detection system, the cavity length L was adjusted and the beat frequency was seen to change accordingly.

4.3 MODE LOCKING

In previous sections beat frequencies have been examined for a laser operating with many random phased modes and also for the case of a few selected random phased modes of nearly equal amplitudes. Here consideration is given to the case of many modes

with fixed phase relationships and nearly equal amplitudes.

Fourier theorem.

Any repetitive pulse train can be made from the sum or interference of a series of discrete sinusoidal functions having integrally related frequencies and fixed phase relationships i.e.

$$E(t) = \frac{E_0}{2} + \sum_{m=1}^{\infty} E_m \cos 2\pi \langle m\Delta\nu \rangle t + E_m \sin 2\pi \langle m\Delta\nu \rangle t \qquad 12.$$

where $m\Delta\nu$ are the discrete frequencies and a zero phase term is assumed. The pulse width $\Delta\tau = 1/\Delta f$ where Δf is the range of frequencies involved in the summation of equation 12. The pulse repetition rate is $\tau = 1/\Delta\nu = 2L/c$. The beat signals discussed in the previous section were for the summation taken over two modes ($m = 1 \rightarrow 2$). The beat signal between two random phased modes lasts for a period equal to the phase memory of the laser. To obtain a sensible periodic output from the superposition of more than two modes, fixed phase relationships must exist between the modes.

A laser supporting a large number of modes (no mode selection) is capable of generating a periodic pulse train. A laser possesses a discrete set of integrally related frequencies (modes) $m\Delta\nu = mc/2L$ across a bandwidth Δf. Phase synchronization is the additional requirement.

It is interesting to calculate the parameters of a pulse train that could be generated by a ruby laser with phase synchronization, assuming strict applicability of the inverse bandwidth relation $\Delta\tau = 1/\Delta f$. The bandwidth of ruby at room temperature is $\Delta f = 9 \times 10^{10}$ Hz (1.5 Å) giving a lower limit of $\tau \approx 10 \times 10^{-12}$ seconds. The repetition rate $\tau = 1/\Delta\nu$

$\approx 8 \times 10^{-9}$ seconds for a 120 cm cavity. The peak power of m phase locked components is m x average power and, assuming fixed phase over the entire bandwidth, $m = \frac{\Delta f}{\Delta \nu} \approx 720$. Using the giant pulse powers observed in chapter 3 i.e. ~ 10 MW the peak power in the mode locked or phase synchronized case would be 7.2×10^9 W.

Achieving synchronization.

If a signal with frequency ν is amplitude modulated at a frequency f side bands are generated at frequencies $\nu + f$ and $\nu - f$. Since the energy in the side bands is intimately related to the parent frequency, the side bands are in phase with the parent signal. If then a laser cavity is modulated at a frequency $\Delta\nu = c/2L$ any mode with a frequency $m\Delta\nu$ generates two side bands at $(m + 1)\Delta\nu$ and $(m - 1)\Delta\nu$. These side bands are situated spectrally on adjacent modes and thus energy in these modes is locked in phase to the parent mode. The same process is impressed on all modes by the modulator with the result that the whole mode spectrum is rapidly phase locked at the onset of oscillations.

4.4 AUTOMATIC MODE LOCKING

Mocker and Collins[37] showed that the bleachable dye used to Q - switch a laser could also automatically provide the amplitude modulation required for phase locking. The intensity dependent transmission characteristic of such a dye is shown schematically in fig. 4.2A. Assuming oscillations start at the mode nearest the peak of the gain profile of fig. 4.1A the action of the dye is to attenuate low level signals preferentially to high level ones, thereby sharpening any amplitude variation within the cavity. Once started, this process provides automatic

A INTENSITY DEPENDENT TRANSMISSION OF BLEACHABLE DYE

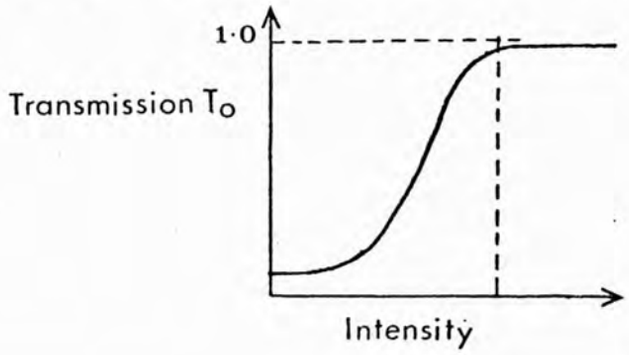

B OPERATION OF BLEACHABLE DYE IN TIME AND FREQUENCY DOMAIN

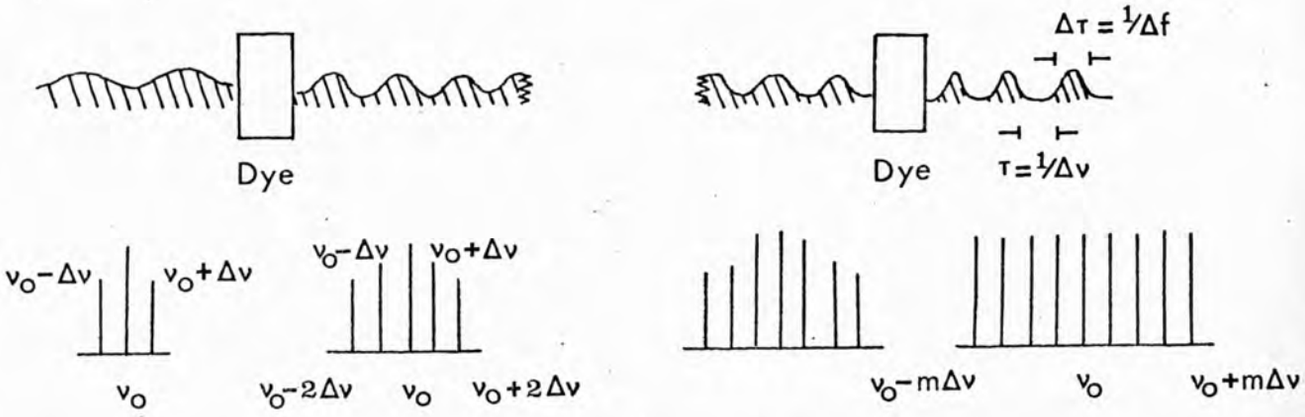

C ABSORPTION OF CRYPTOCYANINE IN VARIOUS SOLVENTS

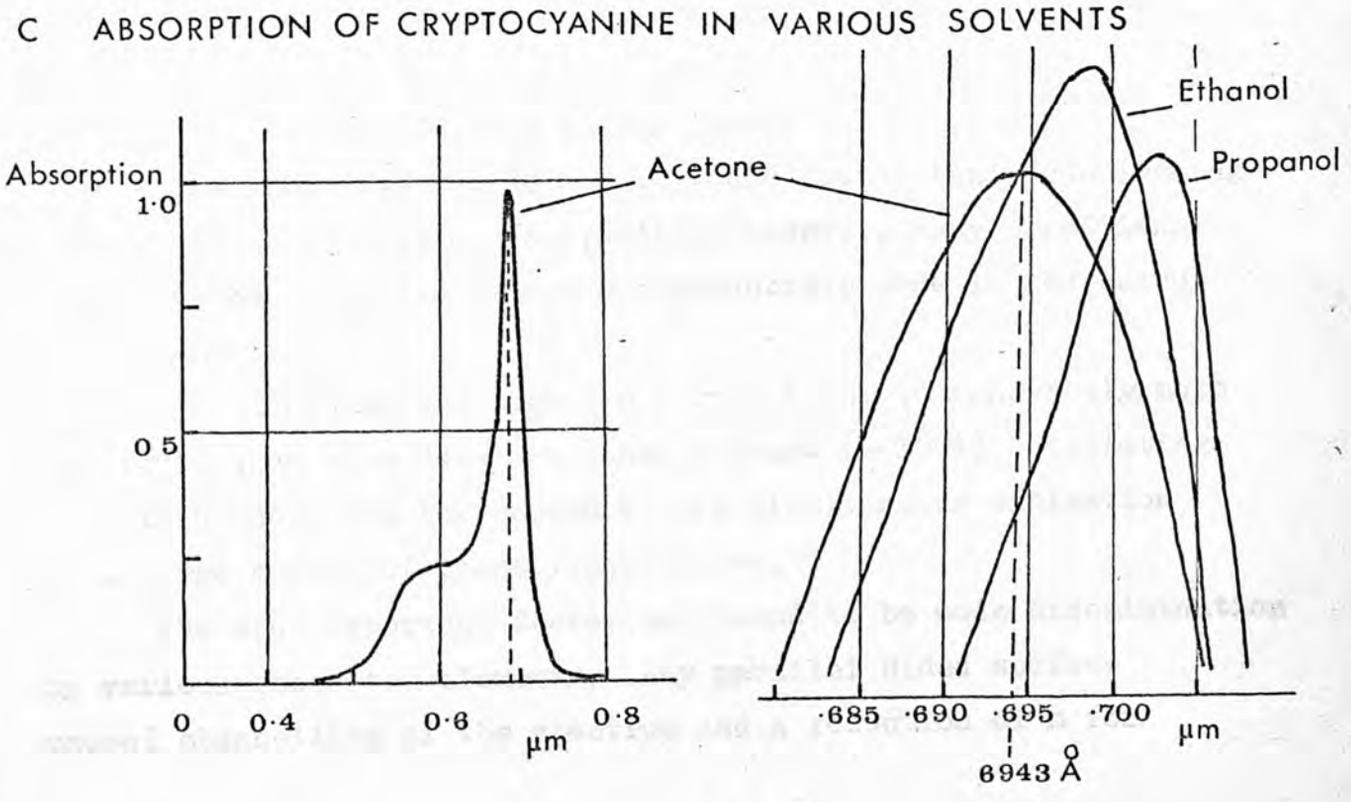

Fig 4·2

modulation at the cavity transit time 2L/c. The harmonics generated by the opening and closing correspond exactly to the axial mode frequency separation $\Delta\nu = c/2L$. The dye automatically provides modulation at the correct frequency without having to compensate for perturbations in the resonator, fig. 4.2B.

The initial spatial variation required to start the process described may be due to the finite extent of the active medium or it may be started by random noise. The latter explanation is supported by the observation of short pulse components in free running lasers.[104,113]

This behaviour of the dye is on a much shorter time scale than the simple bleaching process assumed in Q - switching. The only extra requirement is that the dye should recover in a time less than the cavity transit time 2L/c. This is easily satisfied by cryptocyanine with a relaxation time of 10^{-12} sec.

Experiments in mode locking a ruby laser.

From previous discussions it would appear that mode locking may easily be achieved. In practice, however, many conditions needed to be satisfied before a reproducible mode locked output was achieved.

Synchronizing the modes in a ruby laser is inherently more difficult than with Nd:glass where a broad ($\sim$ 100Å) oscillating bandwidth increases the chance of the simultaneous excitation of a large number of phase locked modes.

The most important factor was found to be mode discrimination by various resonator elements. Any parallel sided surface caused channelling of the spectrum and a reduction of m for

continuous summation of equation 12. The Brewster angled ruby rod prevented any selection by reflection at the rod faces and the dye cell was tilted at its Brewster angle. The effect of a parallel sided surface is shown in fig. 4.3. Fig. 4.3A shows the pulse train monitored on the T 454. Inserting a 3 mm quartz flat inside the cavity (spectral period 1 cm^{-1}) caused sufficient channelling for the generation of a smooth single mode output. Occasionally low amplitude sinusoidal beats were observed.

Increasing the cavity length L increased the mode density and sufficient modes were involved even if the whole spectrum was not simultaneously excited. A further virtue of the long cavity was that it selected a single transverse mode and prevented output in numerous transverse modes, which are difficult (but not impossible[114]) to lock. The long cavity also produced a 'long low' giant pulse F.W.H.M. 70 ns. The giant pulse rise time depends on the speed with which the inversion crosses threshold. This has been examined by Svelto[115] who has shown that if the inversion threshold is crossed too rapidly the modes will not have had time to establish well defined phase relations. The use of a long cavity increased the giant pulse rise time relative to the phase locking time. Fig. 4.3B shows the sinusoidal beat signal observed when L was 86 cm and the repetitive pulse train when L was increased to 120 cm.

The speed of crossing threshold is the single factor which affects the reproducibility of the system. This speed alters dramatically if the dye transmission changes by a few per cent. To this end circulating dye systems have been used to avoid degradation of the dye.

The achievement of mode locking was found to be strongly dependent on the pump level. Pumping the laser 50% above

MODE-LOCKED PULSE TRAINS

A

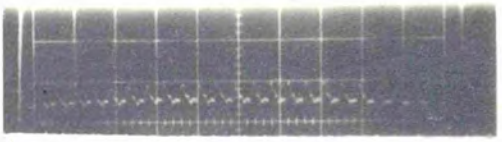

⊣ ⊢ 20 ns Mode-Locked Signal Monitored On T454 With P.I.N. Diode

T = 8·6 ns

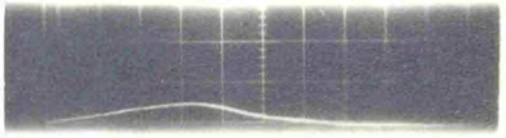

⊣ ⊢ 20ns Insertion Of 3mm Quartz Flat In The Above Cavity

B

⊣ ⊢ 20 ns L = 85 cm

Beat Frequency $F = 1{\cdot}76 \times 10^8$ Hz

($F = N\Delta\nu$, $N = 1$ and $\Delta\nu = c/2L$)

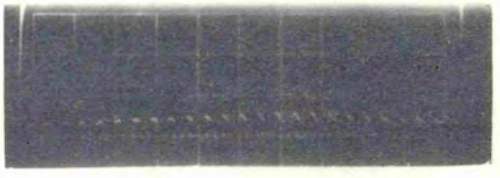

⊣ ⊢ 20ns L = 128 cm

Mode-Locked Signal T = 8·6 ns

C

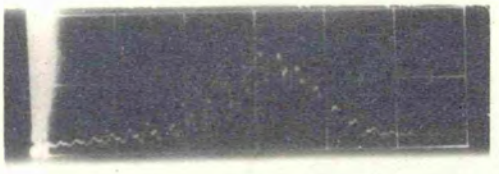

⊣ ⊢ 20 ns

Threshold Dispersion Of Modes

D

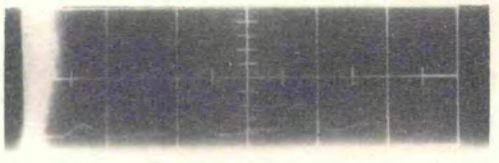

⊣ ⊢ 5 ns. Start Of Mode-Locked Signal. Ten Element Stack Mirror T519 With EMI 9643B Diode

---

E

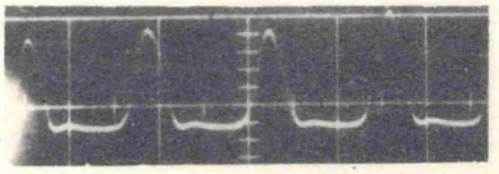

⊣ ⊢ 5 ns

ITL Diode T = 7·2 ns

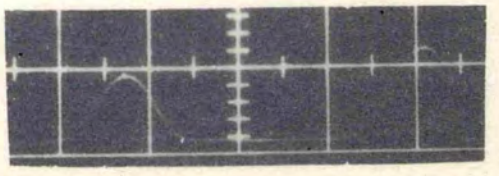

⊣ ⊢ 2 ns

ITL Diode T = 7·2 ns

Fig 4·3

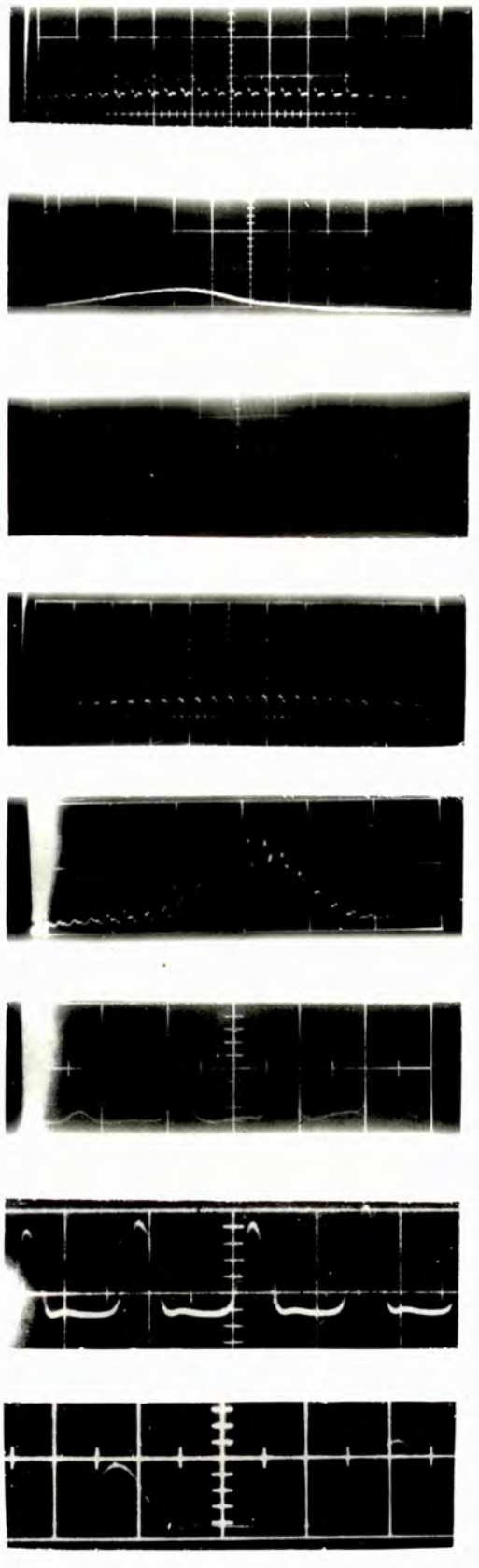

threshold caused a breakaway from a periodic pulse train fig. 4.3C. Besides influencing the speed at which threshold was crossed, pumping in excess of threshold caused many modes to be simultaneously and independently excited. Such behaviour was contrary to the requirement discussed previously of oscillations starting in a single mode and adjacent modes having energy fed into them by the side band generation process.

The position of the dye cell within the cavity was found to be important. If the dye cell was placed at any position other than adjacent to the maximum reflectivity mirror, two pulse trains were generated which competed for the same spectral width.

The choice of saturable absorber for Q -switching ruby lasers is usually cryptocyanine dissolved in such solvents as methanol, ethanol or nitrobenzene. A considerable improvement in consistency of operation was gained by using acetone as the solvent.[38] Spectrophotometer traces of various solutions of cryptocyanine are shown in fig. 4.2C. When acetone was used the absorption peak was coincident with the ruby laser line, whilst in other solvents the absorption peak was displaced by up to 30 Å. It is postulated that this displacement pulls the laser central frequency to one side during the output by providing greater gain for modes closer to the absorption peak. This would cause the frequency spectrum to be swept during emission, reducing the simultaneously available bandwidth. This interpretation is substantiated by results obtained with Nd^{3+} lasers utilizing Kodak 9740 switch solution where the saturable absorber mechanism works on an absorption edge. Treacy[117] found a definite pulling of the laser line during emission resulting in a chirped output signal. The signal could be dechirped (or the pulses compressed) by passing the signal

through a dispersive network to provide a differential delay.

The main portion of the output from the laser was usually 'dumped' on to a piece of black Polaroid film during these experiments. This left a characteristic burn mark and it was possible to tell, from the presence of this mark, that the system had lased. Rotating by 90° the beam splitter, that usually diverted a small portion of the beam to the photodiode, any reflection from the Polaroid was observed. This reflection amounted to 5% of the incident beam and disrupted the mode locked output if the Polaroid surface was roughly aligned with the cavity. To avoid feedback the Polaroid dump was angled at grazing incidence to the laser beam.

4.5 MIRROR DAMAGE

Although the generation of shorter pulses circumvents damage to the active medium, it has been a general observation[37,38] that partially transmitting mirrors are more susceptible to damage when a laser is operated in the mode locked regime. Any slight deterioration in the dielectric mirrors causes a fall off in reproducibility. The change in reflectivity may be considered equivalent to a change in dye concentration since the total cavity loss is changed. It has been shown that the latter affects the locking conditions by changing the speed at which threshold is crossed.

Damage at the maximum reflectivity mirror was alleviated by the use of a roof top prism, but the various schemes devised for the low reflectance end of the cavity e.g. frustrated total internal reflection and electron gun evaporated coatings were not available. The use of etalon type reflectors, with their comparative freedom from damage, unfortunately precludes

mode locking, since these reflectors exhibit mode selective properties.

It was found, however, that a cavity incorporating a 'random stack mirror', fabricated from microscope cover slips could provide the wide band feedback and remain undamaged. The surface of microscope cover slips may be termed random or rough in comparison with optically flat surfaces. The performance of random stack mirrors with conventional Q - switched lasers is the subject of chapter 5. Here the point of importance is that each element in the stack was 0.03 cm thick and the corresponding spectral period was 11 cm^{-1}. Any interference caused by local parallelism therefore did not channel the spectrum and the full band width was available for simultaneous excitation.

A random stack mirror (10 element R = 0.4) was used as the output mirror for the pulse trains monitored with the E.M.I. diode and T 519 and shown in fig. 4.3D. In fig. 4.3E the detection system was the I.T.L. diode and the T 519 oscilloscope. In both cases the pulse shape observed was instrument limited. Photographs like fig. 4.3D,E were typical of many taken with the laser operated with a random stack mirror. The consistency of operation was attributed to the damage free properties of the mirror. In this way a random stack mirror provided an easy to use and reliable component for use with a mode locked ruby laser.

The velocity of light.

The pulse repetition rate c/2L of the mode locked laser enabled a velocity of light determination to be made. Increasing the cavity length by a known amount P increased the ringing time

A MODE-LOCKED RUBY LASER WITH ROUGH STACK MIRROR

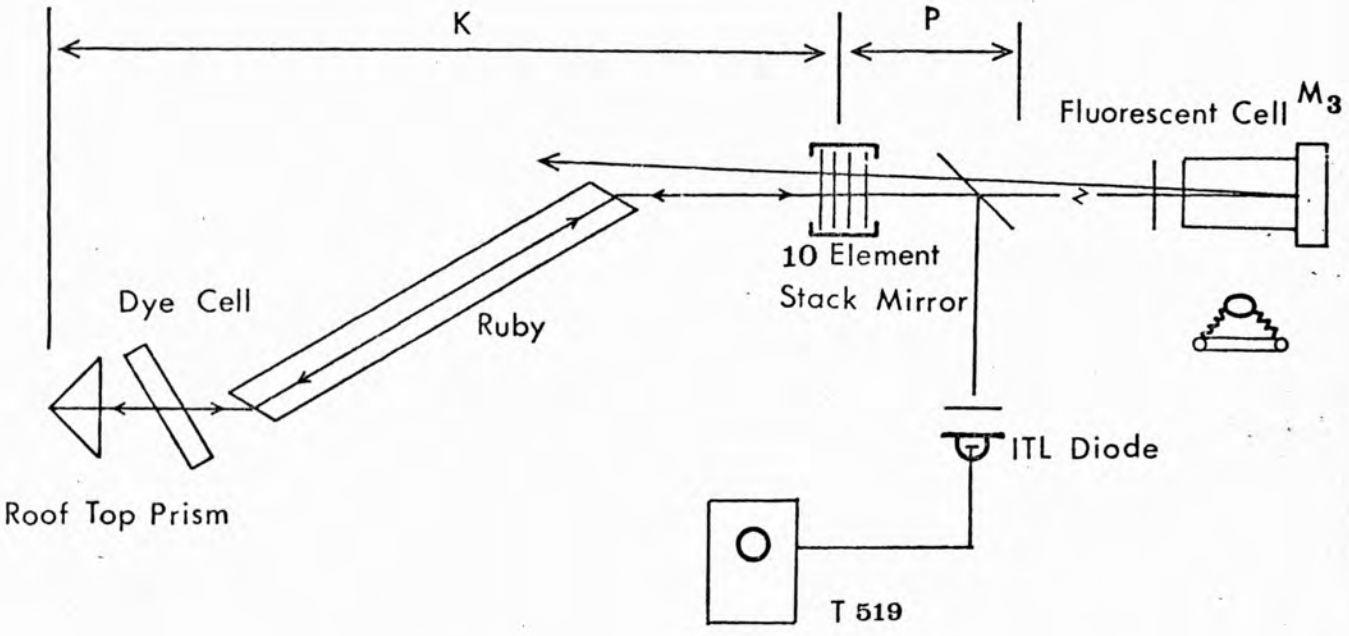

B VELOCITY OF LIGHT

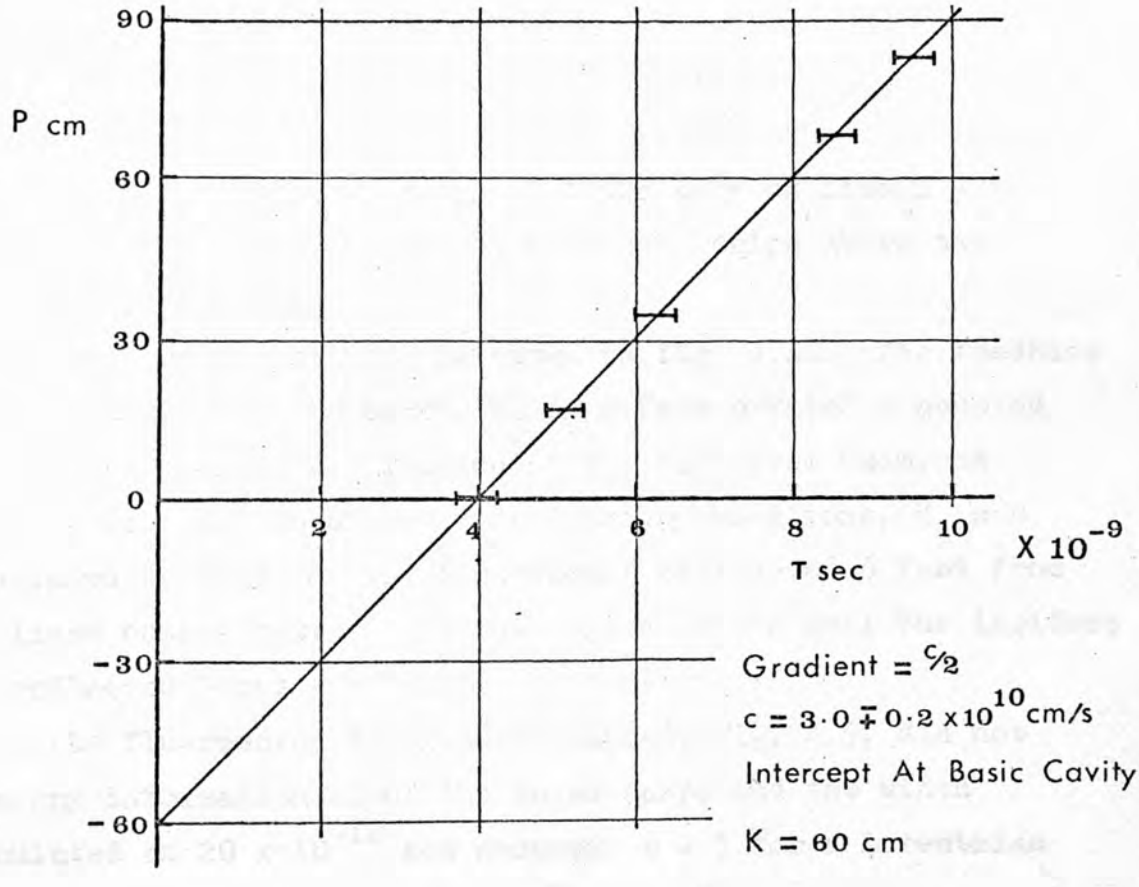

Fig 4·4

of the cavity by 2P/c i.e. $\tau = 2\,(K + P)/c$ where K was the basic cavity length. Fig. 4.4B shows τ as a function of P and from the slope of the graph

$$c = 3.0 \mp 0.2 \times 10^{10} \text{ cm/sec}$$

The basic cavity length K was 60 ∓ 0.1 cm.

Pulse width measurement.

Although the stack mirror did not affect the instrument limited pulse widths, the two photon fluorescence technique was used to estimate real pulse widths. Diphenyl anthracene in benzene hasbeen used for two photon fluorescence, but rhodamine 6G in ethanol was found to be more convenient.

Such a solution is non-absorbing at the fundamental laser frequency ν but absorption may take place via a virtual level at $E = 2h\nu$. From this excited level the atomic system decays to an intermediate level by non-radiative processes and finally radiates a broad fluorescent line. Because of the quadratic intensity dependence of the fluorescence, if means are provided to reflect the pulse train back on itself a profile of the pulse appears as a bright region above the background, fig. 4.5.

The arrangement used is shown in fig. 4.4A. The feedback into the cavity by the mirror M_3 in effect created a coupled cavity. To avoid amplification of the reflected beam, and possible destruction of the mode locking conditions, M_3 was misaligned by 3 mR and the fluorescent cell moved 6 feet from the laser output mirror. In the region of the cell the incident and reflected beams were almost colinear.

The fluorescent track photographed, fig. 4.5, did not give any information about the pulse shape and the width calculated as 20×10^{-12} sec assumed $a = 1$ for a Lorentzian

PULSE WIDTH MEASUREMENT

A Two Photon Fluorescence In Rhodamine 6G

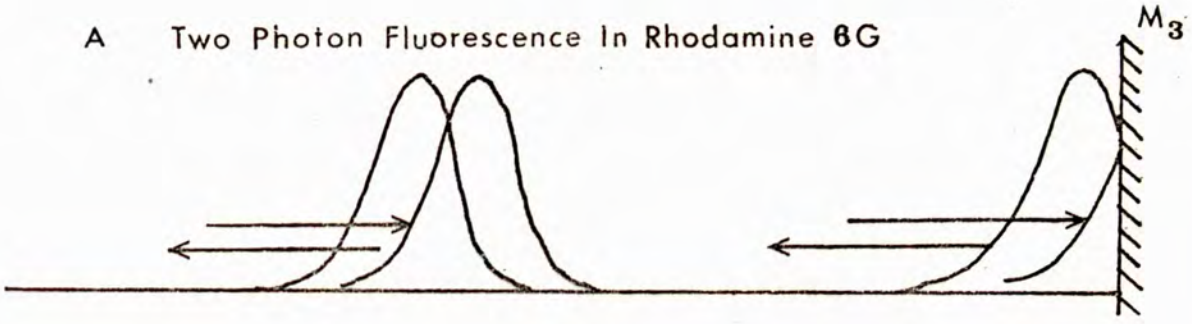

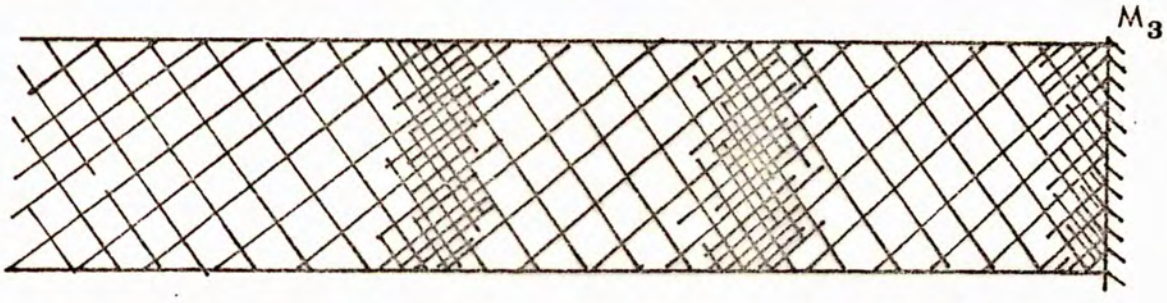

B

100 ps

$X_o = {}^{act}/_{\mu}$ $X_m = {}^{act}/_{2\mu}$ $\mu = 1.36$

$a = 1$ Assumed Lorentzian Pulse Shape

Fig 4.5

pulse. This value agrees well with the inverse bandwidth relation $\Delta\tau = 1/\Delta f$.

The interpretation of such two photon fluorescent patterns is still the subject of violent debate.[118] Theory shows that the contrast ratio of the fluorescence should be 3:1 above background for a completely mode locked signal and that a ratio of 1.5:1 should be observed for the case of random phased modes. Most results, including the track shown in fig. 4.5, yield a ratio of 2.0:1.

The difficulty was thought to have been overcome by the recording of a very narrow spike in the centre of the fluorescent region.[119] Being 50 micron wide with a peak contrast ratio of 2.6, the observation was substantiated by photoelectric measurements of the intensity profile.[120] On the other hand, similar spikes were observed with fluorescence measurements on relaxation oscillations when no mode locking element was present.[104]

The main general impression is that if a periodic pulse train is displayed on an oscilloscope then measurement of the pulse width obtained from two photon fluorescence tracks can be regarded as the true pulse width to a high degree of certainty, without resort to contrast measurements.

* * *

CHAPTER 5

RANDOM STACK MIRRORS

5.1 PERIODIC OPTICAL RESONATORS

Recently the periodic optical resonant reflector has been analysed.[111] Working on the same physical principles as the dielectric thin film a series of parallel sided glass plates can provide a high reflectivity with freedom from damage. The peaked periodic reflectance of such a reflector makes it strongly mode selective, which is desirable for lasers with high spectral brightness, although the opposite is required for mode locked lasers.

Fig. 5.1 shows the computed maximum reflectivity of a periodic resonant reflector for different n and m.[111] To obtain a high reflectivity both n and m must be large (n index, m number of elements). To obtain 85% reflectivity at 6943 Å using Schott L.A.K. 10 glass (n = 1.71383) three such plates are required with a thickness of 0.42087 of the air interval.[111] The six figure accuracy is needed for the operation of this type of mirror. Only a tunable resonator is capable of satisfying such conditions. The plates and spacers need to be flat to $\lambda/10$ and the thickness of the plates and spacers can be varied by heating. The optical thickness of the air interval may be adjusted by varying the atmospheric pressure between the plates.[121,122]

In 1963 Burch[123] reported the use of a stack of dielectric plates as a cavity mirror for a ruby laser. Such a stack

COMPARISON OF REFLECTIVITIES OF RESONANT AND NON-RESONANT PERIODIC REFLECTORS

$$R_{max} = \left| \frac{1 - n^{2m}}{1 + n^{2m}} \right|^2 \qquad \bar{R} = \frac{2m\theta}{1 + (2m-1)\theta} \qquad \theta = \left| \frac{n-1}{n+1} \right|^2$$

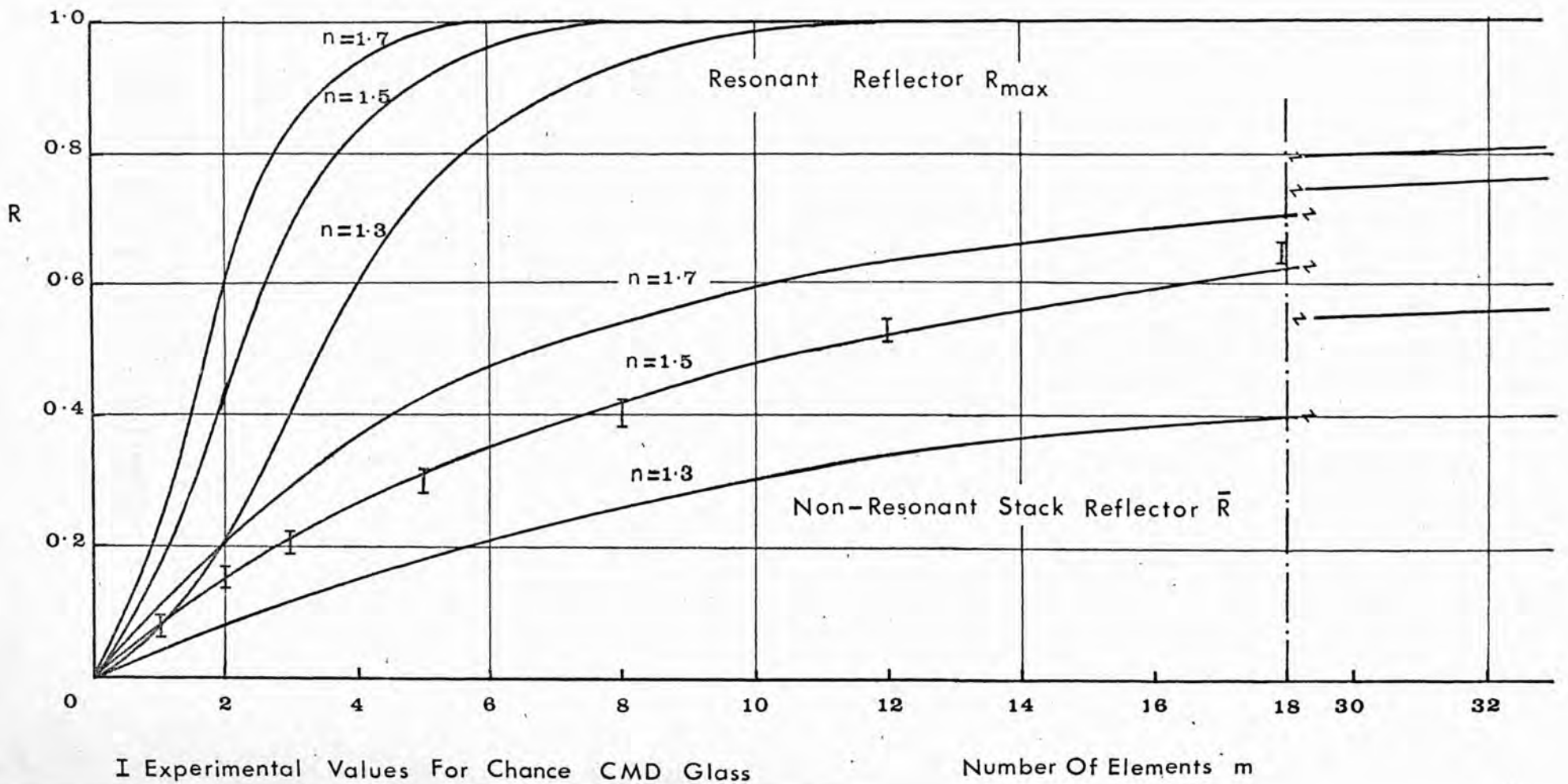

Fig 5·1

consisted of a randomly arranged pile of thin dielectric plates such as microscope cover slips. In contrast to the periodic resonant reflector the optical path varied by several wavelengths across the aperture. Also, the spread of orientations was several minutes of arc. Such a stack provided a white light reflection. Recent interest in high power P.T.M. and mode locked laser systems has required broad band reflectors which are resistant to damage. The random stack mirror fills this need.

5.2 THEORETICAL REFLECTIVITY OF RANDOM STACK MIRRORS

Stokes[124] calculated the white light reflectivity for a pile of plates, ignoring phase effects and interference.

The single plate.

Let θ be the function of incident light reflected by a single surface.

From the Fresnel relation

$$\theta = \left|\frac{\mu - 1}{\mu + 1}\right|^2$$

The fraction of incident light reflected by a single plate (two surfaces) r

$$r = \theta + (1-\theta)^2\theta g^2 + (1-\theta)^2\theta^3 g^4 + \cdots\cdots$$

where g is the fraction of light lost through absorption in a single pass.

Summing to infinity

$$r = \frac{\theta + (1-\theta)^2\theta g^2}{1 - \theta^2 g^2}$$

for $g = 1$ $\qquad r = 2\theta/1+\theta$

A stack of plates.

Consider a stack of m plus n plates in groups of m and n plates. Define the functions ϕm, ψm as the reflection and

transmission of the group of m plates, likewise for n.

Then $\phi_{(m+n)} = \phi m + \psi^2_m \phi n + \psi^2_m \phi m \phi^2_n + \cdots\cdots$

$\psi_{(m+n)} = \psi m \psi n + \psi m \phi n \phi m \psi n + \psi m \phi^2_n \phi^2_m \psi n + \cdots\cdots$

Summing to infinity $\phi_{(m+n)} = \phi m + \dfrac{\psi^2_m \phi n}{1 - \phi m \phi n}$ 13. $\psi_{(m+n)} = \dfrac{\psi m \psi n}{1 - \phi m \phi n}$ 14.

From 13 $\phi_{(m+n)} |1 - \phi m \phi n| = \phi m + \phi n |\psi^2_m - \phi^2_m|$

which is invariant under m,n transform.

Therefore $1/\phi m \left|1 + \phi^2_m - \psi^2_m\right| = 1/\phi n \left|1 + \phi^2_n - \psi^2_n\right| = \text{const}$

Putting the constant equal to $2\cos\alpha$ $\psi^2_m = 1 - 2\phi m \cos\alpha + \phi^2_m$ 15.

Equation 15 must apply for all m, therefore from 14 $\psi^2_{m+n} = 1 - \phi m+n\, 2\cos\alpha + \phi^2_{m+n}$

which from 14 $\psi^2_{m+n} = \dfrac{\psi^2_m \psi^2_n}{(1 - \phi m \phi n)^2}$

Eliminating ψm and ψn by 15

$$\left|1 - 2\phi m \cos\alpha + \phi^2_m\right| \left|1 - 2\phi n + \phi^2_n\right| = \left|1 - 2\cos\alpha\, \phi m+n + \phi^2_{m+n}\right| \left|1 - \phi m \phi n\right|^2$$

Differentiating with respect to n and putting $n = 0$, $\phi n = 0$ and noting that $\left.\dfrac{\delta \phi m+n}{\delta n}\right|_{n \to 0} = \phi' m$

The R.H. side gives $-2\phi'_o \phi m \left|1 - 2\cos\alpha \phi m + \phi^2_m\right| - 2\cos\alpha\, \phi' m + 2\phi m \phi' m$

The L.H. side gives $-2\left|1 - 2\cos\alpha\, \phi m + \phi^2_m\right| \cos\alpha\, \phi'_o$

Equating and dividing by $\phi m - \cos\alpha$

$$\phi' m = \phi'_o \left|1 - 2\cos\alpha\, \phi m + \phi^2_m\right| \qquad 16.$$

Now ϕ'_o is constant $= \beta/\sin\alpha$

Integrating $$\int \frac{\delta\phi m}{1-2\cos\phi m+\phi m^2} = \int \frac{\beta\delta m}{\sin a} + C \qquad 17.$$

This is a standard integral giving $\phi m = \frac{\sin\beta m}{\sin a+\beta m}$

Using 15 $$\psi m^2 = \left|\frac{\sin a}{\sin a+\beta m}\right|^2 \qquad 18.$$

For small losses a and β are small $$\frac{\phi m}{m\beta} = \frac{\psi m}{a} \qquad 19.$$

When $m=1$, $\phi 1 = r = \frac{\beta}{a+\beta}$, $\psi 1 = t = \frac{a}{a+\beta}$ and $t = 1-r = \frac{a}{a+\beta}$ therefore $\beta = \frac{ar}{1-r}$

Using 19 $$\frac{\phi m|1-r|}{mar} = \frac{\psi m}{a}$$

Since $\psi m = 1-\phi m$, $\frac{\phi m|1-r|}{mar} = \frac{1-\phi m}{a}$ therefore $\phi m = \frac{mr}{1+|m-1|r}$

where m is the number of plates and r the value for a single plate

$$r = \frac{2\theta}{1+\theta} \qquad \text{therefore} \quad \phi m = \frac{2m\theta}{1+(2m-1)\theta} \qquad 20.$$

Fig. 5.1 shows the curves relating the mean reflectivity R and the number of plates m for various relative refractive indices, assuming no absorption. A higher number of plates is required with the non-resonant system to achieve a given reflectivity, compared with the resonant reflectors. The equation 20 shows, however, that any substance which is finely divided, so as to present numerous reflecting surfaces, and which is transparent in mass, is brilliant white in reflected light. The intensity of light reflected from snow is due to this effect.

5.3 CONSTRUCTION OF MIRRORS

The mirrors used consisted of 0.3 mm thick microscope cover slips separated by paper spacers which created an air gap between the cover slips of 0.09 mm. The glass was Chance C.M.D. soda - lime - silica with a refractive index of 1.52 and the surfaces were parallel to 5 minutes of arc and flat to 2λ. The density of the stack mirrors was measured on a spectrophotometer. Assuming negligible absorption the measured density was equivalent to a simple reflection. The experimental reflectivities as a function of number of plates are shown in fig. 5.1. Clearly, losses became more important with large numbers of cover slips, but the correlation between theoretical and experimental curves showed that absorption was negligible in stacks of up to 15 elements.

The random stack had a mean reflectance given by equation 20, but enhanced reflectivity was observed in those regions where the local parallelism was better than the mean. This was demonstrated by photographing the reflection pattern when coherent light from a gas laser was incident on the mirror.

Fig. 5.2B shows the observed pattern with reflection from a $\lambda/4$ flat for comparison. The local enhancement and the increased beam divergence can clearly be seen. Fig. 5.2C shows the striated reflection from a stack mirror made visible by chalk dust in the atmosphere. The beam was photographed at an angle and the total path length was 4 metres.

5.4 LASER OUTPUT WITH STACK MIRRORS

Relaxation oscillations.

Fig. 5.3A shows the output energy as a function of the number of elements m in the stack mirror. A 99% dielectric mirror was used at the closed end of the resonator.

Threshold values were higher than those obtained with dielectric mirrors (chapter 3) due to the increased divergence of the beam. However, a relative lowering of threshold was observed with stacks of increasing m. The measured beam divergence was 5 mR with all the mirrors. The far field showed a speckle pattern caused by local enhancement, fig. 5.4B.

The spike power and separation were no different from those obtained previously with good quality dielectric mirrors. However, with a 15 element stack, beat modulation between adjacent axial modes was pronounced.

Magyar and Selden[125] have attributed this to a spectral channelling effect. Though such effects must be present, as the far field pattern shows, the spectral period of the elements forming the stack was 11 cm^{-1}, an order of magnitude greater than the line width of ruby at room temperature.

An alternative mechanism could be a saturable absorption line in the glass caused by impurities. It is known that most microscope cover slips contain iron (in the form of Fe_2O_3), though this is not listed in the typical analysis of the C.M.D. cover

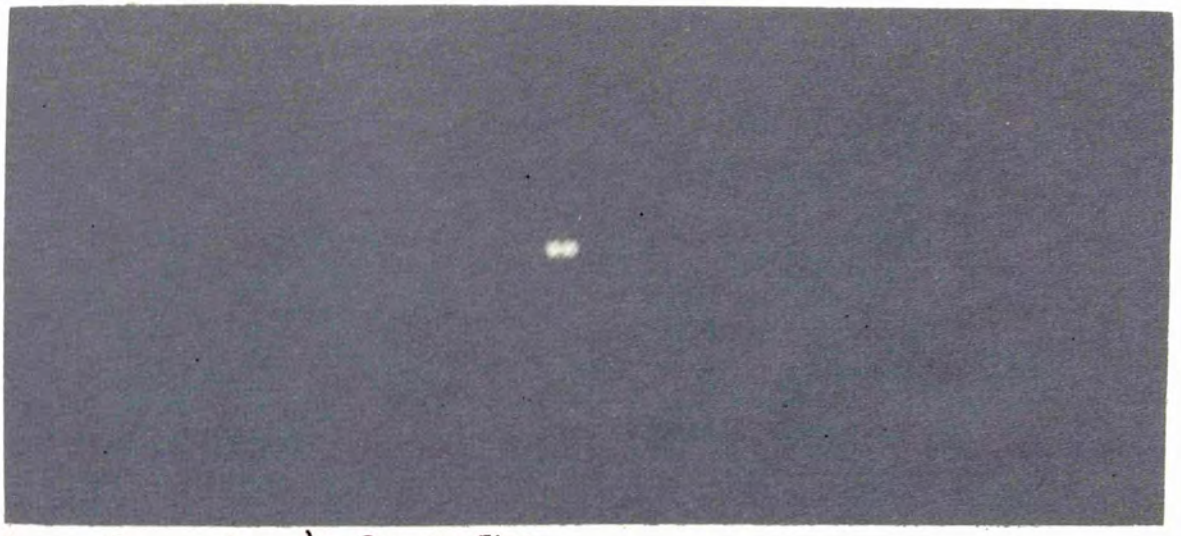

A Comparison $\lambda/4$ Quartz Flat

B Thirty Element Random Stack Mirror

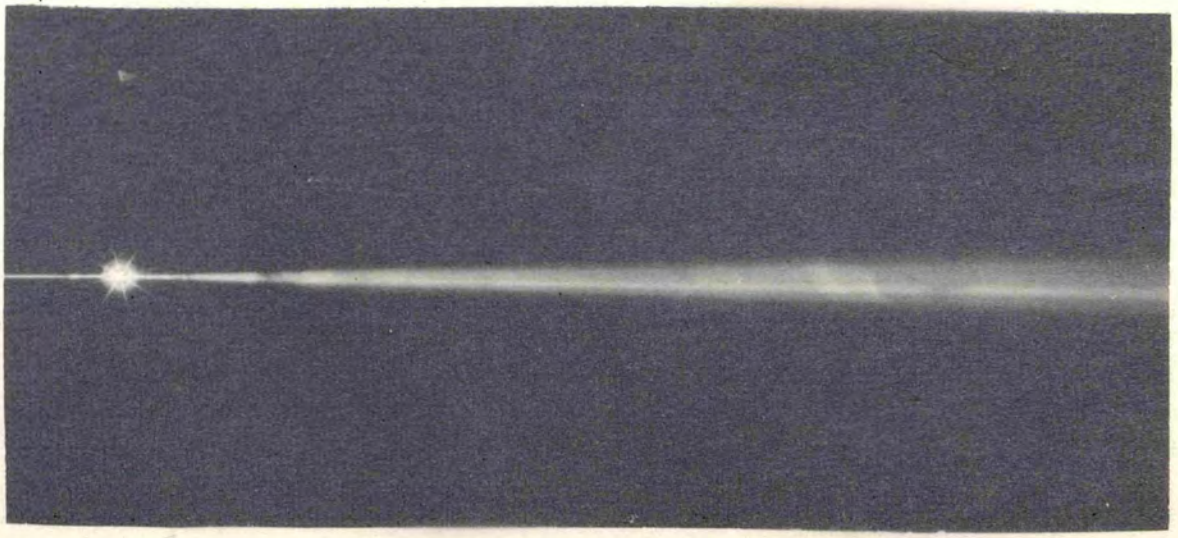

C Striations In Reflected Beam

Light Source:
6328 Å HeNe Gas Laser

Fig 5·2

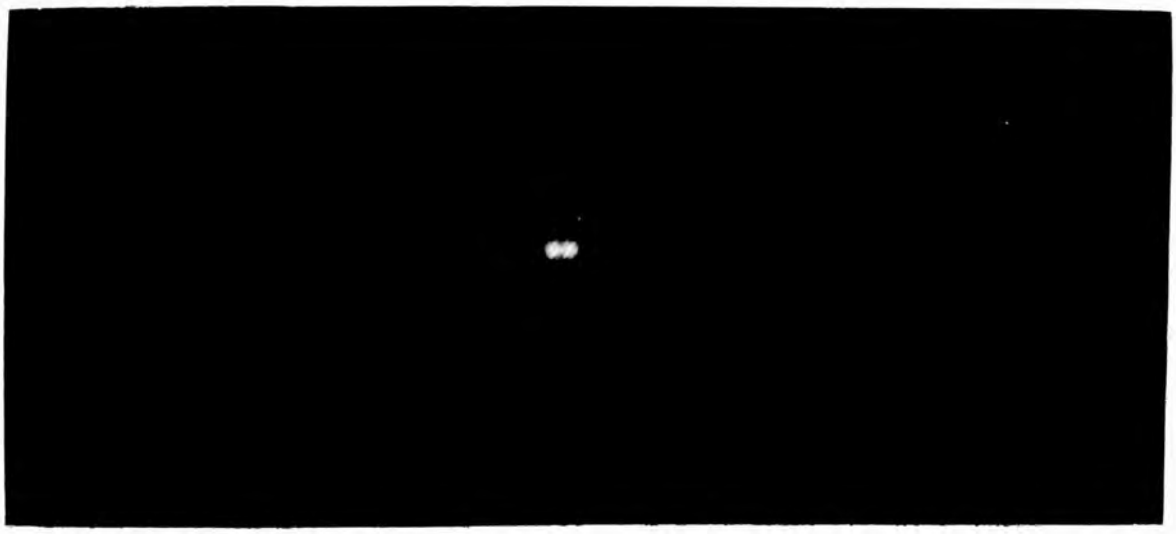

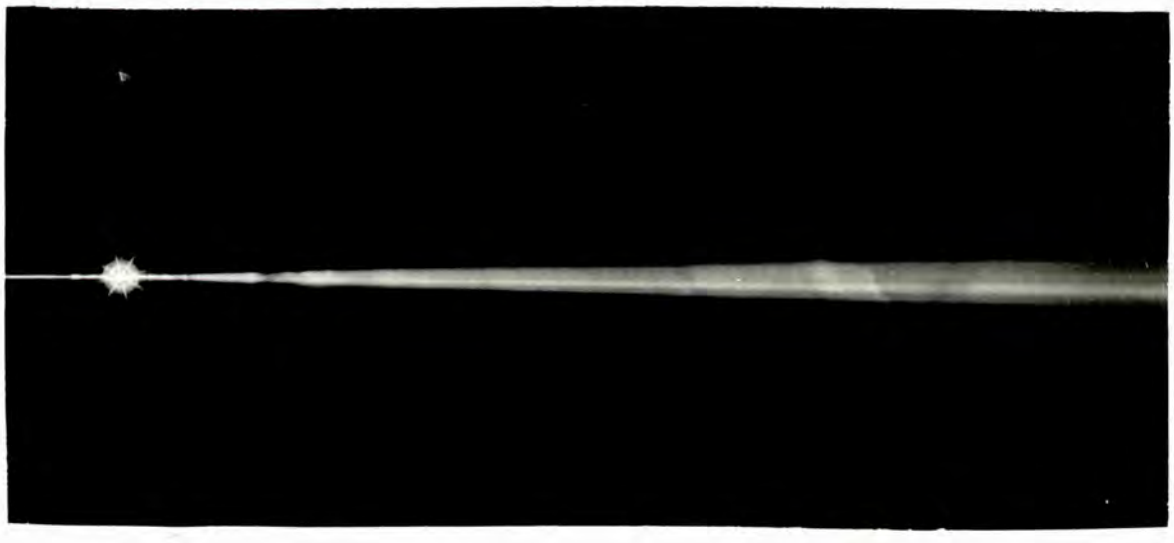

slips used. An iron impurity in glass is saturable and has a relaxation time of 3 ns.[126]

All stack cavity.

Threshold for oscillation was further increased by using stack mirrors at both ends of the laser cavity. The triangular points in fig. 5.3A denote the output from the laser when operated with two stack mirrors of m = 15 and m = 30 elements. That threshold could even be achieved for such a cavity was probably due to the large range of modes which could be supported. A laser consisting of the active medium and two random stack mirrors is a novel arrangement when consideration is given to the normal specifications for laser mirrors.

In fig. 5.3B the total lasing time and the delay before oscillations began are plotted as a function of input energy, E_i. Fig. 5.4A demonstrates the type of spike output observed. At threshold a single pulse F.W.H.M. 300 ns was generated, followed by three or four after pulses. This may have been caused by an increase of any saturable absorption loss within the cavity. With a total of 45 elements saturation may have been sufficient for weak Q - switching. Above threshold a normal chaotic spike ensemble was observed.

Giant pulse output.

A combined mirror and Q - switch cell was made by filling the air gaps in a 45 element stack with a true saturable absorber (cryptocyanine in ethanol). The almost equal refractive indices (1.52 glass, 1.36 ethanol) reduced the reflectivity of the mirror compared with the air glass mirror. This was the reason for an 11 MW peak power output pulse with the combined system and a 5 MW peak pulse when a separate Q - switch cell

RANDOM STACK MIRRORS

A Output As A Function Of Input Energy

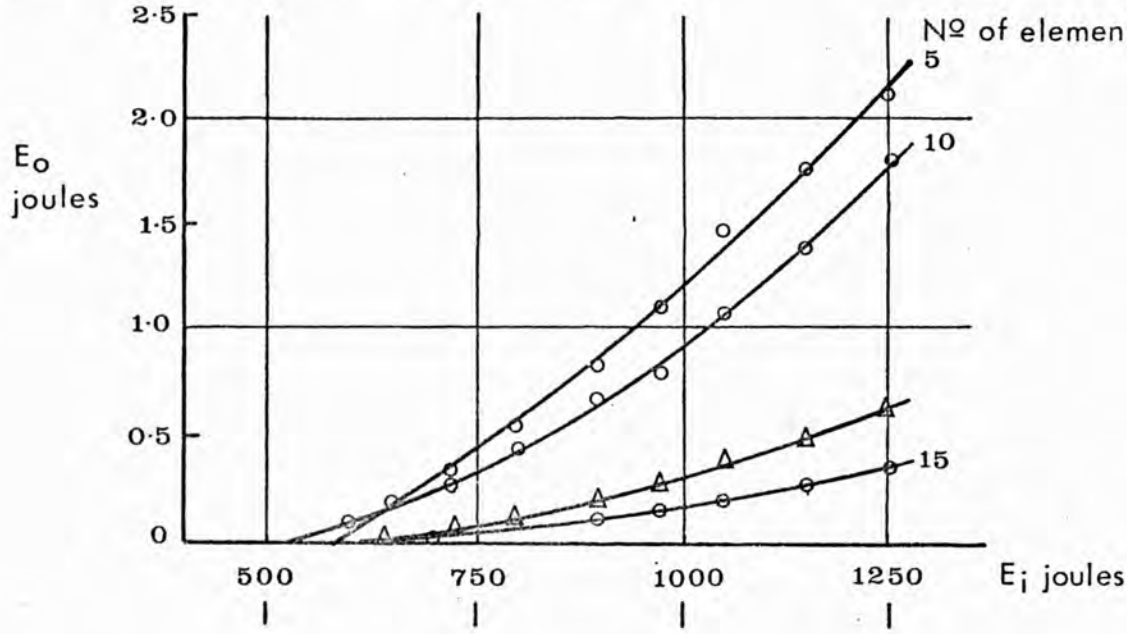

B Timing And Duration Of Output

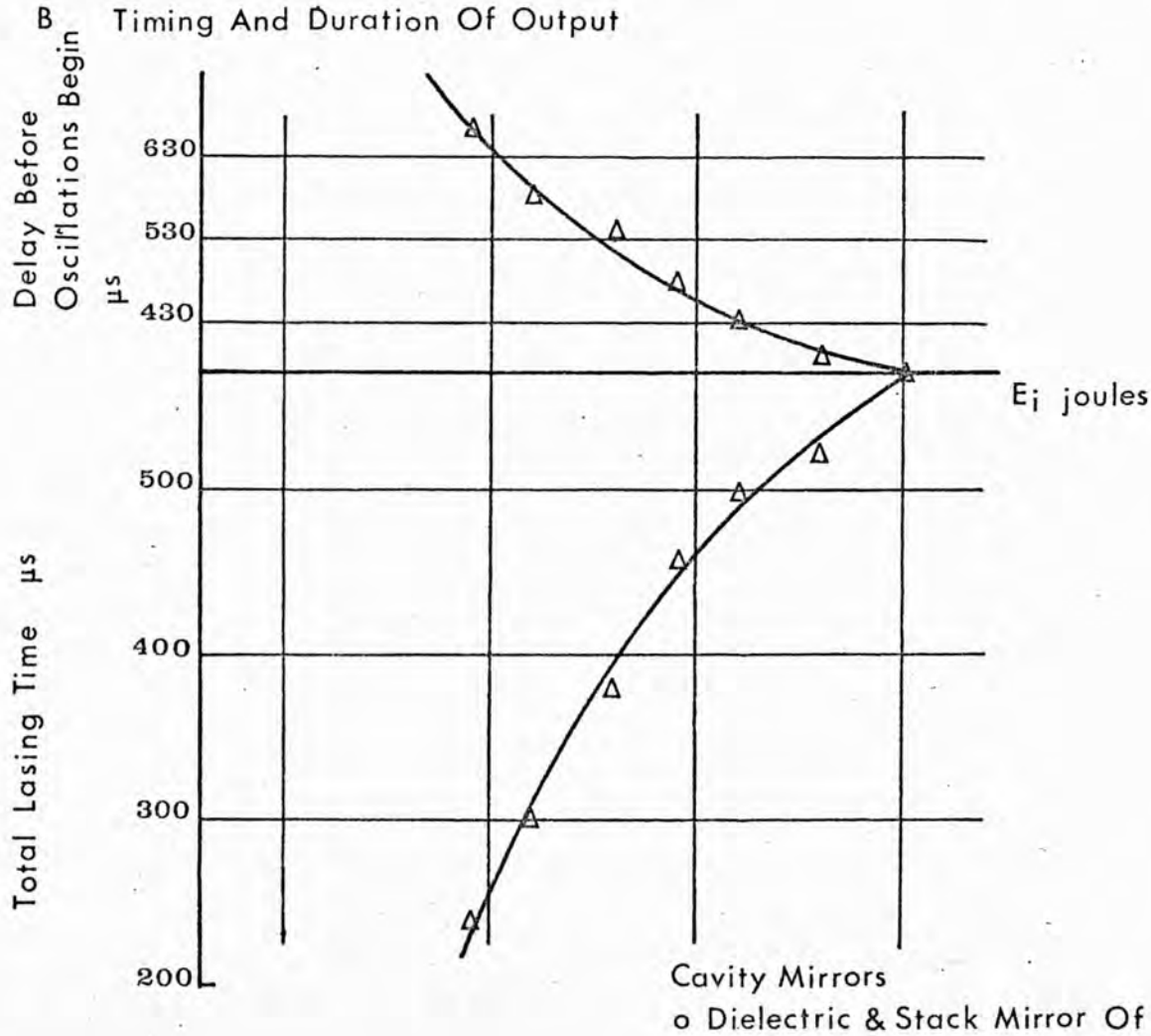

Cavity Mirrors

o Dielectric & Stack Mirror Of m Elements

Δ Stack Mirrors m = 15 , 30

Fig 5·3

LASER WITH RANDOM STACK MIRRORS

A Relaxation Oscillations M_1 15, M_2 30 Elements

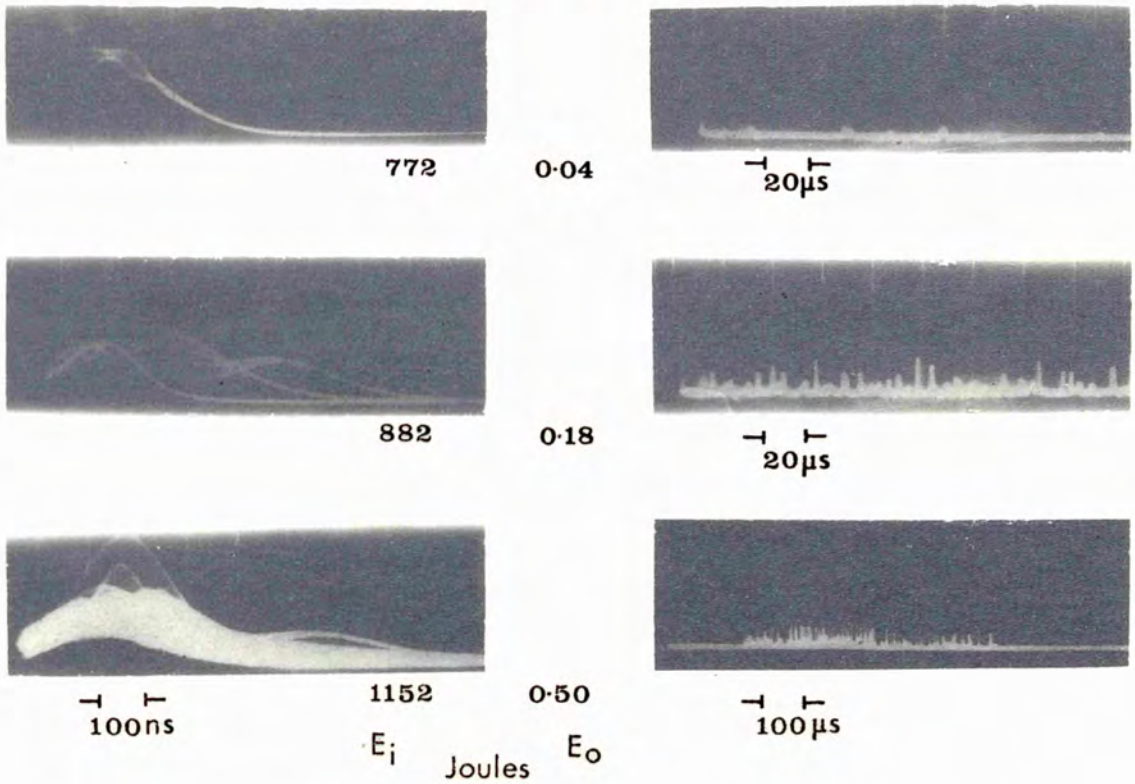

B Far Field Pattern

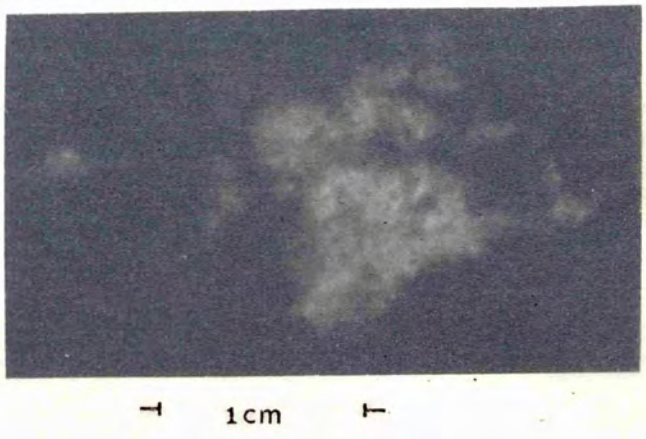

C Combined Mirror And Switch Cell

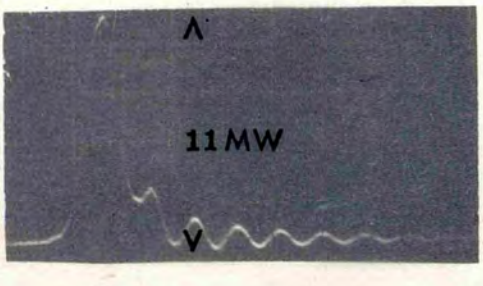

D Separate Switch Cell

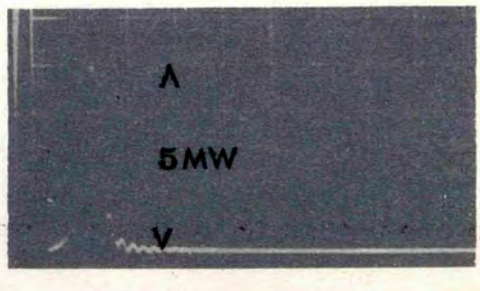

Fig 5·4

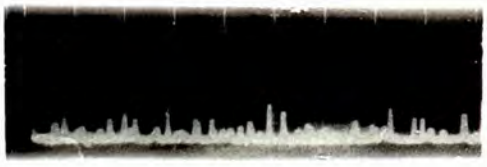

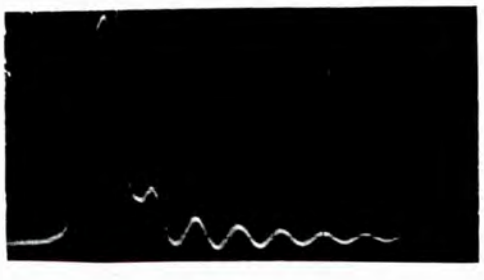

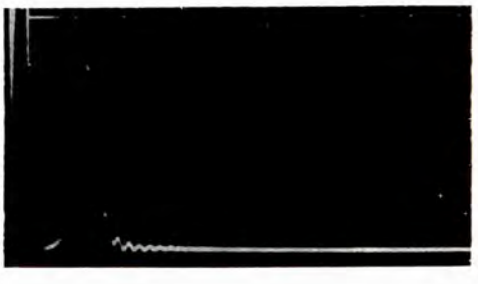

was used with an air glass mirror, fig. 5.4C,D.

The combination of mirror and dye cell reduced the number of components in the laser. Taking this to the limit a unitary design for a laser would consist of a spatially separated active medium. Internal reflections within such a system could be sufficient to offset the losses and the output beam would be equally divided between the two ends.

* * *

CHAPTER 6

LASER INDUCED THERMAL ETCHING IN THIN FILMS

6.1 METALLIC Q - SWITCH FILMS

As a convenient method of analysing laser induced damage in thin films, the Q - switching elements used in the work described in chapter 3 were examined under a microscope. Photograph fig. 6.1 shows the type of feature observed with the carbon films. Photograph fig. 6.1A shows the flaking of the layer whilst the three other figures demonstrate the formation of cracks in the glass substrate. Such cracks are similar to those observed on heat sleeked glass. A large circular chip, approximately 300 micron in diameter, part of which is shown in fig. 6.1C, was the result of thermal shock. Concentric interference bands can be seen due to interference between the substrate and the chip.

The 200 Å gold films used to Q - switch the laser showed the same basic features as the carbon films with the addition of a regular system of parallel straight lines. It was realized that these lines were due to absorption and subsequent evaporation at the antinodes of the standing electromagnetic wave within the laser cavity. Alternatively, the gold film had recorded a two beam hologram of the wavefront. The spacing or spatial period of the modulation is related to the angle of incidence θ between the surface normal and the incident radiation by equation 8

$$d = \frac{\lambda}{2\cos\frac{\theta_2-\theta_1}{2}\sin\frac{\theta_2+\theta_1}{2}}$$

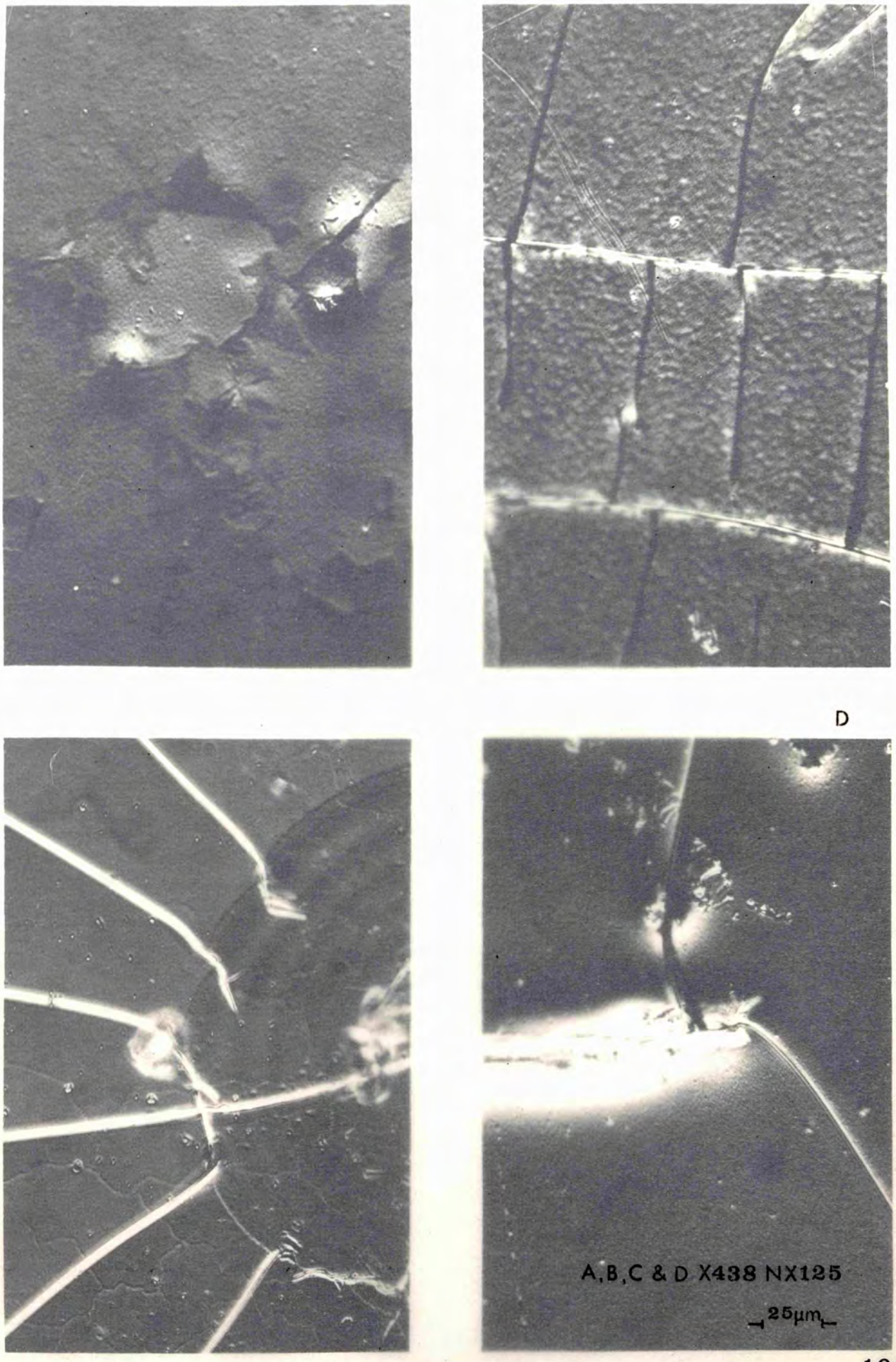

Fig 6·1

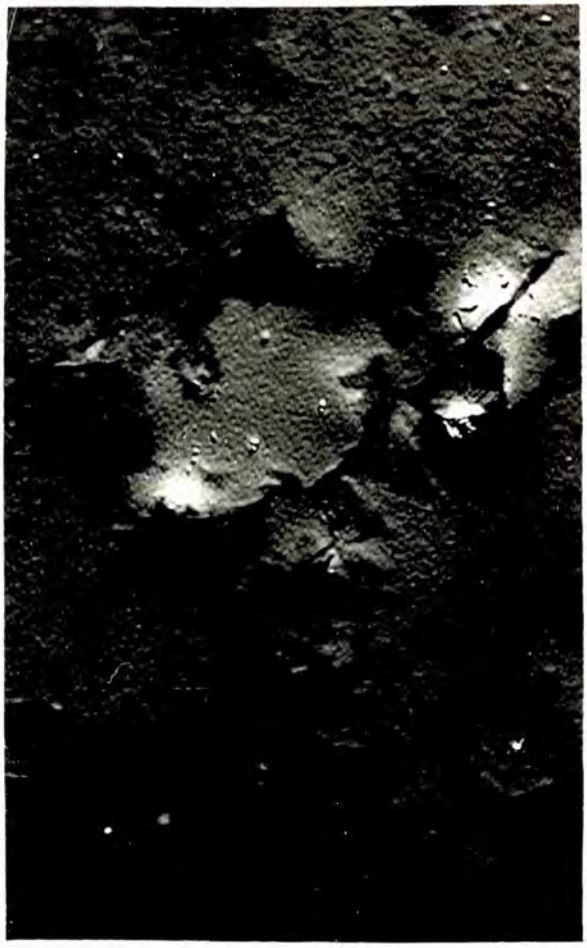

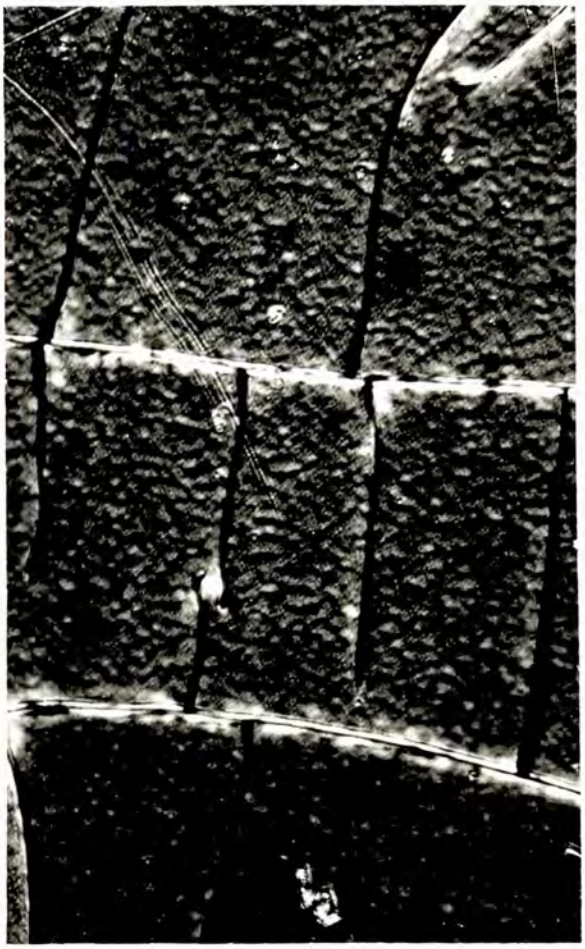

where $\theta = \theta_1 = \theta_2$

Therefore $d = \frac{\lambda}{2\sin\theta}$

Fig. 6.2 shows equation 21 plotted for λ equal to the ruby fundamental and second harmonic radiation.

A series of specimens was prepared and the spatial period of each measured by calibration against a microscope fiducary grid. The experimental points fit the curve well and remove any possibility that the modulations were due to any other effect.[128] Five different ordinate scales are given in fig. 6.2. These enabled the spatial period to be converted from nanometres to line pairs per inch without heartache.

The variation of reflectivity with angle of incidence (chapter 3) for the experimental points in fig. 6.2 caused a corresponding loss variation within the cavity. This put a practical limit on the value of θ that could be utilized. The single pulse peak power decreased to 10 MW as θ was increased to 60°. When θ was greater than 60° the Q of the cavity was so low that oscillations could not be started. This was consistent with θ in the region of 60° being the pseudo-Brewster angle for gold. Above $\theta = 60°$ the reflectivity rapidly increases.[129] Rotating the gold film so that the oscillating electric vector was at right angles to the plane of incidence did not alter the spatial period. However, the reflectivity curve corresponding to this polarization monatomically increased with θ and Q - switched operation could not be obtained for $\theta > 30°$.

The standing wave ratio employed in the experiments was

RELATIONSHIP BETWEEN θ AND SPATIAL PERIOD (d)

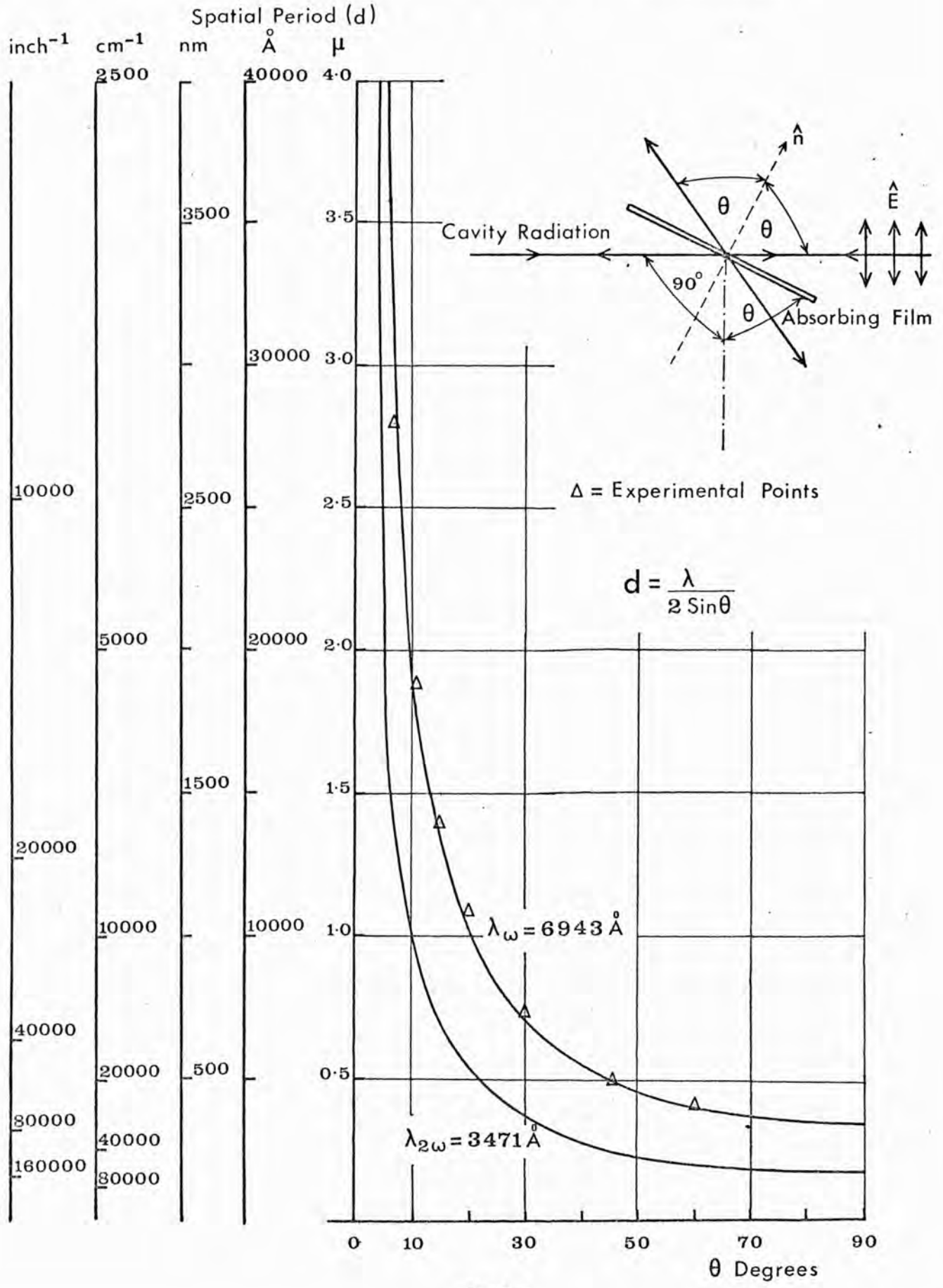

Fig 6·2

almost unity because the gold films were placed between the maximum reflectivity mirror and the ruby. However, placing the film between the ruby and the output coupling mirror (4%) still gave a good modulation profile on the surface. The interpretation was that the absorption of the travelling wave component of the partial standing wave was sufficient to raise the temperature of the gold surface to near its boiling point. Spatially modulated vaporization was then accomplished by the relatively small standing wave component. This is analogous to the pre-fogging technique used with photographic plates to reduce the exposure time.[66] To check that at least a partial standing wave was required the laser was Q - switched with a gold film and the output directed on to a second 200 Å gold film. As expected, the film inside the cavity was found to be spatially modulated, whilst the second film exhibited a uniform damage area.

To study the effect on films other than gold a series of thin films was prepared, using C.M.D. glass substrates. The thickness of the films was such that the reflection at normal incidence was similar to that obtained with 200 Å thick gold films i.e. $R_{pa} = 0.6$. This meant that the peak power generated by the laser was in the region of 10 - 20 MW. Variations for a given incidence angle were due to absorption changes from film to film.

Microscopic examination of each film showed spatial modulations with a period agreeing with equation 21. The definition varied considerably and fig. 6.3A-D are the photomicrographs of the modulations on aluminium, silver, nickel and platinum. The figures at the bottom left of each

A

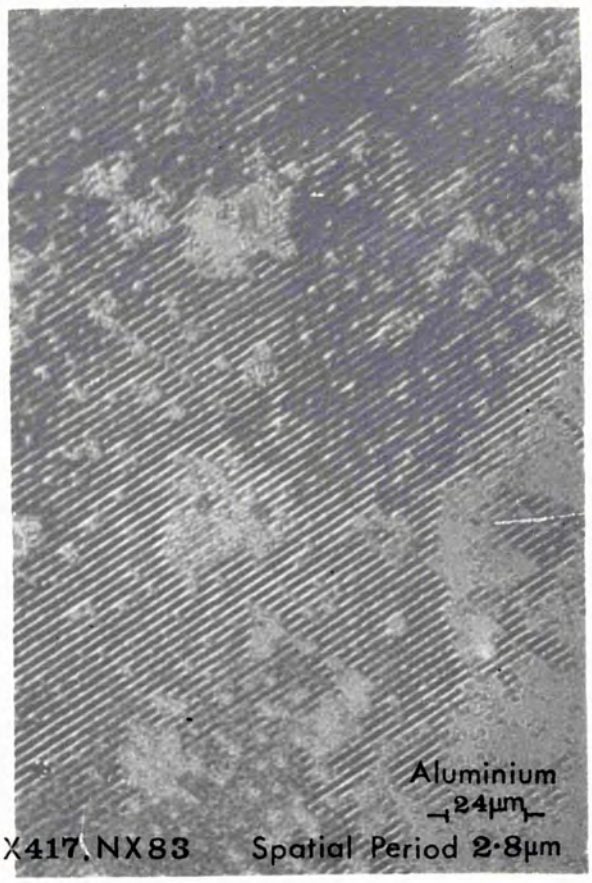
Aluminium
24μm
X417.NX83 Spatial Period 2·8μm

B


Silver
61μm
X166.NX33 Spatial Period 5·5μm

C


Nickel
24μm
X417.NX83 Spatial Period 3·7μm

D

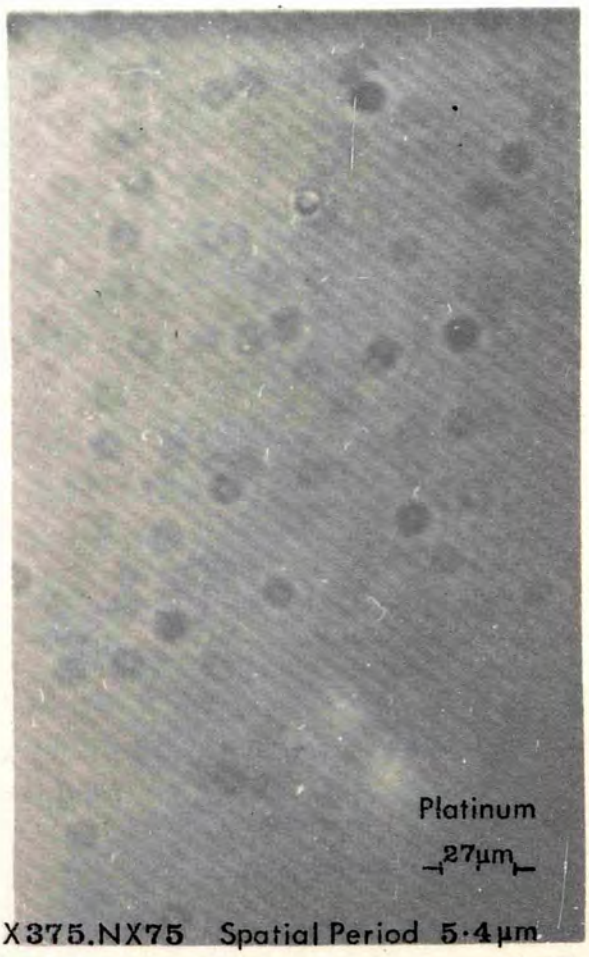
Platinum
27μm
X375.NX75 Spatial Period 5·4μm

Fig 6·3

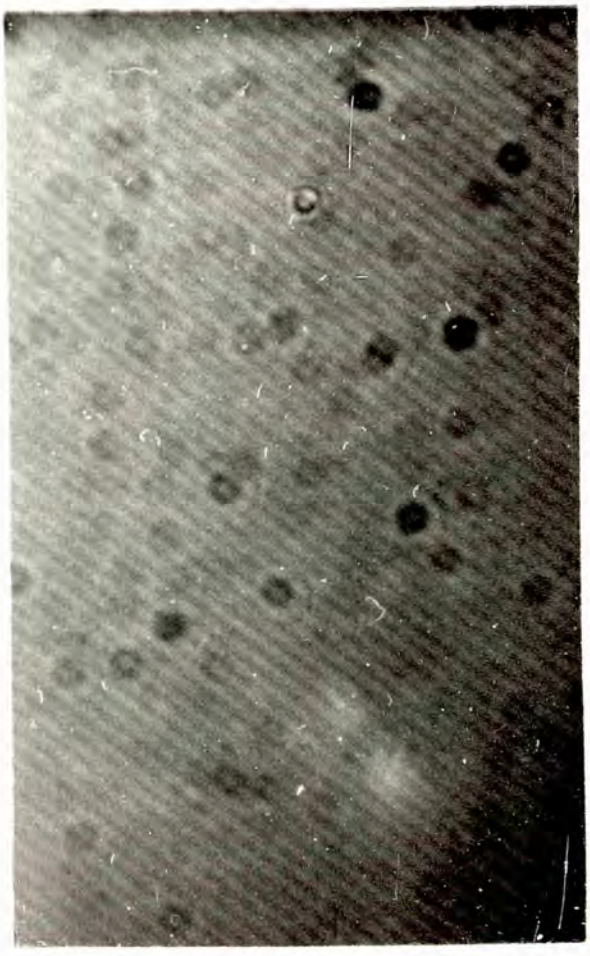

photograph represent the magnification of the reproduced print whilst NX refers to the magnification of the microscope camera system.

Platinum, fig. 6.3D, represented a poorly defined modulation. It was conjectured that this was due to the combination of high boiling point (4500°C) and a thermal skin depth $d = (\alpha\tau)^{1/2}$ of the order of the film thickness. Furthermore, the thermal conductivity of pure carbon is 0.0005 and the thermal skin depth is less than the film thickness. No spatial modulation was observed when carbon films were used, whilst silver (K = 0.86) has a skin depth of 82 micron and exhibits a clearly defined modulation, fig. 6.3B. Modulations were also observed with titanium, copper and bismuth films used to Q - switch the laser.

6.2 SUBSTRATE DAMAGE

The damaged areas of all the films exhibited diffraction properties by glistening different colours when illuminated with white light.

Using the 6328 Å radiation from the gas laser the diffracted beams were observed, fig. 6.4A. Measuring the separation of the orders and using the diffraction relation

$$d(\cos\alpha - \cos\beta) = n\lambda$$

where α and β were the incident and diffracted angles measured from the surface, an additional measurement of the spatial period d could be made. The path of the incident and diffracted beams were made visible by blowing chalk dust into the air.

The exact nature of the diffraction of a freshly formed film was difficult to ascertain. Most of the gold from the

A LASER ETCHED GRATING

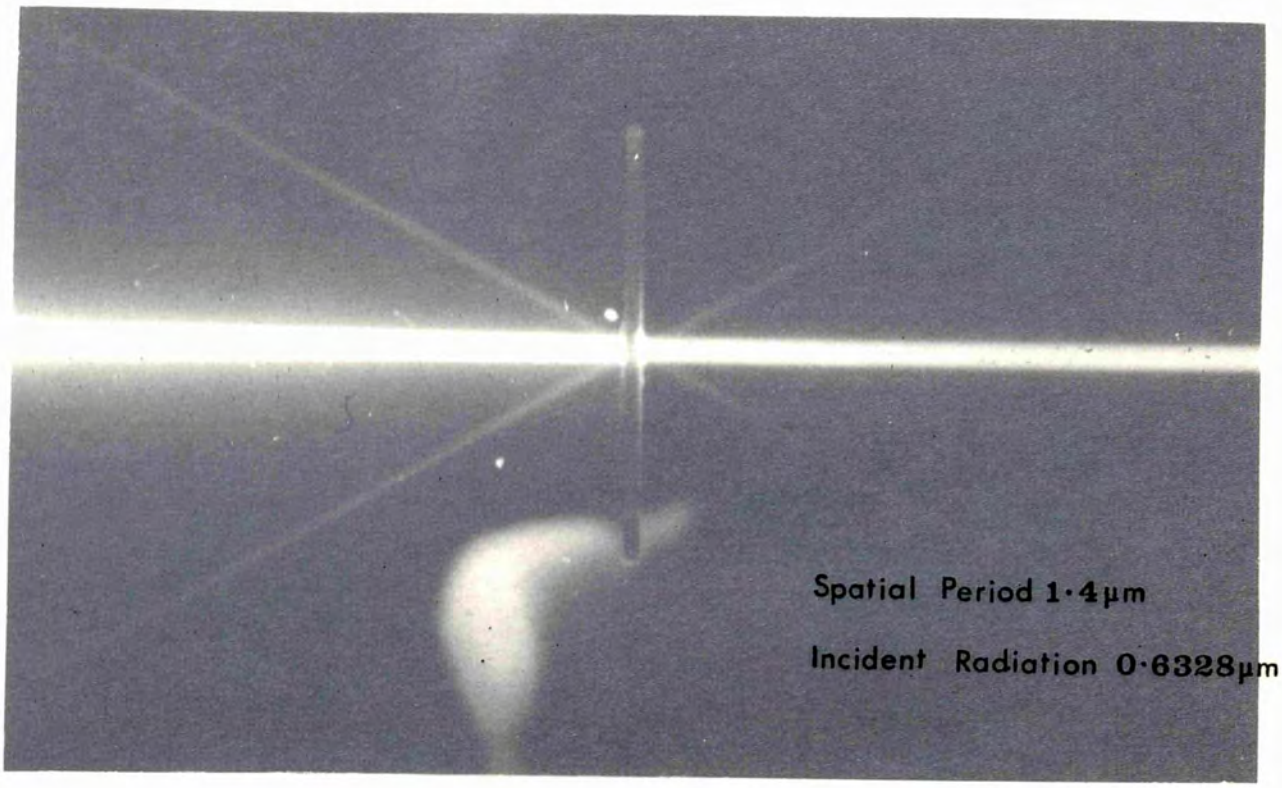

B MICROGRAPH OF ETCHED SUBSTRATE

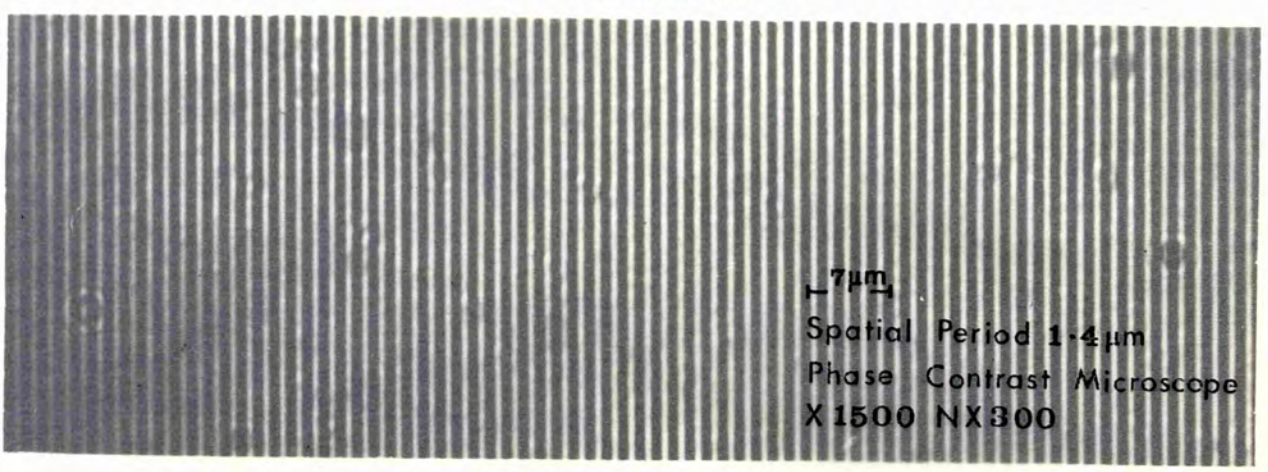

C CPt REPLICA OF (B)

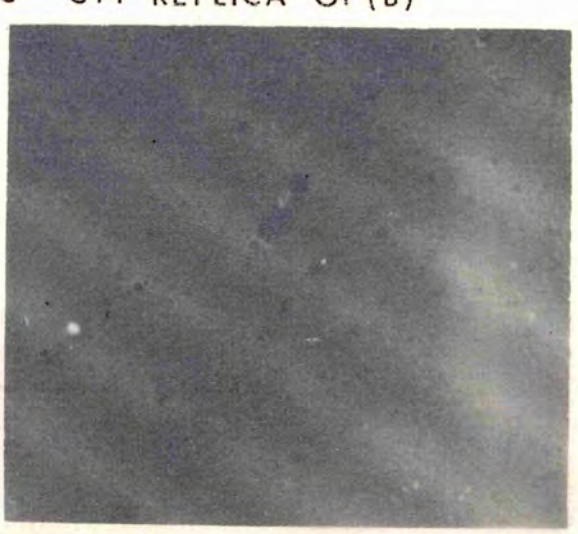

D SODIUM RESONANCE LINES

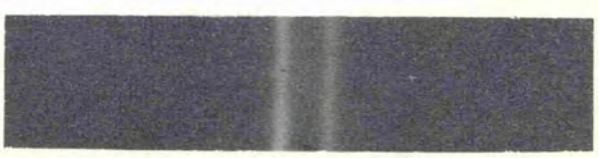

Spatial Period 0·4μm

Angular Separation (1st Order) 5′

Fig 6·4

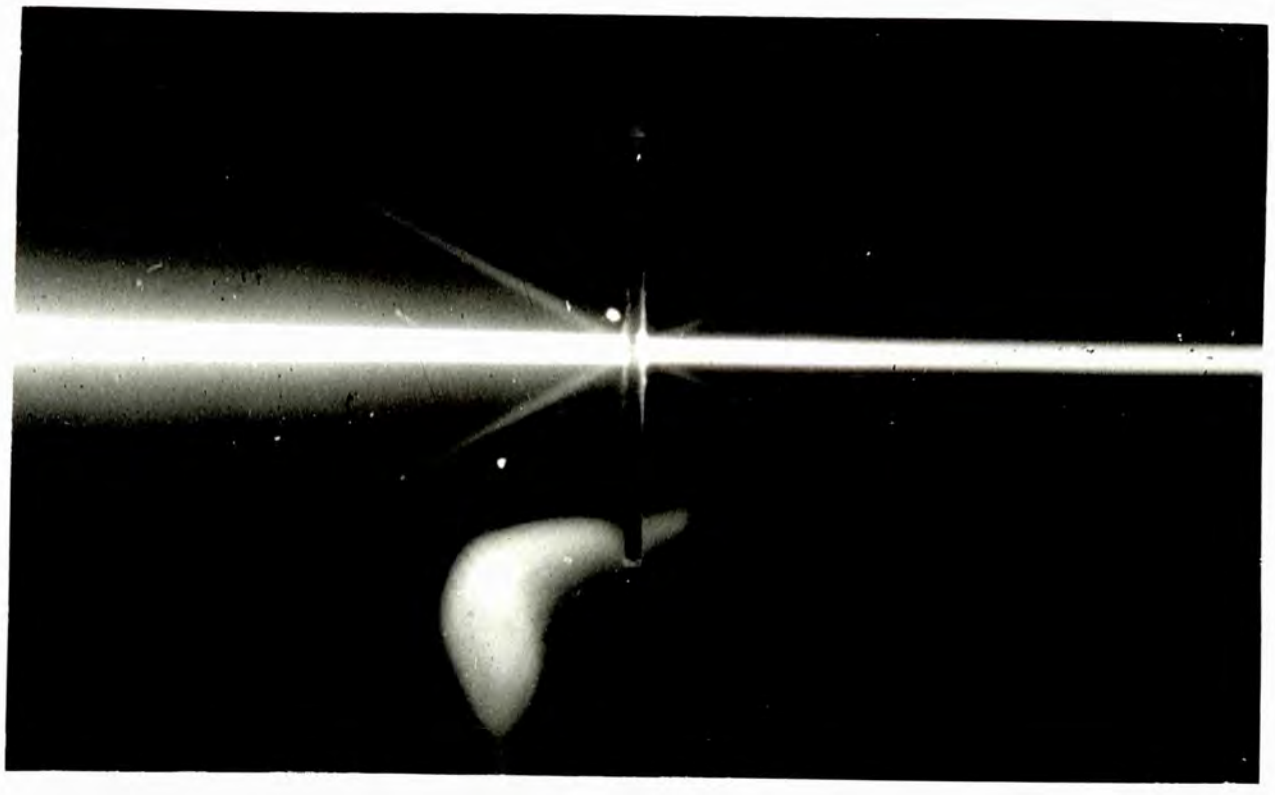

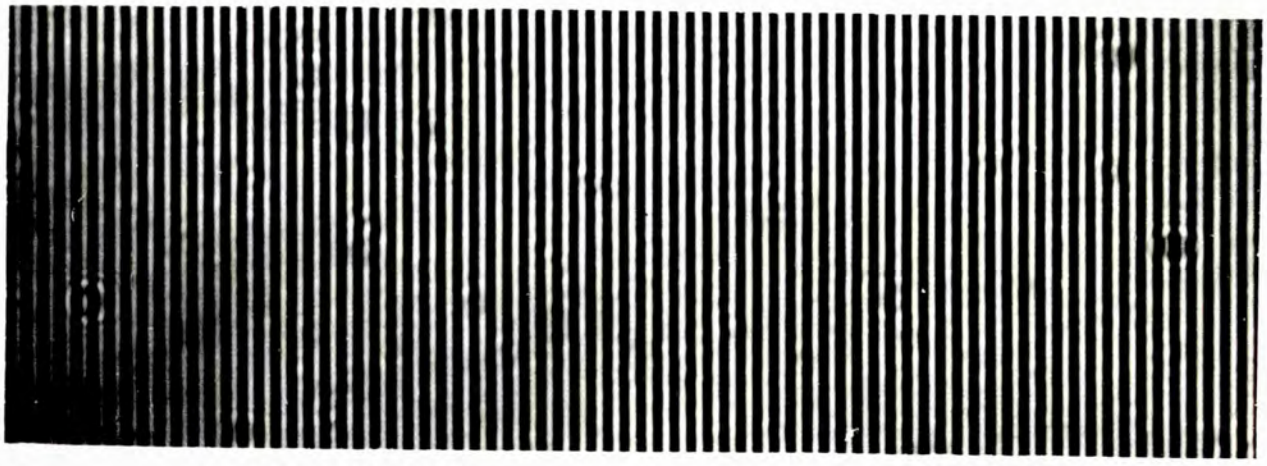

centre of the irradiated region had vaporized. A simple 'amplitude' diffraction process was not applicable. The strength of the diffracted orders suggested that modulation of the glass substrate must have occurred. All traces of gold were removed by soaking the films in aqua regia and after rinsing in distilled water the surfaces were re-examined. The modulations were still present, fig. 6.4B, indicating that the substrate backing had also reached its boiling point. Assuming that the optical absorption of the glass was negligible and that the gold glass interface reached the temperature of boiling gold (2950 C), then thermal diffusion into the substrate duplicated the spatial modulation of the gold.

The modulations observed by optical microscopes did not give any information regarding the modulation profiles. A standing wave results in a $\cos^2$ intensity profile and if it was assumed that the amount of material evaporated from the surface was proportional to the light intensity, the modulation profile should have been similarly defined.

A carbon platinum replica of a cleaned substrate was taken and examined on an electron microscope. The result is reproduced in fig. 6.4C. The smooth undulating nature of the surface is evident. Shadow casting the surface of the replica would have enabled the surface profile to be determined, but this facility was not available.

Subsequent C.Pt. replicas taken from the same area were uniformly successful in recording the profile. This demonstrated that the modulations in the glass substrates were permanent and not composed of loosely adhered glass fragments. The surface

of a cleaned specimen would behave as a phase grating similar to the diffraction from acoustic waves in liquids. By correlating the intensities of the various diffracted orders an assessment of the modulation depth was made (section 6.6).

Resolution as a grating.

To test the resolution of the etched lines when used as a diffraction grating in transmission a 0.4 micron specimen was used. A resolution limit of the order of 1 Å was observed. Specifically the sodium doublet with a separation of 6 Å was easily resolvable, fig. 6.4D. The angular separation of the D lines in first order was 5 minutes. The diffracted intensity was not sufficient for highspeed recording. An exposure of 15 minutes was required and reciprocity failure of the film was responsible for the equal intensities recorded by the D_1 and D_2 lines. (The statistical weights of the upper state in the Principal Series of Alkalis are 4 and 2. Owing to approximately equal excitation energy the population density of $^3P_{3/2}$ state is twice the $^2P_{1/2}$ state and an intensity ratio of 2:1 results.)

6.3 ETCHING WITH FREQUENCY DOUBLED LIGHT

To show that the modulations could also be produced by standing wave systems of different frequencies, gratings were etched with frequency doubled ruby light.

It was necessary to establish first that the absorbing film could be placed outside the laser cavity in the 'extra cavity' arrangement. The standing wave interference system was produced by a third mirror reflecting the laser output normally. To prevent coupled cavity oscillations the external mirror was tilted at an angle larger than the beam divergence.

The laser was Q - switched by a cryptocyanine dye cell and modulations were observed when the absorbing film was close to the third mirror.

The frequency doubled beam $\lambda\omega/2 = \lambda 2\omega$ was generated by passing the laser beam through a 1" x $\frac{1}{2}$" x $\frac{1}{2}$" crystal of ADP.[36] To generate a reasonable amount of frequency doubled light, phase matching conditions had to be satisfied.[45] This was easily accomplished as the cuboid had been specifically cut with its axis at $42\frac{1}{2}^{\circ}$ to the optic axis. At normal incidence to the plane parallel polished faces the laser fundamental and second harmonic travelled as the ordinary and extra-ordinary rays respectively in the birefringent crystal (i.e. $n_{\omega}^{o} = n_{2\omega}^{e}$). Nevertheless, critical 'tuning' of the crystal was required and any deviation gave a sharp decline in frequency doubled power. The 'tunable' range was in the region of $\frac{1}{2}^{\circ}$.

Fig. 6.5 shows the optical arrangement used. The ruby laser in this case was a commercial unit (Bradley 351) and the ruby rod was plane parallel ended and water cooled. This greatly aided 'tuning' of the ADP crystal when high pulse repetition rates were required. The diode D_1 was calibrated in the manner described in chapter 3 and an approximate calibration for D_2 achieved, utilizing the ratio of absolute sensitivity at $\lambda\omega$ and $\lambda 2\omega$ for the S 10 photocathode. The oscilloscope traces, fig. 6.5, gave an approximate second harmonic conversion efficiency of 3% for a 63 MW peak power input pulse. A no. 18A filter efficiently discriminated against the ruby fundamental and allowed only 3471 Å radiation to reach the absorbing plate inclined at an angle θ to the beam. The mirror M_3 was a massive ($\sim 100\mu m$) silver layer on

EXTRA-CAVITY ETCHING WITH FREQUENCY DOUBLED RUBY LIGHT ($\lambda = 0{\cdot}3471\,\mu m$)

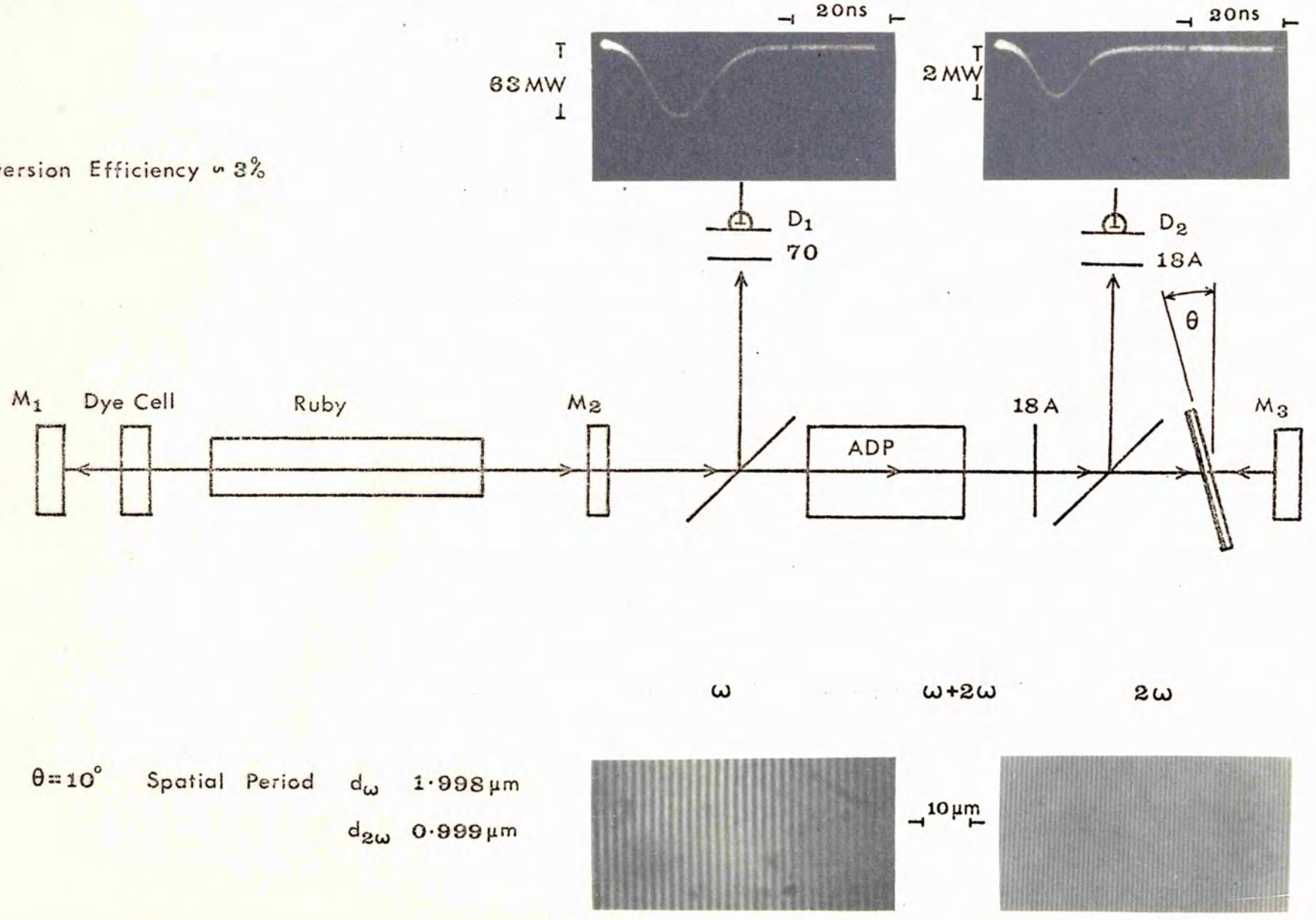

Fig 6·5

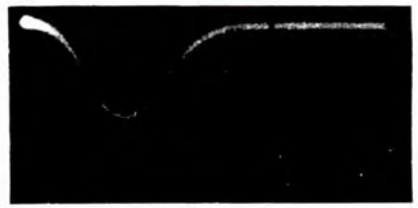

a glass backing. Such a mirror provided good heat transfer and was less susceptible to damage.

At $\theta = 10^\circ$ the expected spatial periods for $\lambda\omega$ and $\lambda 2\omega$ are two and one micron respectively. Spatial periods of one micron were observed with the arrangement shown and, by removing the ADP crystal and filter, modulations at two micron were observed.

It was possible, by counting fringes, to determine the exact ratio of the wavelengths $\lambda\omega/\lambda 2\omega$. It was reckoned that a displacement of one tenth of a fringe could be detected from the microdensitometer traces of the negatives. Taking this as the maximum possible error in a count of 100 frequency doubled fringes the ratio was

$$\frac{\lambda\omega}{\lambda 2\omega} = 2.000 \mp 0.001$$

The point is not a trivial one, as even the slightest departure from a ratio of 2 cannot be explained by currently accepted theories. The only work published on this subject[130] established the ratio as 2 to one part in 10^6 by wavelength comparisons on a twenty one foot grating spectrometer.

The finest line spacing that could be obtained with frequency doubled radiation was closely approximated to at an angle $\theta = 60^\circ$ d = 0.20 micron. The separation was close to the resolution limit for optical microscopes and the lines could not be resolved. However, diffraction of an argon ion laser source at 4880 Å indicated that modulations had been recorded for a film etched with $\theta = 45^\circ$ (d = 0.24 micron). From data obtained a 200 Å gold film was capable of a resolution in excess of 4,000 line pairs per mm.

The spatial period of the small gratings that can be produced by thermal etching closely approaches the limit set by conventional techniques and surpasses photographic techniques by an order of magnitude. The resolving power of a diffraction grating also depends on the total number of lines and a photographic emulsion can record a grating over an area of one square yard with a relatively coarse spatial period.

6.4 OPTICAL MESHES AND FILTERS

Metallic gratings with $d < \lambda$ could form the basis of metallic meshes, filters and grid polarizers at optical wavelengths, similar to those used in the infra-red.[131,132]

Fig. 6.6A shows a laser etched mesh produced by rotating a 200 Å gold film through 90° between successive laser firings. In the array the gold areas show as white squares. The diffraction of 6328 Å radiation by the mesh is shown in fig. 6.6B.

Complete analysis of the optical properties of a mesh is complex. When $\lambda > d$ diffraction does not occur at normal incidence and the transmission is high. As λ decreases to $\lambda = d$ the transmission reaches a minimum. Such a mesh is a short circuit to high frequency signals and may be called a 'capacitative' mesh. The mesh fig. 6.6A should have shown a cut off at $\lambda = 2.5$ micron but no sources or detectors were available. A mesh was fabricated to cut off in the region of 5896 Å but no effect was observed using the sodium resonance line and a photomultiplier. As shown by Auton,[131] by cascading several meshes the transmission is the product of the individual elements and a dramatic improvement can be attained with meshes separated by less than the coherence length of the source used.

A LASER ETCHED MESH

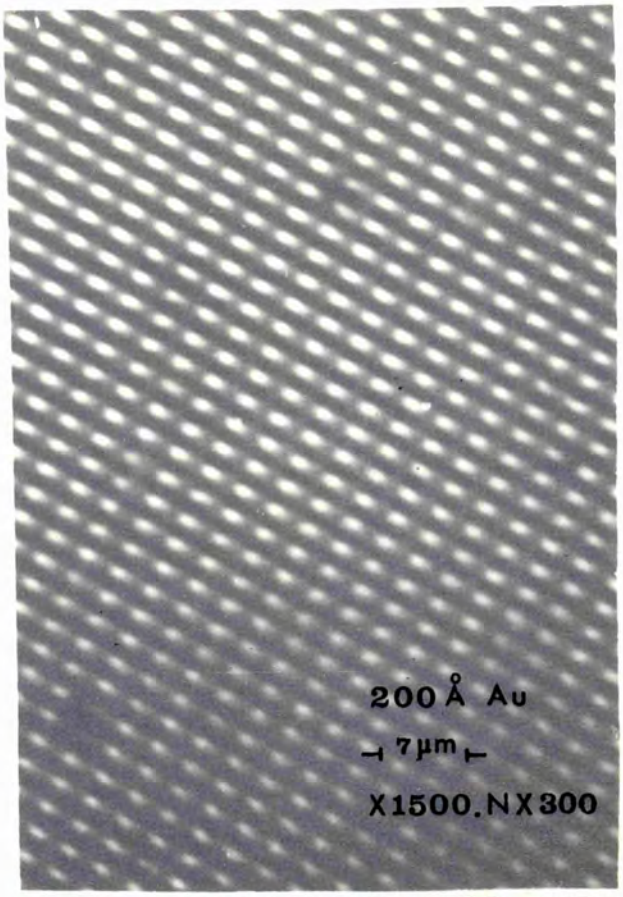

B DIFFRACTION PHOTOGRAPH OF (A)

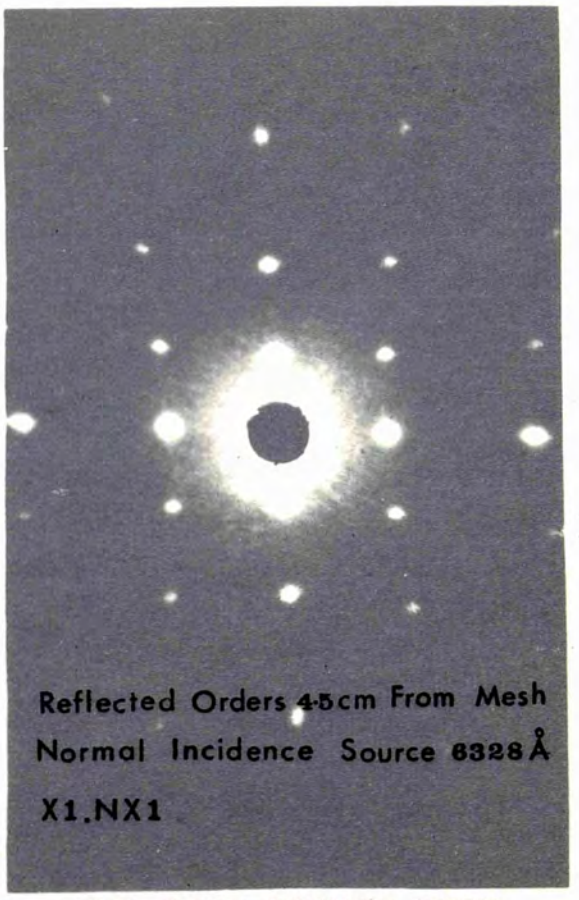

C GRID ETCHED WITH FREQUENCY DOUBLED RUBY LASER LIGHT

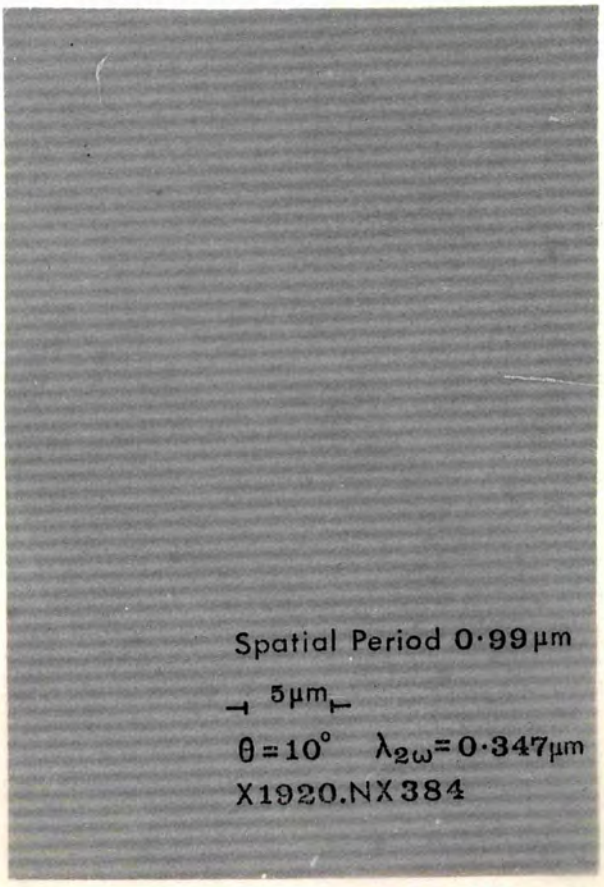

D FINE GRID ETCHED WITH RUBY FUNDAMENTAL

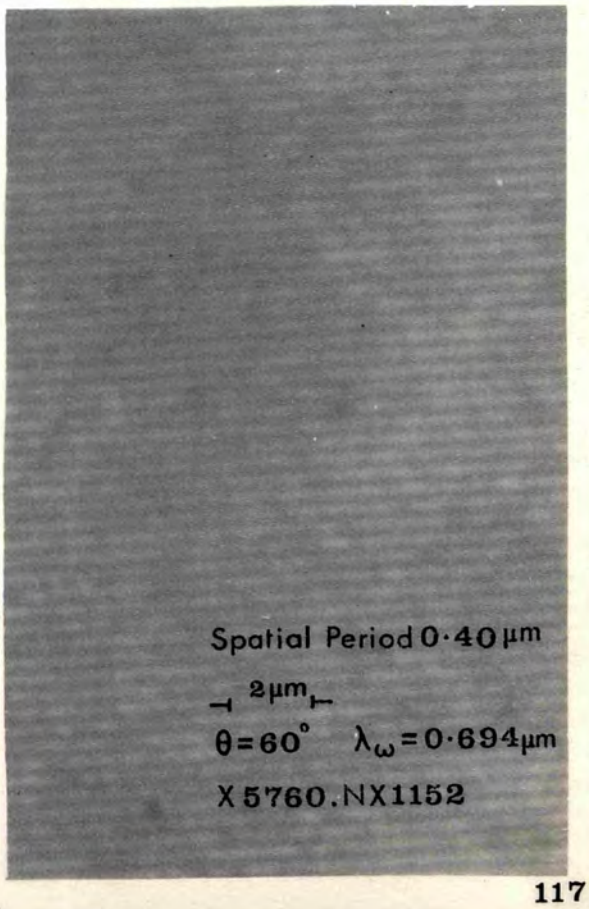

Fig 6·6

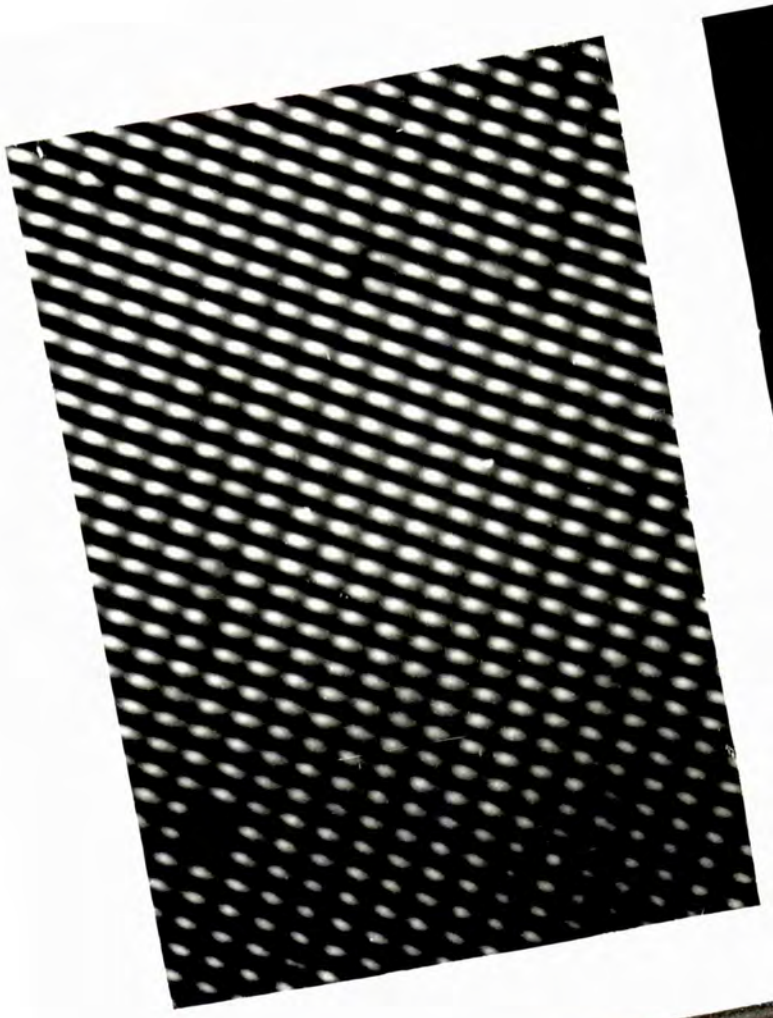

Infra-red interference meshes are commercially available.[133] However, the failure of a single mesh to show any effect was due to the gold thickness being less than the electrical skin depth at optical frequencies. Increasing the film thickness t to a value such that $t = \delta = \left|\frac{2}{\omega g \mu}\right|^{\frac{1}{2}}$. (g conductivity, μ permeability, ω angular frequency) would have precluded the use of the film as a Q - switch.

The fine grids shown in fig. 6.6C,D did not possess the symmetry of the mesh shown in 6.6A and such grids had different transmission and reflection behaviour for orthogonal polarizations. The experimental results on the first diffracted order for orthogonal polarizations are shown in fig. 6.7A. The ratio $I_{\parallel}/I_{\perp}$ is plotted as a function of wavelength for a series of laser etched gratings with spatial periods less than one micron. In this case $I_{\parallel}$ defines the intensity recorded when the incident light was polarized parallel to the grooves and conversely for $I_{\perp}$ Each of the grids was set at a pseudo-Littrow position for the wavelength used; the angle between incident and diffracted radiation was defined by the spectrometer table as 23°. All the grids had been cleaned in aqua regia and recoated with a one micron gold layer.

The behaviour shown in fig. 6.7A cannot be accounted for by the commonly used Huygens formalism. Such an approach incorrectly assumes that the plane diffracted waves are built up by an envelope of 'little wavelets'. It is also a fallacy to assume that when a plane wave is incident on a plane diffraction grating the diffracted waves are also plane and exist only in a discrete set.

A POLORIZATION EFFECTS FOR $E_\perp$ AND $E_{||}$

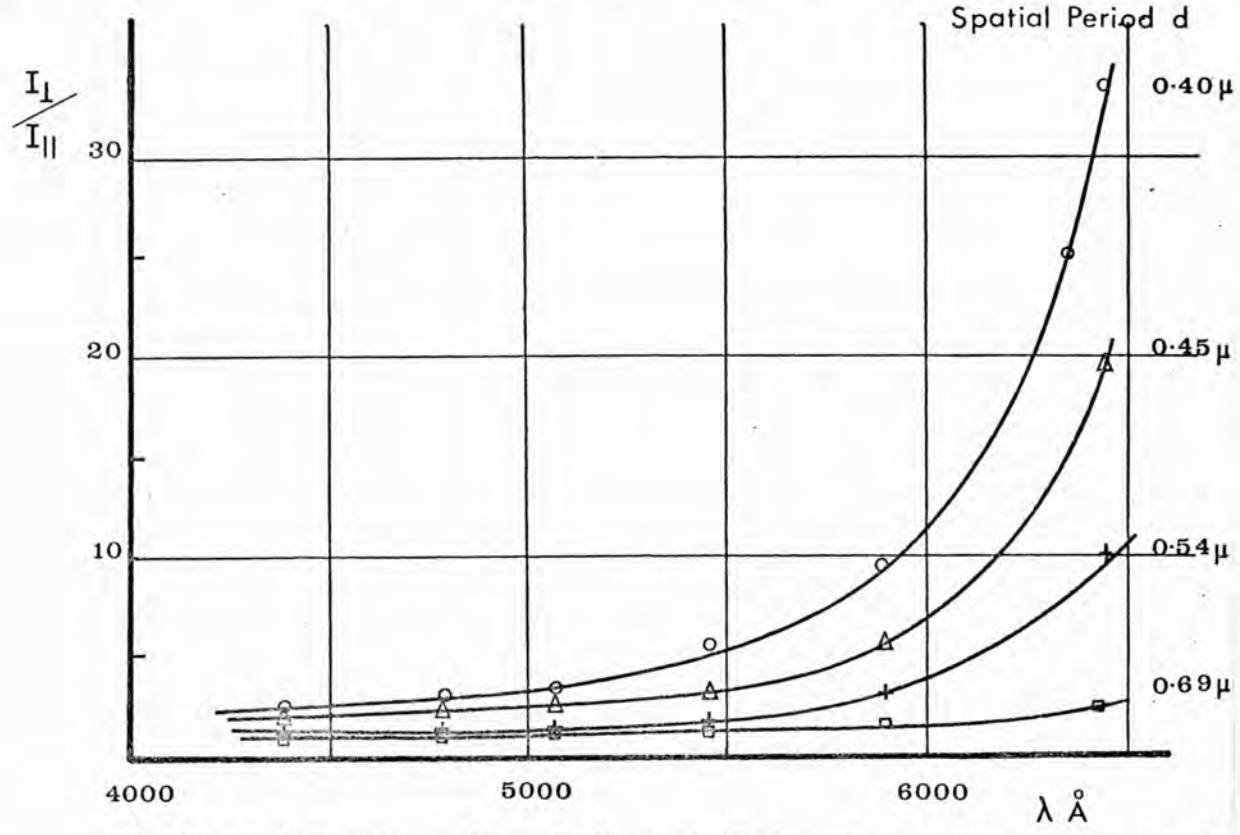

Au Coated Gratings. First Reflected Order. Pseudo Littrow Mounted.

B ORIENTATION SENSITIVITY OF DIFFRACTED INTENSITY

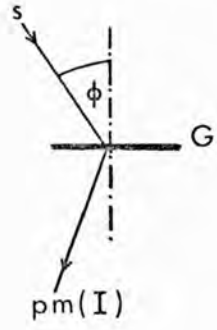

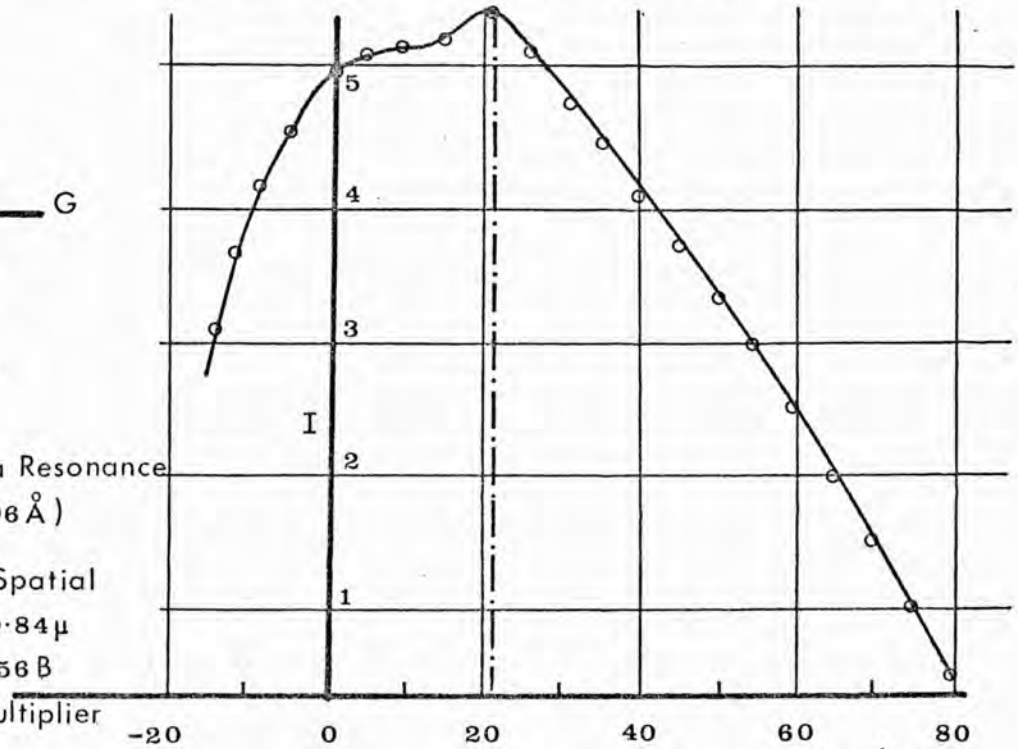

s Source. Na Resonance Line (5896 Å)

G Grating. Spatial Period 0·84μ

pm EMI 6256B Photomultiplier

I Relative Intensity Of First Transmitted Order

Fig 6·7

Consider a two dimensional surface described by the surface function periodic in x

$$S_{x+pa} = S_x \qquad S = f(xy) \qquad p \text{ integer}$$

Although two dimensional problems are essentially scalar, in the case of an electromagnetic field the field may be defined in terms of a single variable E_z or H_z.

E_z must satisfy the wave equation

$$\frac{\delta^2 E_z}{\delta x^2} + \frac{\delta^2 E_z}{\delta y^2} + \frac{\delta^2 E_z}{\delta z^2} = k^2 E_z \qquad 23.$$

where $K = 2\pi/\lambda$ and $e^{j\omega t}$ is implied. An elementary solution of 23 is

$$E_z = \exp\left|jk(x\sin\theta + y\cos\theta)\right|$$

A complete solution of 23 is formed by an angular spectrum of plane waves represented by the Fourier Integral

$$\int_{-\infty}^{\infty} E|\theta| \exp\left|jk(x\sin\theta + y\cos\theta)\right| d\theta$$

Let E_z^i be the component of the incident field

$$E_z^i = \exp\left|-jk(x\sin i + y\cos i)\right|$$

and E_z^d the diffracted field such that

$$E_z = E_z^i + E_z^d$$

Since E_z and E_z^i satisfy the wave equation so must E_z^d . The Fourier Integral of the diffracted waves is

$$E_z^d = \int_{-\infty}^{\infty} E_z^d(i') \exp\left|jk(x\sin i' + y\cos i')\right| di' \qquad 24.$$

where $E_z(i')$ represents the amplitudes of the diffracted waves at i'

Now equation 23 suggests an infinity of diffracted waves but the periodic nature of the boundary and the fact that the boundary conditions must be satisfied by the total field E_z restrict the continuous distribution to a discrete set of waves.

On the surface $E_{z(x+pa)} = E_{z(x)}$

TOTAL TOTAL

Therefore

$$\exp\left|-jk(x\sin i+y\cos i)\right|\exp\left|-jkpa\sin i\right| + \int_{-\infty}^{\infty} E_z^d\left|i'\right|\exp\left|jk(x\sin i'+y\cos i')\right|\exp\left|jkpa\sin i'\right|di'$$

$$= \exp\left|-jk(x\sin i+y\cos i)\right| + \int_{-\infty}^{\infty} E_z^d i'\exp\left|jk(x\sin i'+y\cos i')\right|di'$$

Dividing by $\exp\left|-jk(x\sin i+y\cos i)\right|$

$$\exp\left|-jkpa\sin i\right|\left[1+\int_{-\infty}^{\infty} E_z^d i'\exp jk\left|x+pa\langle\sin i+\sin i'\rangle\right|di'\right]$$

$$= 1+\int_{-\infty}^{\infty} E_z^d i'\exp jky\langle\cos i'+\cos i\rangle\exp jkx\langle\sin i'+\sin i\rangle di' \qquad 25.$$

For a given k, p, a & i $\quad \exp -jkpa\sin i = R = \text{const}$

Therefore for 25 to be satisfied $\quad R\left|1+\exp jkpa\langle\sin i+\sin i'\rangle\right|\int_{-\infty}^{\infty} f\langle i\rangle = 1+\int_{-\infty}^{\infty} f\langle i\rangle$

Therefore $\quad \exp jkpa\langle\sin i+\sin i'\rangle = \text{const}$

i.e. $\quad k\langle\sin i+\sin i'\rangle = m\,2\pi/a \qquad m$ integer

Therefore $\quad \sin i+\sin i' = m\lambda/a$

which is the grating equation and discretness is observed.

This means that equation 24 becomes

$$E_z^d = \Sigma_m (E_z^d)_m \exp jk(x\sin i'_m + y\cos i'_m)$$

It is the boundary conditions and the periodicity of the grating which are at the origin of diffraction. It is remarkable that the exact nature of the boundary condition is not required to derive the grating equation and demonstrate the existence of plane diffracted waves. However, the amplitudes $E_z^d(i_m)$ of the diffracted waves do depend on the precise nature of the boundary, in particular its material as well as the groove shape. In the case of a grating where $d < \lambda$ the boundary condition for $E_{\parallel}$ must be continuous from zero in the metal to non-zero in the groove. On the other hand the boundary condition for $E_{\perp}$ is not continuous across the groove. Assuming that all points within the groove are capable of radiating, $E_{\perp}$ will be greater than $E_{\parallel}$.

This was demonstrated by fig. 6.7A when $I_{\perp}/I_{\parallel}$ reached 35 for the cadmium red line (0.6439 μm) radiation incident on a 0.4 μm grating.

Bragg reflection.

The efficiency of a particular grid defined as $\frac{\text{diffracted power}}{\text{incident power}}$ was found to be dependent on the angle of incidence of the illuminating beam. Fig. 6.7B shows the observed variation of I for the first diffracted order in transmission. The grid had a spatial period d = 0.84 μm and the incident light λ = 5896 Å.

The observed sensitivity with respect to angle is characteristic of grids made with photographic emulsion when the spatial period is less than the emulsion thickness.[71] (For Kodak 649 F film the emulsion is about 10 μm thick after development.) In this case the grid really consists of planes extending through the emulsion and Bragg reflection occurs from

these planes when the angles of incidence and diffraction are equal and the Bragg condition

$$\sin\phi = \frac{n\lambda}{2d} \qquad 26.$$

is satisfied.

Using the known values of λ and d Bragg reflection for the laser etched grating would occur at an incidence angle defined by 26 $\phi = 20^\circ\ 20'$ $(n = 1)$.

As fig. 6.7B shows, the diffracted intensity was not symmetrical about $\phi = 0^\circ$ and a maximum was observed at $\phi = 20^\circ 10'$. There should have been another peak at $\phi = 44^\circ$ but this was not observed.

A Bragg reflection situation should show a sharp angular dependence. The small peak observed was approximately 8° wide and was comparable to the angular width of Bragg peaks observed with thin photographic emulsions.[69]

The width of the peak can be explained by considering the groove profile. A square wave shape would produce a sharp peak; when the profile is continuously variable the groove edge may be described by an average slope, excursions about the mean causing a blurring of the Bragg reflection condition.

6.5 SEQUENTIAL THERMAL ETCHING

The depth of the metallic film is of prime importance for increasing the efficiency of the gratings for applications such as mesh filters. Diffraction efficiency is also a function of modulation depth and a method of increasing the latter was devised.

The laser system could be operated for a second 'shot' after the initial firing with a gold film Q - switch. The

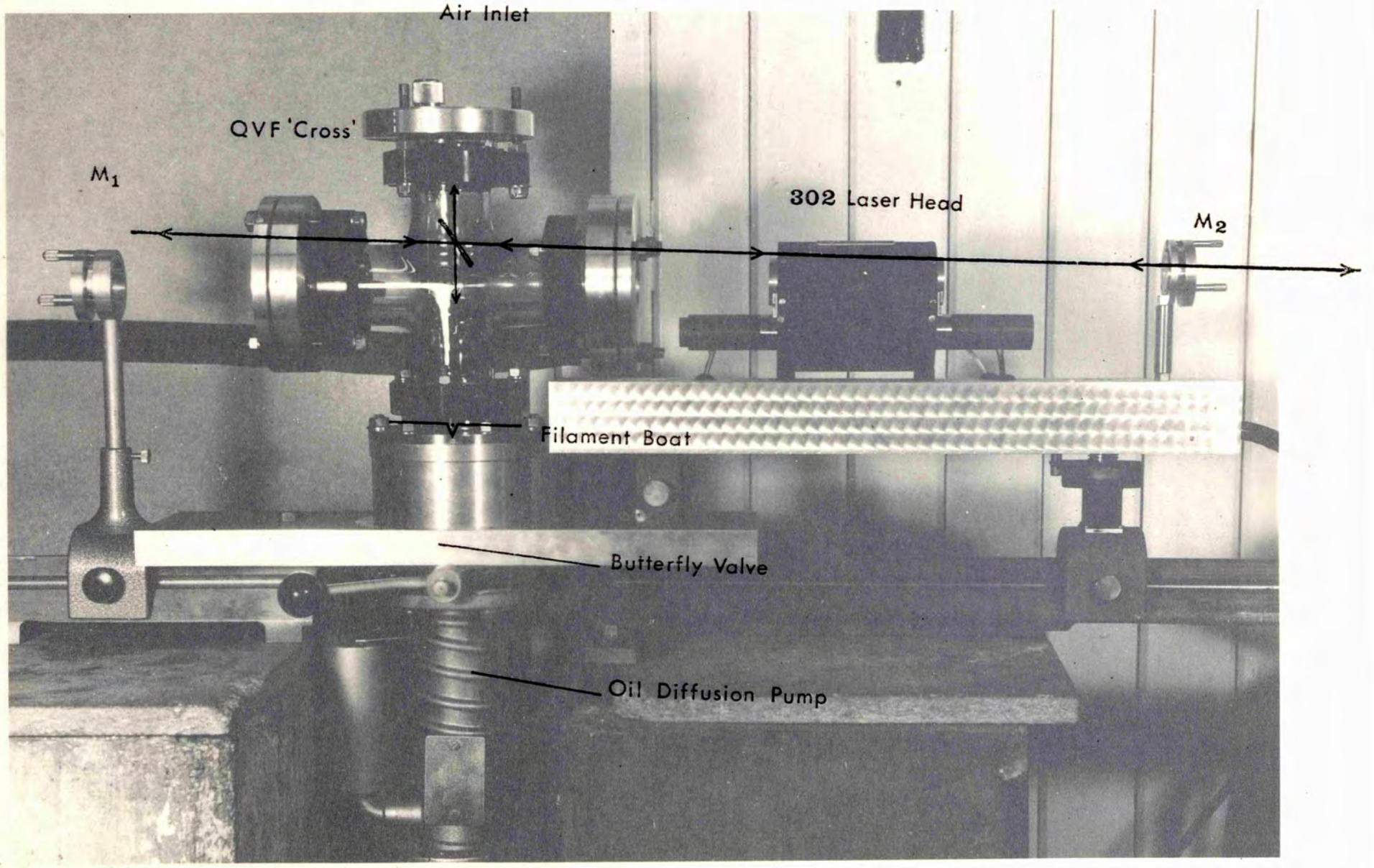

Fig 6.8

ARRANGEMENT FOR IN SITU COATING OF Q-SWITCH FILMS

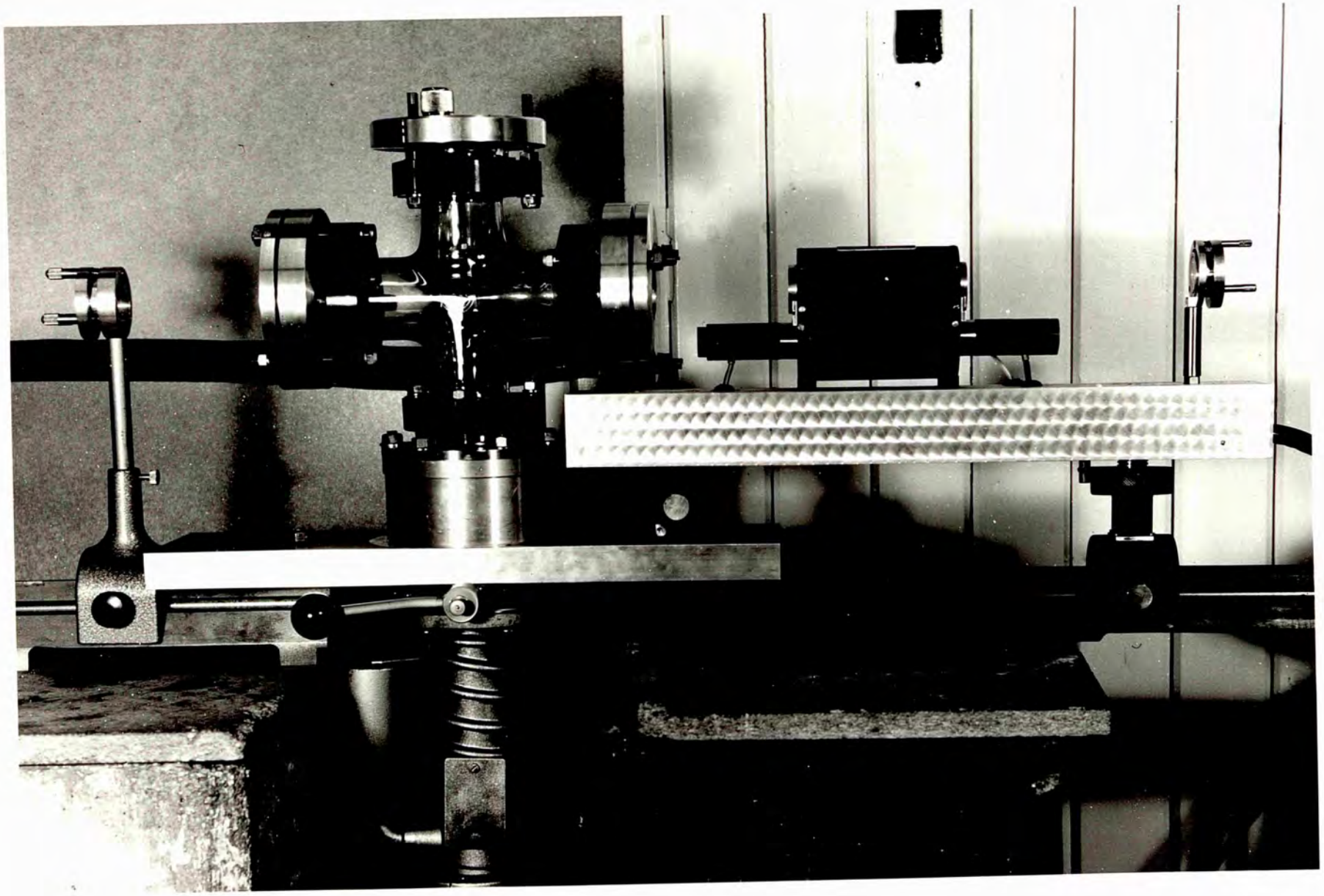

output of these subsequent firings was the same as from a free running laser and consisted of a series of microsecond spikes. Subsequent shots, up to twenty, were uniformly successful and no degradation of the modulation profile was observed. If then the substrate was recoated after each firing with a further 200 Å gold layer, the modulation profile could be built up.

The film must not move between subsequent shots. Fig. 6.8 shows the system built to provide an in situ coating facility for the films. The laser head used was a Bradley 302 and between the rod and the maximum reflectivity rear mirror M_1 a Q.V.F. 'cross' section was mounted with flat glass plates on two of the arms. The bottom arm was connected via a butterfly valve and an oil diffusion pump to a rotary pump. It was not necessary to have a roughing line between the rotary pump and the 'cross' section as the volume of the latter was quite small. An air inlet valve was provided on the metal plate closing the fourth arm. The stirrup arrangement for holding the glass substrates was also fixed to the top plate. A small tungsten boat connected to a filament transformer was mounted in the region between the valve and the bottom arm. The evaporant, produced by electrically heating the boat containing a metal, condensed on the glass substrate above. No vacuum gauge was fitted and the chamber was assumed to be in the region of 10^{-5} torr when the rotary pump made a hard knocking noise. Such an audible gauge was found to be satisfactory as evidenced by the high quality films deposited.

A He Ne gas laser was used to align the optical system and the leakage radiation through M_1 was used as a thickness monitor. Evaporation was stopped when a signal from a P.I.N.

diode placed behind M_1 reached a level previously defined by a 200 Å reference layer produced in the Edwards 18" vacuum system. The evaporation time and current were also noted.

Successful etching of the gold layers evaporated in the integral system was achieved and subsequent evaporations produced giant pulses, albeit of smaller magnitude. The reduction in power was caused by the intensity profile of the laser beam. As shown in chapter 3 the intensity profile across the ruby has a pronounced hump. Subsequent giant pulses generated by the recoated films accentuated the profile and after three shots the lasing area was reduced to fractions of a millimetre until finally threshold could not be reached. This effect was more pronounced in the Bradley 302 laser head which had a focused elliptical pump geometry.

Nevertheless two important facts were established. After three successive evaporations the small central area showed a distinct series of lines clearly thicker than the 200 Å single shot lines. This increase manifested itself in stronger diffracted orders for 6328 Å gas laser radiation. The area also appeared gold coloured as opposed to the greenish blue appearance of a 200 Å gold layer. It had been thought that the impulse caused by the absorption of the light and to a lesser extent the momentum imparted by the vaporizing material may have caused the substrate to move.[134] That surface modulations were observed after three successive shots meant that any such movement was certainly less than $\lambda/2$. Such stability would be required in holographic applications if the high density, multiple storage facility of the thin metallic film were to be exploited.

6.6 MEASUREMENT OF MODULATION DEPTH

6.6I MICROSCOPE FOCUS

An approximate method, using a microscope, was devised to estimate the modulation depth. In fig. 6.9A the surface is assumed to have a curved feature, radius r, of unknown origin. For incident parallel light entering through the glass two foci are formed depending on the curvature being positive or negative. For parallel light in the dense medium n' (glass) the two foci are equally distant from the surface median OX i.e. f = f'. The focal length and curvature are related by

$$\frac{n}{f} = \frac{n' - n}{r} \qquad 27.$$

When reviewing the modulations under a microscope two distinct focal positions existed at positions F_1 and F_2, fig. 6.10A,B and

$$2(f + z) = F_1 \sim F_2 \qquad 28.$$

Finally the geometrical relation

$$z(2r - z) = x^2 \qquad 29.$$

is applicable to the chord formed by the intersect of the median OX with the circle radius r.

The spatial period $d = 4x$ **30.**

Solving 27 to 30

$$\left[\frac{n}{n' - n} + 2\right] z^2 - (F_1 \sim F_2)z + \left[\frac{n}{n' - n}\right]\frac{d^2}{16} = 0 \qquad 31.$$

Two values were derived from equation 31. When $d = 7.2\,\mu m$ $z = 2.9\mu m$ or $0.5\,\mu m$. The higher value was discounted as such a depth would have been resolvable by viewing the substrate 'edge on'. Measurement on the other grids gave values for z in the region of $0.5\,\mu m$ whilst the higher 'discounted' value fluctuated. Over the surface of a single specimen z varied by

MEASUREMENT OF MODULATION DEPTH

A Displaced Focus Method

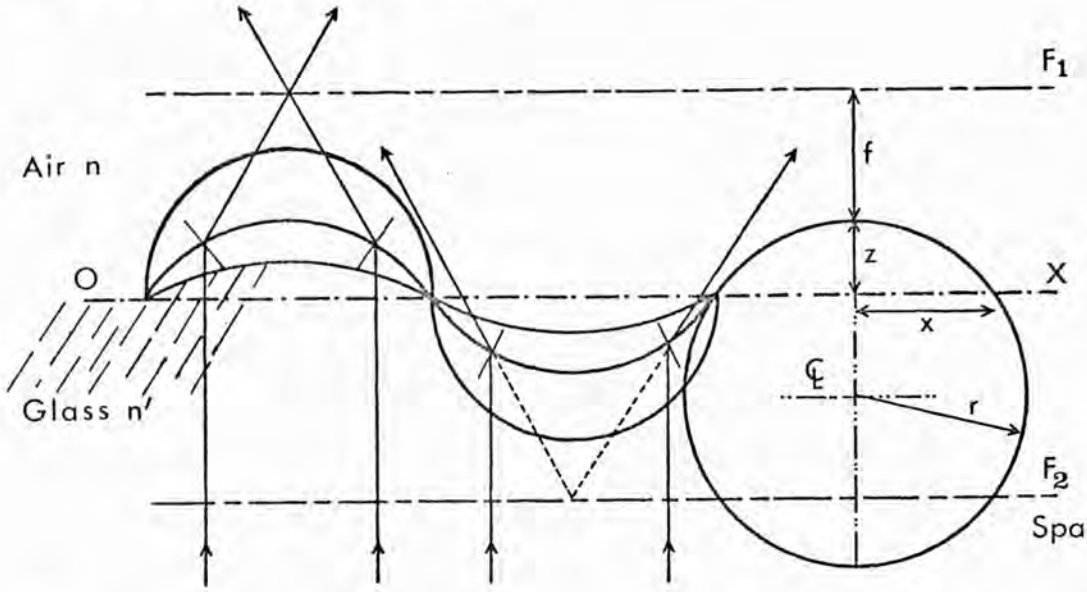

$$\frac{n}{f} = \frac{n'-n}{r}$$

$$2(f+z) = F_1 \sim F_2$$

$$z(2r-z) = x^2$$

B Light Profile Microscope

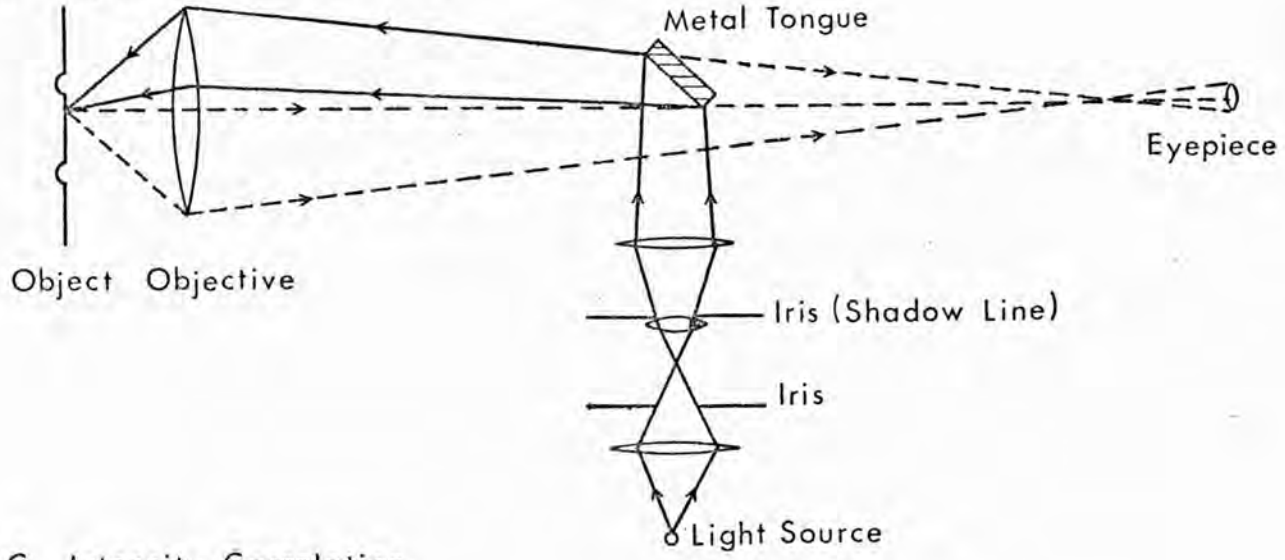

C Intensity Correlation

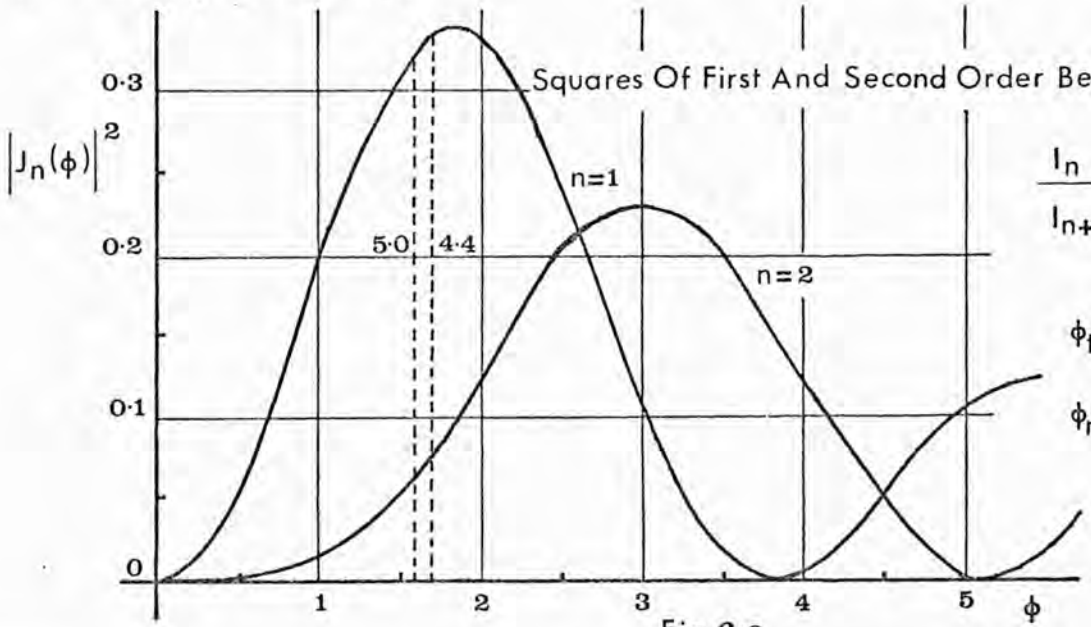

$$\frac{I_n}{I_{n+1}} = \left|\frac{J_n(\phi)}{J_{n+1}(\phi)}\right|^2$$

$$\phi_t = \frac{2\pi(n'-n)D}{\lambda}$$

$$\phi_r = \frac{4\pi D}{\lambda}$$

Fig 6·9

up to 50% especially in the region near the edge of the pattern. It is usual to speak of the peak to peak height of the modulations 2D and by this method 2D was in the region of one micron.

6.6II LIGHT PROFILE MICROSCOPE

The elegant light profile microscope developed by Tolansky[135,136] was used to measure the modulation depth.

The microscope is shown schematically in fig. 6.9B. A microscopic shadow of a straight line is cast at a known angle on the surface. This shadow is displaced, relative to an average position, by any changes in height, similar to the segmented shadow cast by a hand rail on an open staircase. The shadow was cast by a small scratch on a piece of glass placed close to the plane of the field iris, fig. 6.9B. Since the iris was focused on the surface of the object, the scratch was also in focus on the object. The object was viewed in reflected light sent in as an oblique pencil by the metal mirror. Adjusting the relative positions of the scratch and the microscope focus resulted in a fine shadow line contouring the microtopography of the surface. Selection of a previously calibrated lens meant that the magnification in the 'up and down' direction was exactly the same as laterally. Photograph fig. 6.10C shows the microtopography of a 3.6μm grid. The spatial period and displacement of the shadow line were measured with a micrometer eyepiece. In this case the peak to peak height 2D was 0.53 μm whilst measurement by the displaced focus method gave 2D between 0.5 μm and 1.0 μm.

The patchiness of the modulated area, fig. 6.10C was associated with variations of intensity within the laser beam

MEASUREMENT OF MODULATION DEPTH

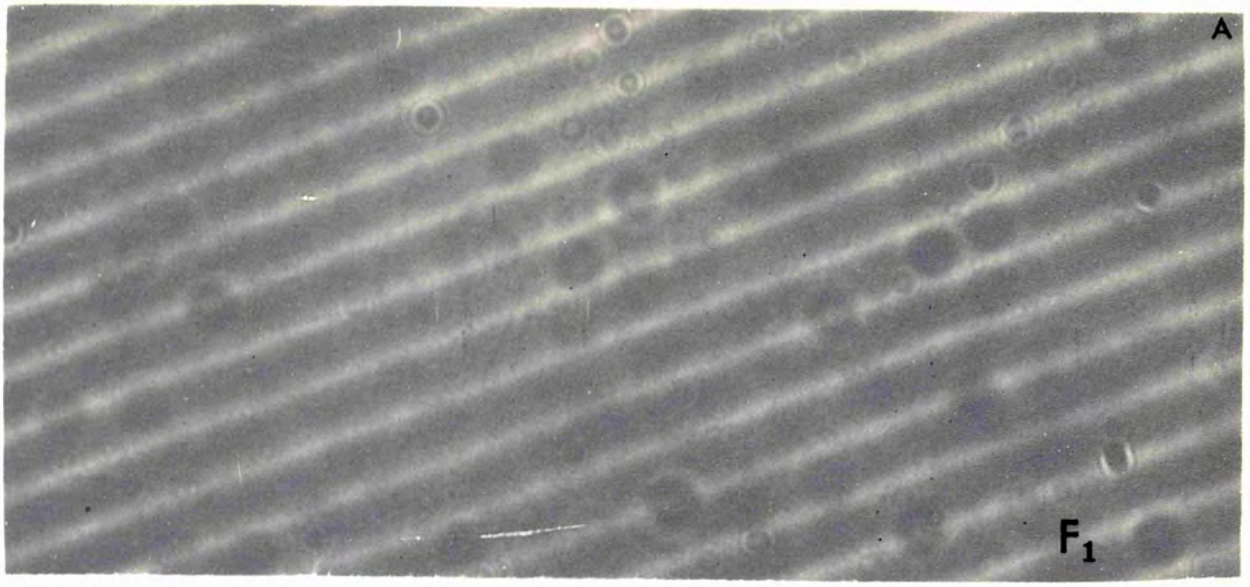

FOCAL SEPARATION METHOD

Spatial Period 7·27μm

$F_1 \sim F_2 = 14\mu m$

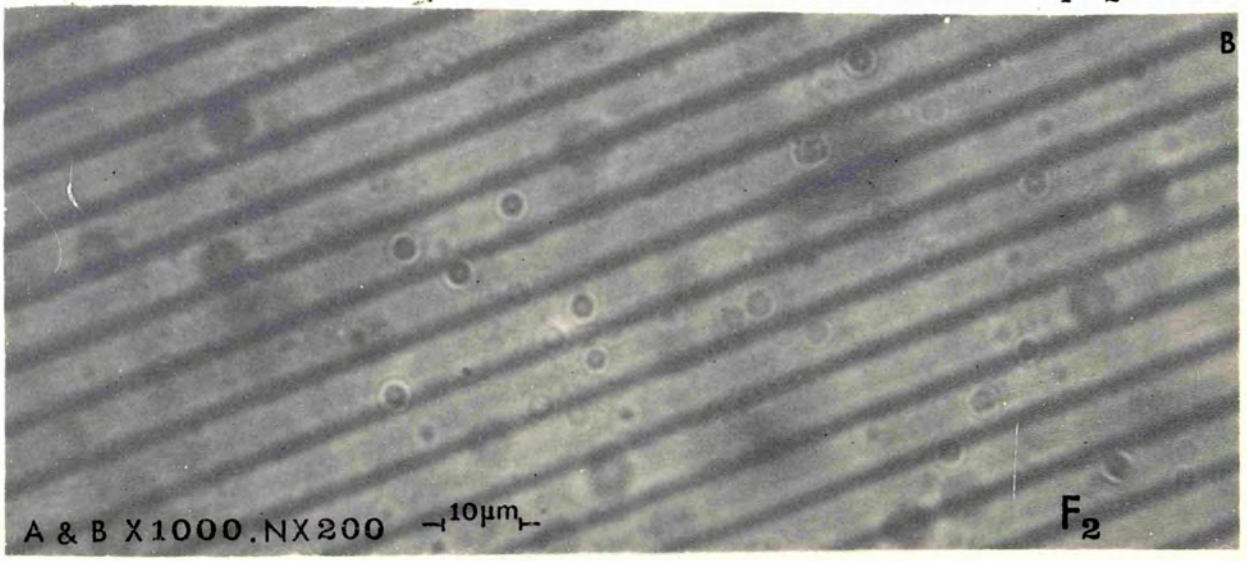

SURFACE PROFILE MICROSCOPE

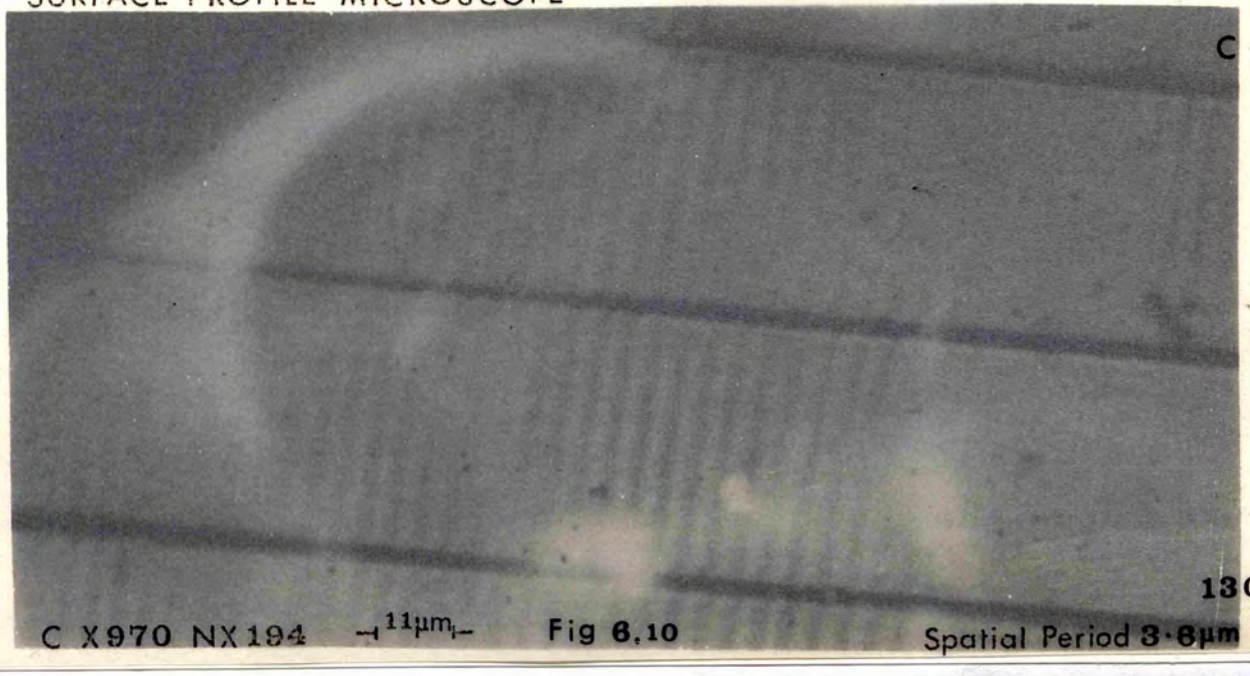

Fig 6.10

Spatial Period 3·6μm

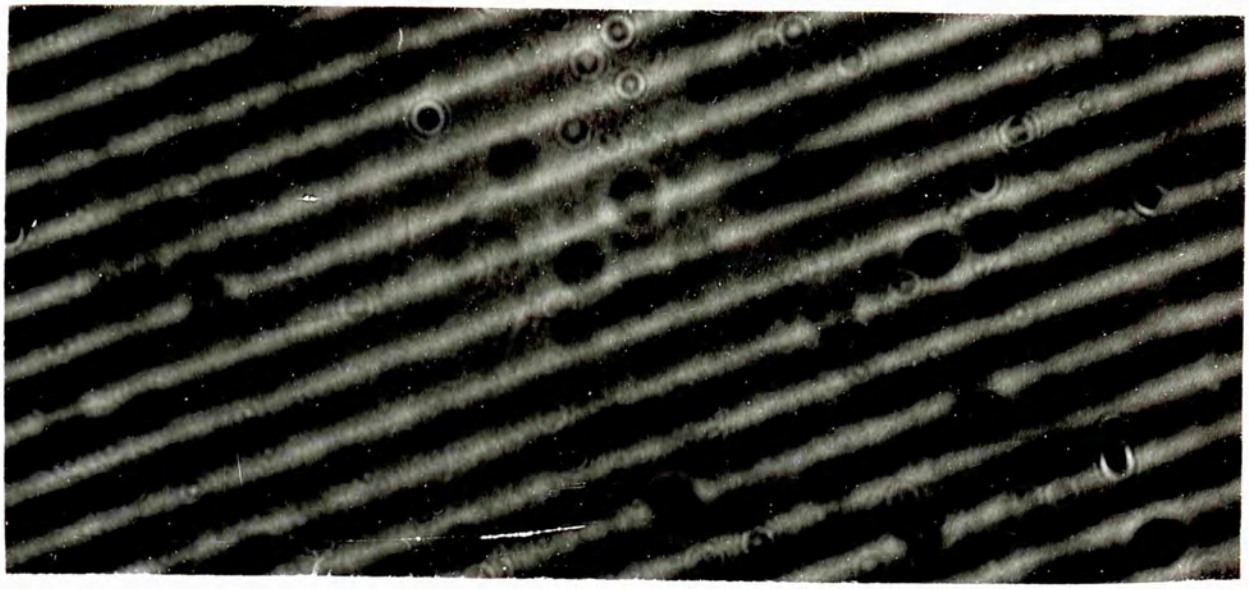

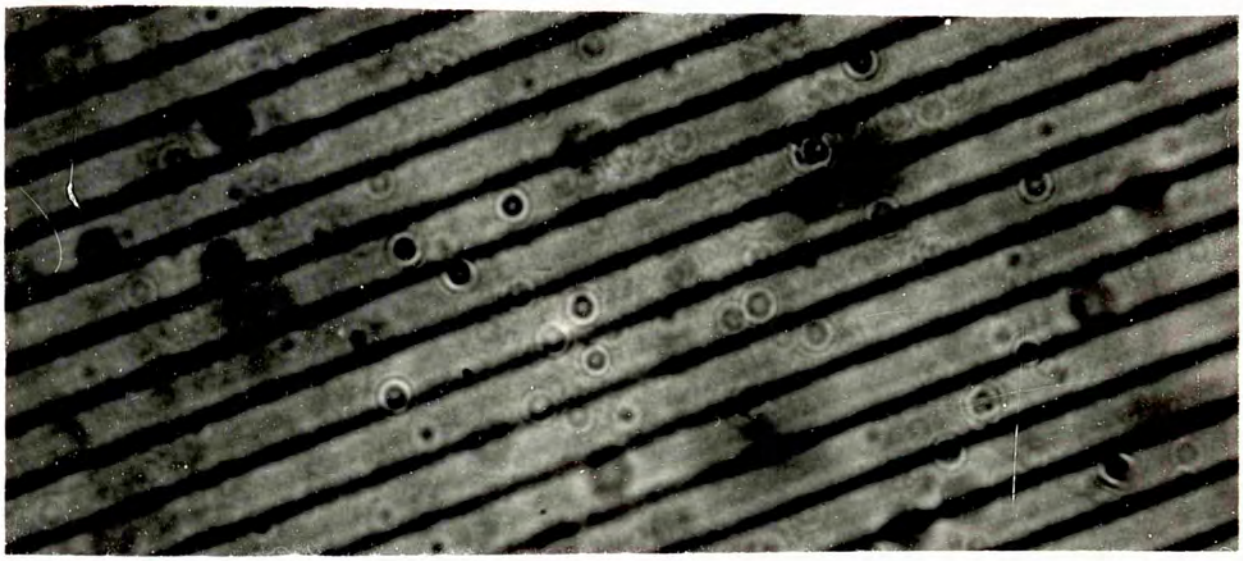

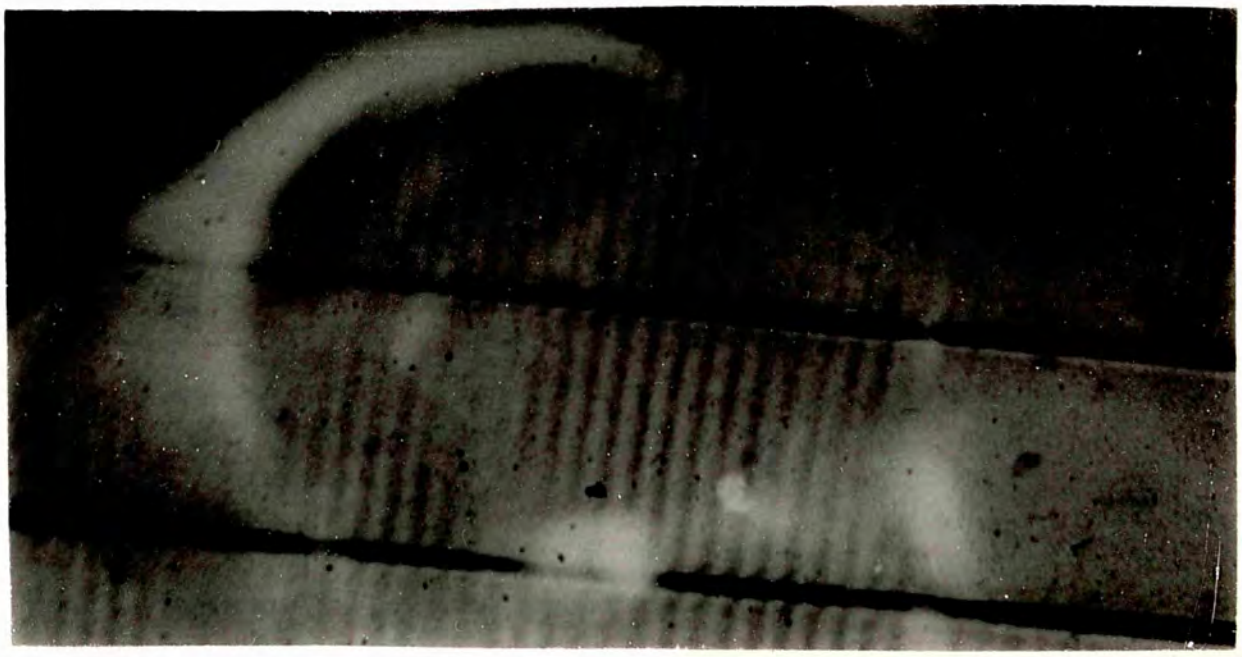

combined with undulations on the surface of the substrate. The use of optical flats in all the experiments would have been prohibitively expensive, but when they were used the region over which uniform etching was observed was $\sim 100\mu m$. Such an area corresponded to the filaments observed in the output from the laser (chapter 3).

6.6III INTENSITY CORRELATION

For a phase grating assume a unit amplitude transmittance and that the incident wave on passing through the corrugated surface receives a periodic phase shift Φx

$$\text{i.e.} \quad \tau(x) = \exp - j\Phi(x)$$

Assuming the modulations are sinusoidal

$$\Phi x = \Phi_0 - \Phi_1 \cos kx$$

$$k = 2\pi/d \qquad \Phi_1 = \frac{2\pi}{\lambda}(\mu - 1)D$$

Therefore $$\tau(x) = \exp -j\Phi_0 \exp \Phi_1 \cos kx \qquad 32.$$

2D being the peak to peak height.
The first term is an arbitrary constant whilst the second term is spatially varying and represents the corrugations imposed on the wavefront by the grating.
A Fourier expansion of the transmittance function $\tau(x)$ corresponds to the Fourier analysis the grating performs

$$\tau(x) = \exp j\Phi_1 \cos kx = \sum_{n=-\infty}^{\infty} f(n)(\Phi_1) \exp jkx \qquad 33.$$

The coefficients of the terms $f(n)(\Phi_1)$ correspond to the amplitudes of the Fourier components.
Now the generating function[137] for Bessel functions is

$$\exp \frac{\beta}{2}\left(t - \frac{1}{t}\right) = \sum_{n=-\infty}^{\infty} J_n(\beta) t^n \qquad 34.$$

Putting $t = \exp j\alpha$, $\beta = \Phi_1$ $\alpha = \frac{\pi}{2} - kx$

$$\exp j\Phi_1 \cos kx = \sum_{-\infty}^{\infty} J_n\langle\Phi_1\rangle \exp jn\left(\frac{\pi}{2} - kx\right)$$

Since $\exp jn\frac{\pi}{2} = j^n$

$$\exp j\Phi_1 \cos kx = \sum_{-\infty}^{\infty} j^n J_n\langle\Phi_1\rangle \exp jnkx$$

From 33

$$\tau(x) = \sum_{-\infty}^{\infty} j^n J_n\langle\Phi_1\rangle \exp jnkx$$

The Fourier amplitude coefficients are seen to be Bessel functions of order n.

The intensities of the diffracted orders are therefore related by the squares of the amplitude terms i.e.

$$\frac{I_n}{I_{n+1}} = \left|\frac{J_n\langle\Phi_1\rangle}{J_{n+1}\langle\Phi_1\rangle}\right|^2$$

where $\Phi_1 = 2\pi(\mu - 1)D/\lambda$ is half the maximum possible phase change between rays incident normal to the surface.

In the case of reflection $\Phi_1 = 4\pi D/\lambda$

First and second order Bessel functions are shown in fig. 6.9C.

The maximum possible efficiency in first order is

$$\left|\frac{J_{n+1}\langle\Phi\rangle}{J_n\langle\Phi\rangle}\right|^2 \times 100 = 34\%$$

($J_0\langle\Phi\rangle$ normalized to unity) and is reached for $\Phi = 1.85$.

Using a spectrometer bench and photomultiplier the intensities of first and second order in transmission were measured for $\lambda = 5896$ Å. The ratio I_1/I_2 was found to vary between 4.4 and 5.0 and this ratio range is marked on the graph fig. 6.9C. It corresponded to $\Phi = 1.6 \mp 0.1$ and assuming $\mu = 1.5$, 2D was 0.60 ∓ 0.04 micron. This value is an average for the surface and compares favourably with the other methods.

The recorded peak to peak depth of the grooves compared

with their spacing suggests that the heat flow from the surface was one dimensional. If two dimensional heat flow had been the case the spatial period would have had to have been at least twice the penetration depth for any contrast to remain. Yet 0.3 μm depths were observed on grids with 0.4 μm spatial periods.

6.7 SURFACE PATTERNS

The system of parallel lines etched on metallic films and their substrates was the most prominent feature. Other surface features were caused by misalignment or dust.

The extra cavity method described in section 6.3 required the tilting of the external mirror M_3. This resulted in a highly complex system of interfering wavefronts. Fig. 6.11A shows the Moiré type modulation of a grid etched with frequency doubled light. The pattern was observed whenever the mirror M_3 was tilted. Although it could not be due to a true Moiré fringe system (the antinodes were moving too fast) the gold film detected a stationary interference pattern.

Fragments of dust and other absorbing centres on the substrates diffracted the laser beam and the Fresnel diffraction pattern was recorded by the gold layer. When the film was at a large θ the shadows cast by various objects were recorded as comet like formations. Fig. 6.11B shows a typical formation and in all observations the direction of propagation of the laser beam was along the longitudinal axis of the comet. At lower values of θ the effective extent of the obstacles perpendicular to the plane of the metallic films was less. In these cases the diffraction was caused by a very small

A

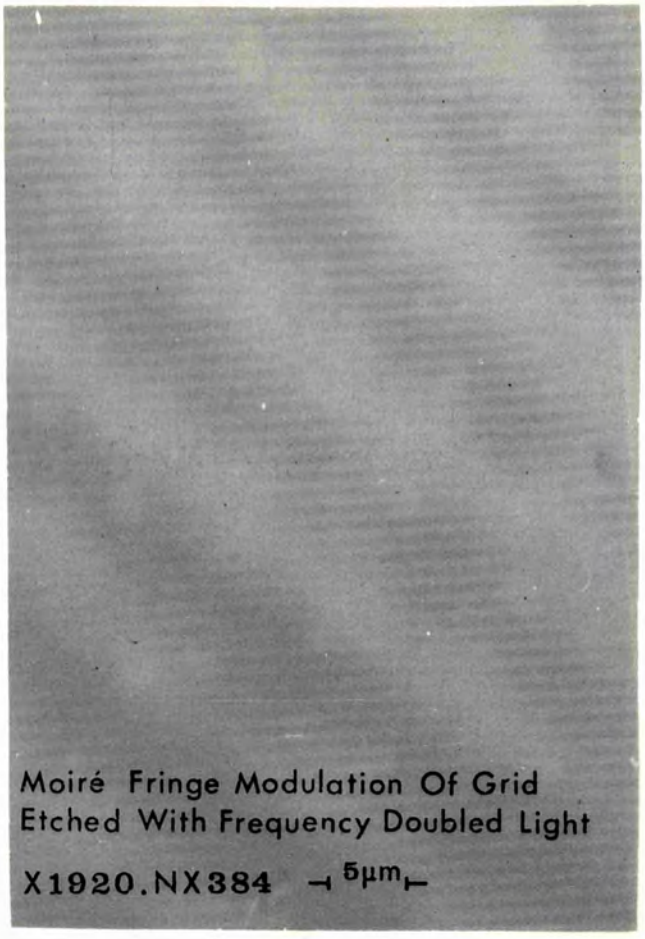

Moiré Fringe Modulation Of Grid
Etched With Frequency Doubled Light

X1920.NX384 ⊣ 5μm ⊢

B

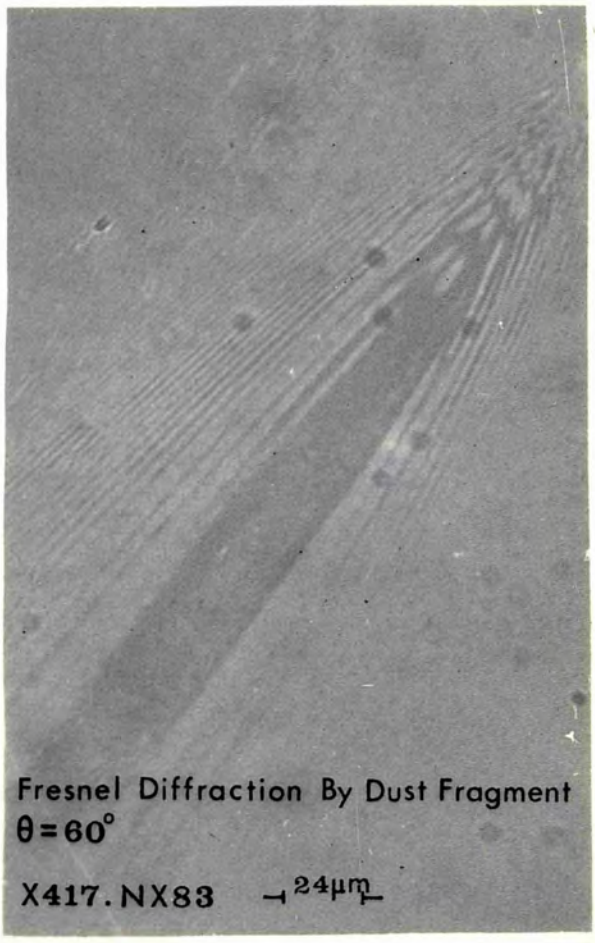

Fresnel Diffraction By Dust Fragment
$\theta = 60^\circ$

X417.NX83 ⊣ 24μm ⊢

C

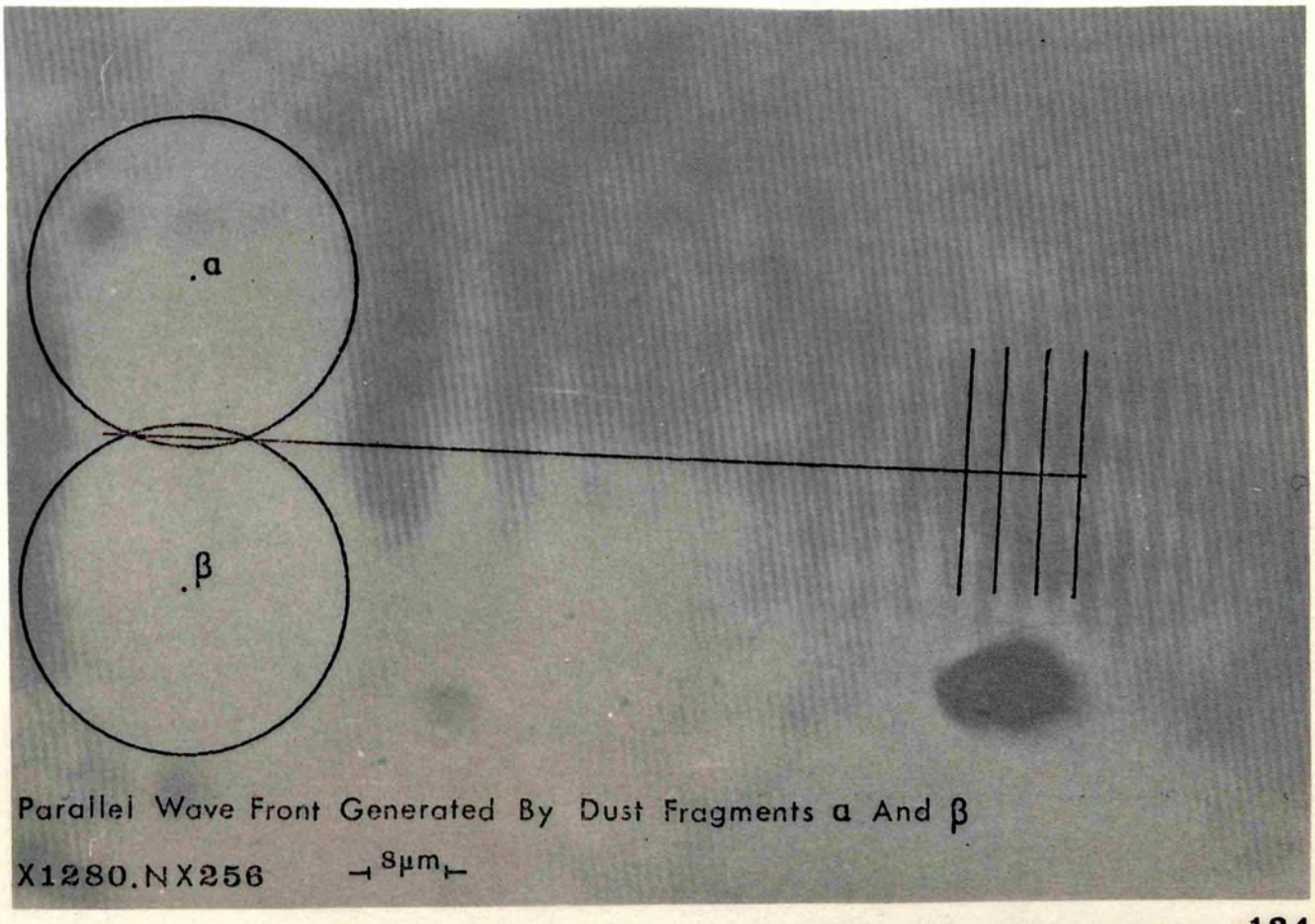

Parallel Wave Front Generated By Dust Fragments α And β

X1280.NX256 ⊣ 8μm ⊢

Fig6·11

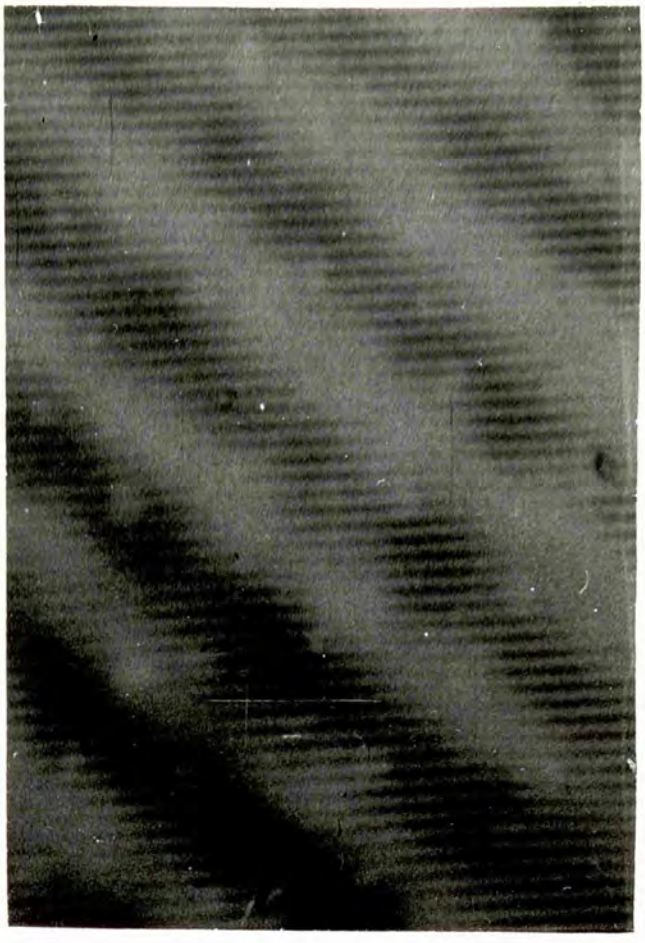

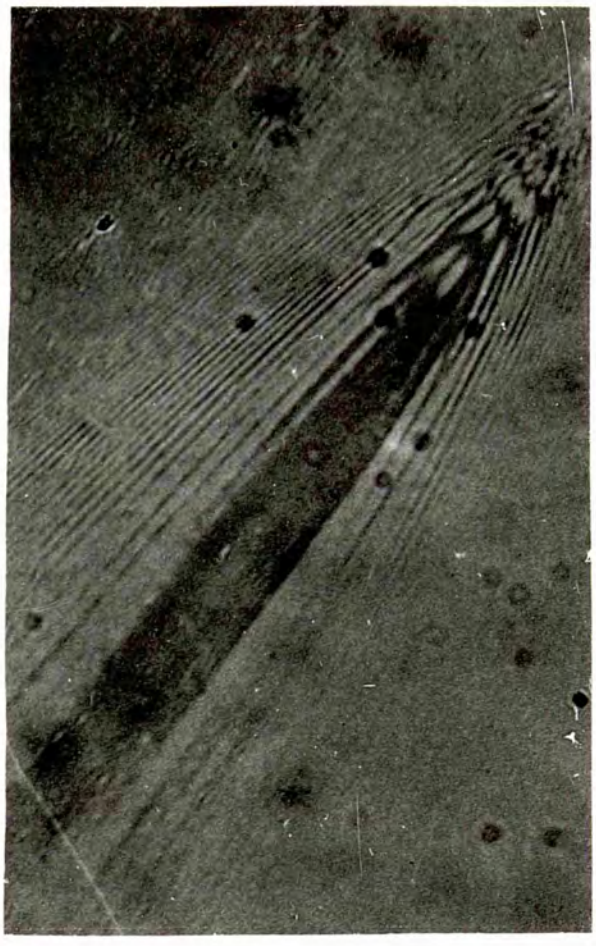

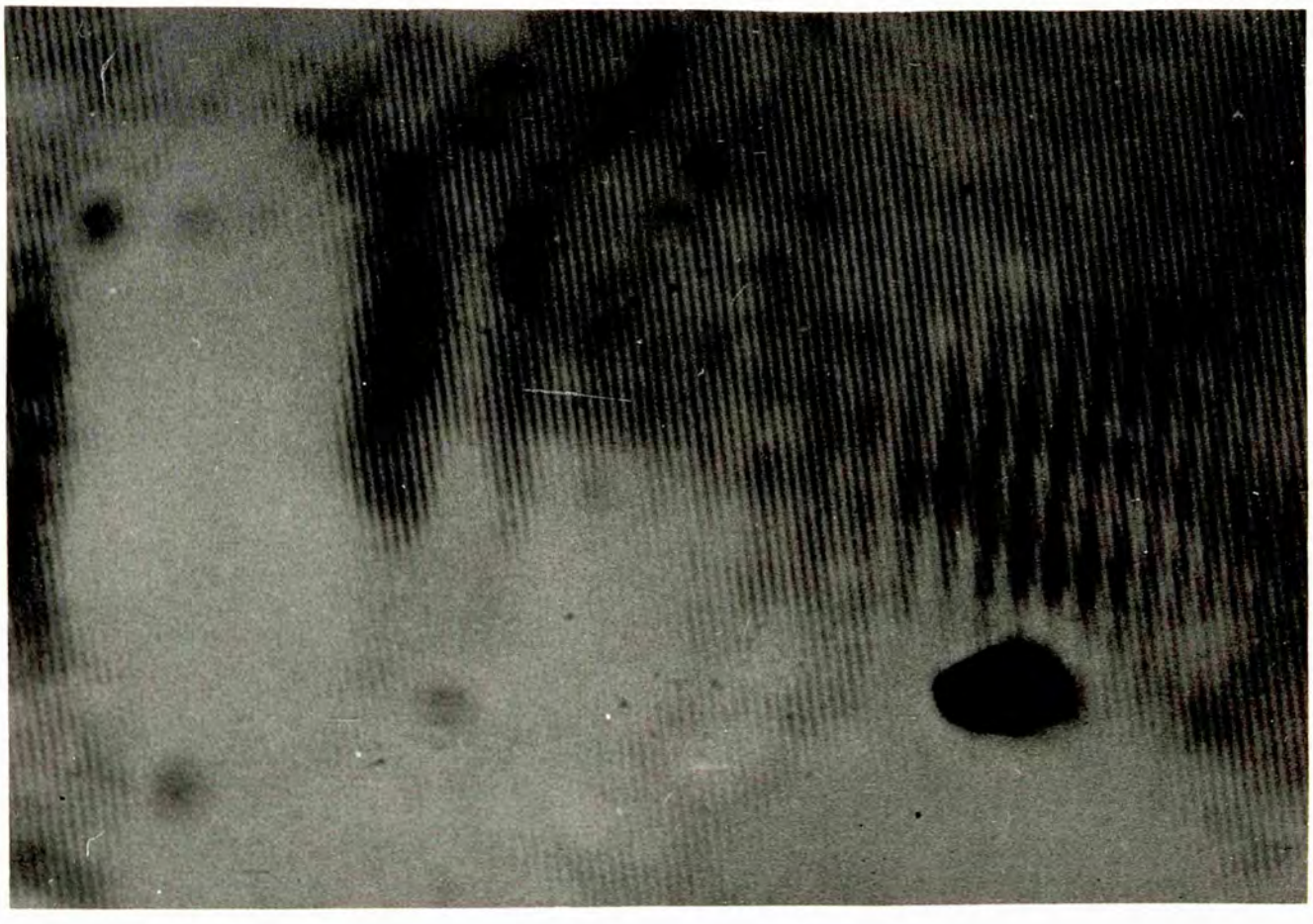

object ($\sim \lambda$) and a spherical wavefront resulted. When two such wavefronts were close together the resultant wavefront was a plane wave. In fig. 6.11C the diffracting centres were on the uncoated side of the substrate at the positions marked α and β.

The spherical wavefront from an isolated absorbing centre casued a series of rings to be etched in the film. The rings corresponded to a Fresnel Zone plate, the radius of the zones being related to the thickness of the substrate r_o (index μ) by

$$S_n = \left| \frac{n \lambda r_o}{\mu} \right|^{1/2} \qquad 35. \qquad (n \text{ integer})$$

Fig. 6.12A shows part of a ring system and by focusing the microscope down to the uncoated side of the substrate the position of the obstacle was located. In all cases this showed as a small chip ~ 50 micron square marking the position of the explosion caused by the vaporization of the obstacle.

Measurements taken of the ring radii were proportional to $(n)^{\frac{1}{2}}$ and using equation 35 the origin of diffraction was located at a distance r_o, equal to the substrate thickness, below the metal film. A two beam hologram of a straight edge, purposely placed on the substrate, was also recorded. In fig. 6.12B the object was a human hair.

Evaporation of dust fragments on the metal surfaces left smaller craters than those on the glass side of the substrate. This was because the metal film dissipated the absorbed energy more efficiently. Fig. 6.13A shows one of the larger craters on the surface previously coated. The same crater is shown in the top left of fig. 6.13C which was taken

A FRESNEL DIFFRACTION BY DUST FRAGMENT

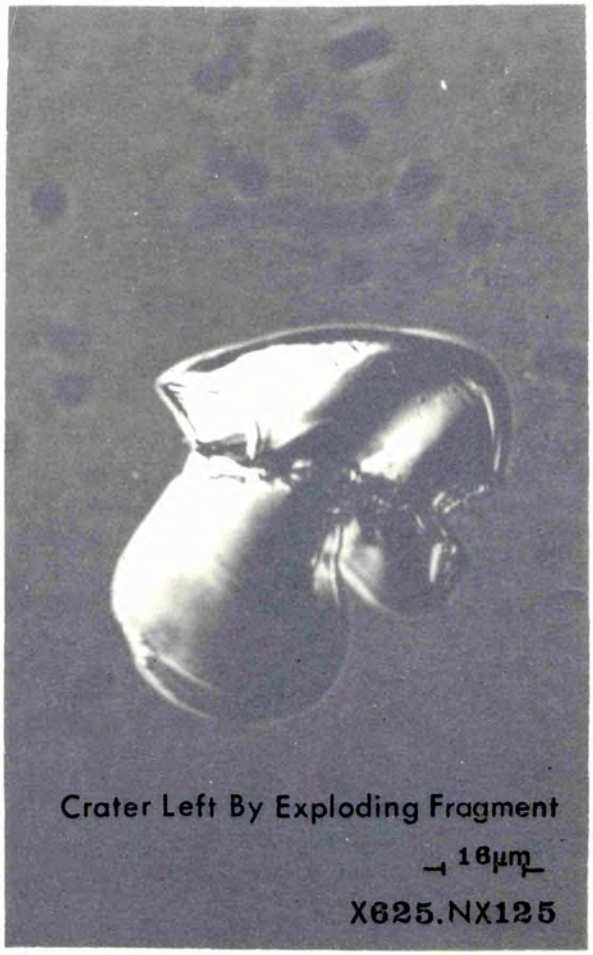

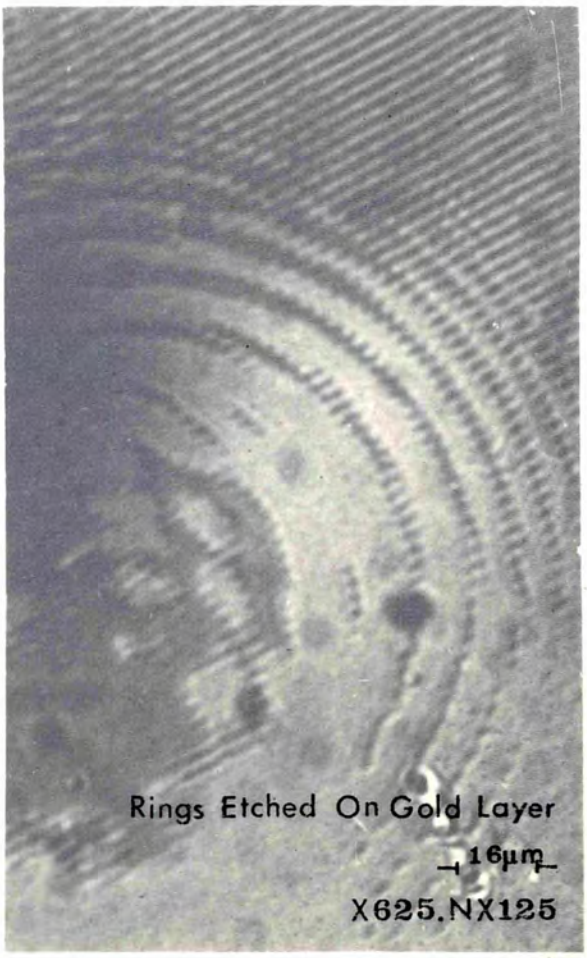

B FRESNEL DIFFRACTION BY A STRAIGHT EDGE

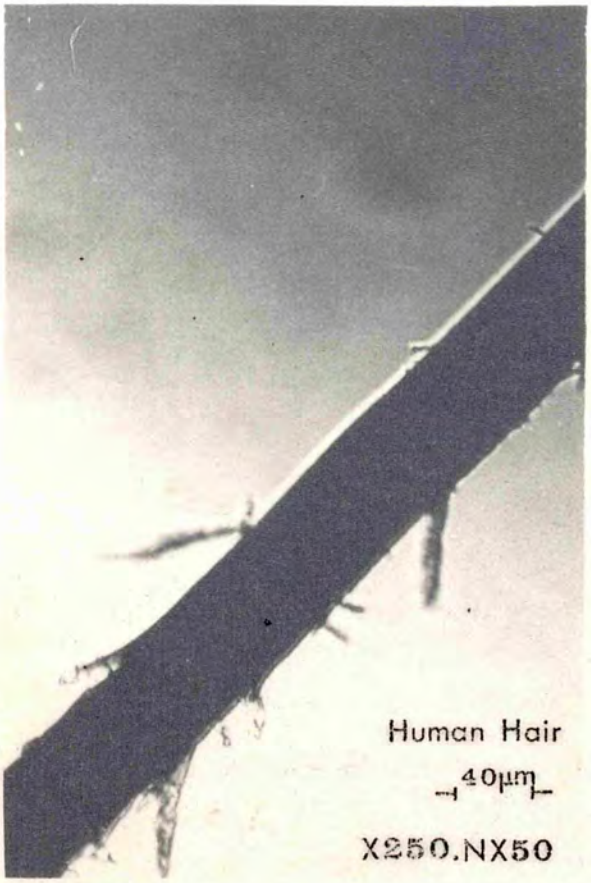

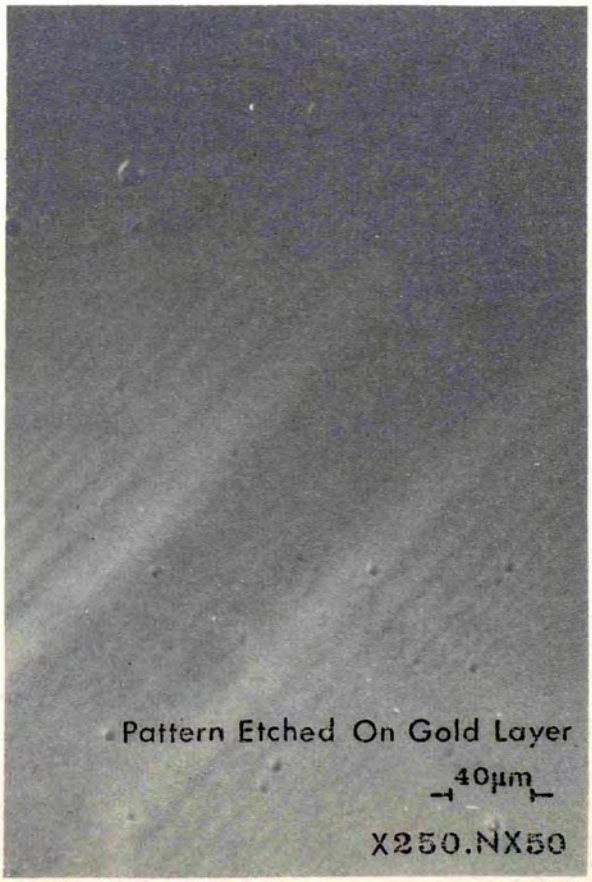

Fig 6·12

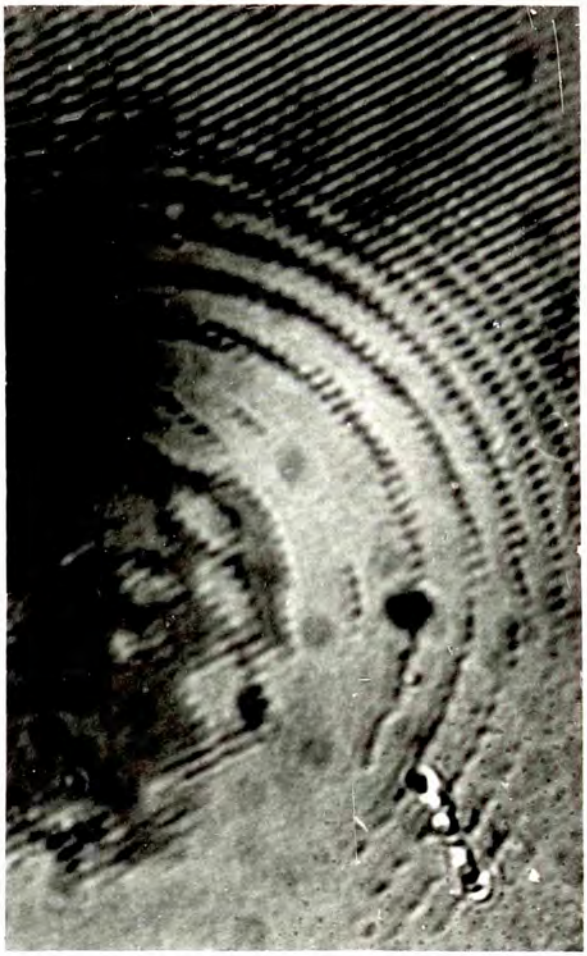

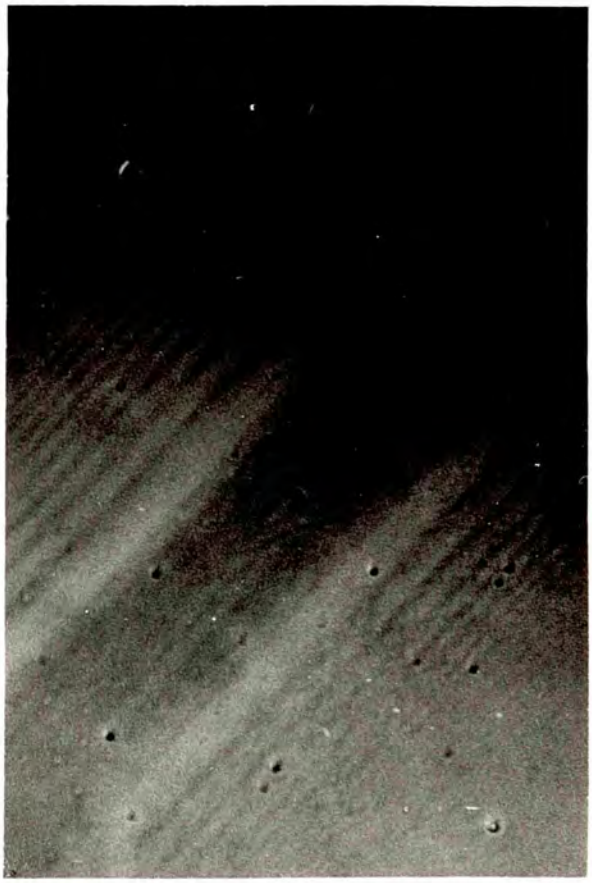

ABSORPTION CENTRE ON Au FILM

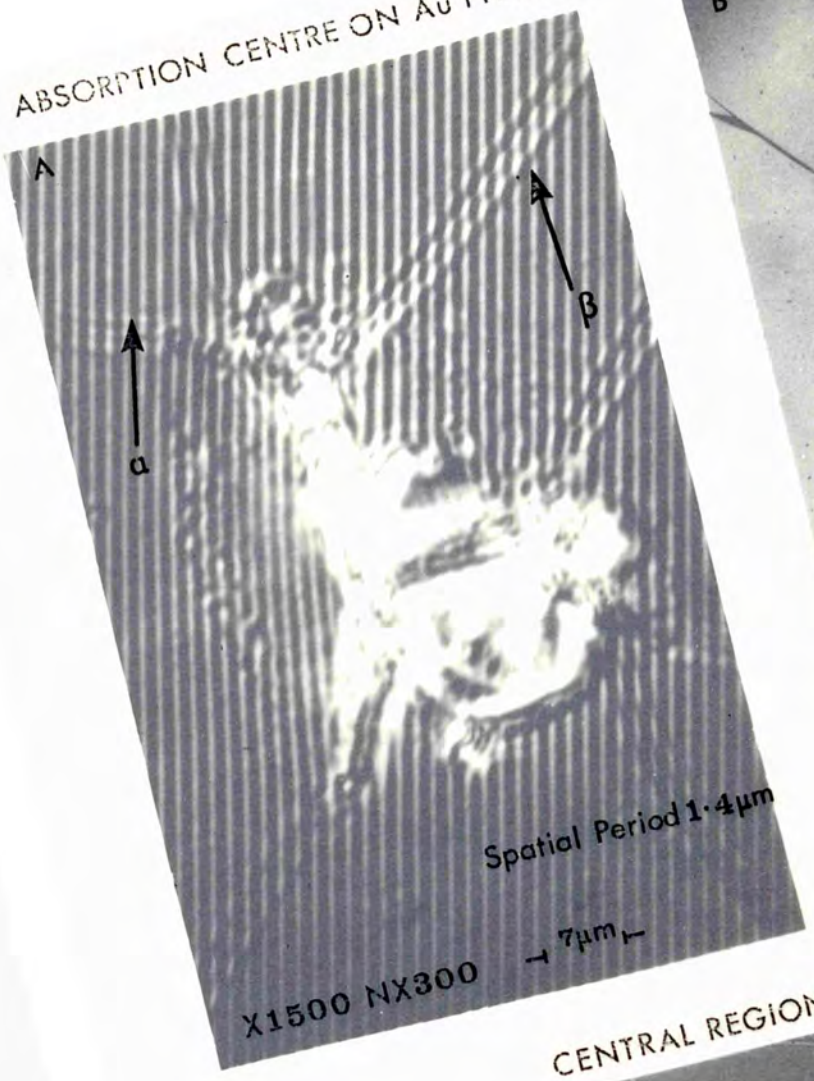

RESTRICTED VAPOUR PLUME

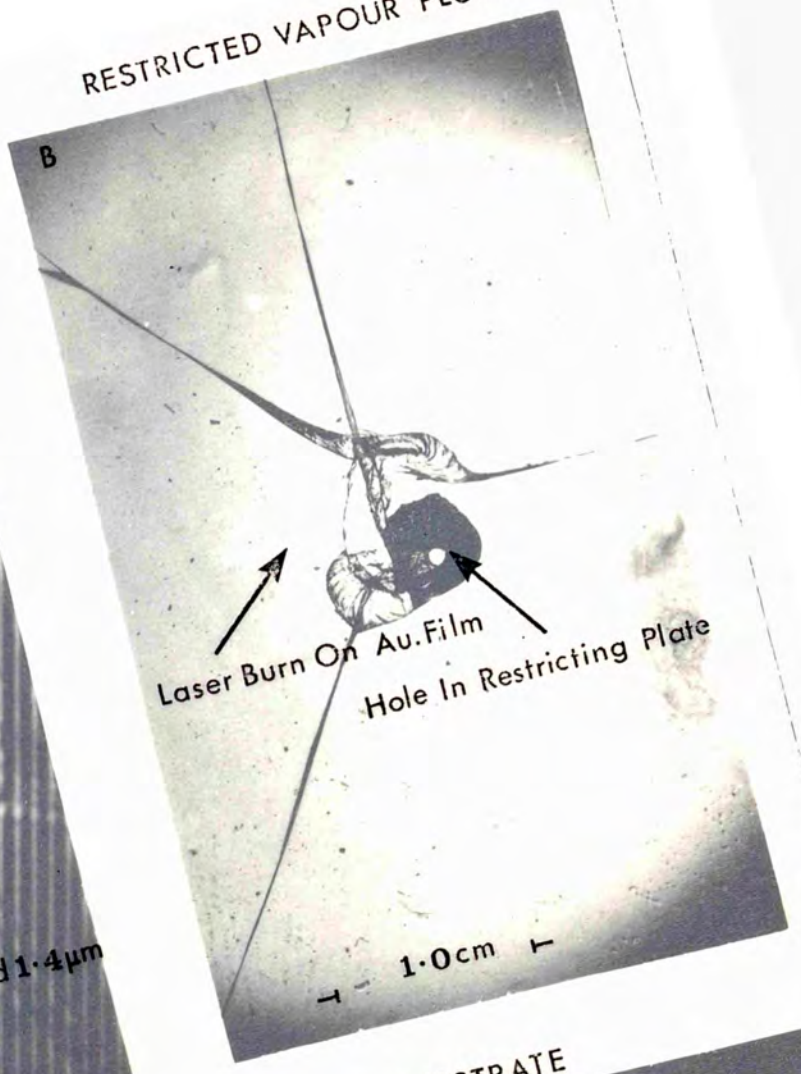

CENTRAL REGION OF CLEANED SUBSTRATE

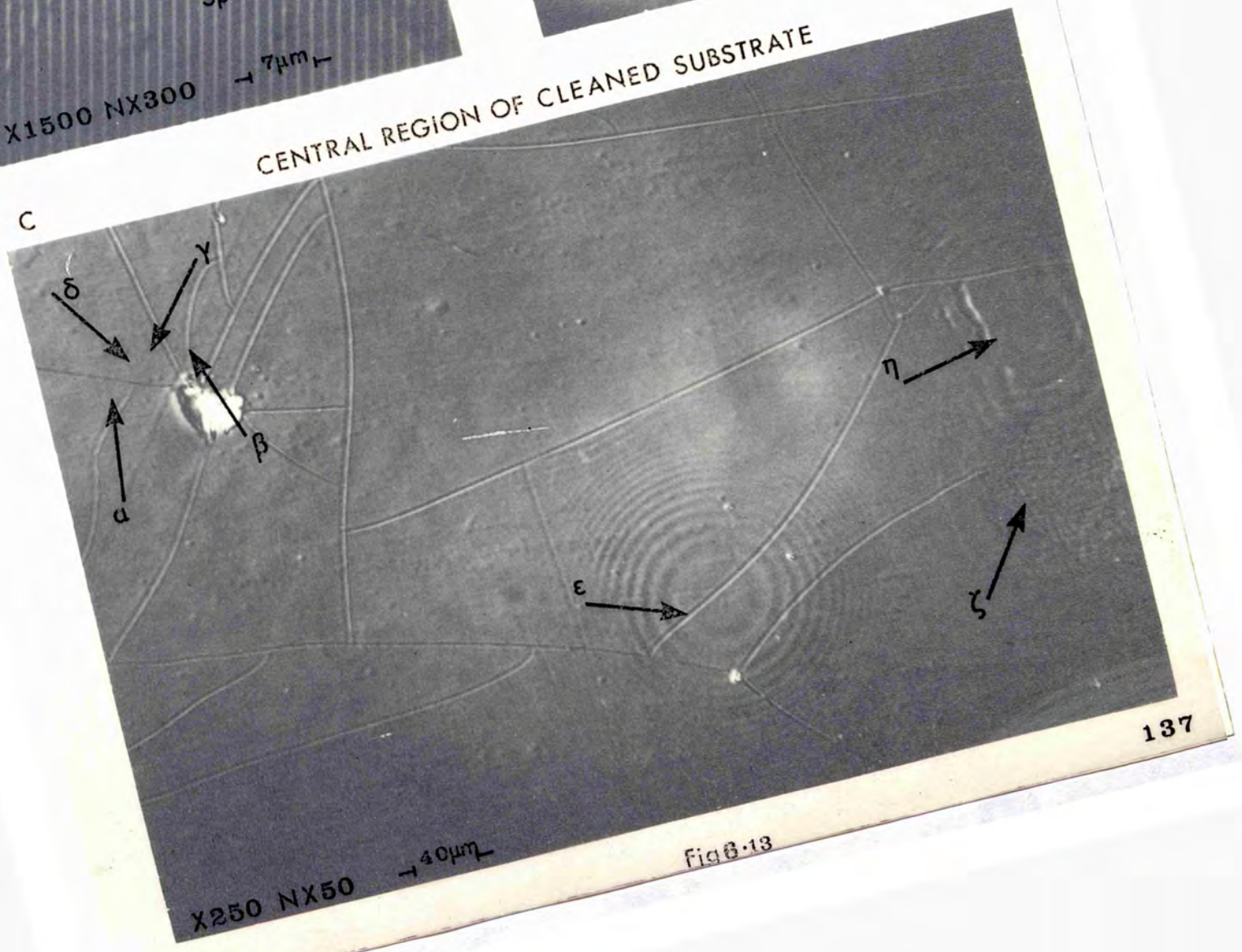

Fig 6·13

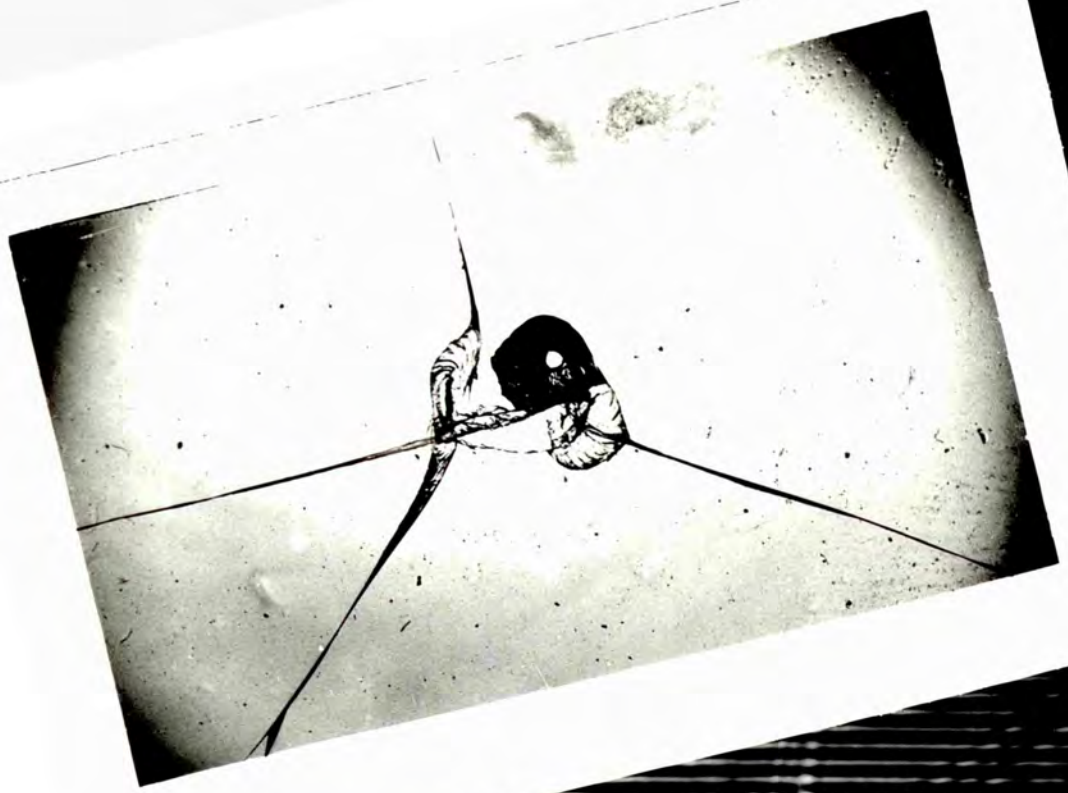

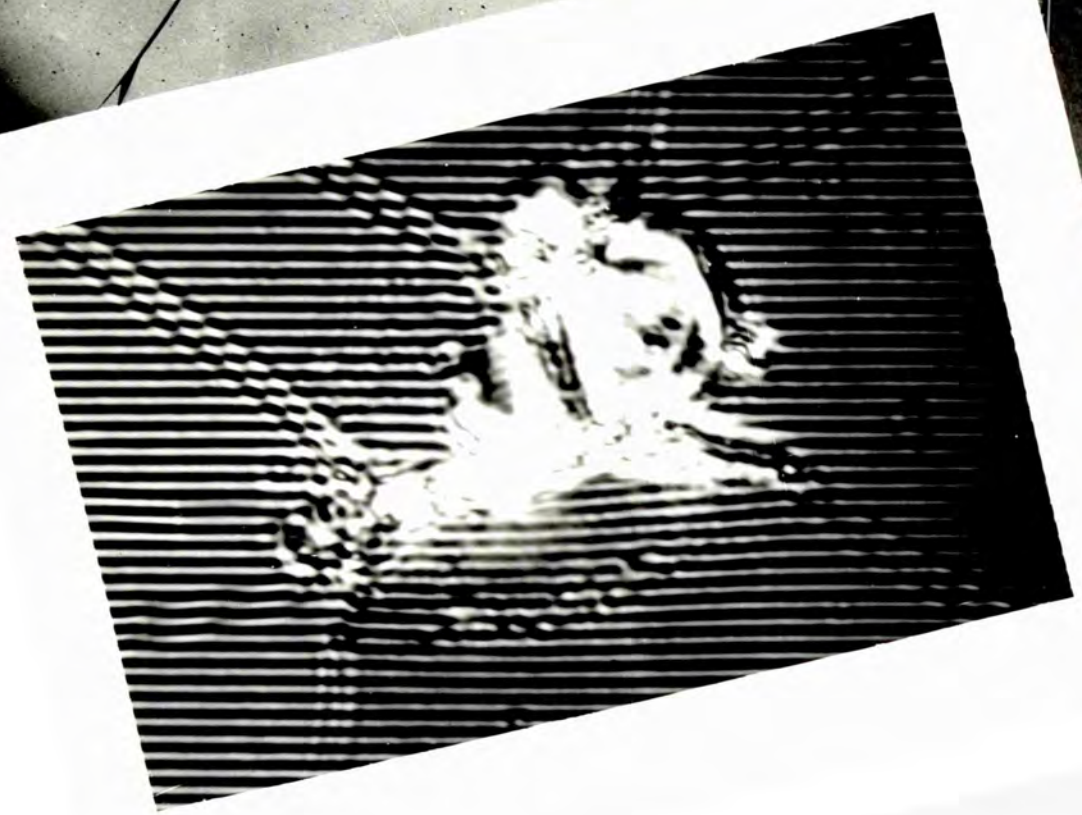

after a period of days relative to 6.13A. The cracks marked α and β are common to both photographs, whilst those marked γ and δ came as a result of 'creep' on the surface. Such behaviour indicated that the origin of the cracks was a tensile stress caused by contraction after viscous flow during heating. The tension was released in the form of cracks with a time constant of days. The absence of cracks at the absorption centres on the uncoated side further suggested that the mechanism causing crazing was tensile stress on cooling and not compression cracking. The craters acted as a nucleus for this process, causing many cracks to terminate in a crater, as shown in fig. 6.13C. This photograph also shows a superb example of a Fresnel Zone at ε and the interference of two such systems at η. The feature marked ξ was a property of the glass substrate and was also observed on unused samples.

Cracking of the substrate could be avoided by the use of fused silica substrates. Grids etched on these substrates were free from cracking and if carefully cleaned crater formation at absorbing centres substantially reduced. The coefficient of thermal expansion is the main factor that influences the cracking process[127] and consideration of the values of α for fused quartz (17×10^{-7} per °C) and C.M.D. glass (73×10^{-7} per °C) verified this.

In the experiments to be described in section 6.9 a second plate of glass was placed almost in contact with the metal layer. Photograph fig. 6.13D shows the effect of restricting the plume of vaporized gold leaving the Q - switch. Calculations assuming that the gold left the substrate with a thermal velocity of its boiling point gave a value for the total momentum

contained in the plume in the region of 10^1 gm cm/sec. This value was commensurate with the damage caused to the second plate. In particular the hole arrowed in 6.13B surrounded by Wallner lines indicated the shock wave nature of the damage. Placing the metal films in a water trough enabled the recondensed gold plume to be observed immediately after Q - switching. The range of the particles in water was in the region of 2 cm and in all cases cracking of the substrate was so dense that the surface was crazed into flakes.

Velocity of crack front.

Photograph fig. 6.14A,B shows two aspects of a branching region of cracks on the substrate surface. Lightly blowing on the microscope stage revealed loosely attached glass fragments at distances along the cracks. Fig. 6.14C,D shows the same effect 0.5 cm from the centre of the target in a region where the cracking stopped. The fragments were more closely spaced towards the end of the crack (bottom of fig. 6.14C,D) and this suggested that the fragments were associated with the velocity of crack propagation. The random siting of the fragments due to intersection with the kind of surface feature arrowed could be discounted by correlating such features on fig. 6.14C and D. The following phenomenological argument is used to calculate the velocity of the crack tip. The rapid expansion of the glass surface directed a compressive wave into the substrate. Subsequent reflection at the air glass boundary resulted in the compression front reaching the surface again after a time $t = 2r_o/v$, r_o being the substrate thickness = 0.1 cm and v the velocity of compressive waves in glass.

A

GLASS FRAGMENTS LOCATED ALONG FRACTURES

B

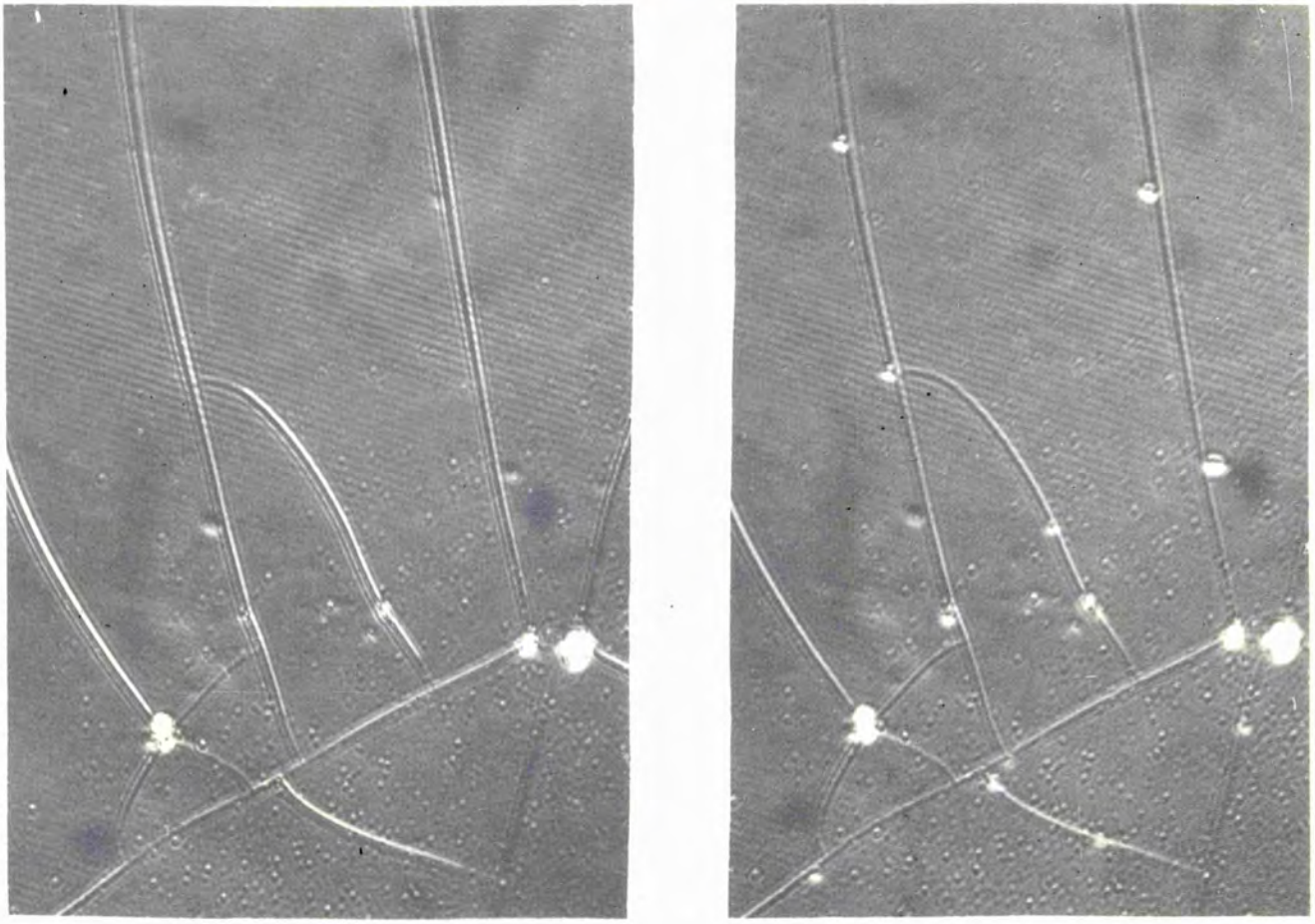

C

D

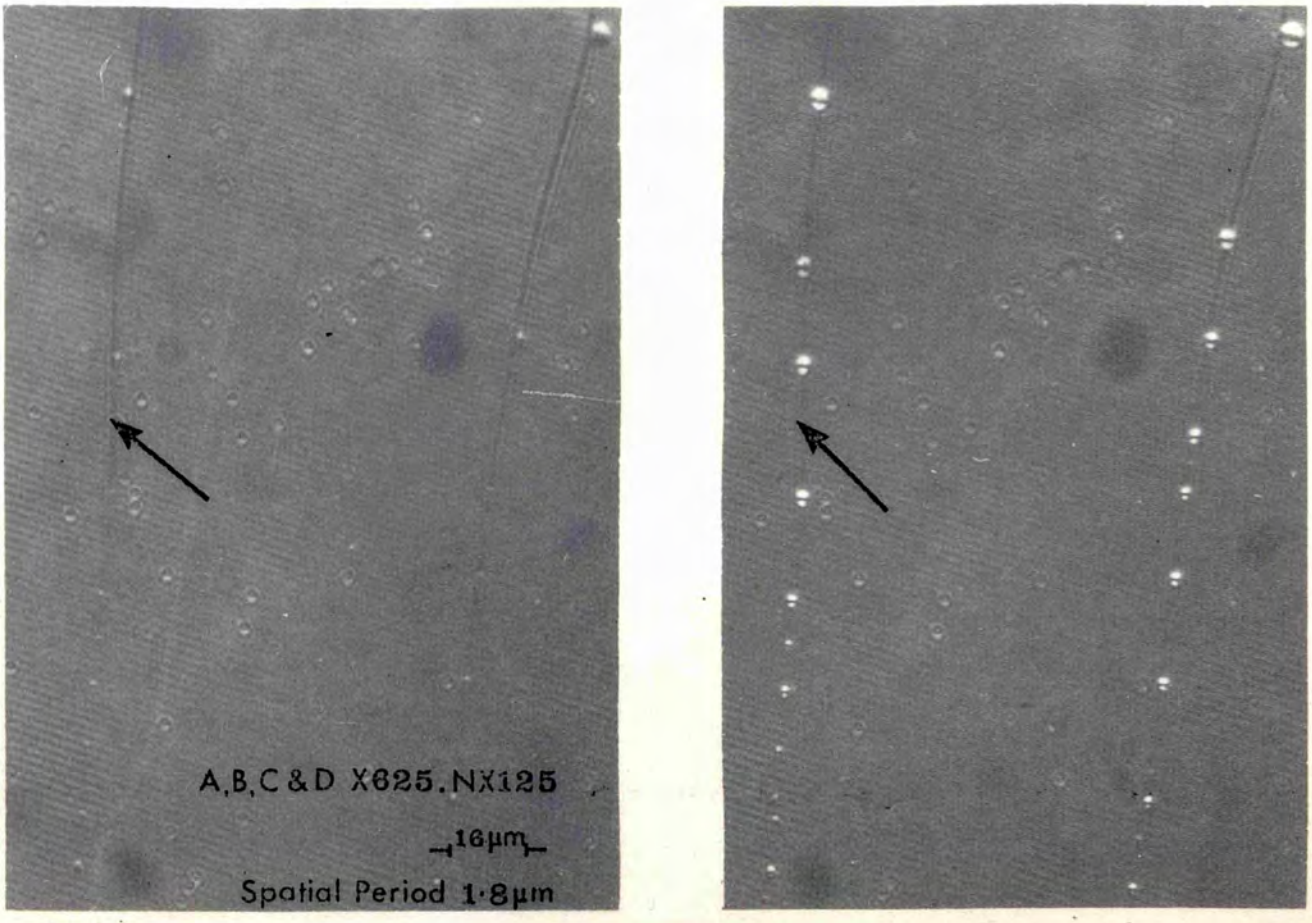

Fig 6·14

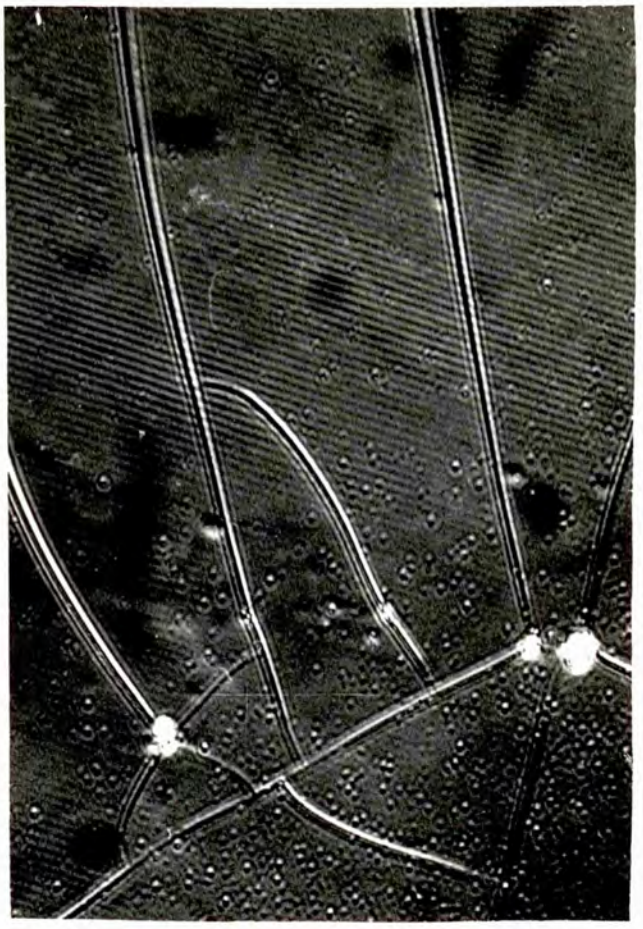

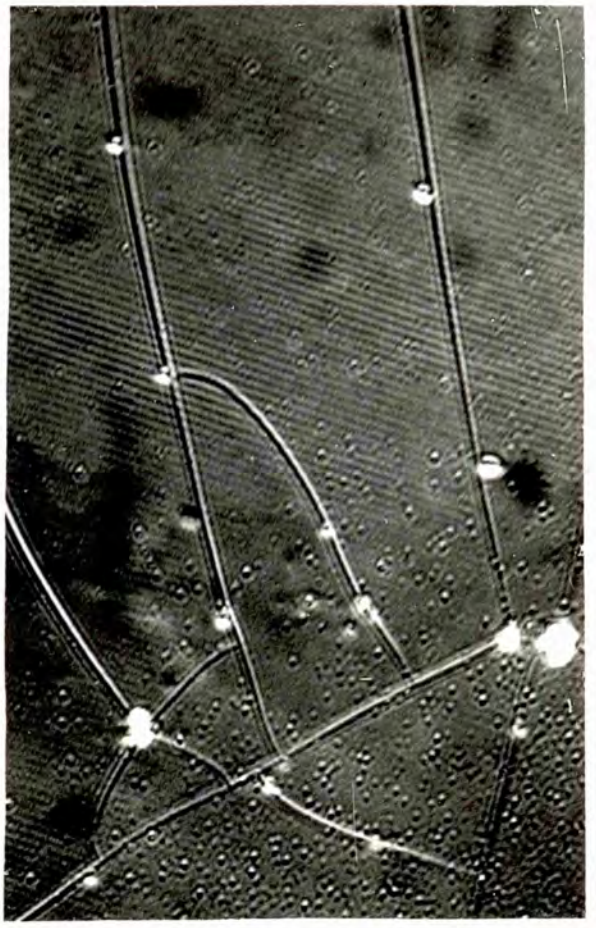

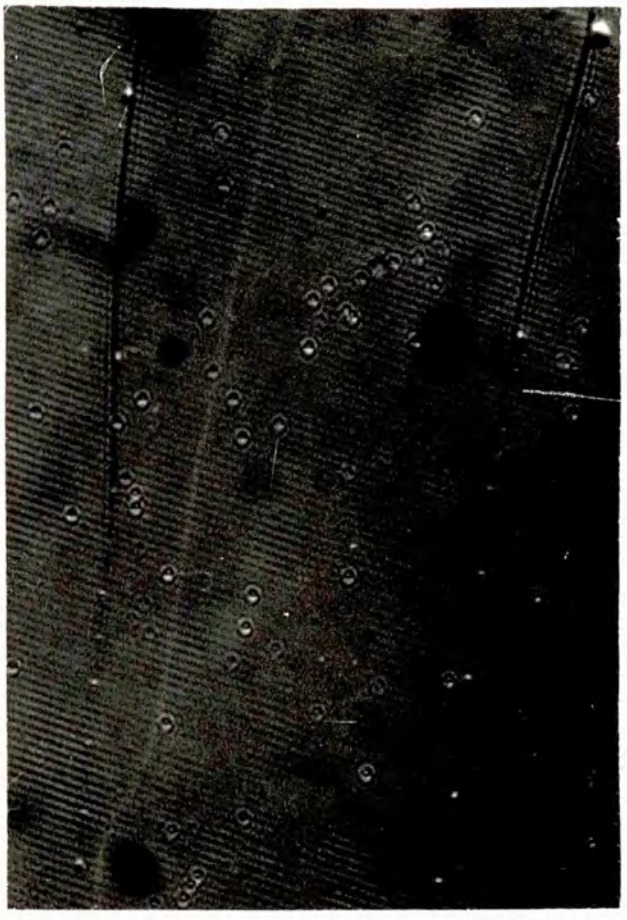

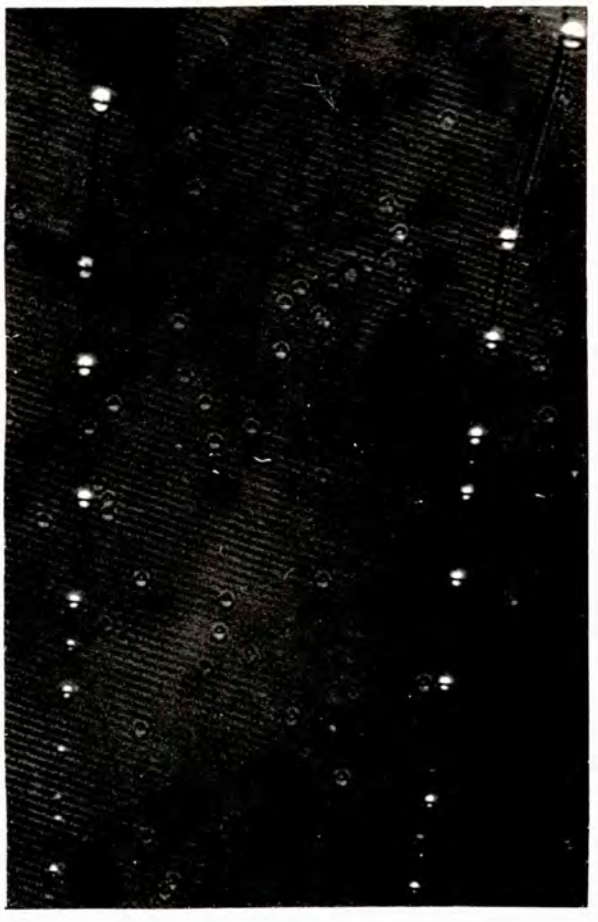

$$v = \left| \frac{E|1-\sigma|}{\rho|1+\sigma||1-2\sigma|} \right|^{1/2}$$

E Young's modulus, ρ density and σ Poisson's ratio.
In this case $v = 5.9 \times 10^5$ cm/sec and $t = 3.3 \times 10^{-7}$ sec.

The localized interference between the compressive wavefront and the crack tip is known to produce a modulation of the crack tip in the same way as the formation of Wallner lines.[138] Such modulation appearing as fragments can be regarded as time markers denoting the position of the crack front every 0.3 μsec in this case. At the top of fig. 6.14D the average crack velocity was 14×10^3 cm/sec, slowing down to 5×10^3 cm/sec, over a distance of 0.018 cm, at the bottom of the photograph. Such timing marks were not always present, indicating that some cracking took place after the compression wave had been dissipated.

6.8 CRYSTALLINE SUBSTRATES

When crystalline substrates were used regular crack patterns were observed on the surface and these could be related to the cleavage habits of the crystals used. Fig. 6.15A demonstrates this feature on mica with the formation of platelets whilst fig. 6.15B shows the cubic nature of a rock salt surface with an X - ray photograph for comparison. Murphy and Ritter[139] demonstrated the possibility of thermally etching metal and semi conductor surfaces by laser irradiation. Such a technique made possible the thermal etching of surfaces under high vacuum and low ambient temperatures. Dielectrics are normally transparent to ruby laser radiation. The results shown in fig. 6.15A,B show that the technique may be extended

A

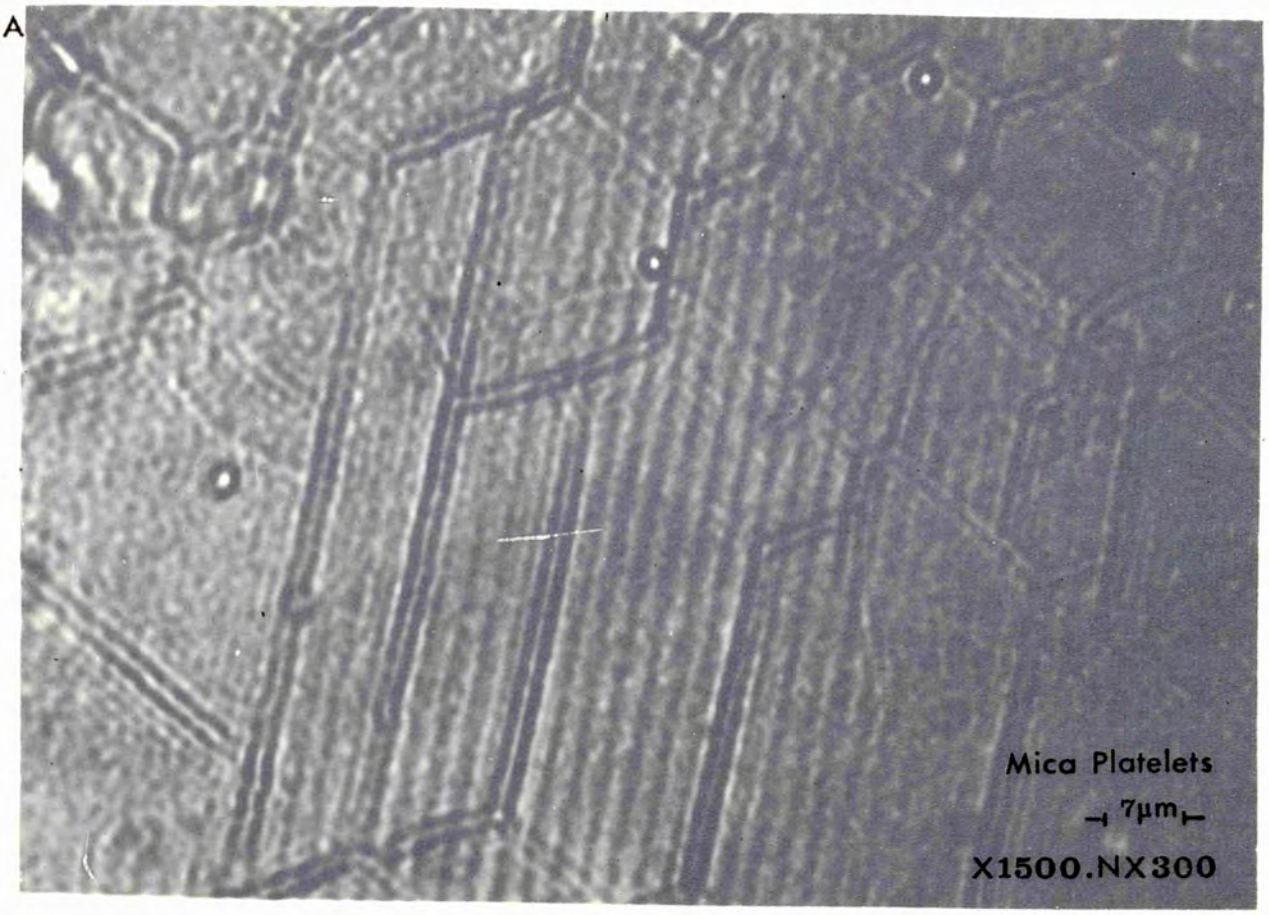
Mica Platelets
7µm
X1500.NX300

B

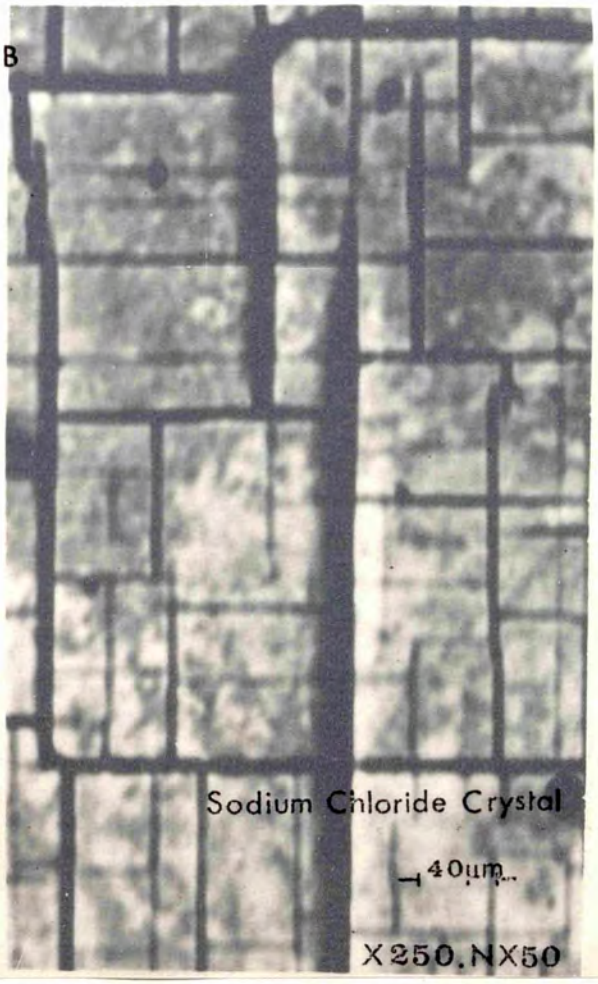
Sodium Chloride Crystal
40µm
X250.NX50

C

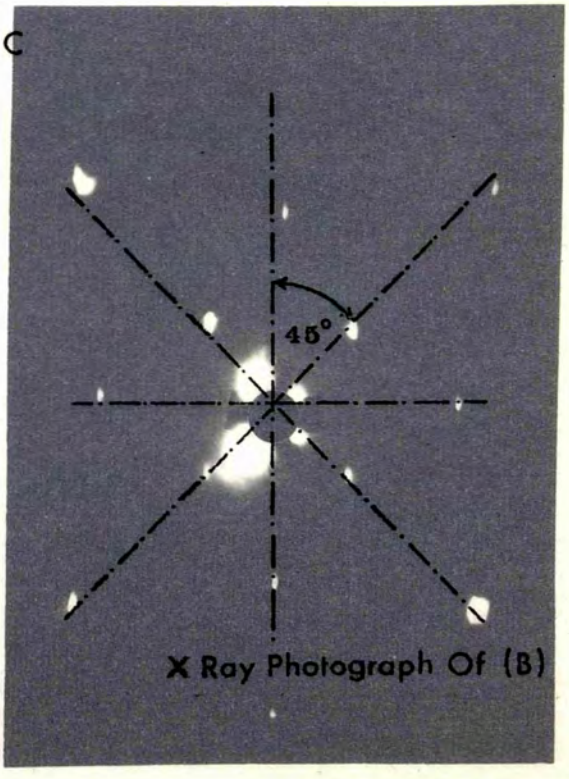
45°
X Ray Photograph Of (B)

Fig 6.15

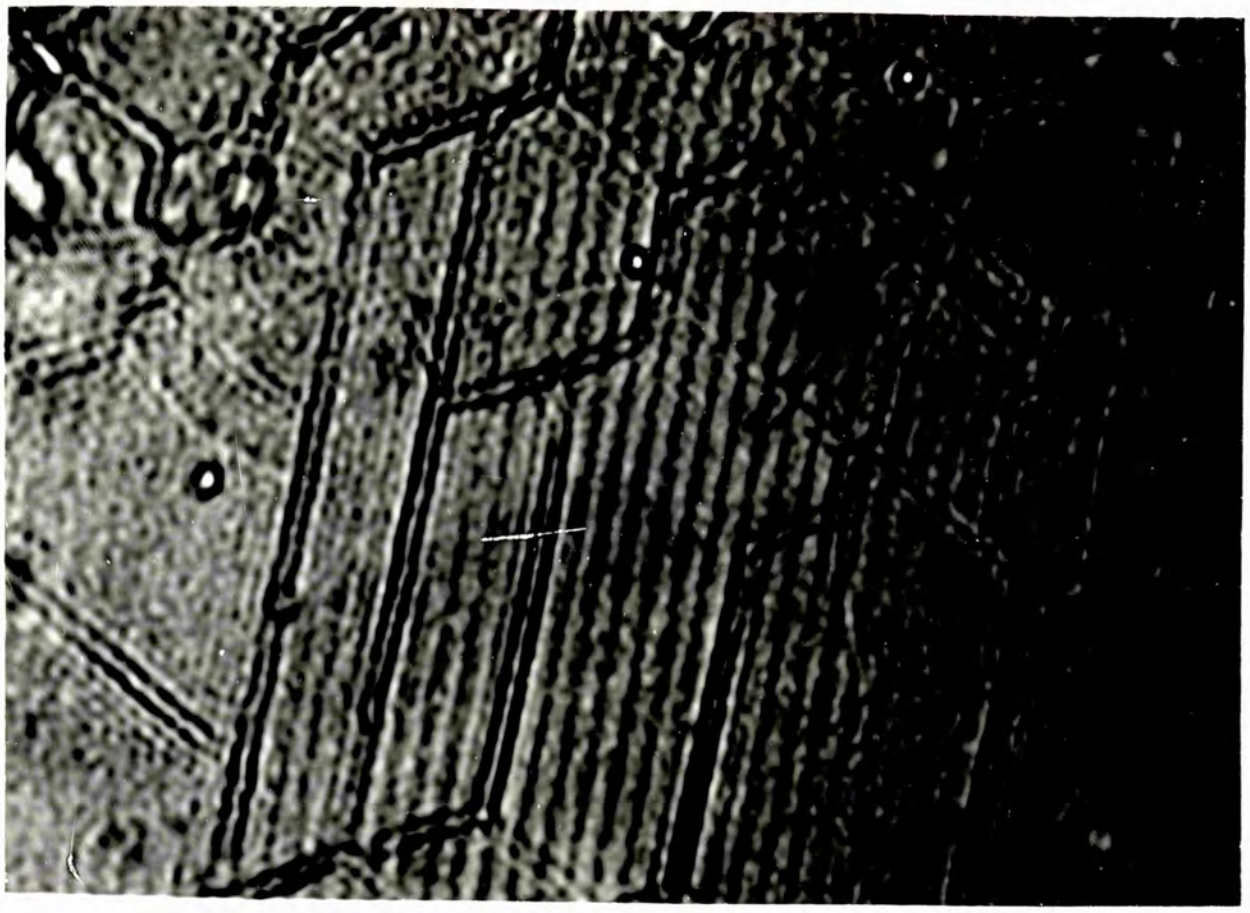

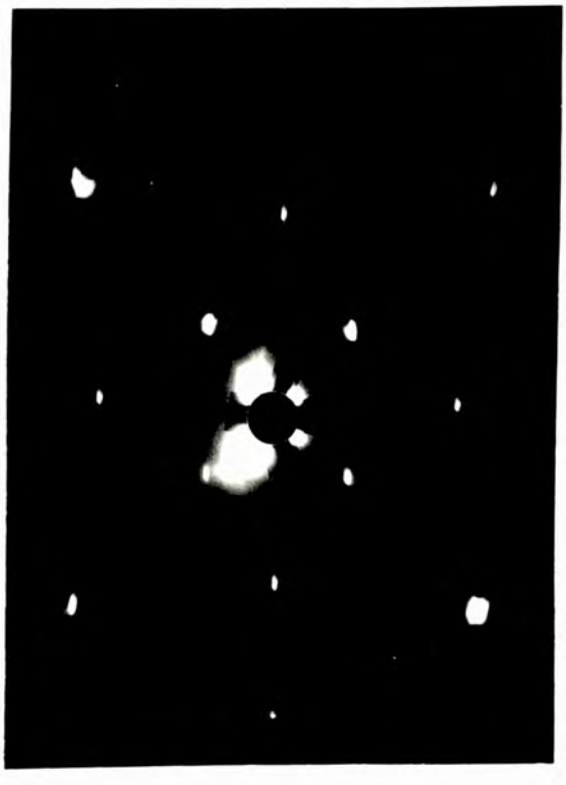

to dielectrics by coating the surface with a thin metallic layer.

6.9 SPATIALLY PERIODIC INHIBITION OF CONDENSATION

The energy required to heat the metal surfaces to boiling point and supply the necessary latent heat for vaporization was in the region of 80 mJ/cm^2 and the high power of a giant pulse was required to accomplish vaporization before thermal diffusion took place.

To use a metal film to record a hologram without destroying the object would require expansion of the beam on the object and subsequent contraction to increase the intensity on the recording material. An alternative approach would be to reduce the power requirement by using a hot metal. In particular, instead of vaporizing a metal at the antinodes of the electric field, it was found possible to use the converse effect i.e. to inhibit the condensation of gold vapour on a substrate in the presence of an intense electromagnetic field.

The gold vapour was produced by a Q - switching gold film and the resultant vapour collected on a microscope cover slip placed nearby. The arrangement is shown in fig. 6.16A which also shows the under attenuated oscilloscope trace of the laser pulse. The trailing edge is seen to decay with a relatively long time constant.

With the separation D between the film and the collector plate equal to 0.01 cm a spatially periodic gold film was observed on the collector plate. Fig. 6.17 shows a series of micrographs of the collector plate at various magnifications.

A INHIBITION OF CONDENSATION

Disposition Of Collector Plate And Q-Switching Film

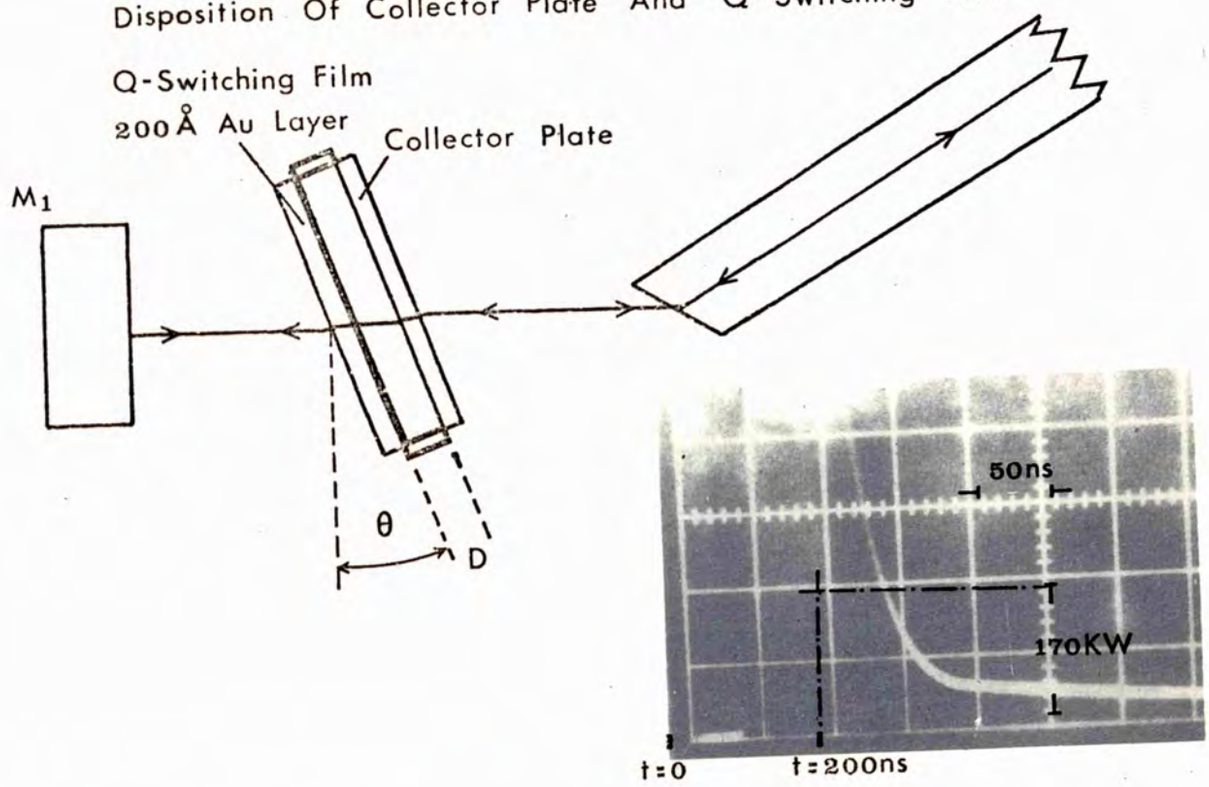

B DISTORTED WAVE FRONTS. RELAXATION OSCILLATIONS

Spatial Period 3·7μ

X150. NX50

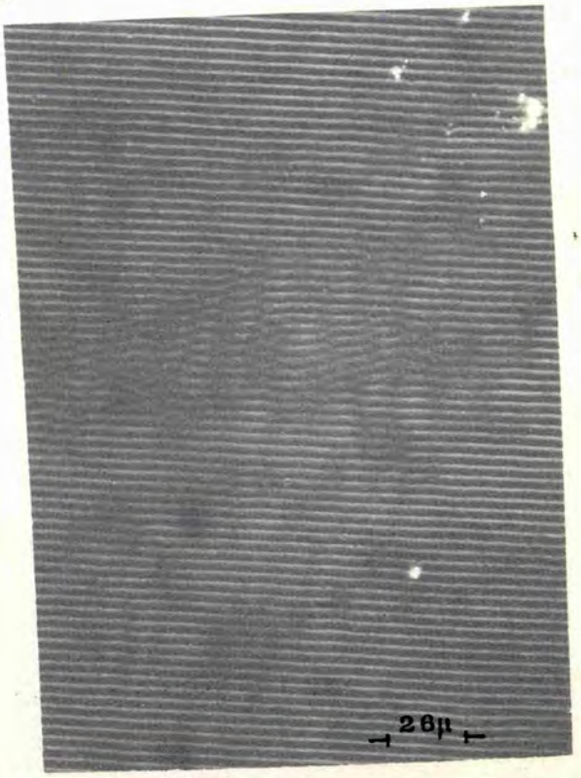

X375. NX125

Fig 8·16

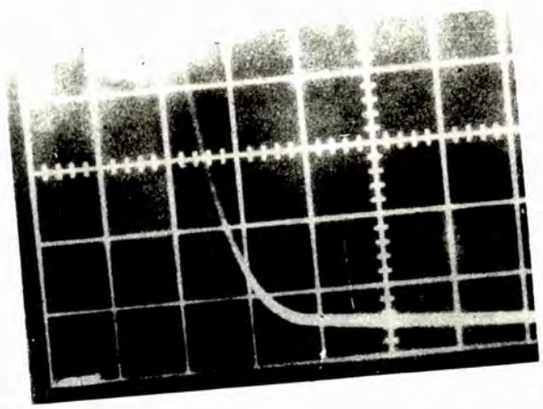

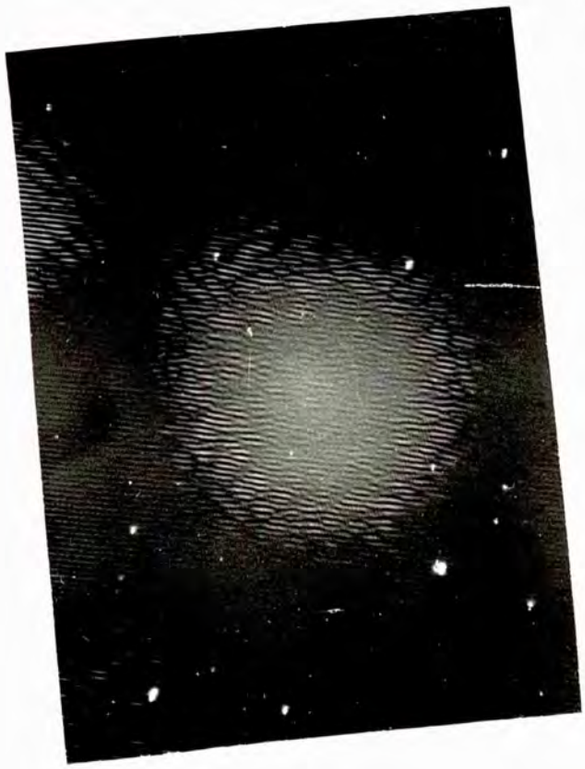

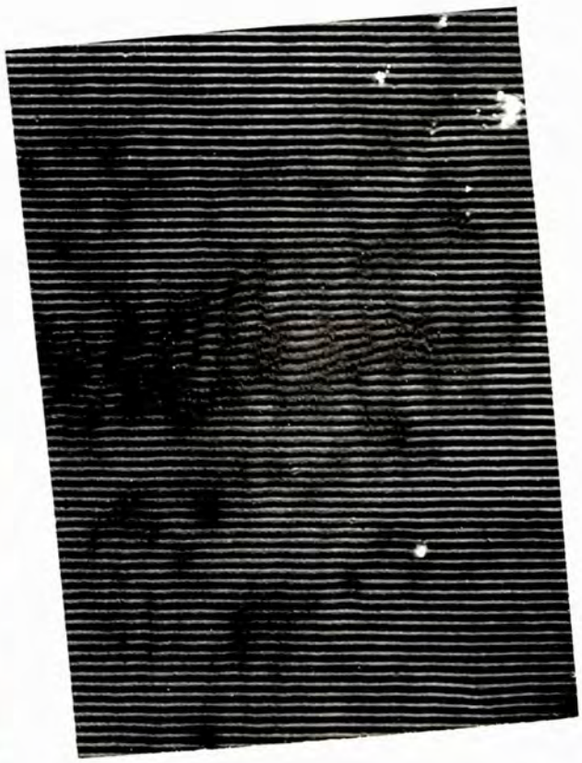

A

INHIBITION OF CONDENSATION

B

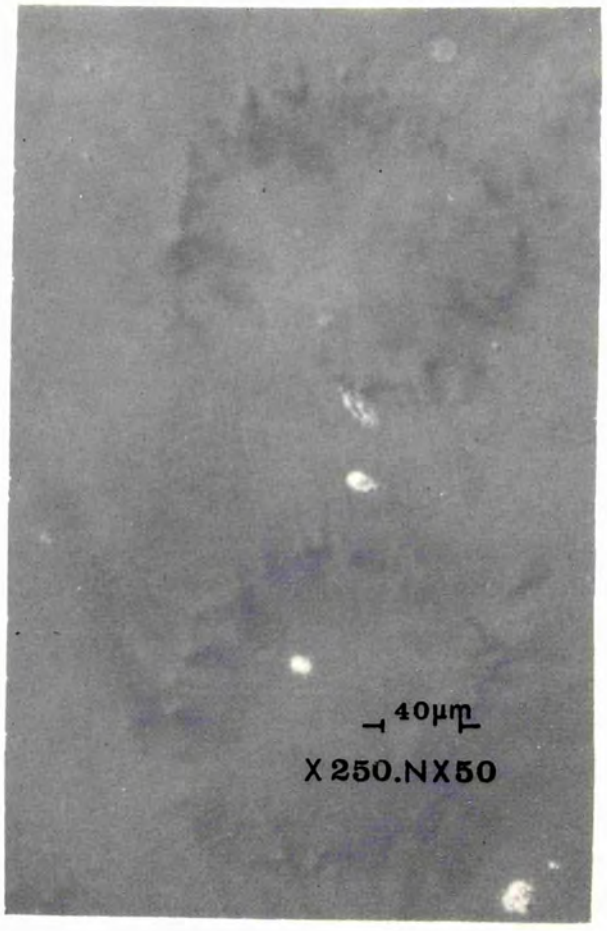

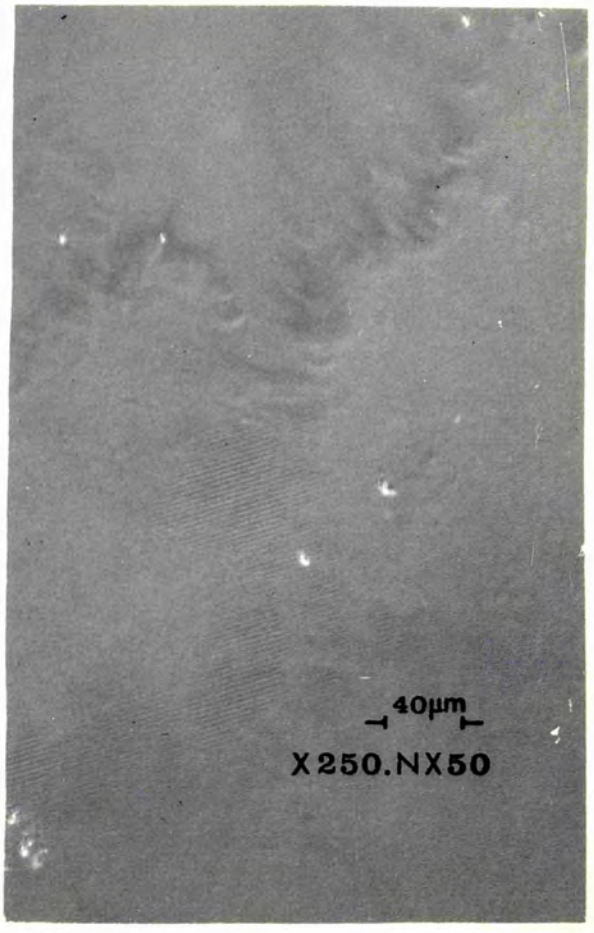

C

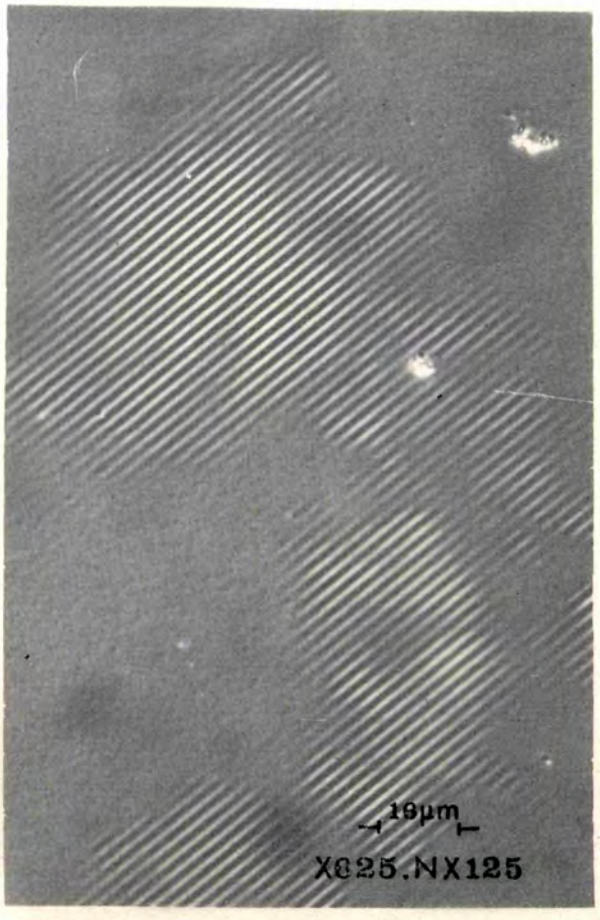

D

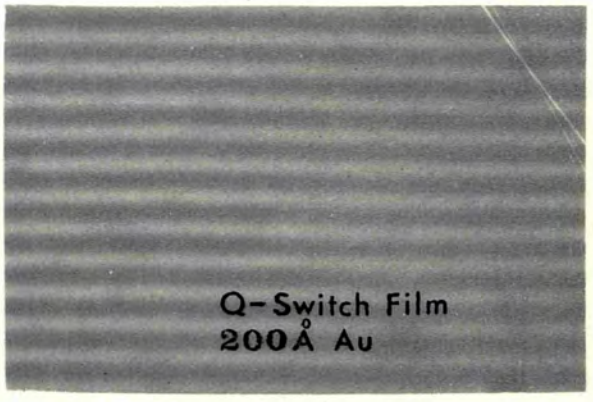

Spatial Period 2·5μm

7μm X1500.NX300

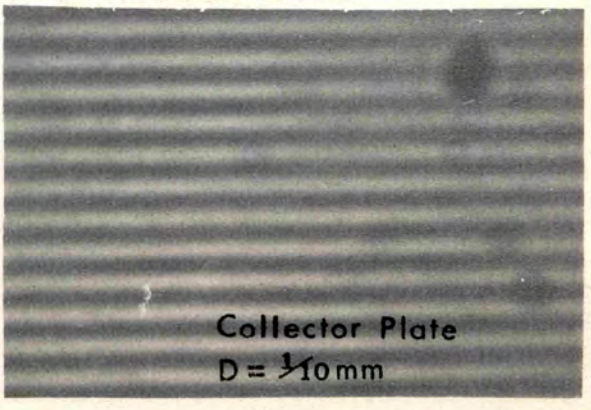

Fig 6·17

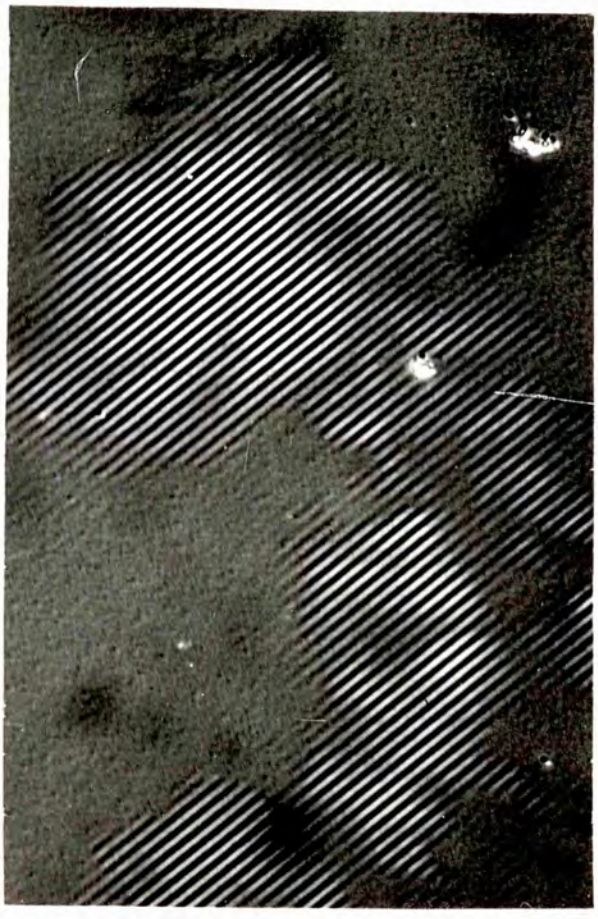

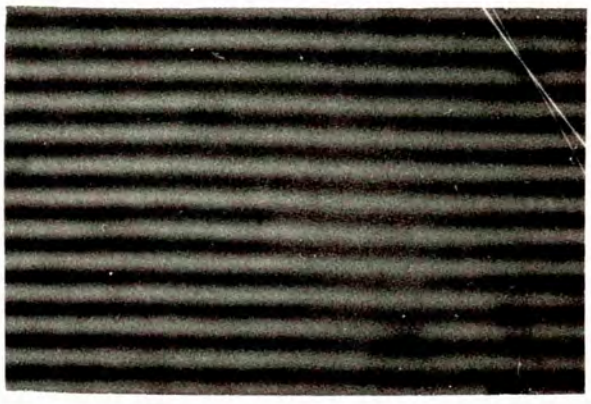

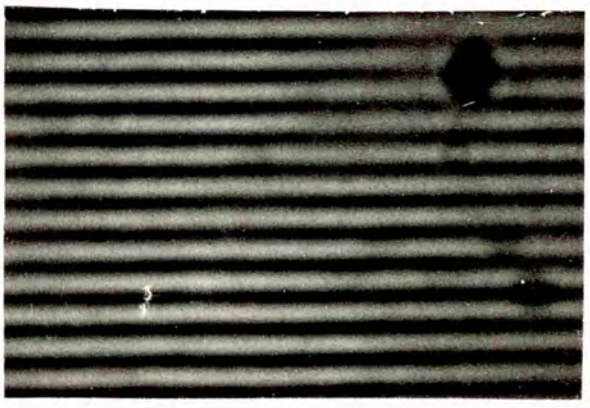

The filamentary nature of the gold layer on the substrate is shown in fig. 6.17A corresponding to the filaments within the laser beam (chapter 3). In the centre of fig. 6.17B the modulations of the gold are just visible in the region between two such filaments. The photograph fig. 6.17D compares the modulations on the collector plate with those on the Q - switching film.

For values of D less than 0.01 cm the collector plate was usually damaged by the rapid expansion of the contained gases. For values of D greater than 0.05 cm no spatial periodicity in the condensed gold could be observed.

It has been shown[89] that although the initial velocity of a vapour produced by laser evaporation agrees with the evaporation temperature, the absorption of laser radiation accelerates the vapour front, increasing the velocity by a factor of twenty over a distance of 0.3 cm for graphite in vacuum. Over the distance D utilized it is reasonable to assume that the velocity was constant and equal to

$$\left| \frac{2\,T_c\,k}{m} \right|^{1/2}$$

where T_c is the boiling point of gold. The vapour front would reach the collector plate in a time τ, measured from the start of the lasing pulse, equal to 200 ns (D = 0.01 cm). From fig. 6.16A the power level inside the cavity at that time had fallen to 150 KW.

This experiment cannot be described by any mechanism other than inhibition of condensation. The recording threshold was substantially reduced. The patchiness of the collected gold

was due to the high pressure gradients in the region between the two plates and the fact that the experiment was performed at atmospheric pressure.

The recording threshold utilizing the inhibition process must be a dynamic one. Using a lower density vapour the threshold should drop dramatically. In particular the condensation of vapours produced by conventional thermal methods in vacuum (section 6.5) could be inhibited by the relatively low power of an argon ion laser.

6.10 SELF PROBING OF LASER ETCHED GRIDS

Considerable interest has been shown in the timing of events when a surface is heated by a laser.[77,82,83,89] It could be argued that, in the systems described previously, the metallic layer must have evaporated to initiate the Q - switched pulse. However, by observing the self diffracted light it was experimentally verified that grid formation and evaporation were initiated at the start of the giant pulse.

Calculations on the positions of self diffracted orders site all four (transmitted and reflected -1 and +1) first orders in either autocollimation or in the same directions as the reflected beams from the film. Observations had therefore to be made on the second diffracted orders. It was convenient to arrange for a second diffracted order to travel at right angles to the probe radiation within the cavity.

If α is the incidence angle of the probe and β the diffracted angle measured relative to the surface then

$$d(\cos\alpha + \cos\beta) = n\lambda$$

is the diffraction relation and the spatial period is

$$d = \frac{\lambda}{2 \cos}$$

Therefore $\cos\beta = (2n - 1) \cos\alpha$

and for the second order to be orthogonal

$$\beta = 270^\circ + \alpha$$

Therefore $\tan\alpha = 2n - 1$

The smallest allowed α is given by $\tan\alpha = 3$, $\alpha = 71^\circ\ 34'$ $n = 2$

The resulting spatial period was 1.098 μm. The corresponding θ (incidence relative to surface normal) was $\theta = 18^\circ\ 26'$.

Fig. 6.18 shows the experimental arrangement used and the film orientation is drawn approximately to scale. The second diffracted order was split into two equal intensity beams by a beam splitter. The reflected beam was photographed through F_3 whilst the undeviated beam, after passing through F_2, was incident on a previously calibrated 56 A.V.P. photomultiplier connected to a T 454 via a 125 ns delay line. The diode D_1 monitored the laser output and also triggered the sweep for the T 454. Detection of the diffracted probe beam had to be accomplished against a high background of scatter from the laser and the xenon flashtube. Interference filters with a 10 Å wide pass band at 6943 Å were incorporated in F_3 and F_2.

The central photograph taken with $\theta = 18\ 26'$ shows the self diffracted beam observed and detuning the film by one degree caused the image to disappear. This verified that the radiation being recorded was the diffracted laser beam. The collimation is self evident and the measured beam divergence of 1.5×10^{-3} radians was consistent with that observed in the main beam. The spot observed may be regarded as an instant 'read out' hologram and as such contained spatial information

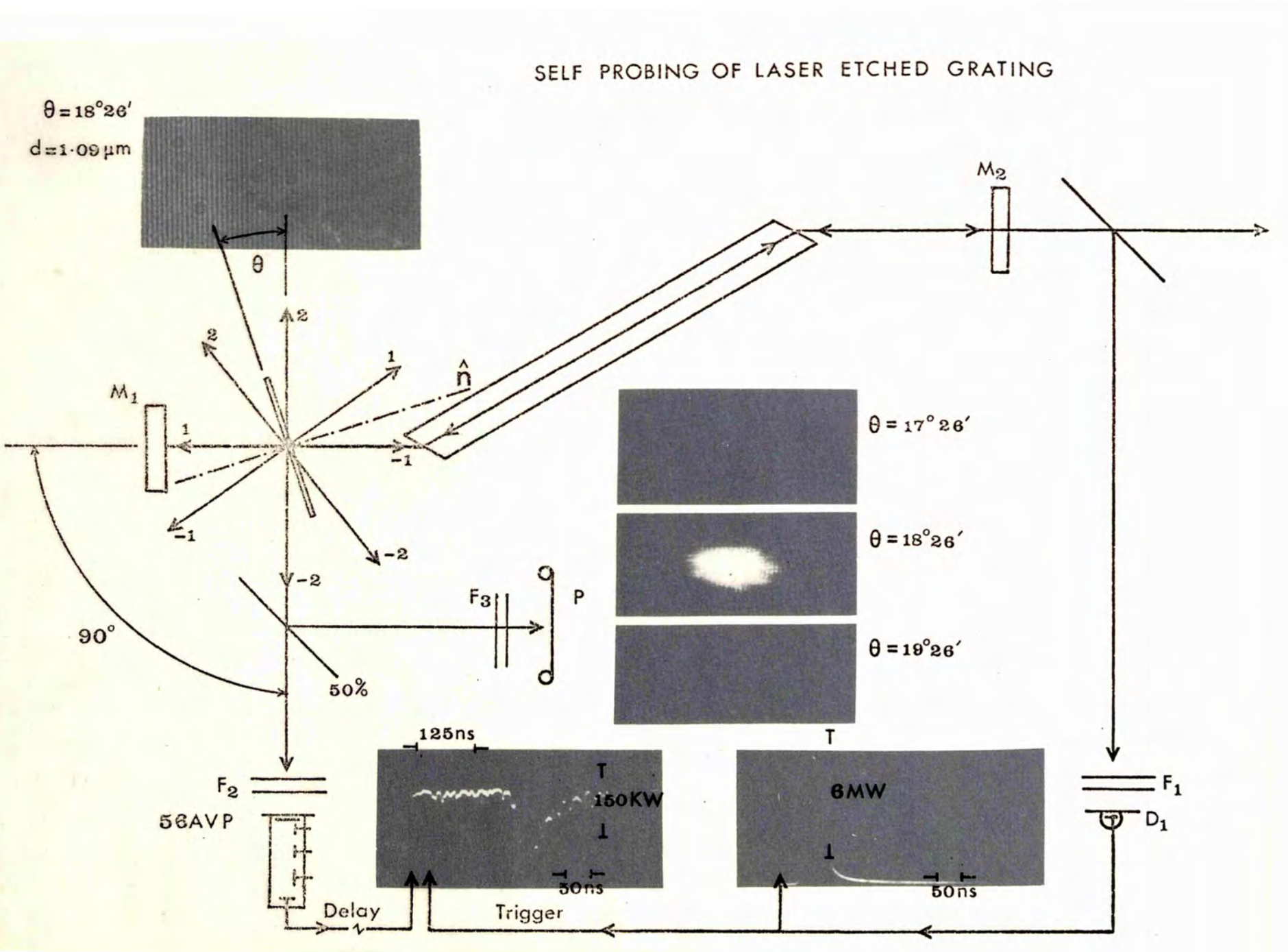
SELF PROBING OF LASER ETCHED GRATING
θ = 18°26′
d = 1·09 μm
θ
M2
M1
n̂
2
1
-1
-2
90°
50%
F3
P
θ = 17° 26′
θ = 18°26′
θ = 19°26′
125ns
T
150KW
50ns
6MW
F2
56AVP
F1
D1
Delay
Trigger

Fig 6·18

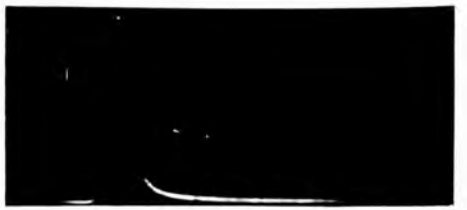

about the surface structure. In all cases the spot was crossed by a parallel system of fringes.

The intensity time characteristic of the diffracted light monitored by the photomultiplier started at the same time as the cavity radiation when allowance was made for the 125 ns delay cable. This coincidence of probe and scattered beam verified that grid formation and cavity radiation were simultaneous.

Generation of sound waves.

The peak power of the second diffracted order was 150 KW compared with 6 MW in the probe beam, representing an efficiency of 2.5%. A similar value was found when a continuous wave gas laser was used on the etched grid. Recently Cachier[140] has demonstrated that high amplitude surface waves may be generated on the surface of a metal by the periodic heating caused by the interference of two laser beams. Auth[141] describes the coupling mechanism as the relaxation of the periodic pressure distribution, caused by local heating at the antinodes of the interfering electromagnetic fields. The decay of the distribution is in the form of two oppositely directed acoustic waves, of wavelength equal to the spacing of the optical fringes. Such a technique provides a tunable source of surface waves by simply varying the angle between the interfering beams. The diffraction of light by similar surface motions has been demonstrated by Soffer.[142]

In the self probing experiment described there was no possibility of the self diffracted beam having been caused by diffraction at a surface wave. In the first place, the generation

of surface waves requires the metallic film thickness to be greater than the thermal skin depth. In the second place, the efficiency of the grid, measured by photographic and photoelectronic methods, was constant and equal to that expected from a 'formed' surface.

* * *

REFERENCES

1. TANG C.L., STATZ H. and DE MARS G., J. Appl. Phys., 34, p. 2289, 1963.

2. MAKOV G., J. Appl. Phys., 33, p. 202, 1962.

3. HELLWORTH R.W., "Advances in Quantum Electronics", Columbia University Press, p. 334, 1961.

4. McCLUNG F.J. and HELLWORTH R.W., Proc. I.E.E.E., 51, p. 46, 1963.

5. HELLWORTH R.W., "Quantum Electronics", vol. 2, Columbia University Press, p. 1203, 1963.

6. WAGNER W.G. and LENGYEL B.A., J. Appl. Phys., 34, p. 2040, 1963.

7. DALY R.T. and SIMS S.D., Appl. Opt., 3, p. 1063, 1964.

8. COLLINS R.J. and KISLUIK P., J. Appl. Phys., 33, p.2009, 1962.

9. BERGSTEIN L. and KAHN W., Proc. I.R.E., 50, p. 1833, 1962.

10. DE MARIA A.J., GAGOSZ R. and BARNARD G., J.Appl. Phys., 34, p. 453, 1963.

11. GEUSIC J.E. and SCOVIL H.E.D., Bell Systems Tech. J., p. 1371, July 1962.

12. SOCY W.R., GELLER M. and BARTFIELD D.P., Appl. Phys. Lett., 5, p.54, 1964.

13. GRANT D.G., Proc. I.E.E.E., 51, p. 604, 1963.

14. MASTERS J.I., WARD J.H. and HARTOUNI E., Rev. Sci. Inst., 34, p. 365, 1963.

15. McCLUNG F.J. and HELLWORTH R.W., J. Appl. Phys., 33, p.828, 1962.

16. GÜRS K., Z. Physik, 172, p. 145, 1963.

17. WOODBURY E.J. and NG W.K., Proc. I.R.E., 50, p. 2347, 1962.

18. KAFALAS P., MASTERS J.I. and MURRAY E.M.E., J. Appl. Phys., 35, p. 2349, 1964.

19. SOFFER B.H., J. Appl. Phys., 35, p. 2551, 1964.

20. RÖSS D., Z. Naturforschung, 204, p. 696, 1965.

21. KATZENSTEIN J., MAGYAR G. and SELDEN A.C., Opto - Electronics, 1, p. 13, 1969.

22 BLISS E.S., National Bureau of Standards Special Publication No. 341, December 1970, p. 105.

23. VUYLSTEKE A.A., J. Appl. Phys., 34, p. 1615, 1963.

24. WEILDER R.C., BURKHALTER J.H. and VUYLSTEKE A.A., J. Appl. Phys., 38, p. 4510, 1967.

25. ERNEST J., MICHON M. and DEBRIE J., Phys. Letts., 22, p. 147, 1966.

26. HOOK W.R., DISHINGTON R.H. and HILBERG R.P., Appl. Phys. Lett., 9, p. 125, 1966.

27. RUNDLE W.J., J. Appl. Phys., p. 5338, 1968.

28. DE MARIA A.J., GLENN W.H. and BRIENZA M.J., Proc. I.E.E.E., 57, p. 2, 1969.

29. DE MARIA A.J., STETSER D.A. and GLENN W.H., Science, 156, p. 1557, 1967.

30. CULTER C.C., Proc. I.R.E., 43, p. 140, 1955.

31. HARGRAVE L.E., FORK R.L. and POLLACK M.A., Appl. Phys. Lett., 5, p. 4, 1964.

32. DI DOMENICO Jr. M., J. Appl. Phys., 33, p.2870, 1964.

33. DEUTSCH T., Appl. Phys. Lett., 7, p. 80, 1965.

34. MICHON M., ERNEST J. and AUFTRET R., Phys. Lett., 23, p. 457, 1966.

35. DI DOMENICO Jr. M., GEUSIC J.E., MARCOS H.M. and SMITH R.G., Appl. Phys. Lett., 8, p. 180, 1966.

36. MAKER P., TERHUME R., NISENHOFF M.and SAVAGE C., Phys. Rev. Lett., 8, p. 21, 1962.

37. MOCKER H.W. and COLLINS R.J., Appl. Phys. Lett., 7, p. 270, 1965.

38. MACK M.E., I.E.E.E. Q-E., 4, 12, p. 1015, 1968.

39. LITTLE V.I. and ROWLEY D.M., J. Phys. E., 3, p. 469, 1970.

40. DE MARIA A.J., STETSER D.A. and HEYNAU H.A., Appl. Phys. Lett., 8, p. 174, 1966.

41. STETSER D.A. and DE MARIA A.J., Appl. Phys. Lett., 9, p. 118, 1966.

42. MALYSHEV V.I., MARKIN A.S., SYCHEV A.A., Zh.E.T.F. Pis'ma, 6, p. 503, 1967.

43. TREACY E.B., Phys. Lett., 28A, p. 34, 1968.

44. WEBER H.P., J. Appl. Phys., 38, p. 2231, 1967.

45. BLOEMBERGEN N., "Non - Linear Optics", 1965.

46. GIORDMAINE J.A., RENTZEPIS P.M., SHAPIRO S.L. and WECHT K.W., Appl. Phys. Lett., 11, p. 216, 1967.

47. ROWE H.E. and LI TINGYE, I.E.E.E. Q.-E., 6, p.49, 1970.

48. KACHEN G., STEINMETZ L. and KYSILKA J., Appl. Phys. Lett., 11, p. 216, 1968.

49. PENNEY Jr. A.W. and HEYNAU H.A., Appl. Phys. Lett., 9,p. 257 1966.

50. MICHON M., ERNEST J. and AUFFRET R., Phys. Lett., 21, p. 514, 1966.

51. DE MARIA A.J., GAGOSZ R., HEYNAU H.A., PENNEY Jr. A.W. and WISNER G., J. Appl. Phys., 38, p. 2693, 1967.

52. BASOV N.G., KRIUKOV P.G., ZAKHAROV S.D., SENATSKY Yu.V. and TCHEKALIN S.V., I.E.E.E. Q.-E., 4, p. 864, 1968.

53. LIPSON S.G. and LIPSON H., "Optical Physics", C.U.P., 1969.

54. GABOR D., Nature, 161, p. 777, 1948.

55. LEITH E. and UPATNIEKS J., J. Opt. Soc. Am., 52, p. 1123, 1962.

56. LEITH E. and UPATNIEKS J., J. Opt. Soc. Am., 53, p. 1377, 1963.

57. STROKE G.W., "Coherent Optics and Holography", Academic Press, 1966.

58. "Methods of Producing Phase Holograms with Conventional Photographic Materials", Special Applications, Eastman Kodak Co., Rochester NY, 1968.

59. MEGLA G.K., Appl. Opt., 5, p. 945, 1966.

60. MOTT N.F. and GURNEY R.W., "Electronic Processes in Ionic Crystals", O.U.P., p. 149, 1957.

61. BEESLEY M.J. and CASTLEDINE J.G., Appl Opt., p. 2720, 1970.

62. URBACK J.C. and MEIER R.W., Appl. Opt., 5, p. 666, 1966.

63. SIEFERT W.A. and ELBRECHT W.F., Photographic Science and Engineering, 5, p. 235, 1961.

64. CHEN F.S., Appl. Phys. Lett., 13, p. 223, 1968.

65. SHANKOFF T.A. and CURRAN R.K., Appl. Phys. Lett., 13, p. 239, 1968.

66. CHANG M.M.T., Cal. Tech. Scientific Report No. 8, May 1969. Clearinghouse, U.S. Dept. of Commerce/N.B.S., AD 696 577 p. 33.

67. BURCH J.M. and PALMER D.A., Optica Acta, 8, p. 73, 1961.

68. RIGLER A.K. and VOGL T.P., Appl. Opt., 5, p. 1086, 1966.

69. GEORGE N. and MATTHEWS J.W., Appl. Phys. Lett., 9, p. 212, 1966. Erratum: equation p. 212 should read $d = \frac{\lambda}{2\cos\frac{\theta_1-\theta_2}{2}\sin\frac{\theta_1+\theta_2}{2}}$

70. KOCK W.E., ROSEN L. and REINDEIRO J., Proc. I.E.E.E., p. 1599, Nov. 1966.

71. FRIESEM A.A., Appl. Phys. Lett., 7, p. 102, 1965.

72. The Angeniuex Corporation of America, 440, Merrick Road, Oceanside N.Y. 11572 (516) 678 3520.

73. LABEYRIE A. and FLAMAND J., Optical Spectra, Nov/Dec, p. 54, 1969.

74. HARRISON G.R., J. Opt. Soc. Am., 39, p. 413, 1949.

75. TURNER G. L'e., Bulletin I.P.P.S., Oct., p. 338, 1967.

76. KOMAR A.I., STABNIKOV M.V., TURUKHANO B.G. and TURUKHANO N., Opt. Spectrosc., 23, p. 450, 1967.

77. GERRITSEN H.J. and HELLER M.E., J. Appl. Phys., 38, p. 2054, 1967.

78. LITTLE V.I., ROWLEY D.M. and WILTSHER R., Nature, 228, p. 49, 1970.

79. AMODEI J.J. and MEZRICH R.S., Appl. Phys. Lett., 15, p. 45, 1969.

80. LITTLE V.I., KEY P.Y., WILTSHER R. and ROWLEY D.M., Nature, 232, p. 165, 1971.

81. Special Issue - Laser Applications, Bulletin I.P.P.S., July 1971.

82. READY J.F., J. Appl. Phys., 36, p. 463, 1965.

83. READY J.F., Appl. Phys. Lett., 3, p. 11, 1963.

84. VOGEL K. and BACKLUND P., J. Appl. Phys., 36, p. 3697, 1965.

85. BASTOW T.J. and BOWDEN F.P., Nature, 218, p. 150, 1968.

86. DUGUAY M.A., SHAPIRO S.L. and RENTZIPIS P.M., Phys. Rev. Lett., 19, p. 1014, 1967.

87. EHLER A.W., J. Appl. Phys., 37, p. 4962, 1966.

88. BASTOW T.J., Nature, 222, p. 1058, 1969.

89. WEICHEL H. and AVIZONIS P.V., Appl. Phys. Lett., 9, p. 334, 1966.

90. LINLOR W.I., Appl. Phys. Lett., 3, p. 210, 1963.

91. RICHARDS F.A. and WALSH D., J. Phys. D., 2, p. 663, 1969.

92. BONCH - BRUEVICH A.M., IMAS Ya. A., LIBENSON M.N. and SPIRIDONOV B.N., Soviet Physics - Technical Physics, 15, p. 512, 1970.

93. LIBENSON M.N., F.Kh.O.M., 2, 1968.

94. LI T. and SIMS S.D., Proc. I.R.E., 50, 4, 1962.

95. CONGLETON R.S., SOOY W.R., DENHURST D.R. and RILEY L.D., "Quantum Electronics", vol. 2, Columbia University Press, p. 1415 and p. 1214, 1963.

96. CALVIELLO J.A., FISHER E.W. and HELLER Z.H., I.E.E.E. Q.-E., 1, p. 132, 1965.

97. EVTUHOV V. and NEELAND J.K., Appl. Opt., 1, p. 517, 1962.

98. NELSON D.F. and BOYLE W.S., Appl. Opt., 1, p. 181, 1962.

99. STATZ H. and DE MARS G., "Quantum Electronics", Columbia Press, p. 530, 1960.

100. DUNSMUIR J., J. Electr. Control, 10, p. 453, 1961.

101. BERKELY D.A. and WOLGA G.J., Phys. Rev. Lett., 9, p. 479, 1962.

102. GRANT D.G., Proc. I.E.E.E., 51, p. 604, 1963.

103. MASTERS J.I., WARD J.H. and HARTOUNI E., Rev. Sci. Inst., 34, p. 365, 1963.

104. BRADLEY D.J., NEW G.H.C., SUTHERLAND B. and CAUGHEY S.J., Phys. Letts., 28A, p. 532, 1969.

105. SZABO A. and ERICKSON L.E., I.E.E.E. Q.-E., 1, p. 692, 1968.

106. FREUND I., Appl. Phys. Lett., 12, 1968.

107. GREENHOW R.C. and SCHMIDT A.J., Appl. Phys. Lett., 12, 1968.

108. COLLINS R.J., BROWN L.O. and DEAN D.R., Appl. Phys. Lett, 12, 1968.

109. ROM - KRICHEVSKAYA I.A. and RATNER A.M., Opt. Spectrosc., 19, p. 149, 1965.

110. MAGYAR G., Rev. Sci. Inst., 38, p. 517, 1967.

111. MAHLEIN H.F. and SCHOLLMEIER G., Appl. Opt., 8, p. 1197, 1969.

112. STATZ H., DE MARS G.A. and TANG C.L., J. Appl. Phys., 38, p. 2212, 1967.

113. RENTZEPIS P.M. and DUGUAY M.A., Appl. Phys. Lett., 11, p. 218, 1967.

114. ARAKELYAN V., KARLOV N. and PROLOROV A., J.E.T.P. Lett., 10, p. 178, 1969.

115. CUBEDDU R., POLLONI R., SACCHI C.A. and SVELTO O., I.E.E.E. Q.-E., 5, p. 470, 1969.

116. SVELTO O.,Research Colloquium on Mode Locked Lasers, Southampton, 28th April 1971.

117. TREACY E.B., Phys. Lett., 28A, p. 34, 1968.

118. SMITH R.L., Phys. Lett., 30A, p. 132, 1969.

119. BRADLEY D.J., NEW G.H.C. and CAUGHEY S.J., Phys.Lett., 30A,p. 78, 1969.

120. SHAPIRO S.L. and DUGUAY M.A., Phys. Lett., 28A, p. 698, 1969.

121. PETERSON D.G. and YARIV A., Appl. Opt., 5, p. 985, 1966.

122. TIFFANY W.B., Appl. Opt., 7, p. 67, 1968.

123. BURCH J.M., "Quantum Electronics", vol. 2, Columbia University Press, p. 1187, 1963.

124. STOKES G.G., Proc. Roy. Soc., 11, p. 545, 1862.

125. MAGYAR G. and SELDEN A.C., Appl. Opt., 9, p. 2040, 1970.

126. Conference on Lasers and Opto Electronics, University of Southampton, March 1969. (Unpublished)

127. DUGDALE R.A., McVICKERS R.C. and FORD S.D., J. Nuclear Materials, 12, p. 1, 1964.

128. BIRNBAUM M., J. Appl. Phys., 36, p. 3688, 1965.

129. JENKINS and WHITE, "Fundamentals of Optics".

130. BOYNE J. and MARTIN F., J. Opt. Soc. Am., 52, p. 880, 1962.

131. AUTON J.P., Appl. Opt., 6, p. 1023, 1967.

132. ULRICH R., Appl. Opt., 7, p. 1987, 1968 and 8, p. 319, 1969.

133. A.I.M. Associates, Cambridge Ltd.

134. STEVERDING B., J. Phys. D, 3, p. 358, 1970.

135. TOLANSKY S., Nature, 169, p. 445, 1952.

136. TOLANSKY S., Scientific American, 191, p. 54, 1954.

137. SNEDDON I.N., "Special Functions of Mathematical Physics and Chemistry", Oliver and Boyd.

138. WALLNER H., Z. Phys., 114, p. 368, 1939.

139. MURPHY R.J. and RITTER G.J., Nature, 210, p. 191, 1966.

140. CACHIER G., Appl. Phys. Lett., 17, p. 419, 1970.

141. AUTH D.C., Appl. Phys. Lett., 16, p. 521, 1970.

142. SOFFER B.H., CLOSE D.H. and PEDINOFF M.E., Appl. Phys. Lett., 15, p. 339, 1969.

References 39, 78, 80 are bound with this thesis.

A C K N O W L E D G E M E N T S

I wish to place on record my appreciation of the help I have received from colleagues during my six year stay at the Royal Holloway College, as an undergraduate and as a postgraduate.

In particular I would like to acknowledge the freely given advice and guidance of my supervisor, Dr. V.I.Little. I must also mention Professor S. Tolansky F.R.S., Dr. P.Y.Key, Dr. A.C.Selden and Dr. G.Magyar for the help they have given.

Many thanks are also tendered to Mrs. R. Wiltsher, with whom I collaborated on this project.

I would also like to acknowledge the considerable financial support of a Science Research Council studentship.

I am indebted for the technical assistance of D.S. Hambley, G. Hayward, M. Thyer and A. Grant.

I am grateful to Marilyn for her literary guidance and typing tenacity.

I would also like to thank Mr. A.J. Taylor for many stimulating discussions, often in the early hours of the morning, mostly concerning boomerangs.

The use of a 'rough stack' mirror in a mode-locked ruby laser

V I Little and D M Rowley
Physics Department, Royal Holloway College, Englefield Green, Surrey
MS *received 18 December 1969, in revised form 5 February 1970*

Abstract The mirror damage problem associated with mode-locked laser systems is discussed. It is shown that a 'rough stack' mirror, fabricated from microscope coverslips, is free from such damage and can be used in mode-locking a ruby cavity.

Mode-locked operation of a ruby laser was first reported by Mocker and Collins (1965) but, despite the advantage of a visible output, authors have chosen to use mode-locked neodymium-in-glass lasers in experiments requiring picosecond pulses. The reason for this choice is twofold. Firstly, neodymium-in-glass has a much broader linewidth than ruby and should theoretically give shorter pulses. Secondly, neodymium-in-glass lasers can be mode locked more easily than ruby.

More recently, Mack (1968) has shown that a carefully designed ruby laser can be mode-locked easily and that by the choice of saturable absorber it is possible to obtain pulses approaching the theoretical limit of the inverse bandwidth.

Even so, as was pointed out in both the above references, at the high power levels involved mirror damage is a severe problem, affecting the reliability of the system. Damage at the 100% mirror can be alleviated by the use of prisms, but the various schemes devised for the low reflectance end of the cavity, e.g. frustrated total internal reflection and electron gun evaporated coatings, are either difficult to use or expensive.

The use of etalon type reflectors (see, for example, Magyar 1967), with their comparative freedom from damage, unfortunately impedes mode-locking by exhibiting mode selective properties. The present work shows, however, that a cavity incorporating a mirror fabricated from microscope coverslips (Burch 1964) can produce the mode-locked output shown in figure 1. The surface of microscope coverslips may be termed

Figure 1 Mode-locked output. Sweep speed 20 ns per large division. Detector rise time ≃ 2 ns

'rough' in comparison with optically flat surfaces. A stack of such coverslips will not be spectrally selective, as is the case of an etalon with precise surfaces. Such a 'rough stack' will, however, have the damage-free characteristics so important in the case of a mode-locked laser.

The mirror used consists of ten 0·3 mm thick microscope coverslips, separated by paper spacers which create an air gap between the slips of 0·09 mm. A mirror of this type can be constructed in the following way. A single coverslip A (see figure 2) of diameter 1 in is placed on a horizontal surface,

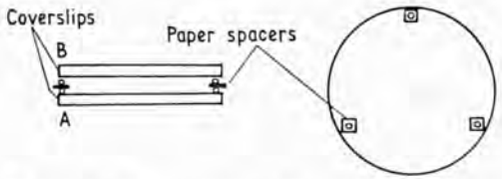

Figure 2 Construction of mirror

and globules of glue applied with a pin at three points. Three paper spacers, 1/10 in square, are placed on top of thess globules with a pin wetted with glue. The next coverslip B ie placed on top of this and the process repeated until the stack is complete. A 50 g weight is carefully placed on top of the stack before leaving the glue to set. It is important that the pin should transfer small amounts of glue only, or when compressed the glue will obscure the optical path. Any extraneous matter trapped in the stack may be blown out with a compressed air line.

Other particulars of the cavity used to obtain consistently

the output shown in figure 1 are as follows. The cavity incorporated a Brewster-angled ruby rod 150 mm long and 10 mm in diameter pumped in an exfocal elliptical geometry by a linear flashtube. The cavity was closed by a roof-top prism and a mirror of the type discussed. The switch cell, with 3 mm path length, was placed close to the prism and tilted at the relevant Brewster angle. The saturable absorber used was cryptocyanine in acetone. Rhodamine 6G was added to this solution in the proportion of 1 mg per 100 cm^3. Cubeddu *et al.* (1969) note that the addition of such a two-photon absorber tends to increase the risetime of the modes relative to their characteristic locking time. The present authors find that this process enhances the mode locking ability of a cavity when either a stack or dielectric mirror is used.

The optical system is simple to align if a helium–neon gas laser is used as an alignment beam. The centre (as judged by eye) of the unusually large area of light resulting from the reflection from the stack mirror is sufficient for its alignment. The mode-locked output of the cavity is found to be relatively insensitive to stack misalignments of up to 5 mrad.

A comparison was made between the stack mirror and a dielectric mirror of 25% reflectivity at 0·6943 μm. The output in both cases was the same and consisted of a train of pulses separated by the cavity ringing time (figure 1). With two-photon fluorescent tracks (Giordmaine *et al.* 1967) pulse widths were found to be of the order of 20 ps. The general Q switch threshold was at 800 J.

The dielectric mirror was, however, found to be damaged after some 40 shots, but the stack mirror showed no detectable damage after 100 shots.

It is in this way that the type of mirror described provides an efficient, easy to use and reliable component for use with a mode locked ruby cavity.

References

Burch J M 1964 *Quantum Electronics: Proc. 3rd Int. Congr., Paris* 1963 (New York: Columbia University Press) pp. 1187–202

Cubeddu R Polloni R Sacchi C A and Svelto O 1969 *I.E.E.E. Trans. Quantum Elect.* **QE-5** 470–1

Giordmaine J A Rentzepis P M Shapiro S L and Wecht K W 1967 *Appl. Phys. Lett.* **7** 216–8

Mack M 1968 *I.E.E.E. Trans. Quantum Elect.* **QE-4** 1015–6

Magyar G 1967 *Rev. Sci. Instrum.* **38** 517–9

Mocker H W and Collins R J 1965 *Appl. Phys. Lett.* **7** 270–3

Journal of Physics E: Scientific Instruments 1970 Volume 3
Printed in Great Britain

(Reprinted from *Nature*, Vol. 228, No. 5266, pp. 49-50, October 3, 1970)

Optical Transmission and Reflexion Gratings by Laser Evaporation

WE wish to report a new technique for the manufacture of optical transmission and reflexion gratings. The gratings are formed by the action of standing light waves in a ruby laser cavity on thin metallic films deposited on glass substrates within the cavity (Fig. 1).

We used two ruby laser systems, one a Bradley laser type 302 which had a very inhomogeneous beam; the other was a more refined system, with a Brewster angled ruby rod. At first two mirrors of 100 per cent reflectivity were used in the cavity, but we found that more controlled evaporation was possible with one of the mirrors only partially reflecting. Rough stack mirrors[1] were also used with success. In both laser systems gratings were produced over an area of about 10 mm², with rulings up to 2,000 lines mm⁻¹.

Most of our experiments have been carried out with gold films 20·0 to 10·0 nm thick, deposited on smooth float glass. Gratings were also produced using silver films. The films cause a loss in the cavity which vanishes when oscillations start the Q of the cavity suddenly increases and the laser output is a high power giant pulse. This is a standard Q-switching method[2,3] producing peak powers of the order of 10 MW in our experiments.

When oscillations start, evaporation takes place at the anti-nodes[4] of the electric field forming a grating within the laser burn. On two films the diffracted first order travelling wave after one reflexion in the cavity mirror also burnt the film. As expected, this burn did not show any diffraction effects.

The number of lines per mm, n, can be varied by changing the angle θ between the film and the normal to the cavity axis, because

$$n = \frac{\sin\theta}{\lambda_R/2}$$

where λ_R is the wavelength of ruby light. Gratings were produced for various values of θ, and n was calculated from the results of normal incidence first order diffraction experiments. The graph (Fig. 2) is a straight line, showing good agreement with theory.

The gratings were examined using a helium–neon laser. Fig. 3 shows the reflected and transmitted first and second order diffracted beams. Spraying the gratings with a protective clear lacquer did not seem to affect their performance. Some of the glass substrates were examined after the metal film had been dissolved, and the glass was found to be etched, giving faint diffraction patterns. We intend to investigate the latter phenomenon as part of the current programme of work at this college on laser damage.

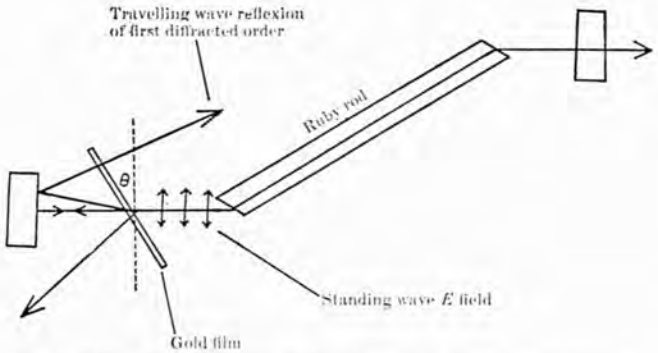

Fig. 1. Technique for producing diffraction gratings by laser evaporation.

The uniformity of the rulings of this kind of grating can be assessed from Fig. 4. In this case the line spacing was 2,500 nm.

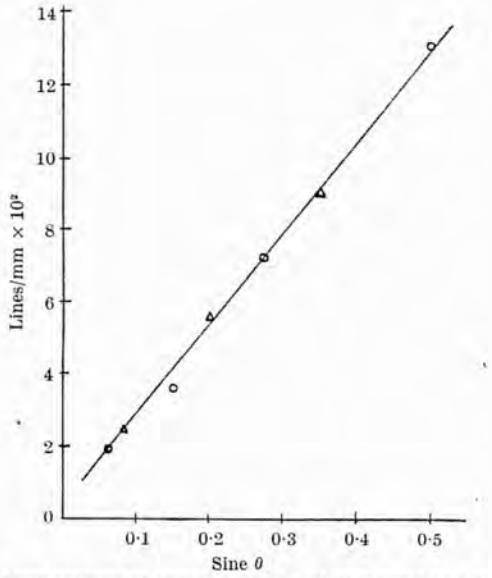

Fig. 2. Laser evaporated gratings. Graph of lines mm⁻¹ as a function of film angle, θ, within the cavity. ○, Bradley type 302 laser; △, Brewster angled laser system.

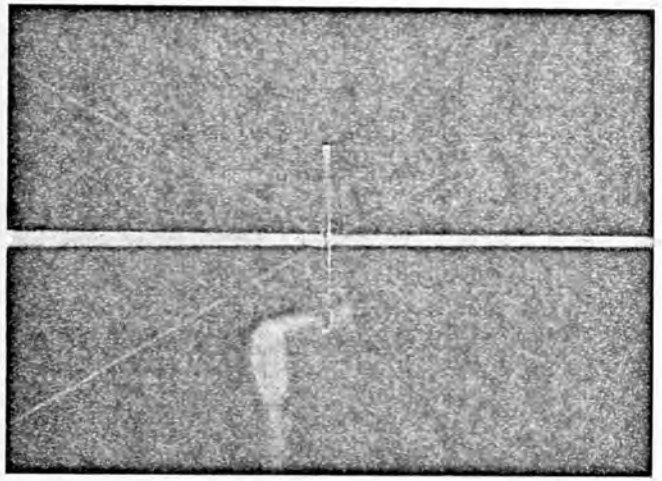

Fig. 3. Transmitted and reflected, first and second diffracted orders by a laser evaporated grating with 715 lines mm^{-1}. Incident radiation 632·8 nm.

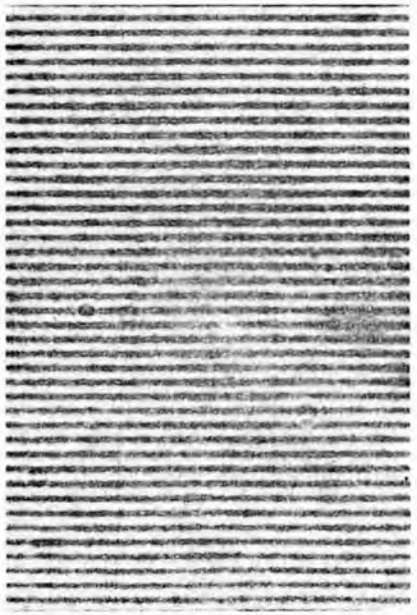

Fig. 4. Laser evaporated grating photographed by transmission microscopy. The grating period is 2,500 nm.

Using this technique the length of grating which can be made seems to be limited only by the length of the laser cavity and the available laser power. The width of the grating is determined by the width of the laser beam—usually only a few mm. The grating spacing could conceivably be as small as 250 nm if frequency doubled ruby laser light were used, and there is no reason to believe that the quality of the rulings would be any worse than those shown in Fig. 4. Development work is proceeding along these lines.

We thank Professor S. Tolansky and Mr M. Thyer for Fig. 4 and Mr D. Hambley for preparing suitable gold films. R. W. and D. M. R. are supported by Science Research Council research studentships.

V. I. Little
D. M. Rowley
R. Wiltsher

Department of Physics,
Royal Holloway College
(University of London),
Englefield Green,
Egham, Surrey.

Received August 3, 1970.

[1] Little, V. I., and Rowley, D. M., *J. Phys.*, E, **3**, 469 (1970).
[2] Masters, J. I., Ward, J., and Hartouni, E., *Rev. Sci. Instrum.*, **34**, 365 (1963).
[3] Grant, D. G., *Proc. IEEE*, **51**, 604 (1963).
[4] Weiner, O., *Ann. d. Physik*, **40**, 203 (1890).

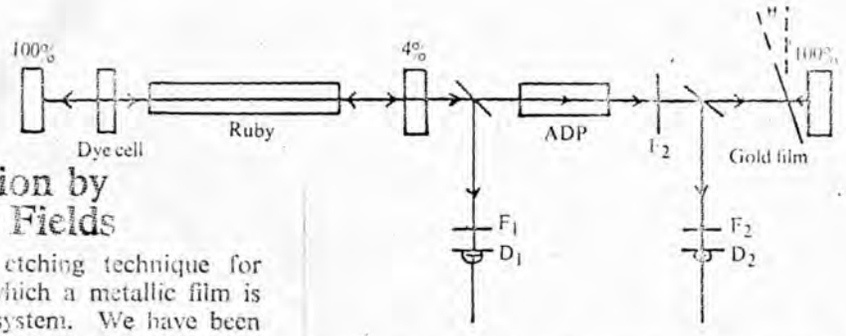

Fig. 1 Optical system for extra-cavity etching with frequency doubled ruby light. Cryptocyanine dye Q-switch; gold thickness 200 Å; F_1 transmission 6943 Å; F_2 transmission 3471 Å.

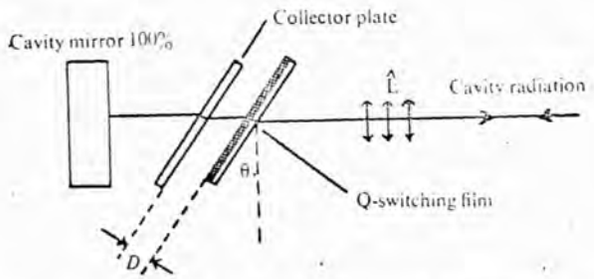

Fig. 2 Disposition of collector plate and Q-switching film.

Inhibition of Condensation by Intense Electromagnetic Fields

V. I. Little
P. Y. Key
R. Wiltsher
D. M. Rowley

Department of Physics, Royal Holloway College, University of London, Englefield Green, Egham, Surrey

Received August 4, 1971.

We recently described[1] an optical etching technique for producing small optical gratings in which a metallic film is used as a Q-switch for a ruby laser system. We have been able to produce line spacings as small as 180 nm using frequency doubled ruby laser radiation in the optical arrangement of Fig. 1; this corresponds to band 13 on Nobert's finest ruled test plate[2]. With further doubling of the laser light, spacings of order 90 nm should be obtainable.

We have now observed the converse of this optical etching effect, namely the spatially periodic inhibition of the condensation of gold vapour by intense optical standing waves. The optical arrangement is shown in Fig. 2; the vaporized plume[3] of gold produced by the Q-switching process was allowed to condense on a clean transparent collector plate (microscope slide). If the gold reaches the collector plate before the laser pulse has decayed to zero, the inhibition of condensation of vapour results in the formation on the collector plate of a spatially periodic gold film similar to that found on the optically etched plate. If the gold arrives after the decay of the laser pulse, the gold deposition on the collector is spatially undifferentiated.

In the present experiment, single laser giant pulses of half width 50 ns and peak power 100 kW mm^{-2} were used. The transit time of the gold atoms from the Q-switching film to the collector plate, distant $D = 10^5$ nm away, was 200 ns according to simple kinetic theory of gases. The operative power density of the laser pulse during condensation of the gold on the collector was 1,500 W mm^{-2} (determined using a calibrated photodiode).

A microphotograph of part of the collector plate is shown in Fig. 3. For $D > 5 \times 10^5$ nm, no spatial periodicity in the condensed gold could be observed and for $D < 10^5$ nm, the collector plate was usually damaged by the rapid expansion of the contained gases.

We are investigating the preferential inhibition of the condensation of vapours *in vacuo* using an argon ion laser system.

1 Little, V. I., Rowley, D. M., and Wiltsher, R., *Nature*, 228, 49 (1970).
2 Turner, G. L'E., *Bull. I.P.P.S.*, 338 (1967).
3 Ready, J. F., *Appl. Phys. Lett.*, 3.1. 11 (1963).

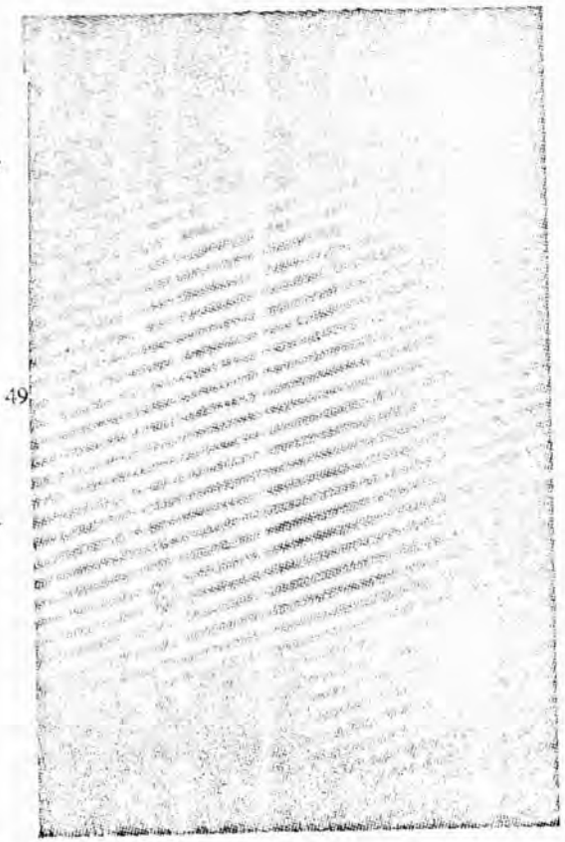

Fig. 3 Microphotograph of part of collector plate showing spatially periodic (2,580 nm) gold layer.